



University  
of Glasgow

Kredi, Doaa (2016) *Improving interfaces for nerve repair*. PhD thesis.

<http://theses.gla.ac.uk/7255/>

Copyright and moral rights for this work are retained by the author

A copy can be downloaded for personal non-commercial research or study, without prior permission or charge

This work cannot be reproduced or quoted extensively from without first obtaining permission in writing from the author

The content must not be changed in any way or sold commercially in any format or medium without the formal permission of the author

When referring to this work, full bibliographic details including the author, title, awarding institution and date of the thesis must be given

Enlighten:Theses  
<http://theses.gla.ac.uk/>  
theses@gla.ac.uk



University  
of Glasgow

# Improving interfaces for nerve repair

Doaa Kredi

Submitted in fulfilment of the requirements for the  
Degree of Doctor of Philosophy (PhD)

Centre for Cell Engineering  
College of Medical, Veterinary and Life Sciences  
Institute of Molecular, Cell and Systems Biology  
University of Glasgow  
Glasgow, G12 8QQ

**October 2015**

## Thesis Abstract

Autologous nerve grafts are the current gold standard for the repair of peripheral nerve injuries. However, there is a need to develop an alternative to this technique, as donor-site morbidities such as neuroma formation and permanent loss of function are a few of the limitations concerned with this technique. Artificial nerve conduits have therefore emerged as an alternative for the repair of short peripheral nerve defects of less than 30 mm, however they do not surpass autologous nerve grafts clinically. To develop a nerve conduit that supports regeneration over long nerve gaps and in large diameter nerves, researchers have focused on functionalizing of the conduits by studying the components that enhance nerve regeneration such as micro/nano-topography, growth factor delivery systems, supportive cells and extracellular matrix (ECM) proteins as well as understanding the complex biological reactions that take place during peripheral nerve regeneration.

This thesis presents strategies to improve peripheral nerve interfaces to better the regenerative potential by using dorsal root ganglions (DRGs) isolated from neonatal rats as an *in vitro* model of nerve regeneration. The work started off by investigating the usefulness of a frog foam protein Ranaspumin-2 (Rsn2) to coat biomaterials for compatibility, this led to the discovery of temporary cell adhesion on polydimethylsiloxane (PDMS), which was investigated as a suitable tool to derive cell-sheets for nerve repair. The influence of Rsn2 anchored to specific adhesion peptide sequences, such as isoleucine-lysine-valine-alanine-valine (IKVAV), a sequence derived from laminin proven to promote cell adhesion and neurite outgrowth, was tested as a useful means to influence nerve regeneration. This approach improves the axonal outgrowth and maintains outgrowth long term.

Based on the hypothesis that combinational modulation of substrate topography, stiffness and neurotrophic support, affects axonal outgrowth in whole DRGs, dissociated DRGs were used to assess if these factors similarly act at the single cell level. Rho associated protein kinase (ROCK) and myosin II inhibitors, which affect cytoskeletal contractility, were used to influence growth cone traction forces and have shown that these factors work in combination by interfering with growth cone dynamic creating a different response in axonal outgrowth at the single cell level.

# Table of Contents

<b>Thesis Abstract .....</b>	<b>2</b>
<b>Table of Contents .....</b>	<b>3</b>
<b>List of Tables.....</b>	<b>6</b>
<b>List of Figures .....</b>	<b>7</b>
<b>Presentations .....</b>	<b>12</b>
<b>Acknowledgments .....</b>	<b>13</b>
<b>Author’s Declaration.....</b>	<b>14</b>
<b>Definitions/Abbreviations.....</b>	<b>15</b>
<b>Chapter 1.....</b>	<b>17</b>
<b>1.1 General introduction.....</b>	<b>18</b>
<b>1.2 Peripheral nervous system (PNS).....</b>	<b>18</b>
1.2.1 The Neuron .....	18
1.2.2 Peripheral nerves.....	20
1.2.3 Peripheral nerve injury .....	21
1.2.4 Wallerian degeneration.....	24
1.2.5 Neural regenerative response .....	27
1.2.6 Growth cone and elongation.....	30
1.2.7 The cytoskeleton and the ECM.....	31
1.2.8 Cell adhesion molecules (CAMs).....	34
1.2.9 Experimental model <i>in vitro</i> : DRGs.....	37
<b>1.3 Nerve regeneration.....</b>	<b>38</b>
1.3.1 Nerve conduits – Biomaterials.....	39
1.3.2 Nerve conduits – Topography .....	40
1.3.3 Nerve conduits – supporting cells .....	41
1.3.4 Nerve conduits – Growth Factors.....	42
<b>1.4 PDMS .....</b>	<b>44</b>
1.4.1 Chemistry.....	44
1.4.2 Hydrophobicity .....	45
<b>1.5 Rsn2 .....</b>	<b>46</b>
<b>1.6 Aims &amp; goals.....</b>	<b>49</b>
<b>Chapter 2.....</b>	<b>50</b>
<b>2.1 Introduction .....</b>	<b>51</b>
<b>2.2 Materials and methods .....</b>	<b>53</b>
2.2.1 Molecular biology .....	53
2.2.1.1 Overnight culture.....	53
2.2.1.2 Expression of protein .....	53
2.2.1.3 Harvesting of protein .....	54
2.2.1.4 Protein purification .....	54
2.2.1.5 Protein concentration.....	55
2.2.2 Cell engineering .....	56
2.2.2.1 Organotypic culture of DRGs .....	56
2.2.2.2 DRG immunofluorescence .....	56

2.2.2.3	Cell culture.....	57
2.2.2.4	Caco-2 cell Immunofluorescence.....	57
2.2.2.5	Material fabrication .....	57
2.2.2.6	Sample preparation .....	58
2.2.2.7	PDMS swelling.....	58
2.2.2.8	X-ray photoelectron spectroscopy (XPS) .....	59
2.2.2.9	Topas® sample preparation .....	60
2.2.2.10	Data analysis – cell number timeline.....	60
2.2.2.11	Quantification of linear ZO-1 staining.....	61
<b>2.3</b>	<b>Results.....</b>	<b>63</b>
2.3.1	Expression and purification of Rsn2 and iLOV-Rsn2.....	63
2.3.2	Adsorption of Rsn2 onto a hydrophobic surface.....	65
2.3.3	Verification of protein attachment – XPS.....	66
2.3.4	DRG cultures .....	67
2.3.5	Caco -2 cell cultures.....	70
<b>2.4</b>	<b>Discussion/conclusion.....</b>	<b>77</b>
<b>Chapter 3.....</b>	<b>81</b>	
<b>3.1</b>	<b>Introduction .....</b>	<b>82</b>
<b>3.2</b>	<b>Materials and methods .....</b>	<b>86</b>
3.2.1	PDMS fabrication (flat and Grooves).....	86
3.2.2	Sample sterilization and preparation .....	86
3.2.3	Dissociation of DRGs into single cells .....	86
3.2.4	Immunofluorescence.....	87
3.2.5	Rho & ROCK inhibitors .....	88
3.2.6	Cell sizing analysis.....	88
3.2.7	Branching analysis .....	88
3.2.8	Neuron length analysis .....	88
<b>3.3</b>	<b>Results.....</b>	<b>89</b>
3.3.1	Cell characterisation .....	89
3.3.2	Length of individual neurons (10 day culture).....	92
3.3.3	24-hours outgrowth and contractility tests.....	98
<b>3.4</b>	<b>Discussion/Conclusion .....</b>	<b>105</b>
<b>Chapter 4.....</b>	<b>109</b>	
<b>4.1</b>	<b>Introduction .....</b>	<b>110</b>
<b>4.2</b>	<b>Materials and methods .....</b>	<b>112</b>
4.2.1	Protein expression.....	112
4.2.2	Size Exclusion Chromatography.....	112
4.2.3	PDMS fabrication .....	112
4.2.4	Sample preparation .....	113
4.2.5	Dissociation of DRGs into single cells .....	113
4.2.6	Immunofluorescence staining .....	114
4.2.7	Water Contact Angle (WCA) .....	115
4.2.8	PDMS microcontact stamp .....	116
4.2.9	Data analysis.....	116
<b>4.3</b>	<b>Results.....</b>	<b>117</b>
4.3.1	Expression and purification of the proteins .....	117
4.3.2	WCA measurements .....	118
4.3.3	Axonal outgrowth on all protein variations.....	119
4.3.4	Analysis of axonal outgrowth on IKVAV-Rsn2 and RGD-Rsn2 .....	121
4.3.5	Long term time points (10-day).....	128

4.3.6 PDMS microcontact stamp .....	130
<b>4.4 Discussion &amp; conclusion .....</b>	<b>133</b>
<b>Chapter 5.....</b>	<b>136</b>
<b>Discussion-Conclusion.....</b>	<b>136</b>
<b>5.1 General discussion .....</b>	<b>137</b>
5.1.1 Rsn2 for temporary surface modification of PDMS.....	138
5.1.2 Physical substrates factors affect NGF response in individual neurons.....	139
5.1.3 Rsn2 modifications and neural response .....	140
<b>5.2 Future work.....</b>	<b>142</b>
5.2.1 Further investigation in using Rsn2 in culture .....	142
5.2.2 Quantifying myosin II.....	143
<b>5.3 General conclusion.....</b>	<b>144</b>
<b>List of References .....</b>	<b>145</b>

## List of Tables

<i>Table 1: CA measurement values of the eleven different conditions tested. Measurements were taken immediately after coating with the proteins. Values and standard deviation were calculated using 30 readings per data set, which were taken across 3 substrates.....</i>	<i>119</i>
---	------------

## List of Figures

Figure 1: A schematic representation of a neuron. The cell body called the soma contains the nucleus; extending from the cell body are dendrites, which receive signals from other neurons and an axon that conveys the signals to its destination by an action potential (orange arrow). Schwann cells surround the axon in layers of myelin (a lipid-rich membrane) that supports the axon and enhances signal transduction. Gaps between the Schwann cells are known as nodes of Ranvier, which further enhance signalling by a process known as saltatory conduction. ....	19
Figure 2: A schematic representation of a peripheral nerve. Axons are grouped together into fascicles that are surrounded by connective tissue, the endoneurium and blood vessels. This is all bound together by the perineurium and all these structures are held together by another connective tissue layer the epineurium. Adapted from (Evans, 2001).....	21
Figure 3: Schematic representation of peripheral nerve injuries as classified by Seddon and Sunderland. In neurapraxia all the connective structures are intact and full recovery is achieved without any surgery. In axonotmesis (grade 2) the axons are disturbed and Wallerian degeneration (detailed in section 1.2.4) takes place; recovery is achieved by axonal regeneration. Axonotmesis (grade 3) the endoneurium is also disturbed leading to incomplete and misdirected axonal regeneration. Axonotmesis (grade 4) is same as grade 3, with the perineurium also being disturbed – little recovery without surgery. Neurotmesis is the total disruption of the nerve with no recovery without surgery. ....	23
Figure 4: Mechanism of Wallerian degeneration. At the site of nerve injury (A) a process known as Wallerian degeneration occurs (B) Schwann cells at the distal part of the nerve, stop making myelin and are fragmented with their myelin sheaths along with the axon by macrophages and activated Schwann cells. Schwann cells then migrate to the site of injury and bridge the gap by forming bands of Bungner (C). Within 24 hours the axons start to regenerate and bridge the injury site at a rate of 0.25 to 1 mm a day – the leading segment of the axon is termed the growth cone (D) Myelin is formed around the axon as it regenerates – axons continue to regrow until the target is reached. Adapted from (Allodi et al., 2012).....	26
Figure 5: Signaling in peripheral nerve injury. Upon injury, signals from the injury site are sent to the soma informing it of the disconnection which in turn results in activation of transcription factors responsible for the regenerative state. The main changes that occur is a burst of action potentials, interruption of the trophic molecules retrograde transport system, and the transfer of phosphorylated proteins like MAP2 which is one of the positive signals that is generated. All these contribute to the activation of RAGs which induce production of GAP-43 and neurotrophic factors. Adapted from (Allodi et al., 2012).....	29
Figure 6: Cytoskeleton composition of an axon. A schematic representation of an axon is shown with a cell body (a), and an axon and growth cone (b). Diagrams e, f and g are schematic representation of the 3 components of the cytoskeleton microtubules, neurofilaments and actin filaments respectively. From (Fletcher and Mullins, 2010) with permission. ....	32
Figure 7: A schematic representation of focal adhesion formation of a growth cone. In red are the integrin $\alpha\beta$ heterodimeric receptors that bind to proteins within the ECM, such as collagen (col), laminin (LN) and fibronectin (FN). In purple are the scaffolding proteins talin, paxillin and vinculin that bind to the cytoplasmic tail of the integrins linked to actin filaments (blue). Focal adhesion kinase and Src are activated by clustering of integrin receptors (orange) and modulate adhesions through phosphorylation of key residues that allow binding of many additional proteins. Adapted from Myres et al (Myers et al., 2011). ....	36
Figure 8: Solution structure of Rsn-2. (A) Ribbon diagram illustrating the Rsn-2 fold and (B) rotated 90° about the vertical axis. (Mackenzie et al., 2009). ....	47
Figure 9: A secondary structure schematic indicating how RSN-2 molecules might lie in a more extended conformation at the air-water interface (a) compared with the compact closed form in solution (b)(Mackenzie et al., 2009).....	48
Figure 10: PDMS weight change with swelling. The above graph represents the average weight changes of 18 PDMS samples. A total decrease of 5% was established.....	59
Figure 11: Image analysis using the Analyse particle tool of Image J software. (A) Represents the cell nuclei selected by adjusting the threshold. (B) Represents the particles counted and (C) is the completed computation of the number of particles selected. Scale bar = 50 $\mu\text{m}$ . ....	61
Figure 12: Image analysis using Neuron J tool of Image J software. The fluorescence image of the ZO-1 immunostaining (A) in the process of tight junction selection – once a trace has been made the line changes colour to pink (B). Once all the tight junctions are selected the program is run to compute the length of the selection and the results are obtained in $\mu\text{m}$ . scale bar = 50 $\mu\text{m}$ . ....	62
Figure 13: SDS-PAGE analysis of iLOV-Rsn2 (left) and Rsn2 (right) expression samples. A distinct band is visible for iLOV-Rsn2 at ~ 27 KDa (arrow) and ~14 KDa for Rsn2 (arrow) indicating the presence of protein which could be confirmed by purification. ....	63

- Figure 14: SDS-PAGE analysis of Rsn2 (A) and iLOV-Rsn2 (B) nickel affinity column samples. To elute the bound His-tagged protein, a solution containing a high concentration of Imidazole is used which displaces the bound histidines. Contaminant proteins seen in columns (5-7) were removed by a series of washes using (5-30mM) imidazole concentrations before eluting for the target protein. The gels confirm that the protein was eluted successfully as a distinct band is visible in the first elution wash ~ 27 kDa for iLOV-Rsn2 and ~14 kDa for Rsn2. .... 64
- Figure 15: Fluorescence images of iLOV-Rsn2 adsorbed surfaces with holly leaf shaped patterned hydrophilic (contact angle  $45.0^{\circ} \pm 2.8^{\circ}$ ) and hydrophobic ( $71.5^{\circ} \pm 2.5^{\circ}$ ) surfaces. (A) hydrophilic surface inside, hydrophobic outside, and (B) Hydrophilic surface outside, hydrophobic inside. These images show that the surface properties guide the differential adsorption of iLOV-Rsn2. Imaging of iLOV fluorescence showed consistently, that the relative amount of iLOV-Rsn2 was lower on the hydrophilic substrate and that this difference was independent of the pattern type (inside/outside hydrophobic). Scale bar = 30 $\mu$ m. .... 65
- Figure 16: XPS spectra (MgK $\alpha$  X-ray source) of blank PDMS substrate (lower, red trace) and PDMS coated with Rsn2 (upper, brown trace). The nitrogen 1s signal is a clear marker for the presence of protein on the surface, and can only be seen on the Rsn-2 coated surface. The respective peaks are indicated. The inset table gives the relative percentage surface coverage for C1, Si2p, O1s, and N1s. .... 66
- Figure 17: Immunofluorescence images of DRG explants immuno-labelled for  $\beta$ 3-tubulin (red) and nuclei (blue) grown for 6 days on: (A) PLL coated PDMS (grooves). (B) On Rsn2 coated PDMS (grooves) (C) on iLOV-Rsn2 coated PDMS (grooves). Images B and C are showing the retraction of the nerve fibres when cultured on Rsn2/iLOV-Rsn2 surfaces (see arrows), whereas the positive control (A) is showing extended and growing nerve fibres. (Observation of n=9 DRG cells) Scale bar = 100 $\mu$ m. .... 67
- Figure 18: Immunofluorescence images of DRG explants immuno-labelled for F-Actin (red) and nuclei (blue) cultured on PCL for 10 days coated with (A&B) PLL, (C&D) Rsn2 and (E&F) iLOV-Rsn2. The images show that the DRG cells adhered onto the PCL surfaces without showing any neurite retraction. (Observation of n=9 DRG cells) Scale bar for images A, C&E = 100  $\mu$ m and B, D&F = 50  $\mu$ m. .... 68
- Figure 19: Bright field images of DRG explants cultured on PC substrates for 10 days coated with (A) PLL (B) Rsn2 and (C) iLOV-Rsn2. The images show that the DRG cells adhered onto the PC substrates without showing any neurite retraction. (Observation of n=9 DRG cells) Scale bar = 50  $\mu$ m. .... 69
- Figure 20: Immunofluorescence images of DRG explants immuno-labelled for  $\beta$ 3-tubulin (red) grown for 10 days on (A), PLL coated PC (B), iLOV-Rsn2 coated PC (C), iLOV-Rsn2 coated PC and pre incubated in L15 media 6 days prior to seeding (D), iLOV-Rsn2 coated PC and pre incubated in L15 media (in absence of FBS). (Observation of n=9 DRG cells) Scale bar = 50 $\mu$ m. .... 70
- Figure 21: The graph represents the average number of Caco-2 cells/mm<sup>2</sup> after 1,5 and 7 days on plain PDMS – negative control, PLL coated PDMS –positive control, and Rsn2 and iLOV-Rsn2 coated PDMS. Stars indicate significant differences between groups as determined by ANOVA and a Dunnett post hoc test \*p<0.05 \*\*p<0.01 and \*\*\*P<0.001. (n=3 biological repeats, multiple fields of view (9 per sample) were examined for analysis). The bars indicate standard deviation. .... 71
- Figure 22: ZO-1 tight junction staining 5, 10 and 15 days (A-C) on iLOV-Rsn2 coated PDMS and analysis of tight junction length ZO-1 (red), and DNA (blue). Scale bar = 30 $\mu$ m. The graph (D) shows the average length of tight junction formation (ZO-1) by Caco-2 cells after 5, 10 and 15 days on PLL coated –positive control and iLOV-Rsn2 coated PDMS. Stars indicate significant differences between groups as determined by ANOVA and a Dunnett post hoc test \*p<0.05 and \*\*\*P<0.001. (n=3 biological repeats, multiple fields of view (10 per sample) were examined for analysis). The bars indicate standard deviation. .... 72
- Figure 23: Immunofluorescence images of Caco-2 cells immuno-labelled for nuclei (grey-scale) cultured for 28 days on (A) PLL coated PDMS- no cell peeling on the edge (edge indicated by white line). (B) iLOV-Rsn2 coated PDMS – cell-peeling starting from the edge. (C) Rsn2 coated PDMS – cell peeling on the edges (indicated by the arrow). (Observation of n=9 samples) Scale bar = 50 $\mu$ m. .... 73
- Figure 24: Immunofluorescence images of Caco-2 cells immuno-labelled for fibronectin cultured on (A) PLL-coated PDMS: there is no cell peeling and ECM is associated with the whole surface. (B) Post cell peel-off from iLOV-Rsn2 PDMS (peeling indicated by arrow): no fibronectin is present on surface after peeling. (Observation of n=9 samples) Scale bar = 50 $\mu$ m. .... 73
- Figure 25: XPS spectra (AlK $\alpha$  X-ray source) to verify the use of Cu<sup>2+</sup> as a tag to detect Rsn2. Cu<sup>2+</sup> is observed when bound to Rsn2 on the surface (upper trace) – two control samples (middle and lower trace) were tested to ensure that Cu<sup>2+</sup> does not bind the material and that the signal is only observed when Cu<sup>2+</sup> is chelated by Rsn2. The respective peaks are indicated, and the inset table gives the relative percentage surface coverage for C1, Si2p, O1s, and N1s. .... 74
- Figure 26: XPS spectra (AlK $\alpha$  X-ray source) analysing the PDMS surface post peel off. Neither Cu2p nor N1s peak are observed on the PDMS surface post cell peel off (upper trace) confirming that Rsn2 is no longer present on the surface and that the PDMS as the blank substrate (lower trace) is reverted back to its original

- chemistry before being coated with Rsn2. The respective peaks are indicated, and the inset table gives the relative percentage surface coverage for C1, Si2p, O1s, and N1s. .... 75
- Figure 27: Phase contrast images of Caco-2 cell sheets cultured on (A) PC and (B) leached PDMS cultured for 21 days. Both show no peeling and similar cell clustering morphology. Representative images. Scale bar = 50  $\mu\text{m}$ . .... 76
- Figure 28: Signal transduction pathway of the Rho GTPases in regulation of cytoskeleton organisation. Adapted from (Guan and Rao, 2003). The Rho GTPases are regulated by GEFs (guanine nucleotide exchange factors) and inactivated by GAPs (GTPase activating protein). Activated ROCK regulates MLC and its phosphorylation results in an increase in actomyosin contractility. .... 83
- Figure 29: Immunofluorescence images of sensory neurons immuno-labelled for neuroactive peptides NF200 (red), SP or CGRP (green) and nuclei (blue) to determine cell population distribution. The cells were cultured on PLL coated PDMS (flat). The images represent NF200 positive cell (A), CGRP positive cells (B) and SP positive cells (C). No SOM positive cells were detected. Representative images. Scale bar = 50  $\mu\text{m}$ . .... 90
- Figure 30: The graph represents the cell area ( $\mu\text{m}^2$ ) of individual sensory neurons after seeding on PLL and laminin coated PDMS (flat). The variation of cell size is due to the presence of different cell subpopulations within the DRG neurons. (n= 3 biological repeats, multiple fields of view were examined for analysis, total of 686 cells). .... 91
- Figure 31: Immunofluorescence images of sensory neurons immuno-labelled for  $\beta$ 3-tubulin (A-C inverted grey-scale images) on PLL coated PDMS (flat). Cells were cultured for 10 days at (A) 10 ng/ml (B) 50 ng/ml (C) 100 ng/ml of NGF. The axons extend from the neurons after plating, with the length of the axons increasing with NGF concentration. Images (D-F) show the S100 $\beta$  positive Schwann cells (red) that follow the outgrowth of the axons and the nuclei (blue, DNA) of all other structural cells. Scale bar = 50  $\mu\text{m}$ . .... 93
- Figure 32: Immunofluorescence images of sensory neurons immuno-labelled for  $\beta$ 3-tubulin (inverted grey-scale images) on laminin coated PDMS (flat). Cells were cultured for 10 days at (A) 10 ng/ml, (B) 50 ng/ml, and (C) 100 ng/ml of NGF. The axons branch out in a random manner, the length of the total axonal outgrowth decreases with NGF concentration. Scale bar = 50  $\mu\text{m}$ . .... 94
- Figure 33: Immunofluorescence images of sensory neurons immuno-labelled for  $\beta$ 3-tubulin (inverted grey-scale images) on PLL coated PDMS (grooves). Cells were cultured for 10 days at (A) 10 ng/ml, (B) 50 ng/ml, and (C) 100 ng/ml of NGF. The axons extend by following the orientation of the grooves, but less so with increasing NGF concentration as seen in B (50 ng/ml) and C (100 ng/ml). The length of the total axonal outgrowth decreases with NGF concentration. Arrows show groove orientation. Scale bar = 50  $\mu\text{m}$ . .... 94
- Figure 34: Immunofluorescence images of sensory neurons immuno-labelled for  $\beta$ 3-tubulin (inverted grey-scale images) on laminin coated PDMS (grooves). Cells were cultured for 10 days at (A) 10 ng/ml, (B) 50 ng/ml, and (C) 100 ng/ml of NGF. The axons extend along the grooves following their orientation, the length of the total axonal outgrowth decreases with increasing NGF concentrations. Arrows show groove orientation. Scale bar = 50  $\mu\text{m}$ . .... 95
- Figure 35: Axon length of individual sensory neurons after a 10-day culture on PLL coated (flat or microgrooved) and laminin coated (flat or microgrooved) PDMS. On the PLL coated PDMS (flat), axonal length increased significantly with increasing NGF concentration. Compared to the flat, on microgrooves axon length was reduced with increasing NGF concentration. On the laminin coated PDMS (flat) axon length decreased significantly from 10ng/ml to 100ng/ml as did the length of the axons on the microgrooves. Stars indicate significant differences between groups as determined by ANOVA and Tukey's post hoc test \* $p < 0.05$  \*\* $p < 0.01$  and \*\*\* $p < 0.001$ . (n=3 biological repeats, multiple fields of view (10 per sample) were examined for analysis). The bars indicate standard deviation. .... 96
- Figure 36: The graph represents the number of branches formed on PDMS (grooves) coated with either PLL or laminin (LAM) cultured for 10 days in varying NGF concentrations of 10 ng/ml, 50 ng/ml and 100 ng/ml ng/ml. No change in branching was observed with increasing NGF concentrations, however the laminin surface reduced the number of branches. (n=3 biological repeats, multiple fields of view (10 per sample) were examined for analysis)..... 97
- Figure 37: Immunofluorescence images of sensory neurons immuno-labelled for  $\beta$ 3-tubulin (grey-scale) cultured on PLL coated PDMS (flat). Cells were cultured for 24hs at (A) 10 ng/ml, (B) 50 ng/ml and (C) 100 ng/ml of NGF. The axons extended from the neurons after plating, with the length of the axons increasing with NGF concentration. Scale bar = 50  $\mu\text{m}$ . .... 98
- Figure 38: Axon length of individual sensory neurons after 24-hour culture on PLL coated PDMS (flat) samples with varying NGF concentrations of 10 ng/ml, 50 ng/ml and 100 ng/ml. Positive control – PLL coated PDMS (non-treated). Inhibition of myosin II was achieved by the addition of Blebbistatin (50  $\mu\text{M}$  or 100  $\mu\text{M}$ ). The Rho-ROCK pathway was inhibited by the addition of Y-27632 (50 $\mu\text{M}$ ). The pattern observed on the control was comparable to the 10-day time point where the axon length increased significantly with increasing NGF concentration. Upon the addition of blebbistatin, the pattern of outgrowth was similar to that of the control but with larger axonal extensions. Y-27632 inhibited the pattern of outgrowth observed

- with increasing NGF concentrations. Stars indicate significant differences between groups as determined by ANOVA and a Dunnett post hoc test  $***P<0.001$ . (n=3 biological repeats, multiple fields of view (10 per sample) were examined for analysis). The bars indicate standard deviation. ....100
- Figure 39: Immunofluorescence images of sensory neurons immuno-labelled for  $\beta$ 3-tubulin (grey-scale) cultured on PLL coated PDMS (flat) at 10 ng/ml, 50 ng/ml and 100 ng/ml of NGF. Inhibition of myosin II was achieved by the addition of Blebbistatin (50  $\mu$ M or 100  $\mu$ M). The Rho-ROCK pathway was inhibited by the addition of Y-27632 (50  $\mu$ M). Pattern observed on the control was comparable to the 10-day time point where the axonal length increased significantly with increasing NGF concentration. Upon the addition of Blebbistatin, the pattern of outgrowth was similar to that of the control but with longer axonal extensions. Y-27632 grossly inhibited overall outgrowth and no change in outgrowth could be seen with increasing NGF concentrations. Scale bar = 50  $\mu$ m. ....101
- Figure 40: Axon length of individual sensory neurons after 24-hour culture on PLL coated PDMS (grooves) samples with varying NGF concentrations of 10, 50 and 100 ng/ml. Positive control – PLL coated PDMS (non-treated). Inhibition of myosin II was achieved by the addition of blebbistatin (50  $\mu$ M or 100  $\mu$ M). The Rho-ROCK pathway was inhibited by the addition of Y-27632 (50 $\mu$ M). The pattern observed on the control was comparable to the 10-day time point where the axonal length decreased significantly with increasing NGF concentration. The addition of blebbistatin resulted in larger axonal extensions. Y-27632 inhibited the pattern of outgrowth observed with increasing NGF concentrations. Stars indicate significant differences between groups as determined by ANOVA and a Dunnett post hoc test  $***P<0.001$ . (n=3 biological repeats, multiple fields of view (10 per sample) were examined for analysis). The bars indicate standard deviation. ....102
- Figure 41: Immunofluorescence images of sensory neurons immuno-labelled for  $\beta$ 3-tubulin (grey-scale) cultured on PLL coated PDMS (grooves) at 10 ng/ml, 50 ng/ml and 100 ng/ml of NGF. Inhibition of myosin II was achieved by the addition of Blebbistatin (50  $\mu$ M or 100  $\mu$ M). The Rho-ROCK pathway was inhibited by the addition of Y-27632 (50  $\mu$ M). Pattern observed on the control was comparable to the 10-day time point where the axonal length decreased significantly with increasing NGF concentration. Upon the addition of Blebbistatin, the pattern of outgrowth was similar to that of the control but with larger axonal extensions (non-responsive to topographical cue). Y-27632 inhibited the pattern of outgrowth seen with the differing NGF concentrations. Scale bar = 50  $\mu$ m. ....103
- Figure 42: Immunofluorescence images of sensory neurons immuno-labelled for F-actin (red), the focal adhesion marker talin (green), and DNA in nuclei (blue). The cells were cultured for 24-hours on glass coverslips where (A&B) No inhibitor (C) 100  $\mu$ M Blebbistatin (D) 50  $\mu$ M Y-27632. Scale bar = 10  $\mu$ m. ....104
- Figure 43: Contact angles were measured using the static drop technique on a PDMS surface and fitted with a circular line to determine angles. As depicted the contact angle varies depending on the hydrophobicity of the surface (WCA  $<90^\circ$  = high wettability, WCA  $>90^\circ$  = low wettability). ....115
- Figure 44: SDS-PAGE analysis of RGD-Rsn2 nickel affinity column samples. To elute the bound His-tagged protein, a solution containing a high concentration of Imidazole is used which displaces the bound histidines. Contaminant proteins seen in columns (5-7) were removed by a series of washes using (5-30mM) imidazole before eluting the target protein. The gels confirm that the protein was eluted successfully, as a distinct band is visible in the first elution wash at the molecular weight (~14 kDa) expected for RGD-Rsn2. ....117
- Figure 45: SDS-PAGE analysis of purified and buffer exchanged protein samples. Distinct bands are present at ~ 14 kDa for (from left to right after the markers): Rsn2, RGD-Rsn2, IKVAV-Rsn2, LDVP-Rsn2, PHSRN-Rsn2, FHRIKKA-Rsn2. For iLOV-Rsn2 a distinct band is present at ~ 27 kDa. The other much weaker bands seen at 75 kDa (Rsn2, RGD-Rsn2, PHSRN-Rsn2) and 25 kDa could be E.coli proteins. ....118
- Figure 46: Immunofluorescence images of sensory neurons immuno-labelled for  $\beta$ 3-tubulin (grey-scale) cultured for 24 hours on PDMS (flat) coated with (A) Rsn2, (B) LDVP-Rsn2, (C) PHSRN-Rsn2, (D) iLOV-Rsn2, (E) FHRIKKA-Rsn2, (F) RGD-Rsn2, (G) IKVAV-Rsn2 and highlighted in red are the two controls for this experiment (H) laminin (LAM) and (I) PLL. IKVAV-Rsn2 and RGD-Rsn2 were taken forward as suitable coatings to promote axonal outgrowth, Rsn2 was also used as a control. (Observation of n=9 cells) Scale bar = 50  $\mu$ m. ....120
- Figure 47: This graph represents the average length of axon outgrowth of individual neurons cultured for 24-hours PDMS (flat) coated with: PLL, LAM, Rsn2, RGD-Rsn2, IKVAV/RGD-Rsn2 mix and IKVAV-Rsn2 in 10 ng/ml NGF. The outgrowth on IKVAV-Rsn2 was significantly higher than on all the other substrates tested. Stars indicate significant differences between groups compared to control sample PLL as determined by ANOVA and a Dunnett post hoc test  $**p<0.01$  and  $***P<0.001$ . (n=3 biological repeats, multiple fields of view (10 per sample) were examined for analysis). The bars indicate standard deviation. ....122
- Figure 48: The graph represents the number of branches of individual neurons cultured for 24-hours on PDMS (flat) coated with: PLL, LAM, Rsn2, RGD-Rsn2, IKVAV/RGD-Rsn2 mix and IKVAV-Rsn2 in 10 ng/ml NGF. Neurons growing on IKVAV-Rsn2 branched significantly more than those seeded onto the other coatings tested. Stars indicate significant differences between groups compared to control sample PLL as determined

- by ANOVA and a Dunnett post hoc test  $*p < 0.05$  and  $***P < 0.001$ . ( $n=3$  biological repeats, multiple fields of view (10 per sample) were examined for analysis). The bars indicate standard deviation. ....123
- Figure 49: Immunofluorescence images of sensory neurons immuno-labelled for  $\beta 3$ -tubulin (inverted grey-scale images) cultured for 24-hours on PDMS (flat) coated with (A) Laminin, (B) PLL, (C) RGD-Rsn2, (D) Rsn2, and (E) IKVAV-Rsn2. A large network of axons was formed on the IKVAV-Rsn2 coating, fewer and smaller networks were formed on all the other surfaces. Scale bar = 50  $\mu\text{m}$  applies to all parts of the figure. ....124
- Figure 50: The graph represents the average axon length of individual neurons cultured for 24-hours on PDMS (grooves) coated with: PLL, LAM, Rsn2, RGD-Rsn2, IKVAV/RGD-Rsn2 mix and IKVAV-Rsn2 in 10 ng/ml NGF. The neurite length of cells cultured on IKVAV-Rsn2 and LAM were significantly longer in comparison to PLL. Stars indicate significant differences between groups compared to control sample PLL as determined by ANOVA and a Dunnett post hoc test  $**p < 0.01$  and  $***P < 0.001$ . ( $n=3$  biological repeats, multiple fields of view (10 per sample) were examined for analysis). The bars indicate standard deviation. ....125
- Figure 51: The graph represents the number of branches of individual neurons cultured for 24-hours on PDMS (grooves) coated with PLL, LAM, Rsn2, RGD-Rsn2, IKVAV/RGD-Rsn2 mix and IKVAV-Rsn2 in 10 ng/ml NGF. Axons on IKVAV-Rsn2 branch significantly, more often in comparison to RGD-Rsn2 and plain Rsn2. Stars indicate significant differences between groups compared to control sample PLL as determined by ANOVA and a Dunnett post hoc test  $*p < 0.05$  and  $**p < 0.01$  ( $n=3$  biological repeats, multiple fields of view (10 per sample) were examined for analysis). The bars indicate standard deviation. ....126
- Figure 52: Immunofluorescence images of sensory neurons immuno-labelled for  $\beta 3$ -tubulin (grey-scale inverted images) cultured for 24-hours on PDMS (grooves – arrows represent direction of grooves) coated with (A) laminin (B) IKVAV-Rsn2 (C) PLL (D) RGD-Rsn2 and (E) Rsn2. All the surfaces allowed for guided directional outgrowth where laminin provided the best outgrowth compared to the other surfaces. Scale bar = 50  $\mu\text{m}$  applies to all substrates. ....127
- Figure 53: Immunofluorescence images of sensory neurons immuno-labelled for  $\beta 3$ -tubulin (green), Schwann cell marker S100 $\beta$  (red) and DNA (blue) cultured for 24-hours on (A) PDMS (flat) and (B) PDMS (grooves) coated with a 1/1 mix of RGD-Rsn2/IKVAV-Rsn2. The peptide mix seems to have increased the attachment of Schwann cells and other structural cells (only nuclei, not S100 $\beta$  positive). (Observation of  $n=10$  cells) Scale bar = 50  $\mu\text{m}$ . ....128
- Figure 54: Immunofluorescence images of sensory neurons immuno-labelled for  $\beta 3$ -tubulin (green), Schwann cell marker S100 $\beta$  (red) and DNA (blue) cultured for 10 day on PDMS (flat) coated with IKVAV-Rsn2. At the 10-day time point, the axons formed a very complex network. Also evident were a large number of Schwann (e.g. see arrows, S100 $\beta$  positive) and other supporting cells (e.g. arrowheads, only nuclei, not S100 $\beta$  positive). Scale bar = 50  $\mu\text{m}$ . ....129
- Figure 55: Immunofluorescence images of sensory neurons immuno-labelled for  $\beta 3$ -tubulin (inverted grey-scale images) cultured for 10 days on (A) PDMS (grooves) and (B) PDMS (flat) both coated with IKVAV-Rsn2. The grooves resulted in aligned outgrowth whereas the flat cultures have formed a very complex network of axons. Scale bar = 50  $\mu\text{m}$ . ....129
- Figure 56: Fluorescence images of iLOV-Rsn2 adsorbed surfaces on (A) PDMS (grooves) – plasma treated and iLOV-Rsn2 coated after  $\mu\text{CP}$  (B) non-treated PDMS (flat) after  $\mu\text{CP}$  transferred iLOV-Rsn2 from (A). These images show that the lines formed by the ridges were successfully transferred from sample A to B (arrows show direction of grooves). Scale bar = 50  $\mu\text{m}$ . ....130
- Figure 57: The graph represents the average axon outgrowth length of individual neurons cultured for 24-hours on PDMS (flat) (with and without plasma treatment) coated with either IKVAV-Rsn2 or RGD-Rsn2 in 10 ng/ml NGF. The differences between plasma and no plasma treatment were not considered significant at  $p < 0.05$  using ANOVA ( $n=3$  biological repeats, multiple fields of view (10 per sample) were examined for analysis). The bars indicate standard deviation. ....132

## Presentations

Presentations made by the candidate relating to research in this thesis

(2015) Poster presentation at The Tissue and Cell Engineering Society (TCES), Southampton UK. Kredi, D and Riehle, MO. Physical substrate factors, NGF concentration and Rho-ROCK inhibition affect outgrowth response in individual neurons.

(2015) Poster presentation at UK Society for Biomaterials Annual Conference and Postgraduate Day, Belfast Ireland. Kredi, D and Riehle, MO. Physical substrates factors and NGF affect outgrowth responses in individual neurons.

(2015) Rapid-fire presentation at UK Society for Biomaterials Annual Conference and Postgraduate Day, Belfast Ireland. Kredi, D and Riehle, MO. Physical substrates factors and NGF affect outgrowth responses in individual neurons.

(2014) Poster presentation at Tissue Engineering and Regenerative Medicine Symposium (TERMIS), Genoa Italy. Kredi, D; Pedersen, RH; Steinmetz, N; Gadegaard, N; Smith, B and Riehle, MO . Frog foam protein for temporary surface modification of PDMS.

(2013) Oral presentation at DTC in Cell and Proteomic Technologies Symposium, Glasgow UK. Kredi, D; Pedersen, RH; Steinmetz, N; Gadegaard, N; Smith, B and Riehle, MO . Frog foam protein for temporary surface modification of PDMS.

## Acknowledgments

Firstly, I would like to thank my supervisor Dr Mathis Riehle for his continuous support, patience and motivation. His guidance, ideas and immense knowledge helped me throughout the project. I have been very lucky to be supervised by Mathis, who has always been fun to work with throughout the whole process. I could not have imagined having a better supervisor. I would also like to thank my second supervisor Dr Brian Smith for his help and guidance throughout the project. Big thanks to everyone at the Centre for Cell Engineering (CCE) for being great colleagues; particularly Dr Jemma Roberts who read over drafts of this thesis and helped me on numerous occasions in solving DRG mysteries, your help is greatly appreciated. A special thanks to Ricky and Anil for all the laughs and banter, it's been pure awesomeness.

My parents are owed a huge debt of gratitude for their continuous support and encouragement during this PhD. Huge thanks goes to the best sister in the world Zainab and brother in law Omar for inviting me to stay during the past few years, and to my beautiful nieces Tabarak and Safa who never fail to make me smile. It has been very fun living with you all and I appreciate everything you have done for me.

Of course I have to thank Louisa and Ya Hua who have been amazing friends, our long chats, series nights and dinners will surely be missed. I couldn't have survived without you guys. Finally I want to big up my "Curryhouse Crew" who make me laugh on a daily basis on our WhatsApp group chat, although we are all in different cities, I never feel distant from you guys and you are truly friends that I cherish, our daily banter has been a great way to keep me motivated.

## **Author's Declaration**

I hereby declare that the research presented within this thesis is my own work unless otherwise stated, and has not been submitted elsewhere for any other academic degree.

Doaa Kredi

## Definitions/Abbreviations

<b>1B-LIF</b>	1B leukaemia inhibitory factor
<b>ADSCs</b>	Adipose derived stem cells
<b>AFT3</b>	Activating transcription factor 3
<b>ANOVA</b>	Analysis of variance
<b>BDNF</b>	Brain derived neurotrophic factor
<b>BSA</b>	Bovine serum albumin
<b>cAMP</b>	Cyclic adenosine monophosphate
<b>CAMs</b>	Cell adhesion molecules
<b>CAP-23</b>	Cytoskeleton-associated protein-23
<b>Cdc42</b>	Cell division control protein 42
<b>CGRP</b>	Calcitonin gene related peptide
<b>cm</b>	Centimetre
<b>CNS</b>	Central nervous system
<b>CNTF</b>	Ciliary neurotrophic factor
<b>CSPG</b>	Chondroitin sulphate proteoglycans
<b>DMEM</b>	Dulbecco's modified Eagle medium
<b>DRG</b>	Dorsal root ganglia
<b><i>E.coli</i></b>	Escherichia coli
<b>ECM</b>	Extracellular matrix
<b>EDTA</b>	Ethylenediaminetetraacetic acid
<b>FAK</b>	Focal adhesion kinase
<b>FBS</b>	Fetal bovine serum
<b>FDA</b>	Food and drug association
<b>FGF</b>	Fibroblast growth factor
<b>FGFR</b>	Fibroblast growth factor receptor
<b>FHRRIKA</b>	Phenylalanine-histidine-arginine-isoleucine-lysine-lysine-alanine
<b>FMN</b>	Flavin mononucleotide
<b>GAP-43</b>	Growth associated proteins
<b>GDNF</b>	Glial cell line-derived neurotrophic factor
<b>GDP</b>	Guanosine-5'-diphosphate
<b>GEFs</b>	Guanosine exchange factors
<b>GFLs</b>	Glial-cell-line-derived neurotrophic factor family ligands
<b>GGF</b>	Glial growth factor
<b>GTP</b>	Guanosine-5'-triphosphate
<b>IKVAV</b>	Isoleucine-lysine-valine-alanine-valine
<b>IPTG</b>	Isopropyl $\beta$ -D-1-thiogalactopyranoside
<b>kDa</b>	KiloDalton
<b>L15</b>	Leibovitz's medium
<b>LB</b>	Luria-Bertani
<b>LCST</b>	Lower critical solution temperature
<b>LDVP</b>	Leucine-aspartic acid-valine-proline
<b>LMWC</b>	Low molecular weight chains
<b>LOV</b>	Light-Oxygen-Voltage-sensing
<b>MAPK</b>	Mitogen-activated protein kinases
<b>MLC</b>	Myosin light chain
<b>mm</b>	Millimetre
<b>MPa</b>	Megapascal
<b>MSCs</b>	Mesenchymal stem cells
<b>MW</b>	Molecular weight
<b>NCAMs</b>	Neural cell adhesion molecules

<b>Nde1</b>	NudE Neurodevelopment Protein 1
<b>NF200</b>	200-kilodalton subunits of neurofilaments
<b>NGF</b>	Nerve growth factor
<b>nm</b>	Nanometre
<b>NMR</b>	Nuclear magnetic resonance
<b>NSCs</b>	Neural stem cells
<b>NT3</b>	Neurotrophin 3
<b>NT4</b>	Neurotrophin 4
<b>NTA</b>	Nitrilotriacetic acid
<b>PBS</b>	Phosphate-buffered saline
<b>PC</b>	Polycarbonate
<b>PCL</b>	Polycaprolactone
<b>PDMS</b>	Polydimethylsiloxane
<b>PGA</b>	Poly glycolic acid
<b>PHSRN</b>	Proline-histidine-serine-arginine-asparagine
<b>PI3-K</b>	Phosphoinositide 3-kinase
<b>PLGA</b>	Poly(lactic-co-glycolic acid)
<b>PLL</b>	Poly-L-lysine
<b>PLLA</b>	Poly-l-lactic acid
<b>PLUNC</b>	Palate, lung and nasal epithelium clone protein
<b>PNIPAM</b>	Poly-N-isopropylacrylamide
<b>PNS</b>	Peripheral nervous system
<b>PPE</b>	Polyphenyl ether
<b>PPy</b>	Polypyrrole
<b>RAGs</b>	Regeneration associated genes
<b>RGD</b>	Arginine-glycine-aspartic acid
<b>Rho</b>	Ras homolog gene family
<b>RNA</b>	Ribonucleic acid
<b>ROCK</b>	Rho-associated protein kinase
<b>Rsn2</b>	Ranaspumin-2
<b>SDS-PAGE</b>	Sodium dodecyl sulfate polyacrylamide gel electrophoresis
<b>SOM</b>	Somatostatin
<b>SOX</b>	Sex determining region Y (SRY)- Box 11 transcription factor
<b>SP</b>	Substance P
<b>STAT-3</b>	Signal transducer and activator of transcription 3
<b>TCP</b>	Tissue culture plastic
<b>TH</b>	Tyrosine hydroxylase
<b>TNF<math>\alpha</math></b>	Tumour necrosis factor $\alpha$
<b>TrkA</b>	Tropomyosin receptor kinase A
<b>WCA</b>	Water Contact Angle
<b>XPS</b>	Xray photoelectron spectroscopy
<b>YIGSR</b>	Tyrosine-isoleucine-glycine-serine-arginine
<b><math>\mu</math>CP</b>	Microcontact printing
<b><math>\mu</math>l</b>	Microlitre
<b><math>\mu</math>m</b>	Micrometre

# **Chapter 1**

## **General introduction**

## Chapter 1

### **1.1 General introduction**

Nerve repair is still a major challenge in surgery. There is on-going effort to develop improved treatments for peripheral nerve repair. This thesis focuses on improving interfaces of polymers for nerve repair using isolated nerve cells as a means to assess the effectiveness of different interfaces. The work started off investigating the usefulness of a frog foam protein to coat biomaterials for enhanced compatibility, which went on to explore how surface topography and growth factors interact to affect regeneration, and an assessment of the effectiveness of specific adhesion peptide sequences on neural outgrowth. Thus the background to peripheral nerve histology, peripheral nerve injury, pathophysiological and the cellular and biomolecular aspects of nerve regeneration will be introduced in sequence. Followed by an overview of nerve regeneration challenges and the problems of existing conduits and what is necessary to come to a better solution using materials, surface modifications, topography, surface compatibility and growth factor strategies.

### **1.2 Peripheral nervous system (PNS)**

#### **1.2.1 The Neuron**

The main structural constituent of the nervous system is the neuron (figure 1). The prime function of neurons of the PNS is to connect the central nervous system (CNS) to limbs and organs. The PNS consists of two types of neurons; motor neurons that relay nerve impulses away from the CNS found in the spinal cord and sensory neurons that relay nerve impulses towards the CNS, which are located in the dorsal root.

## Chapter 1

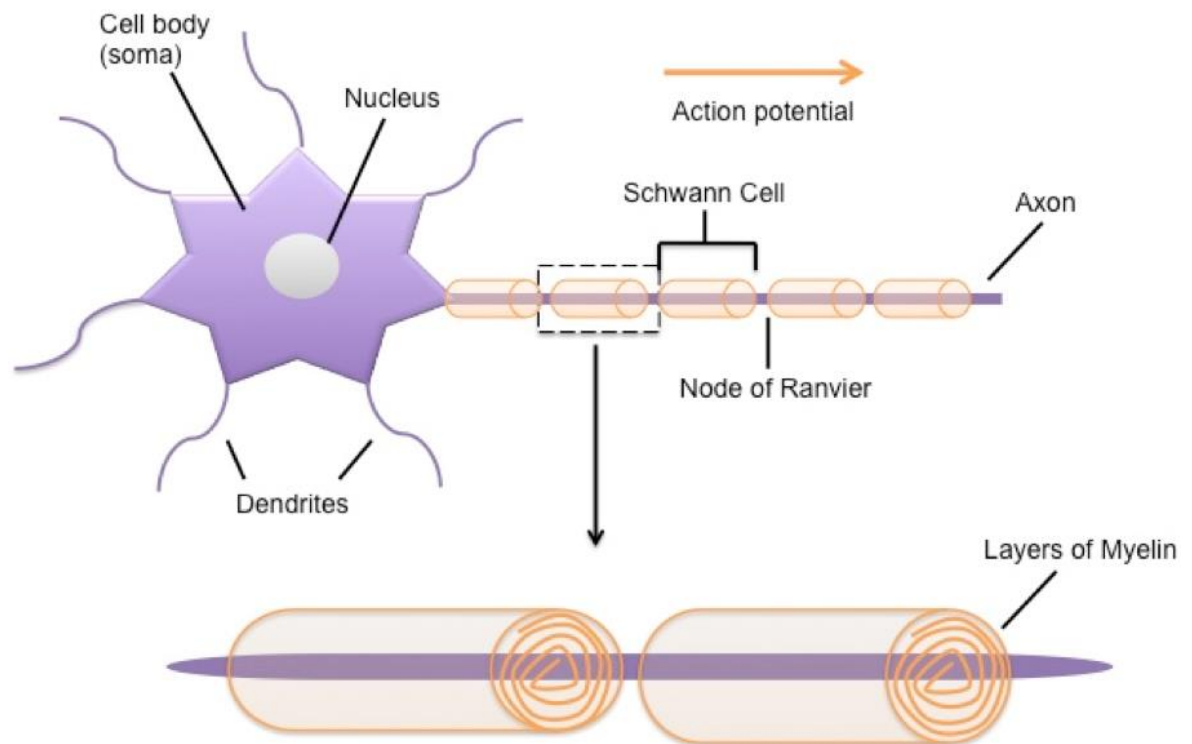


**Figure 1:** A schematic representation of a neuron. The cell body called the soma contains the nucleus; extending from the cell body are dendrites, which receive signals from other neurons and an axon that conveys the signals to its destination by an action potential (orange arrow). Schwann cells surround the axon in layers of myelin (a lipid-rich membrane) that supports the axon and enhances signal transduction. Gaps between the Schwann cells are known as nodes of Ranvier, which further enhance signalling by a process known as saltatory conduction.

All neurons have a cell body (soma); this contains the nucleus, where the synthesis of neural proteins and membranes takes place. Also found in the soma are Nissl bodies which are granules of rough endoplasmic reticulum. Extending from the cell body are the dendrites, which are specialised to receive afferent nerve input from the axons of other neurons (Hakim, 1999). Also extending from the cell body is the axon its role is to conduct an electrical signal known as an action potential, propagating signals to other neurons and, target tissues and organs. Supporting the axons are Schwann cells, which can wrap the axon in their myelin sheath speeding up action potential transmission (figure 1). The action potential originates at the axon hillock -, the junction of the axon and cell body. When a neuron is in the resting state, the electrical potential across the axonal membrane is approx. -70 mV. At the peak of an action potential, the membrane potential can be as much as +40 mV. Myelination of the axon allows the action potential to take place at the node of Ranvier, which is where two

## Chapter 1

adjacent segments of myelin on one axon are separated (Quarles *et al.*, 2006), allowing the impulse to jump from node to node, speeding up the process, this form of impulse propagation is called saltatory conduction (Quarles *et al.*, 2006). Neurons make contact with other cells or target tissues at a junction called a synapse, where neurotransmitters are released to transmit chemical signals, or are directly coupled via electrochemical synapses (Akins and Biederer, 2006).

### 1.2.2 Peripheral nerves

Three connective tissue layers are associated with peripheral nerves; these are the epineurium, perineurium and endoneurium (figure 2). Individual axons are in close contact with Schwann cells, which either myelinate axons of large calibre ( $> 2\mu\text{m}$ ) on a one-to-one basis, or wrap groups of small ( $< 2\mu\text{m}$ ) unmyelinated axons in pockets of cytoplasm (Hall, 2005). Assisting the Schwann cells is the endoneurium, which separates the axons from one another by surrounding each one individually thereby ensuring the signal is projected to the correct destination along one axon. In a peripheral nerve, bundles of axons are grouped together into fascicles (figure 2) by a dense connective tissue called the perineurium, a multi-layered structure composed of flattened polygonal cells interspersed with layers of collagen fibrils (Gamble and Eames, 1964, Sunderland and Bradley, 1961, Tillett *et al.*, 2004). Enclosing the entire peripheral nerve is the outer connective tissue layer, the epineurium. It contains longitudinal collagen fibrils, elastic fibres and adipose tissue (Tillett *et al.*, 2004).

## Chapter 1

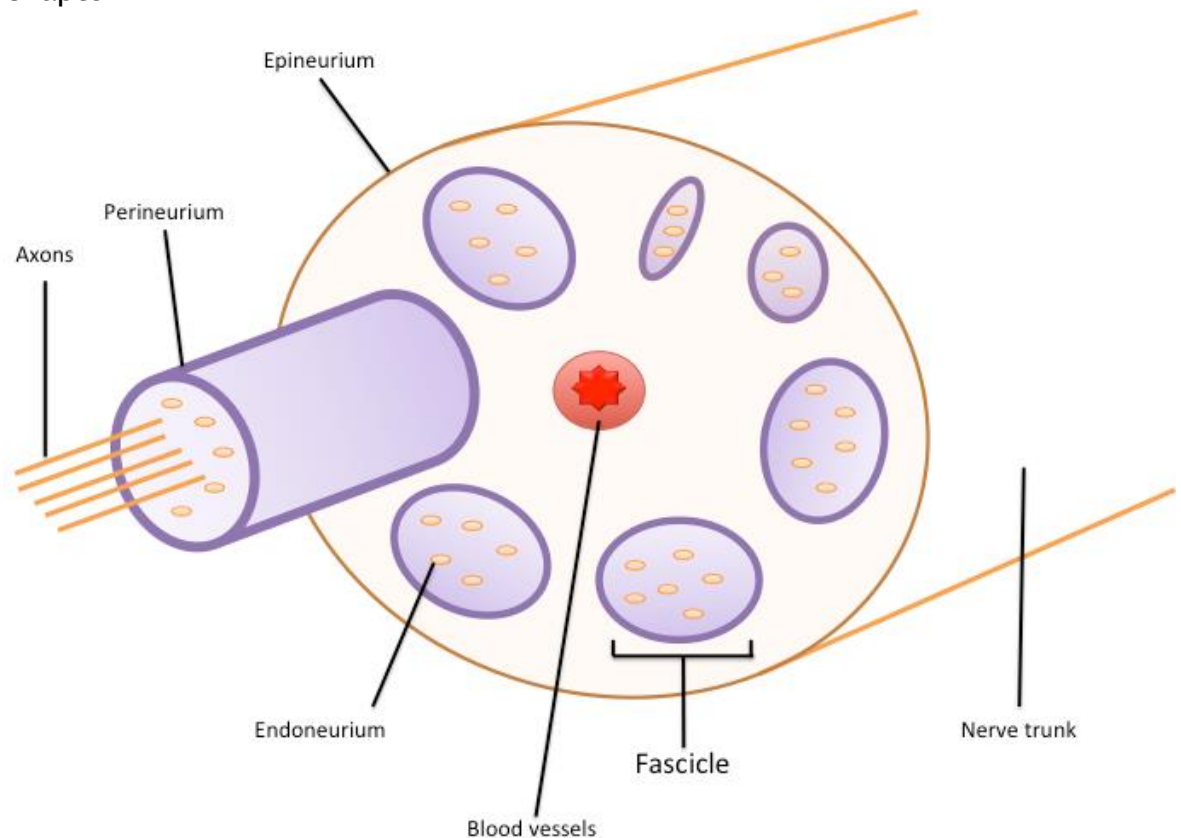


**Figure 2: A schematic representation of a peripheral nerve. Axons are grouped together into fascicles that are surrounded by connective tissue, the endoneurium and blood vessels. This is all bound together by the perineurium and all these structures are held together by another connective tissue layer the epineurium. Adapted from (Evans, 2001).**

### 1.2.3 Peripheral nerve injury

Peripheral nerve injuries are serious health problems that can lead to loss of sensation and mobility, as the resulting loss of innervation impairs voluntary muscle movements and normal sensation. In Europe more than 300 000 cases of peripheral nerve injuries occur annually and in the United States, 360 000 people suffer from upper extremity paralytic syndromes on an annual basis (Ciardelli and Chiono, 2006). The most widely used systems to compare and determine the extent of injury are the two scales developed by Seddon (Seddon, 1942) and Sunderland (Sunderland, 1969)

Seddon classified nerve injuries as neurapraxia, axonotmesis and neurotmesis (figure 3). Neurapraxia is the mildest nerve injury where full recovery is achieved in days-weeks without any surgery, as all the supportive structures (endoneurium, perineurium, epineurium) remain intact. However there can be

## Chapter 1

disruption of conduction (electrical and chemical) due to myelin sheath damage known as segmental demyelination (Campbell, 2008). Axonotmesis is where the axon is damaged with the endoneurial connective tissue still intact; this provides a guide for axonal regeneration. Finally a neurotmesis injury is where the nerve is completely disturbed, with surgery being the only possible solution for regeneration.

In comparison to the Seddon classification system, the Sunderland classification system is divided into five classes. The first, second and fifth groups correspond with Seddon's classifications, while the third and fourth degrees are additional subclasses of axonotmesis. In a grade 3 injury, there is axonotmesis but also endoneurial discontinuity, while the perineurium is preserved. The endoneurial disruption inhibits regeneration, the scaffolding created by the Schwann cell tubes is distorted and the environment is less receptive to regenerating axons, which tends to decrease successful regeneration (Campbell, 2008). In grade 4 injuries, the perineurium is also disrupted which means there is little recovery without surgery.

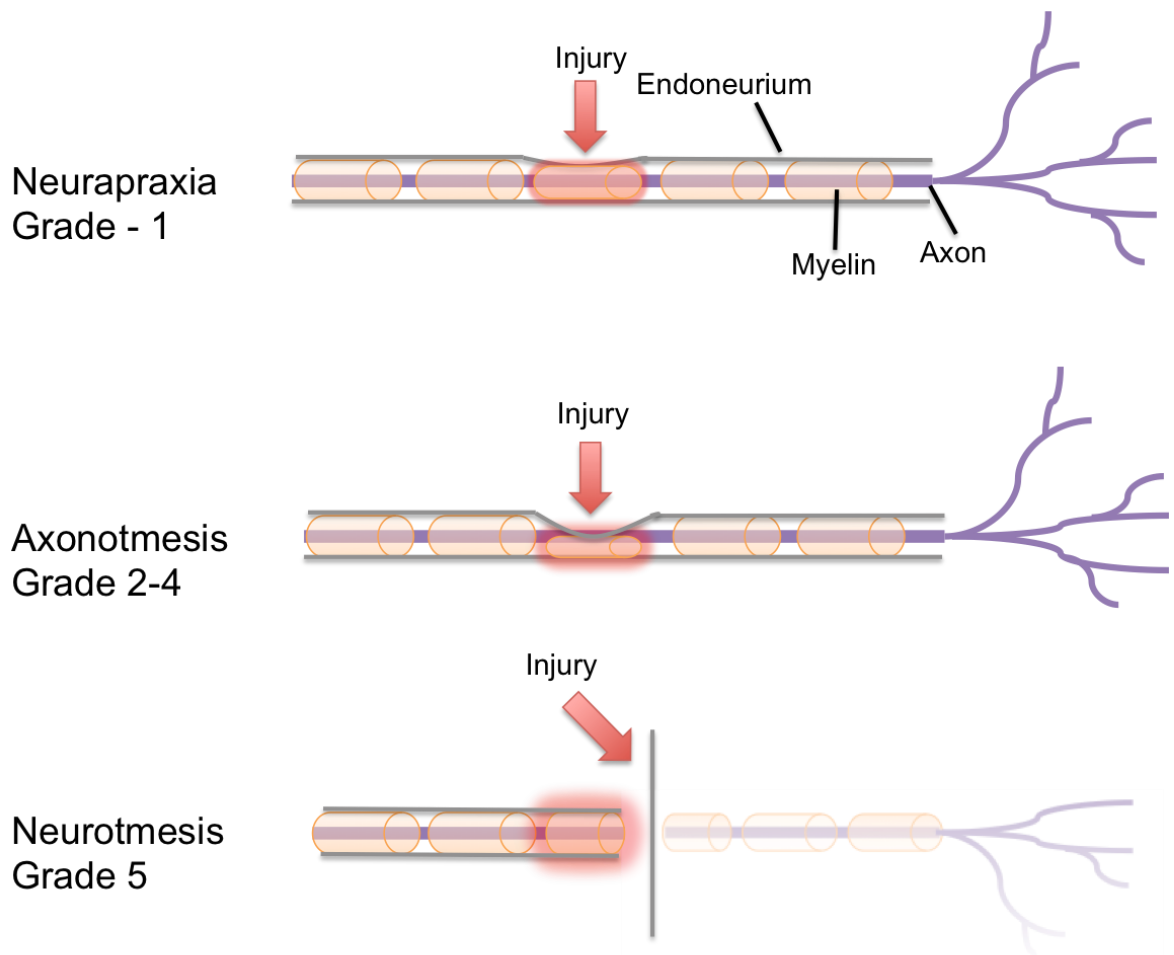


**Figure 3: Schematic representation of peripheral nerve injuries as classified by Seddon and Sunderland. In neurapraxia all the connective structures are intact and full recovery is achieved without any surgery. In axonotmesis (grade 2) the axons are disturbed and Wallerian degeneration (detailed in section 1.2.4) takes place; recovery is achieved by axonal regeneration. Axonotmesis (grade 3) the endoneurium is also disturbed leading to incomplete and misdirected axonal regeneration. Axonotmesis (grade 4) is same as grade 3, with the perineurium also being disturbed – little recovery without surgery. Neurotmesis is the total disruption of the nerve with no recovery without surgery.**

### 1.2.4 Wallerian degeneration

Unlike the CNS, the PNS has a remarkable ability to regenerate. The time and success of the peripheral nerve repair process depends on the extent of injury. As a consequence of loss of target, 30-40% of small diameter sensory neurons that contribute to a dorsal root ganglion apoptose after nerve transection (Hall, 2005, Fu and Gordon, 1997, Ygge, 1989). Neurons that survive begin to express genes to compensate for the loss of target-derived neurotrophic factors in order to regrow their axons across the site of the injury and back to the periphery (Xiao *et al.*, 2002, Rosen and Lundborg, 2004). First-degree injuries have little pathological changes and no true degeneration or regeneration occurs. However in second degree injuries or Axonotmesis, distal to the injury site, a process known as Wallerian degeneration (figure 4) takes place (Waller, 1850) where the primary histological change involves physical fragmentation of both axons and myelin (Burnett and Zager, 2004). While the axons distal to the injury are undergoing Wallerian degeneration, axons of the proximal nerve stump undergo “die back” to the first node of Ranvier (Fu and Gordon, 1997). The cell body of axotomized PNS neurons undergoes characteristic morphological changes that are collectively referred to as “chromatolysis”. This is where the nissl bodies found in the cell soma begin to break up and the nucleus enlarges moving away from the centre of the cell body.

After physical interruption, the ends of the severed axons are sealed; this leads to swelling of the axon as they fill with organelles that are unable to progress beyond the site of the lesion (Hall, 2005). The degeneration process is dependent on an increase in calcium that activates calcium-dependent proteolytic enzymes. Calcium-dependant ubiquitin and calpain-proteases are responsible for the degradation of the endoplasmic reticulum, mitochondria, cytoskeletal elements of the axon and neurofilaments (Allodi *et al.*, 2012, George *et al.*, 1995). Schwann cells detach from the dying axons and become activated after 24 hours of injury by exhibiting nuclear and cytoplasmic enlargement (Burnett and Zager, 2004) as well as an increased mitotic rate and react by stopping myelin production from taking place. This is associated with a down regulation of genes that transcribe proteins linked to myelin and begin to express regeneration-associated genes (RAGs) (Fenrich and Gordon, 2004).

## Chapter 1

Schwann cells begin to remove the degenerated axonal- and myelin-debris before macrophages take over. Macrophages play an essential role both in the phagocytosis of myelin following nerve injury and in the change in the functional state of the Schwann cells (Bruck, 1997). Macrophages are recruited by chemoattractive factors, including cytokines such as interleukin - 1 $\beta$  leukaemia inhibitory factor (1 $\beta$ -LIF) and tumor necrosis factor (TNF-  $\alpha$ ) secreted by Schwann cells. The dedifferentiated Schwann cells scavenge myelin debris, proliferate and form so called bands of Bungner, which are strings of linked Schwann cells. These bands of Schwann cells guide and support the axons that regenerate from the proximal nerve stump into and through the endoneurial tubes of the distal nerve stumps (Liu *et al.*, 1995). The process of Wallerian degeneration begins within a few hours of injury and is completed by 6-8 weeks, leaving a distal stump comprising only endoneurial tubes lined by Schwann cells (Kang *et al.*, 2003).

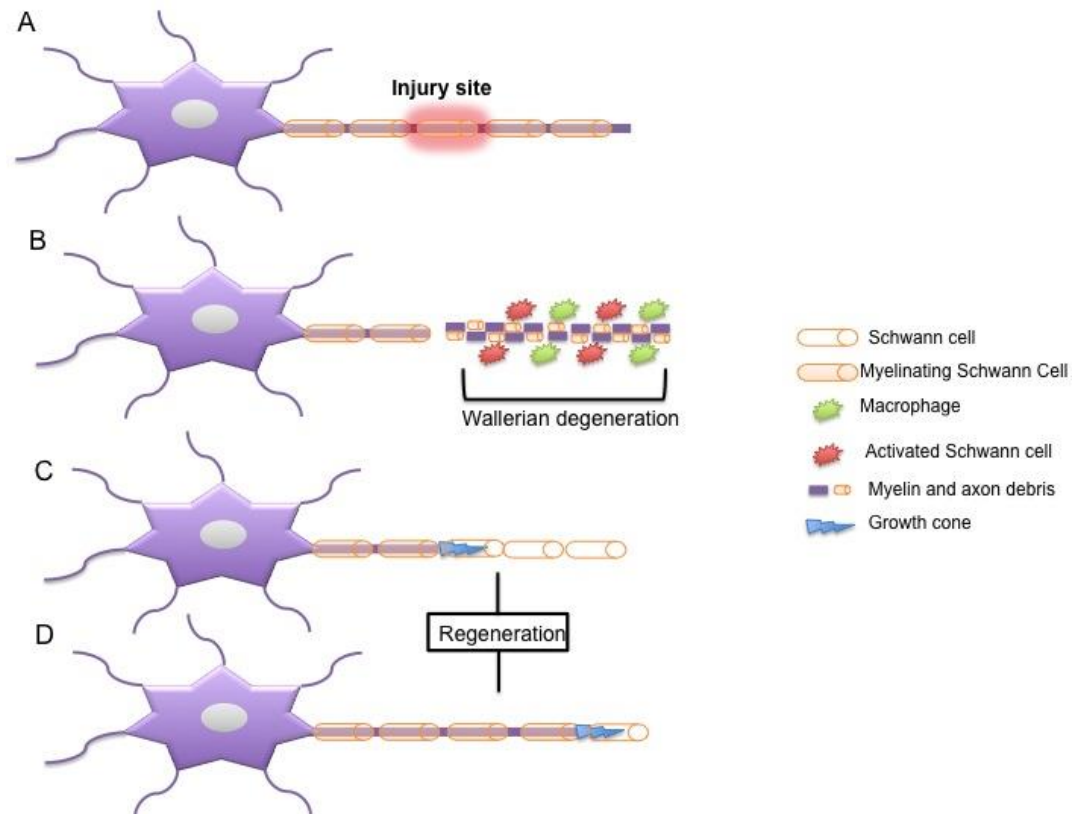


**Figure 4: Mechanism of Wallerian degeneration. At the site of nerve injury (A) a process known as Wallerian degeneration occurs (B) Schwann cells at the distal part of the nerve, stop making myelin and are fragmented with their myelin sheaths along with the axon by macrophages and activated Schwann cells. Schwann cells then migrate to the site of injury and bridge the gap by forming bands of Bungner (C). Within 24 hours the axons start to regenerate and bridge the injury site at a rate of 0.25 to 1 mm a day – the leading segment of the axon is termed the growth cone (D) Myelin is formed around the axon as it regenerates – axons continue to regrow until the target is reached. Adapted from (Allodi et al., 2012).**

### 1.2.5 Neural regenerative response

The affected neuron attempts to regenerate its axon soon after injury (Thomas, 1989). In adults the growth capacity of a neuron is repressed to allow proper synaptic development but post-injury neurons switch back to their embryonic growth state (Allodi *et al.*, 2012). When an injury occurs changes in the gene expression switch the neuron from a “transmission” state to a growth or regenerative state. The axotomy-associated change in the gene expression encodes for transcription factors, which in turn regulate the expression of genes involved in cell survival and neurite outgrowth (Herdegen *et al.*, 1991, Allodi *et al.*, 2012, Navarro *et al.*, 2007). The first warning signal sent to the soma, that marks the beginning of the regenerative process, is the calcium-induced burst of action potentials emanating from the injury site. This elevates intracellular calcium and cyclic adenosine monophosphate (cAMP) that in turn triggers chromatolytic changes in the cell body (Mandolesi *et al.*, 2004). Additional signals are sent to the soma informing it of the disconnection; these signals can be negative or positive. The main negative signal is the decrease in nerve growth factor (NGF) levels due to disruption of the retrograde transport system caused by the injury; this informs the neuron that the axon has been disconnected from its target (NGF biology discussed in detail in section 1.3.4). Positive injury signals are sent to the soma by the release of ciliary neurotrophic factor (CNTF), neurotrophin 3 (NT3) and fibroblast growth factor (FGF), are released from the Schwann cells to support the neuron in recovery. An example of how the growth factor CNTF supports the neuron is by making contact with the tip of the injured axons and promoting phosphorylation of signal transducer and activator of transcription (STAT3) (Kirsch *et al.*, 2003).

Activated proteins termed “positive injury signals”, are endogenous axoplasmic proteins that undergo post-translational modifications at the lesion site upon axotomy (Allodi *et al.*, 2012). The carrier proteins vimentin and importins are synthesised and interact with the motor protein dynein (Hanz *et al.*, 2003), and allow retrograde transport of phosphorylated Mitogen-activated protein kinases (MAPK) and STAT3, that in turn activates mitogen associated kinase cascades such as MAPK, protein kinase B known as Akt and p38 which assist in triggering neurite outgrowth (Lindwall and Kanje, 2005) and early signalling responses (Michaevlevski *et al.*, 2010). Nuclear localization and phosphorylation of

## Chapter 1

transcription factors such as c-Jun, JunD, activating transcription factor (ATF3), sex determining region Y (SRY)-Box 11 (Sox11) and STAT3 lead to a change in gene expression, in turn up regulating RAGs which include genes that transcribe cytoskeletal proteins such as tubulin and actin as well as the growth associated protein 43 (GAP-43) and cytoskeleton-associated protein 23 (CAP-23), as they are all required for mediating growth cone elongation (Fenrich and Gordon, 2004, Strittmatter *et al.*, 1994)(summarised in figure 5).

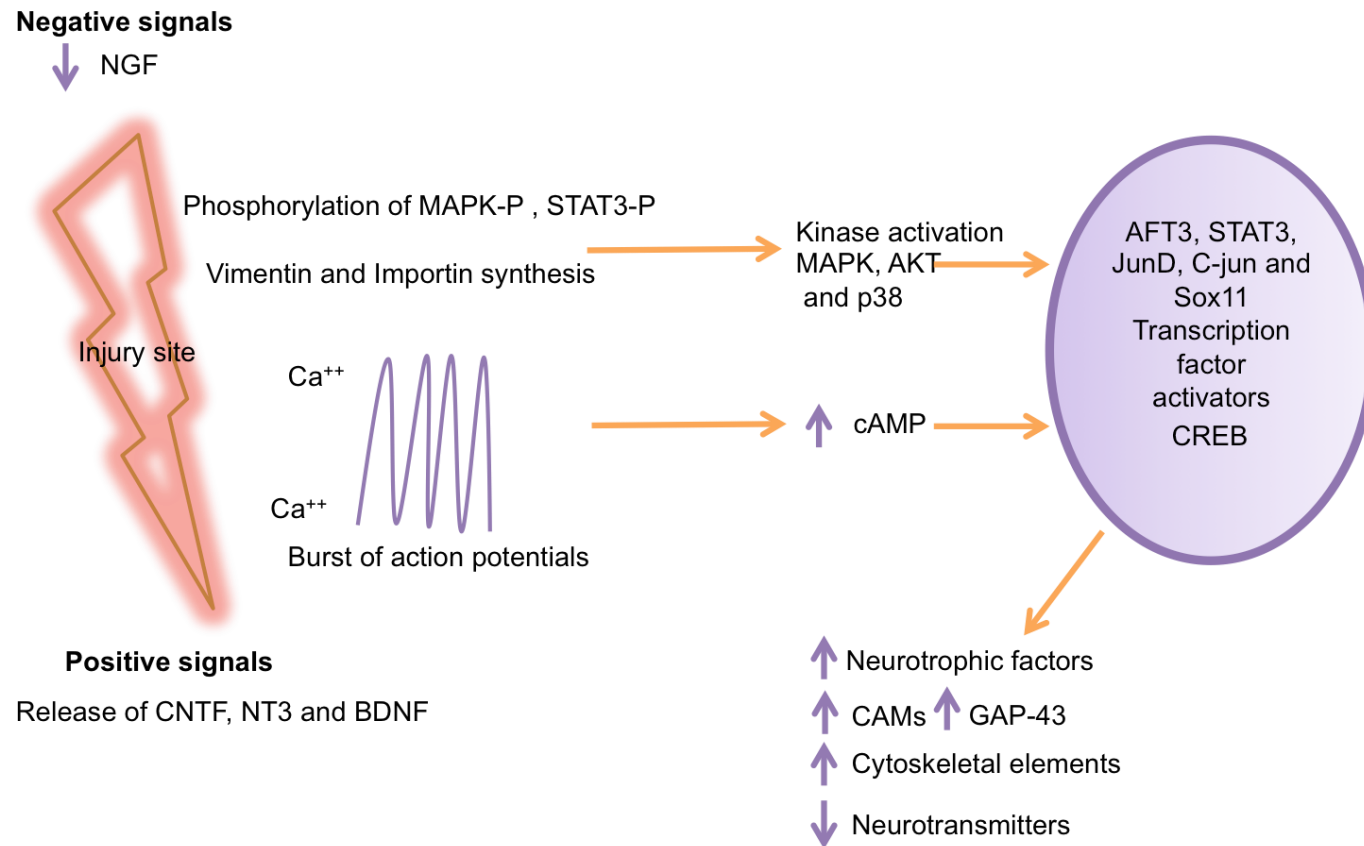


**Figure 5: Signaling in peripheral nerve injury.** Upon injury, signals from the injury site are sent to the soma informing it of the disconnection which in turn results in activation of transcription factors responsible for the regenerative state. The main changes that occur is a burst of action potentials, interruption of the trophic molecules retrograde transport system, and the transfer of phosphorylated proteins like MAP2 which is one of the positive signals that is generated. All these contribute to the activation of RAGs which induce production of GAP-43 and neurotrophic factors. Adapted from (Allodi et al., 2012).

## Chapter 1

### 1.2.6 Growth cone and elongation

Growth cones are finger-like extensions, with filopodia that explore and sample the environment, and act as long distance sensors at the tips of axons (Kater and Rehder, 1995). Within hours after injury, the process leading to growth cone formation begins and sprouts begin to form from the axons. In a process called chemotaxis, the tip is guided to move forward by neurotrophic factors such as NGF, Glial cell line-derived neurotrophic factor (GDNF), Brain-derived neurotrophic factor (BDNF) and NT3, are produced by non-neural cells as well as neurotropic factors such as laminin, fibronectin and collagen IV, which lay down a gradient for the advancing tip. Each regenerating axon may give rise to over 10 axonal sprouts but the number of branches decreases with time in the distal segments as sprouts that do not make peripheral connections undergo atrophy and eventually disappear (Allodi *et al.*, 2012). To reach target organs the axon survives by maturing and enlarging in size. Growth cones are controlled by mechanisms that help it navigate its way following signals that determine how it advances, turns and branches: these are contact-mediated attraction, chemoattraction, contact-mediated repulsion and chemorepulsion. These mechanisms seem to act simultaneously and in a coordinated manner to direct path finding (Goodman, 1996). To reach complete regeneration the growth cone must elongate following the endoneurial tubes of the distal nerve to reach their target organ. If the gap is too big and the growth cone is not able to find its way to the distal nerve stump, a neuroma is formed. In a neuroma the nerve tries to regrow, but fibrous scar tissue prevents it from growing uniformly and instead a tangled, painful mass in the scar tissue is formed. As well as playing an important role in helping to guide the axons after injury, the growth cone is also heavily involved in responding to topography, as extracellular topography controls the direction of leading axons (Hoffman-Kim *et al.*, 2010).

Positive signalling by neurotrophic factors and proteins like Gap-43 are important for the regulation of the growth cone during development and regeneration, the growth cone also receives signals that disrupt the extracellular cues that the regenerating axon encounters. Such signals inhibit the assembly of actin, resulting in growth cone collapse forcing the microtubules to retract. ROCK, has been shown to modulate growth cone stability by regulation of actin dynamics (Tonges *et al.*, 2011). The small G protein Rho which has been

## Chapter 1

identified as a main binding partner of ROCK (Ishizaki *et al.*, 1996), is one of the proteins that is responsible for causing repulsive guidance signal into the growth cone cytoskeleton reorganization leading to repulsive turning (Patel and Van Vactor, 2002).

### **1.2.7 The cytoskeleton and the ECM**

The cytoskeleton of a cell provides structure and organization. Typically the three main components that make up the cytoskeleton of a cell are actin filaments, microtubules and intermediate filaments (Fletcher and Mullins, 2010). These three components combined control the shape and the mechanics of the cell in responding both to positive and negative signals. As detailed above, the regenerating axon is lead by the growth cone (detailed in section 1.2.6), and in turn its mobility is dependent on receptors that receive guidance cues from the local environment (Campbell, 2008). The cytoskeleton of the growth cone is composed of microtubules and actin filaments (green and red respectively in figure 6a), which control its directionality and movement by forming sheet-like dendritic actin filament networks and parallel actin-filament filopodia at the leading edge (Fletcher and Mullins, 2010). The cytoskeleton of the axon itself is composed of flexible, but strain-resistant neurofilaments that form a structural matrix with embedded microtubules.

## Chapter 1

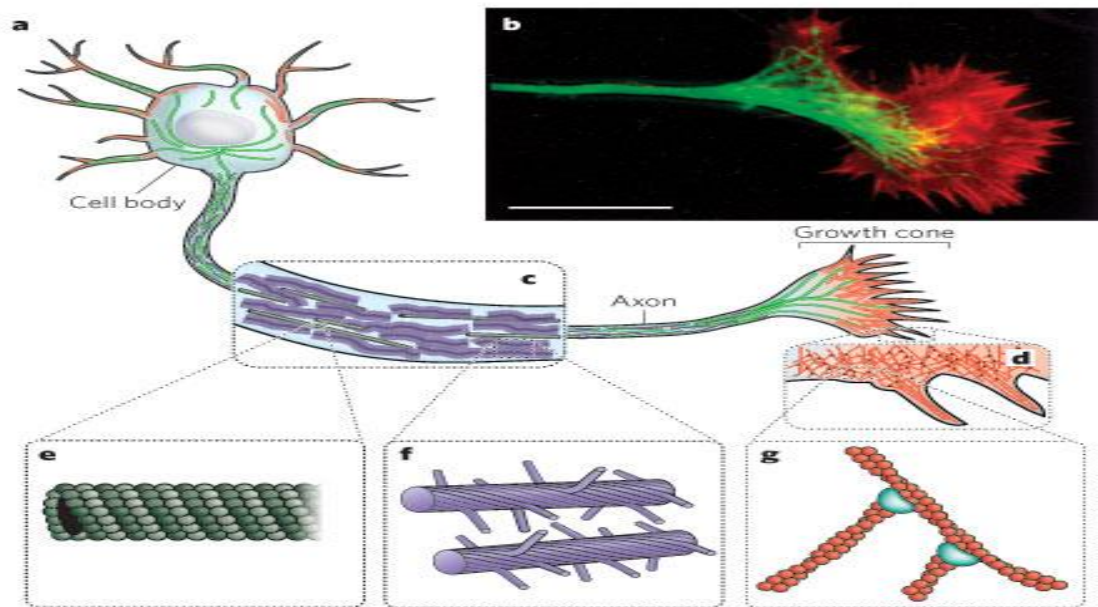


**Figure 6: Cytoskeleton composition of an axon.** A schematic representation of an axon is shown with a cell body (a), and an axon and growth cone (b). Diagrams e, f and g are schematic representation of the 3 components of the cytoskeleton microtubules, neurofilaments and actin filaments respectively. From (Fletcher and Mullins, 2010) with permission.

The ECM is composed of a mixture of glycoproteins and proteoglycans that provide the cell with external structural functions and support. In the nervous system, ECM molecules are synthesized and secreted by neurons and supporting cells into the interstitial spaces surrounding developing neurons (Myers *et al.*, 2011). The growth cone, the leading section of the axon, as described above can respond to both stimulating and inhibiting cues provided by different ECM molecules, and dependant on the neurons status (“transmission” vs. “repair/growth”). An example of proteoglycans found in the peripheral nerve that can cause inhibition are chondroitin sulphate proteoglycans (CSPG) which do so by interfering with integrin signalling (detailed in 1.1.8) (Zuo *et al.*, 1998).

Playing a major role in enhancing the regeneration process are three glycoproteins: collagen, laminin and fibronectin.

Collagens are trimeric molecules formed by three  $\alpha$  chains with 28 varying isoforms subclassed into three groups; fibrillar-forming, fibrillar-associated and non fibrillar (Kalluri, 2003). These proteins not only play an important role in the ECM of most tissues, but also are also involved in the development of the

## Chapter 1

nervous system (Fox, 2008, Hubert *et al.*, 2009). Collagens have been shown to be important in neural cell migration, neurite adhesion and outgrowth (Bradshaw *et al.*, 1995). A study by Fox *et al.*, (2008) highlights the important role of collagen in regulating axon path finding and maintenance of synaptic connection, where zebrafish motor axon growth failed to extend without the presence of collagen.

The second class of important/relevant ECM proteins are the fibronectins. Fibronectins are dimers formed by two almost identical monomers, with 20 alternative spliced isomers (Leiss *et al.*, 2008). Fibronectins have an integrin binding domain arginine-glycine-aspartic acid (RGD), which is located near the middle of the molecule. The function it carries out in neural development and regeneration is to mediate cell adhesion (Muller *et al.*, 1995), to stimulate migration (Stettler and Galileo, 2004), and axon outgrowth (Humphries *et al.*, 1988, Hikita *et al.*, 2003), as well as neural differentiation (Tate *et al.*, 2004).

The third type of ECM molecules important for regeneration are Laminins, which are heterotrimeric glycoproteins consisting of  $\alpha$ ,  $\beta$  and  $\gamma$  subunits, the  $\alpha\beta\gamma$  subunits can assemble differently and form up to 15 subtypes each with a specific function and time and tissue dependant distribution (Aumailley *et al.*, 2005). The laminins are important as they carry out critical and diverse functions within the nervous system. These include promoting cell adhesion (Lallier and Bronner-Fraser, 1993), stimulating migration (Anton *et al.*, 1999), neurite control and guidance during outgrowth (Rivas *et al.*, 1992, Gupton and Gertler, 2010), assisting in growth cone guidance (McKerracher *et al.*, 1996), as well as path finding and synapse formation, and most importantly in the regeneration process after injury (Luckenbill-Edds, 1997).

The multi domain structure of laminin means that specific domains are associated with distinct functions such as cell attachment, promotion of neurite outgrowth, and binding to other glycoproteins (Luckenbill-Edds, 1997). In particular two peptide sequences of laminin have been shown to have specific biological activity related to neuronal regeneration and differentiation, these are IKVAV and tyrosine-isoleucine-glycine-serine-arginine (YIGSR). Tashiro *et al.*, (1989) highlights the use of the IKVAV sequence (in the form of a synthetic peptide) as a means to mediate cell attachment, migration and neurite outgrowth. As described above, collagen and fibronectin are both promoters of

## Chapter 1

neurite outgrowth but the most rapid and extensive process formation is observed with laminin (Kleinman *et al.*, 1990) with cell sensitivity being much higher on laminin, as picomolar amounts of laminin can still promote outgrowth.

### 1.2.8 Cell adhesion molecules (CAMs)

Both the ECM and CAMs play a crucial role in guiding and supporting axonal regeneration. In particular CAMs are very important in regeneration as they translate attraction/repulsion cues aimed at the tip of the re-growing axon into appropriate intracellular signalling (Allodi *et al.*, 2012). There are three main families of CAMs that are found in the nervous system: cadherins, neural CAMs (NCAMs), and integrins.

The cadherins are transmembrane proteins. Their extracellular domain contains repetitive subdomains called cadherin repeats, which contain sequences that are involved in calcium binding (Shapiro *et al.*, 1995) and mediate cell-cell adhesions. N-cadherin, a subtype of this group has been shown to be an important mediator in axon outgrowth, fasciculation and synapse formation (Ranscht, 2000, Takeichi, 2007). The second relevant family, the NCAMs are responsible for axon path finding and target recognition. They achieve this by two main pathways: Fibroblast growth factor receptor (FGFR) phosphorylation and Fyn association (Allodi *et al.*, 2012). Integrins are a family of heterodimeric receptors, composed of an  $\alpha$  and  $\beta$  subunit, initially characterized for their role in anchoring cells to the ECM (Hynes, 1996). The family has 18  $\alpha$  and 8  $\beta$  subunits that combine to form 24 different integrin complexes. The integrin subunits are more or less ligand-specific, with different ECM molecules being bound and recognised by different combinations of subunits. Integrins are activated upon extracellular ligand engagement and clustering (Myers *et al.*, 2011). This process involves integrins associating intracellularly with adapter proteins that connect the integrin to the cytoskeleton. Upon attachment to the ECM, clustering occurs at the cell membrane and associate with a cytoskeletal and signalling complex that in turn promotes the assembly of actin filaments (Giancotti and Ruoslahti, 2006). Integrin-mediated interactions activate several cytoplasmic protein kinases, in particular focal adhesion kinase (FAK) and the Src family kinases (Giancotti and Ruoslahti, 2006). FAK and Src signalling also modulate cell adhesion assembly and turnover, as well as regulation of the actin

## Chapter 1

cytoskeleton (Myers *et al.*, 2011). These proteins are recruited to the site of integrin-mediated cellular attachment along with the structural proteins paxillin, talin and vinculin (Tucker *et al.*, 2005) (figure 7). The interaction of the integrins with the cytoplasmic kinases and in combination with structural proteins, leads to the formation of focal adhesions that in turn can lead to changes in cell morphology. Integrins play a big role in the peripheral nervous system as many of the laminin isoforms are recognised by the integrins. Their main role is in the involvement of focal adhesion formation (cell to basal lamina interactions) (Allodi *et al.*, 2012). By direct binding to paxillin, integrins serve to transduce signals from the ECM matrix as well as from growth factors, to the organisation of the actin cytoskeleton (Snider *et al.*, 2002). Most importantly, neurons after injury overexpress 4 different subunits of integrins  $\alpha 4\beta 1$ ,  $\alpha 5\beta 1$ ,  $\alpha 6\beta 1$  and  $\alpha 7\beta 1$  that are known to promote nerve regeneration (Kloss *et al.*, 1999, Wallquist *et al.*, 2004), and specifically recognise and bind laminin-2 and -8 in peripheral nerves (Wallquist *et al.*, 2004). A study by Werner *et al.*, (2000) showed that deletion of the integrin subunit  $\alpha 7$  slows down the speed of motor axon regeneration. Another important role of the integrins is their function in growth cone formation by the assembly of dynamic adhesion complexes on ECM substrata - which is regulated not only by ligand binding but also appears to be regulated by receptor trafficking (Ezratty *et al.*, 2009).

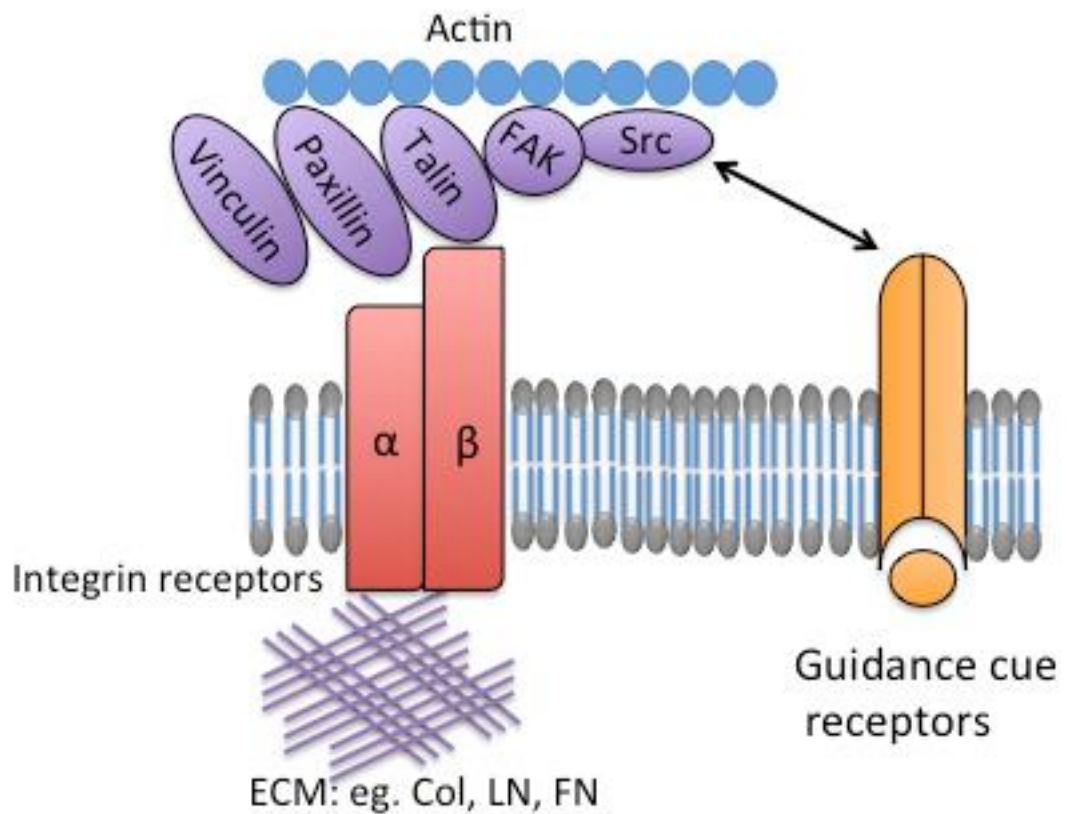


**Figure 7:** A schematic representation of focal adhesion formation of a growth cone. In red are the integrin  $\alpha\beta$  heterodimeric receptors that bind to proteins within the ECM, such as collagen (col), laminin (LN) and fibronectin (FN). In purple are the scaffolding proteins talin, paxillin and vinculin that bind to the cytoplasmic tail of the integrins linked to actin filaments (blue). Focal adhesion kinase and Src are activated by clustering of integrin receptors (orange) and modulate adhesions through phosphorylation of key residues that allow binding of many additional proteins. Adapted from Myres et al (Myers et al., 2011).

## Chapter 1

**1.2.9 Experimental model *in vitro*: DRGs**

The experimental model that is used in this work is an organotypic culture of DRGs. Each DRG contains approximately 10,000 pseudo-unipolar sensory afferent neurons with their associated support cells and are located near the entrance of dorsal roots into the spinal cord (Hanani, 2005). They are the most widely used neuronal populations to investigate and gain an understanding of regenerative interactions in the PNS. DRG neurons mount a robust regeneration response after injury that can result in functional recovery (Snider *et al.*, 2002). Both explants of DRGs with nerve stumps attached, and dissociated DRG neurons are used to gain an understanding of how the parameters being investigated influence the outgrowth response on the cells. When DRG explants are used the relationships between neurons, satellite cells and Schwann cells is preserved; this is also a good model as it is closely representative to that which occurs in a natural environment (Tonge *et al.*, 1997). Dissociating the DRG is advantageous for the fine analysis of the morphology and the behaviour of individual neurons (Lindsay, 1988). Another advantage of using DRGs is that they can be readily cultured from rat pups allowing a suitable model for *in vitro* regeneration studies. Instead of doing *in vivo* experiments, which are costly and cause pain to the animal, this model reduces animal use as ~20 DRGs can be extracted per pup.

### 1.3 Nerve regeneration

Nerve autografts are still considered to be the gold standard for bridging nerve gaps and have been for the past 50 years (Lee and Wolfe, 2000). Autografts offer optimal results in nerve regeneration as they are more biocompatible than artificial materials, less toxic, will not elicit an immune response, and provide a support structure to promote cell adhesion and migration (Evans, 2001).

However, with any technique there are always limitations, and for autografts it is that only 50% of surgeries are successful due to a great potential of size mismatch, which limits the regeneration process (Bellamkonda, 2006). Moreover, the possibility of painful neuroma formation and scarring are also drawbacks of this technique (Daly *et al.*, 2012), and the use of autografts is limited to a transfer of 5 cm (typically of the sural nerve).

Research into aids for peripheral nerve research so far has been targeted towards the development of artificial or engineered nerve guidance channels, which aim to enhance regeneration across nerve gaps as a promising alternative to autografts. In general the advantages that these hold over the standard method is that they limit scar formation, can provide sufficient mechanical properties for structural support, and exhibit a low immune response and biodegradability, which removes the need for secondary surgery (Daly *et al.*, 2012). The food and drug association (FDA) has approved several devices based on both natural and synthetic biomaterials to repair nerve defects (Kehoe *et al.*, 2012). Current research is focused on functionalizing the conduit, aiming to improve the outcome. The 4 essential components of which have been highly researched with the aim of getting to a better solution to enhance the clinical outcome of conduits are: choice of growth permissive substrates (biomaterial, hydrogels, extracellular matrix proteins or peptides), surface modifications (nano/micro topography), trophic factors (NGF, BDNF) and glial cells or other support cells (Bellamkonda, 2006).

## Chapter 1

### 1.3.1 Nerve conduits – Biomaterials

Non-biodegradable materials such as silicone (Chen *et al.*, 2000), acrylic polymers (Scaravilli, 1984), polyethylene (Cordeiro *et al.*, 1989) and elastomeric hydrogels (Keeley *et al.*, 1991) were used for PNS research, and although these studies have shown axonal regeneration, their suitability long term, is questionable as their inflexibility makes their use complicated in larger nerve gaps. The incorporation of natural polymers with silicone for instance laminin and collagen, enhanced the regeneration of a 6 mm mouse sciatic nerve (Labrador *et al.*, 1998). Other natural polymers, which have been used for their desirable properties are gelatin (Liu *et al.*, 2004) and chitosan (Itoh *et al.*, 2003).

With growing understanding of the optimal characteristics of a conduit, research is focusing on employing biomaterials that are biocompatible thus provoking no inflammatory response, biodegradable materials, which degrade within a reasonable period and only show mild foreign body reactions (Ciardelli and Chiono, 2006), and to maintain a mechanically stable architecture during the regeneration process. Permeability of the material is also important therefore it is desirable to have a permeable biomaterial to allow the diffusion/influx of oxygen and nutrients from interstitial fluid to the surviving nerve tissue through pores in the conduit wall (Kokai *et al.*, 2009). Polymers that belong to the polyester group, such as polycaprolactone (PCL) (Bender *et al.*, 2004, Kokai *et al.*, 2010), poly-L-lactic acid (PLLA) (Yang *et al.*, 2004, Lu *et al.*, 2009) and polyglycolic acid (PGA) (Nakamura *et al.*, 2004) have all gained considerable interest in this particular research field as they are biodegradable and, degrade via the hydrolysis of ester bonds along the polymer backbone (Ciardelli and Chiono, 2006), releasing water, lactic, glycolic and carbonic acid which can be broken down by the body.

In addition to the use of a single material, the blending of synthetic and natural polymers is a well-established strategy for the improvement of biocompatibility and the biodegradability of synthetic polymers (Chiono *et al.*, 2008). Bender *et al.*, (2004) utilized porous collagen-based beads (CultiSphers) with PCL. The incorporation of the collagenous beads resulted in enhanced cortical neuron adhesion, viability, and neurite extension as compared to PCL alone.

## Chapter 1

Finally electrically conductive polymers have also been evaluated for their use to enhance nerve regeneration. Conductive polypyrrole (PPy) has been used to enhance restoration of lost nerve function for its desirable properties such as controllable charge density, erodability, and wettability. Conductive polymer nerve guides placed in transected rat sciatic nerves have been shown to support nerve regeneration over an 8-week time period (George *et al.*, 2009). The main material used in this work was PDMS discussed in detail in section 1.4.

### 1.3.2 Nerve conduits – Topography

Cells, and that includes neurons respond to the topography and physical features of their environment, this has already been shown by Harrison in (1912). Nerve cells encounter topography early on, when the nervous system is developing, an example of that is during histogenesis of the cerebral cortex, cortical neurons are guided along radial glial cells (Nadarajah *et al.*, 2002). The alignment of ECM proteins and the Schwann cells is crucial in axon alignment and guidance. The bands of Bungner play an especially important role in this process, orienting the Schwann cells and ECM resulting in regenerating peripheral nerves (Hoffman-Kim *et al.*, 2010, Gesellchen *et al.*, 2014). The aim of utilising topography in nerve conduits is to rewire the pathways that are damaged from injury or disease by aligning neurite extensions in a desired direction. Grooved topography has been used to guide neurites in *in vitro* models of the PNS and CNS with success (Miller *et al.*, 2002, Johansson *et al.*, 2006, Su *et al.*, 2013, Sorensen *et al.*, 2007).

A lot of research has focused on the neurite response on different groove depths and results have indicated that alignment and outgrowth increase with increasing groove depth from around 0.2 to 4  $\mu\text{m}$ , no effects is observed on grooves smaller than 200 nm (Miller *et al.*, 2002, Clark *et al.*, 1990). Choosing the optimal depth of a groove is critical, as the combination of depth and the angle at which an approaching neurite contacts the feature (wall or edge) has been shown to influence whether the neurite turns to follow the cue, or crosses the step to preserve its original direction (Hoffman-Kim *et al.*, 2010, Li *et al.*, 2008).

## Chapter 1

### 1.3.3 Nerve conduits – supporting cells

Discussed previously, is the importance of Schwann cells in supporting axons. Schwann cells remain to be the most important cell type to use in peripheral nerve regeneration as they produce molecules such as laminin and collagen as well as secreting growth factors like NGF and BDNF, which are essential for supporting neural cell growth and survival (Evans, 2001). Schwann cells are also essential for the guidance and support of a regenerating axon; this is mainly regulated by glial growth factor (GGF) and has been shown to be the most effective growth factor for Schwann cell proliferation (Terenghi, 1999). Aligned monolayers of Schwann cells can aid regenerating axons by directing neural outgrowth to follow the direction of their alignment even in the absence of topography (Thompson and Buettner, 2006). A study by Novikova *et al.* (2008) showed that the scaffold they used combined with cultured adult Schwann cells and ECM molecules was successful in bridging the spinal trauma zone and promoted axonal regeneration across the conduit. More specific to nerve regeneration, Kalbermatten *et al.*, (2008) showed that the use of optimally seeded Schwann cells on a strip of fibrin glue has shown great promise to bridge a gap in a rat model.

Neural stem cells (NSCs), mesenchymal stem cells (MSCs) and adipose derived stem cells (ADSTs) have all been shown to have a positive effect on nerve regeneration (Terenghi *et al.*, 2009, Walsh and Midha, 2009). NSCs have the ability to self-renew, and are capable of differentiating into neurons, astrocytes and oligodendrocytes (Kennea and Mehmet, 2002). A study by Zhang *et al.*, (2008) showed that the use of NSCs together with a chitosan conduit and NGF was successful in promoting regeneration to bridge a 10 mm facial nerve defect. MSCs have been shown to differentiate into cells expressing neuronal cell markers when exposed to mitogens such as BDNF and NGF, once differentiated, MSCs can myelinate axons and act like Schwann cells (Sanchez-Ramos *et al.*, 2000). The use of mesenchymal stem cells in their undifferentiated state *in vivo* to aid regeneration stimulates the advancing axons and native Schwann cells, creating a conducive environment for nerve regeneration by differentiating into multiple pathways (Oliveira *et al.*, 2010, Kemp *et al.*, 2008). A study carried out by Oliveira *et al.*, (2010) revealed that the addition of undifferentiated stem cells to a median mouse model increased functional recovery significantly,

## Chapter 1

where the number of myelinated fibres and angiogenesis had increased within the conduits including the stem cells. In the last few years, adipose tissue has been identified as possessing a population of multi-potent stem cells. Studies have shown that stem cells isolated from rat visceral fat mimic the differentiation process of human ADSCs and can adopt adipocyte, osteoblast, chondrocyte and neural phenotypes (Tholpady *et al.*, 2003). Kingham *et al.*, (2007) showed that rat ADSCs expressed all the markers found in Schwann cells and enhanced neurite outgrowth *in vitro*, suggesting transition into a Schwann cell phenotype. ADSC derived Schwann cells have enhanced peripheral nerve regeneration as shown by di Summa *et al.*, (2010) a significant increase in axonal regeneration was recorded in the group of fibrin seeded with Schwann cells compared with the empty fibrin.

### 1.3.4 Nerve conduits – Growth Factors

Neurotrophic factors primarily belong to three distinct families: (i) the neurotrophins; (ii) the glial-cell-line-derived neurotrophic factor family ligands (GFLs); and (iii) the neuropoietic cytokines (Deister and Schmidt, 2006). Each family has distinct functional characteristics with overlapping cellular responses (Deister and Schmidt, 2006). Growth factors enhance functional regeneration by supporting axonal growth, Schwann cell migration and proliferation.

Research using growth factors to aid repair has focused on the use of NGF which belongs to the neurotrophins family, as it is a known promoter of neuron outgrowth and branching (Evans, 2001, Sterne *et al.*, 1997) and is the most studied of the trophic factors. Others belonging to this family include NT3, Neurotrophin 4 (NT4) and BDNF, and all exhibit a homology of approximately 55% with NGF.

NGF acts through the high affinity Tropomyosin receptor kinase A (trkA) that is mostly found in sensory neurons. The low affinity receptor NGF activates is the p75 receptor. There is evidence that trkA and p75 function cooperatively to mediate the cellular effects of NGF, with p75 acting as a chaperone to improve the binding to trkA. NGF exerts its trkA-mediated effects by becoming internalised and activating diverse signalling pathways.

## Chapter 1

NGF has been used in many studies for therapies in nerve regeneration (Chang, 2009, Dodla and Bellamkonda, 2008, Gravvanis *et al.*, 2004). A study by Xu *et al.*, (2003) using a polyphenyl ether (PPE) conduit in a rat sciatic model to bridge a 10 mm gap has shown that NGF increased nerve regeneration versus control conduits with no NGF.

The growth factors can be used singly or in combination to achieve the best regeneration results. Madduri *et al.*, argues in his study that co-delivery is essential for increased functional regeneration as a peripheral nerve contains different neural and glial subpopulations (Madduri *et al.*, 2010). The main drawback for using a single growth factor delivery system is usually down to the poor release kinetics; where there is a high initial burst release.

Gradients of growth factors or ECM components have been used and show that gradients exploit an innate response of growth cones that is not possible with uniform, isotropic distribution. Dodla and Bellamkonda (2008) suggest that gradients of such factors might exert synergy and enable the neurostimulatory cues to be more effective than when they are distributed isotropically.

## Chapter 1

### 1.4 PDMS

#### 1.4.1 Chemistry

PDMS belongs to the family of polymeric organosilicone compounds commonly known as silicones that have been widely used in microfluidics (El-Ali *et al.*, 2006) and cell mechanics (Palchesko *et al.*, 2012). It has become one of the most favourable polymers for rapid prototyping of designs and for fabrication of microdevices due to its many attractive properties such as low cost, ease of use and high compliance (Berthier *et al.*, 2012). The chemical formula of PDMS is  $(C_2H_6OSi)_n$  where  $n$  is the number of repeating monomers. The fabrication of PDMS involves a cross-linking reaction between the PDMS base mixed with a cross linking agent- the most widely used form of PDMS is Sylgard 184. The crosslinking of PDMS is achieved through a hydrosilylation reaction of the vinyl group from the siloxane oligomers and the silicon hydride group from the siloxane crosslinker. When the two react and crosslink a Si-C bond is formed (Oulad Hammouch *et al.*, 1996). The standard ratio of the base and curing agent is 10:1. Changing the ratio in turn affects the stiffness of the polymer produced (Lee *et al.*, 2004). PDMS is therefore useful to use in studies where altering stiffness of the cellular environment is targeted and understanding the effect stiffness has on cell behavior is important for creating biomaterials targeted towards regeneration. A study looking at the effect of substrate stiffness on adult neural stem cells revealed that the substrate stiffness is an important factor to the proliferation and differentiation of the adult neural stem cells where the optimal stiffness for proliferation (3.5 kPa) and differentiation to neurons (<1 kPa) (Leipzig and Shoichet, 2009). A study on the effect of branching of disassociated DRGs on different PDMS stiffness's has shown that neurons branch on softer substrates whereas glial cells prefer stiffer substrates for survival (Flanagan *et al.*, 2002). Trappmann *et al.*, (2012) focused their investigation on human epidermal cells to study the effects of stiffness on cell differentiation using a PDMS stiffness range of 0.1 kPa to 2.3 MPa where cell spreading and differentiation was unaffected by PDMS stiffness, however cells on a polyacrylamide gel of low elastic modulus (0.5 kPa) couldn't form stable focal adhesions confirming that cells do not attach to loosely bound ECM proteins on the gels.

## Chapter 1

**1.4.2 Hydrophobicity**

After the cross-linking and the curing process, PDMS becomes a hydrophobic elastomer. When used in cell culture or any biological application it is often exposed to oxygen plasma (Owen and Smith, 1994) to render its surface hydrophilic before coating the surface with a protein that promotes cell adhesion. The plasma changes the chemistry of PDMS and produces silanol (SiOH) terminations on its surface allowing the adhesion of cell supportive proteins. The thermodynamically unstable hydrophilic surface regains its hydrophobicity in less than an hour if not coated with protein (Jo *et al.*, 2000) , as a result of low molecular weight (LMW) chains diffusing to the surface (Kim *et al.*, 2001). The polymer chains diffuse from the bulk of the surface, thereby replacing hydroxyl groups on the surface that had been produced by plasma treatment.

As well as its use for biological research, PDMS has been widely researched as a polymer insulator as it is thermally stable due to the strong Si-O bond energy and excellent water repellency resulting from low intermolecular interactions (Kim *et al.*, 2001). Kim *et al.*, (2001) analysed the hydrophobic recovery of samples that were exposed to partial electrical charges; the examined samples were seen to undergo mild oxidation of pendent methyl groups and simultaneously produced very small amount of LMW species. The subsequent hydrophobic recovery is then possibly due to the migration of *in situ* produced species from the bulk to the surface of the elastomer (2001). Eddington *et al.*, demonstrated that eliminating these LMW species by thermal aging allows the hydrophilic surface to be more permanent (Eddington *et al.*, 2006).

## Chapter 1

### 1.5 Rsn2

Recently natural adhesives such as those based on the byssus fibre protein (Lee *et al.*, 2007), and amphiphilic proteins such as hydrophobins (Linder *et al.*, 2005) have been used as alternatives to native ECM proteins to render inherently hydrophobic materials biocompatible. In a study by Janssen *et al.*, (2002) Teflon® (a material that is comparatively hydrophobic and not supportive of cell adhesion) was coated with a genetically modified hydrophobin SC3, as well as two other modified versions TrSC3 and RGD-SC3. The results indicated that the RGD-modified protein served as a better platform for fibroblast cell growth.

Rsn2 initially isolated from the foam nests of the túngara frog as one of the constituent proteins is a monomeric protein of 11 kDa (Mackenzie *et al.*, 2009). Rsn2 with its unique characteristics can modulate biomaterial surface properties e.g. of hydrophobic materials by rendering these more hydrophilic, and more favourable for cells to attach to. Rsn2 has been shown to be cell supportive without the incorporation of adhesive ECM protein derived sequences, however to improve the outcome for nerve outgrowth, the protein has been engineered to incorporate an adhesive ECM protein derived sequence IKVAV and RGD (discussed in section 1.2.7) have been specifically developed for this project as a method to coat the hydrophobic surface of the PDMS polymer.

One interesting feature of the protein Rsn2 is the presence of six consecutive aspartic acids found at the C-terminus, this motif gives the protein its amphiphilic amino acid distribution, with a slightly hydrophobic N-terminus and hydrophilic C-terminus. This amphiphilic feature would suggest that Rsn2 is a surface-active protein. This was confirmed by a study carried out by Fleming *et al.*, where Rsn2 was observed to produce a significantly greater reduction in surface tension at substantially lower concentrations when compared to control proteins (2009).

Hydrophobins are produced by filamentous fungi (Linder *et al.*, 2005) and represent a different class of surface-active proteins, and recombinant versions are used for many applications including biomedical, as fusion partners for protein purification, and anti-fouling agents (Hektor and Scholtmeijer, 2005). In solvents with a high dielectric constant, hydrophobins associate together to form

## Chapter 1

multimers, which is critical for them to remain in solution. Rsn2 in contrast does not multimerise, therefore it employs some other mechanism and thus represents a potential new class of surfactant proteins (Mackenzie *et al.*, 2009). The Nuclear magnetic resonance (NMR) structure of Rsn2 (figure 8) was solved to understand the mechanism the protein undergoes to achieve its surface-active functionality, however the structure of Rsn2 in solution had no resemblance to its amphiphilicity and therefore further analysis was required.

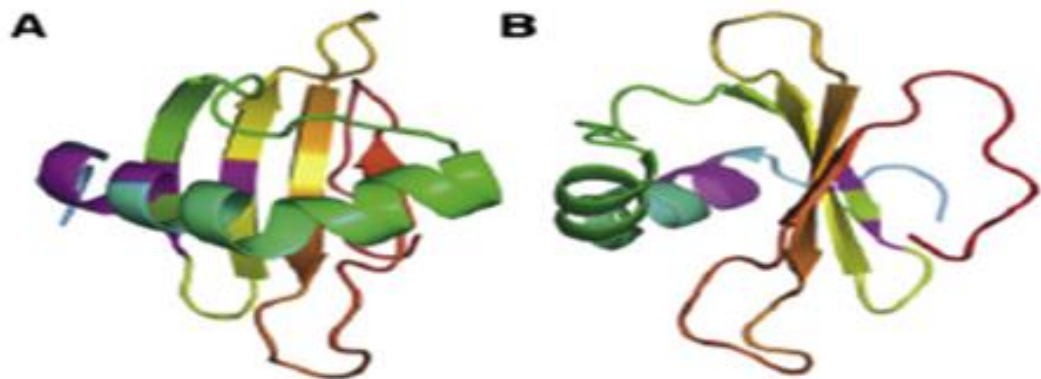


**Figure 8: Solution structure of Rsn-2. (A) Ribbon diagram illustrating the Rsn-2 fold and (B) rotated 90° about the vertical axis. (Mackenzie *et al.*, 2009).**

It was more important to understand the structure not in solution but the structure at the air water interface. A study was carried out where neutron reflectivity was used to investigate the protein at the interface. From this data it was possible to produce a two-layer model around the air-water interface (Mackenzie *et al.*, 2009). From this analysis it was concluded that Rsn2 undergoes a conformational change in order to fulfil its observed role. The model proposed is that the alpha helix (blue in Figure 9) unfolds away from the beta-sheet (orange in Figure 9), exposing the protein's hydrophobic core to the air and aligning the hydrophilic exterior in one plane, directed to the water. This was described as a “clam-shell” like opening of the protein and would give rise to the amphiphilicity required for the surfactant activity (Mackenzie *et al.*, 2009). The data also proposed different functions for the C and N terminus respectively, where the hydrophobic N-terminus acts as a trigger on interaction with the air pulling Rsn2 to the surface whereas the charged C terminus acts as an anchor remaining in the water. The secondary structure at the air-water interface is difficult to obtain as NMR spectra cannot be obtained and therefore

## Chapter 1

the data presented in the study by Mckenzie *et al.*, remains hypothetical (Mackenzie *et al.*, 2009).

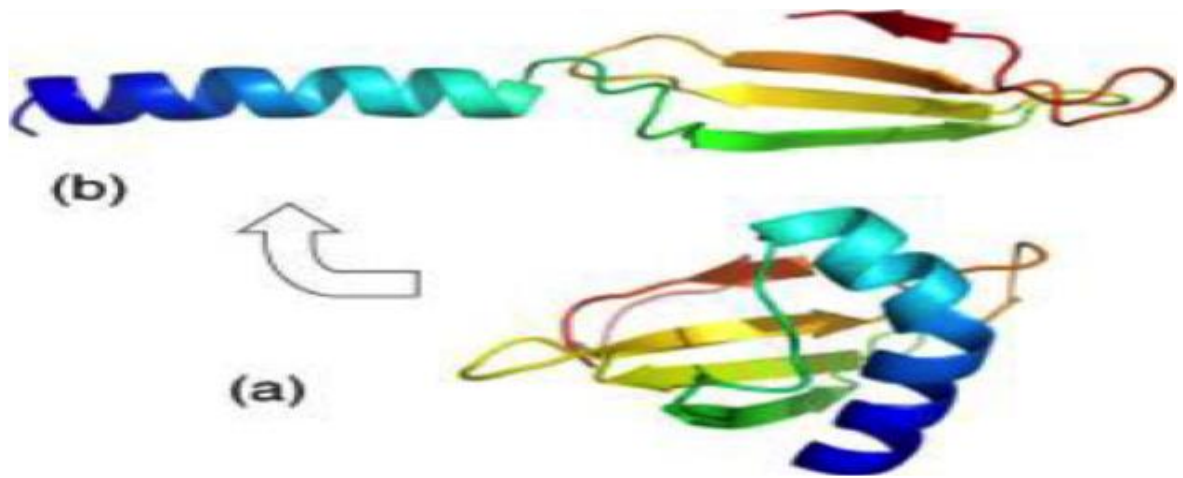


**Figure 9: A secondary structure schematic indicating how RSN-2 molecules might lie in a more extended conformation at the air-water interface (a) compared with the compact closed form in solution (b)(Mackenzie *et al.*, 2009).**

The advantages of using protein-based materials to render materials cell-compatible is that these often offer inherent biocompatibility, can be degraded into non-cytotoxic fragments, and possess similar properties to native tissue, greatly facilitating their use as part of engineered cell scaffolds (Straley and Heilshorn, 2009). The method of using an amphiphile to coat hydrophobic surfaces does not rely on a specific surface chemistry but on a physical surface parameter that is given by most if not all aliphatic polymers allowing its wide adoption (Janssen *et al.*, 2002).

## 1.6 Aims & goals

The aim of this research was to enhance the regenerative potential of nerve repair tubes by studying parameters that aim to improve the interfaces of polymers by:

- I. Investigating the potential use of Rsn2 to coat hydrophobic polymers (PDMS, PCL and polycarbonate (PC)), which requires no plasma treatment to render a hydrophilic and cell compatible surface.
- II. Understanding the reasons that cause cell peeling on Rsn2 coated PDMS and develop this into a cell harvest method (based on outcome of aim I).
- III. Studying parameters such as substrate coating, topography and NGF concentration and how these interact to affect growth cone guidance and axonal outgrowth.
- IV. Analysis of axonal outgrowth of individual sensory neurons on different peptide sequences (IKVAV, RGD) engineered onto Rsn2 for well-defined adhesion.

## **Chapter 2**

### **Rsn2 for temporary surface modification of PDMS**

## Chapter 2

### 2.1 Introduction

Biocompatibility of a biomaterial surface is very important for its role in being used as an artificial implant to minimize foreign body reaction and to promote normal wound healing (Ratner and Bryant, 2004). Biomaterials such as PDMS, PGA and PCL, which are used in medicine and tissue engineering, are fairly hydrophobic (contact angle  $>90^\circ$ ) and therefore need surface treatment before cells will readily attach to them (Ciardelli and Chiono, 2006). In order to engineer biocompatibility, the physico-chemical properties of the polymer surface can be modified using a variety of techniques. One such approach is the immobilisation of cell-interactive synthetic peptide sequences (e.g. RGD) on the polymer surface (Ruoslahti and Pierschbacher, 1986, Janssen *et al.*, 2002), or the adsorption of native ECM adhesion promoting proteins such as fibronectin (Ruoslahti and Pierschbacher, 1986), laminin (Aumailley *et al.*, 1990) and collagen (Statz *et al.*, 1991). PDMS is a favourable polymer for rapid prototyping for topographic and mechanical surface features, and for fabrication of biomedical microdevices due to its many attractive properties such as low cost, ease of use, high replication fidelity, high compliance (Berthier *et al.*, 2012) and biocompatibility (Sherman and Kennedy, 1998, McDonald and Whitesides, 2002, Lee *et al.*, 2004). In our lab, PDMS is used to culture DRGs as its mechanical properties can be easily adjusted and biocompatibility achieved after treatment with poly-L-lysine (PLL). Additionally, PDMS can be microstructured to incorporate grooves to direct the growing neurons in culture.

Recently, a natural adhesive based on the byssus fibre protein produced by the mussel, *Mytilus edulis* family (Lee *et al.*, 2007), and amphiphilic proteins such as hydrophobins (Linder *et al.*, 2005), have been used as alternative strategies to immobilise aspects of native ECM molecules on polymeric substrates. Proteins contained in natural foams such as horse sweat (Vance *et al.*, 2013, Beeley *et al.*, 1986), human airway (Gakhar *et al.*, 2010), and the foam nests of certain amphibians (Mackenzie *et al.*, 2009, Fleming *et al.*, 2009) have suitable amphiphilic properties comparable to hydrophobins, and thus may be suitable for the same task.

Here Rsn2, a protein found in the foam nests of the túngara frog, which is a surface-active amphiphile, is used to modify polymer substrates. In principle,

## Chapter 2

this protein could be used to modulate the surface properties of a biomaterial by, for example, rendering hydrophobic materials more hydrophilic, and more favourable for cells to attach to. The technology of cell sheet engineering has become increasingly important in regenerative medicine. Stimulus responsive polymers have allowed the harvesting of cell sheets that can achieve high cell density, retain cell-cell junctions and deposited ECM (Patel and Zhang, 2013). The most widely used system is the thermo-responsive smart polymer poly (N-isopropylacrylamide) (pNIPAAm) (Kumashiro *et al.*, 2010, Haraguchi *et al.*, 2012). Once the temperature of pNIPAAm is dropped below its lower critical solution temperature (LCST), the polymer chains unfold, rehydrate and repel the cells, which induces them to peel off forming a monolayer of cells that possess their ECM and which can be transferred to new culture dishes, overlaid on top of other cell sheets, or over living tissue (Hannachi *et al.*, 2009). After extensive research into this polymer by Okano's group, one particular field well established is the use of cell sheets for cardiac repair (Shimizu *et al.*, 2006b, Shimizu *et al.*, 2006a). In these works, thermo-responsive culture dishes were used to grow sheets of beating neonatal cardiomyocytes, confluent cardiac cell sheets were harvested without any enzymatic treatment. The stacked cardiac cell sheets developed sheet-to-sheet communication via cell-cell junctions and could pulsate synchronously (Haraguchi *et al.*, 2006) which, when attached to a heart, improved cardiac function significantly. While there is no doubt that the thermo-responsive system is the most recognised in this field, there are other systems that are also well established such as electro-responsive (Yeo *et al.*, 2001), photo-responsive (Higuchi *et al.*, 2004), pH responsive (Guillaume-Gentil *et al.*, 2011) and finally magnetic systems (Ito *et al.*, 2004).

The aim of this chapter was to investigate the potential use of Rsn2 to coat hydrophobic polymers (PDMS, PCL, PC) for DRG cell growth. The surfactant protein Rsn2 was initially tested as an alternative to PLL treatment to make PDMS substrates biocompatible for the outgrowth of DRG explants, but although outgrowth was observed, after 6 days in culture, axon retraction was observed. This was not seen on the comparison material PC, or the plasma treated PLL coated controls. This serendipitous observation was further explored as a tool for cell sheet production of a suitable cell type, and a hypothesis for the basis of the peeling effect generated and tested.

## Chapter 2

## 2.2 Materials and methods

### 2.2.1 Molecular biology

Rsn-2 was overexpressed as a thrombin-cleavable N-terminal His<sub>6</sub> fusion-tagged form in *Escherichia coli* (*E.coli*) BL21 (DE3) cells (Novagen) using the pET28-Rsn2 plasmid. A second construct containing an additional fluorescent tag (iLOV) (Chapman *et al.*, 2008) was prepared by sub cloning a synthetic, codon optimised iLOV insert into the NdeI site of pET28-Rsn2 to create pET28-iLOV-Rsn2 (vector made and characterised by Dr. S.Vance, I grew the stably transfected bacteria from glycerol stocks, expressed, isolated, cleaned, and characterised the proteins and did all the work otherwise described in this chapter). iLOV is a flavin-based fluorescent protein derived from the LOV (light, oxygen or voltagesensing) domain of Arabidopsis thaliana phototropin 2 (Chapman *et al.*, 2008). The LOV domains form a covalent adduct between a bound flavin mononucleotide (FMN) and a conserved cysteine residue (Cys426 of Arabidopsis phototropin 2) following excitation by blue light.

Within the pET system, gene expression is controlled by the bacteriophage T7 promoter. This system yields high quantities of recombinant protein as T7 RNA is more active than *E.coli* and is not recognised by *E.coli* RNA polymerase, making it highly selective. Expression of the target gene is promoted upon the addition of Isopropyl β-D-1-thiogalactopyranoside (IPTG), this works by binding to the lac repressor releasing the promoters and allowing the transcription of T7 RNA polymerase and the target gene of interest.

#### 2.2.1.1 Overnight culture

A colony was selected from the Luria-Bertani (LB) plate and was introduced into 10 ml of LB media containing 30 mg/ml kanamycin. This was left to grow at 37°C, shaking at 230 rpm, overnight.

#### 2.2.1.2 Expression of protein

One litre of LB media containing 30 mg/ml kanamycin was placed in 4 flasks. Each flask was inoculated with 10 ml of high-density overnight culture. The cultures were left to grow at 37°C, with 200 rpm shaking until optical density

## Chapter 2

(OD<sub>600</sub>) reached ~0.8. The culture was induced with IPTG (1mM, Sigma) and left to express at 37° C for 4 hours.

### 2.2.1.3 Harvesting of protein

The cells were harvested after 4 hours by centrifugation at 1000 g for 20 mins, after which the cells were re-suspended in binding buffer (50 mM Na<sub>2</sub>HPO<sub>4</sub>, 300 mM NaCl and 5 mM Imidazole) containing Benzonase (0.01%, Novagen).

Sonication was employed to disrupt the cells and release the protein into the solution. This was carried out on a Sanyo Soniprep 150 at 10 amplitude microns for 30 cycles of 30 sec on, 30 sec off. An ice bath was used to prevent the sample from over-heating. Insoluble cell debris was removed by centrifugation at 20000 g for 20 mins, leaving a cell lysate containing the protein Rsn2 or iLOV-Rsn2.

### 2.2.1.4 Protein purification

The method utilised is Ni<sup>2+</sup> affinity chromatography, which works by having a high affinity for histidine residues. The metal is bound to the resin within a nitrilotriacetic acid (NTA) moiety and the protein of interest containing a His-tag is retained on the column leaving other untagged proteins to wash through. To elute the bound protein imidazole (300 mM) is used to displace the bound histidines, therefore releasing the bound protein. Contaminant proteins that may have a natural affinity for the Ni<sup>2+</sup> ions were removed by washes with solutions containing low imidazole concentrations (5-30 mM).

The column was prepared by washing 5x column volume with water followed by equilibration of the column by the addition of 5x volume of binding buffer (20 mM Tris.HCL, 0.5 M NaCl and 5 mM Imidazole). The supernatant was passed through a syringe filter (0.8 µm, Nalgene) and loaded onto the Ni-NTA column (Novagen) followed by 2 x 5 column volume washes of binding buffer to allow setting followed by 3 x 3 column volume washes with wash buffer (20 mM Tris.HCL, 0.5 M NaCl and 20 mM imidazole) before the addition of 4 x 1 volume of elution buffer (20 mM Tris.HCL, 0.5 M NaCl and 0.3 M imidazole). Finally 3x volume of matrix of 1 M imidazole was used to remove any remaining protein. Samples were collected from each column wash and analysed by sodium dodecyl

## Chapter 2

sulphate-polyacrylamide gel electrophoresis (SDS-PAGE). The samples were allowed to buffer exchange by dialysis overnight in (10 mM NaH<sub>2</sub>PO<sub>4</sub>, 10 mM Na<sub>2</sub>HPO<sub>4</sub> and 50 mM salt).

### 2.2.1.5 Protein concentration

After the protein was purified, a measurement of protein concentration was made using a Nano drop 1000 (Thermo Scientific). For Rsn2 the absorption at 280 nm was used and the apparatus was blanked with water. However, the absorbance signal at 280 nm overlaps with that of iLOV-Rsn2 as the FMN chromophore absorbs at 270 nm, making the UV reading invalid. To overcome this, a small volume of the protein was heated to 85 °C for 5 mins to denature the protein and release the bound FMN. The solution was then centrifuged at 20000 g for 5 mins to pellet the denatured protein. The concentration of free FMN in the supernatant was then calculated based on the extinction coefficient of 12500 ± 500 M<sup>-1</sup> cm<sup>-1</sup> at 450 nm (Drepper *et al.*, 2007).

To determine the protein concentration the following equation was used:

$$C = \frac{M * A}{E}$$

Where: C = concentration, M= molecular weight, A = Absorbance measurement, and E = extinction coefficient<sup>1</sup> (M<sup>-1</sup> cm<sup>-1</sup>).

$$\text{Rsn2 MW} = 13415.2 \quad \epsilon_{280} = 6085 \text{ M}^{-1} \text{ cm}^{-1}$$

$$\text{Rsn2 - iLOV MW} = 26682 \quad \text{Ex.co} = 16055 \text{ M}^{-1} \text{ cm}^{-1}$$

Protein samples were concentrated using a Vivaspin20 with a 5000 molecular weight cut off column (vivascience). Columns were pre-rinsed in water after which they were centrifuged with protein samples at 5000 g until the desired concentration was achieved.

---

<sup>1</sup> The extinction coefficient is a parameter used to describe how strong a substance absorbs light at a given wavelength.

## Chapter 2

### 2.2.2 Cell engineering

#### 2.2.2.1 Organotypic culture of DRGs

DRGs were isolated from neonatal (1-5 days old) Sprague-Dawley rats. Rats were euthanized by Euthatal® injection (500mg/Kg) according to Home Office regulations, and then dissected. Before seeding, the nerve stumps were removed after which the DRGs were seeded on the middle of the PDMS, PC and PCL samples. DRGs were then cultured for 10 days at 37°C 5% CO<sub>2</sub> in 15.1 mm diameter well plates in L15 culture media (Sigma, UK) supplemented with fetal bovine serum (FBS, 10%, Life technologies, UK) N-acetyl-cystein and vitamin C (50 mg/ml), antibiotic mix (1%, L-glutamine, penicillin streptomycin and fungizone) and NGF (10ng/ml, 2.5 S Invitrogen, UK). Cultures were split fed 1:1 every day.

#### 2.2.2.2 DRG immunofluorescence

After 10 days growth, DRGs were washed with phosphate buffered saline (PBS) and fixed in formaldehyde (10%, Fisher Scientific)/PBS solution also containing sucrose (2% w/v, Fisher Scientific) for 15 mins. Following fixation, the cells were permeabilised in sucrose (10.3%), NaCl (0.292%, AnalaR Normapur), MgCl<sub>2</sub> (0.06%, AnalaR Normapur), HEPES (0.476%, Fisher Scientific) and Triton X-100 (0.5%, Sigma, UK) per 100ml PBS at 4°C for 5 mins, followed by an incubation at 37°C in PBS/BSA (1%, Sigma, UK) for 5 mins. The blocking solution was replaced by PBS/BSA solution containing anti- $\beta$ <sub>3</sub>-tubulin antibody (1:100, mouse anti-TU-20 Santa Cruz, California). The samples were incubated at 37°C for 2 hours. The samples were then washed thrice with a PBS/Tween@20 (0.5%, Sigma, UK). The samples were further incubated for an hour in PBS/BSA solution containing biotinylated anti-mouse antibody (1:50, Vector Laboratories) after which they were washed thrice with PBS/Tween. Texas red streptavidin (1:50, Vector Laboratories) in PBS/BSA was then added to the sample and kept at 4°C for 30 mins before washing thrice with PBS/Tween. To prepare the slides, a small drop of mounting medium containing DAPI (Vectorshield-DAPI) was placed on a labelled microscope slide. Samples were viewed on a fluorescence microscope (Zeiss Axiovert200 or Olympus - BX51). DAPI Excitation/Emission (nm) = 358/461 and Texas red (FITC) Excitation/Emission (nm) = 596/615.

## Chapter 2

### 2.2.2.3 Cell culture

Caco-2 cells were cultured in Dulbecco's Modified Eagle Medium (DMEM, 71%, Sigma UK) supplemented with Medium 199 (17%, Sigma UK), FBS (9%, Life Technologies, UK), L-glutamine (1.6%, 200mM, Life Technologies UK) and, sodium pyruvate (0.9%, 100mM, Life Technologies UK). The cells were seeded into a 24 well plate at a density of 23,000 cells per surface and incubated at 37°C in a humidified, 5% CO<sub>2</sub> containing atmosphere.

### 2.2.2.4 Caco-2 cell Immunofluorescence

After culture the cells were washed with PBS and fixed with 10% formaldehyde/PBS 2% sucrose for 15 mins. After fixation the cells were permeabilised in perm buffer at 4°C for 5 mins followed by an incubation at 37°C in PBS/BSA for 15 mins. This was replaced by PBS/BSA solution containing anti-ZO-1 (Rabbit anti-ZO-1, Invitrogen). The samples were incubated at 37°C for 2 hours. The samples were then washed thrice with PBS/Tween®20 (0.5%, Sigma, UK). The samples were further incubated for 1 hour in PBS/BSA solution containing biotinylated anti-Rabbit antibody (1:50, Vector Laboratories) and washed thrice with PBS/Tween. Texas red streptavidin (1:50, Vector Laboratories) in PBS/BSA was then added to the sample and kept at 4°C for 30 mins before washing thrice with PBS/Tween. To prepare the slides, a small drop of mounting medium containing DAPI (vectorshield-DAPI) was placed on a labeled microscope slide. Samples were viewed on a fluorescence microscope with appropriate filters (Zeiss Axiovert200). Monoclonal Anti Fibronectin antibody (Sigma, UK) was used to stain for the extracellular protein fibronectin and samples were prepared as described above. DAPI Excitation/Emission (nm) = 358/461 and Texas red (FITC) Excitation/Emission (nm) = 596/615.

### 2.2.2.5 Material fabrication

PDMS 184 polymer solution 90% (wt/wt) (Sylgard® 184 Silicone Elastomer, Dow Corning, UK) was added to 10% (wt/wt) curing agent. This was mixed very well in a disposable cup. The mixture was degassed under vacuum for 20 mins. The degassed PDMS was poured into a petri dish or a silicon wafer mould and cured in an 80°C oven for 2 hours, it was left to cool before removing and cutting the

## Chapter 2

samples to individual 11 mm diameter devices with a cork borer. For PC, a sheet (0.5 mm thickness, Good fellow) was cut into 1cm x 1 cm squares.

### 2.2.2.6 Sample preparation

Samples were sterilised prior to seeding: by immersing in 70% ethanol for 30 mins after which each sample was rinsed 2x in PBS followed by drying with a flow of 0.22µm filtered, compressed air in a laminar flow cabinet to avoid contamination.

For Rsn2 and iLOV-Rsn2 coating no plasma treatment was required, protein solution (0.1 mg/ml) was added to each surface and was left to incubate for up to an hour. After this the surfaces were rinsed in water and air-dried ready for seeding with cells.

The positive control samples of PDMS and PC surfaces were treated for 1 min with air plasma generated using a Harrick Plasma PDC-002 Plasma Cleaner at 29.6 W. After plasma treatment, the surfaces were coated with PLL (13 µg/ml, Sigma) solution for 30 mins at 37°C before seeding with cells.

### 2.2.2.7 PDMS swelling

Un-reacted base component of the crosslinked PDMS was extracted by two cycles of swelling the polymer in n-hexane (Riedel-de Haën), followed by n-hexane extraction and shrinking of the samples in ethanol. The polymer was weighed before the washing cycles and mass loss was monitored to ensure all unreacted LMWC chains were removed (figure 10).

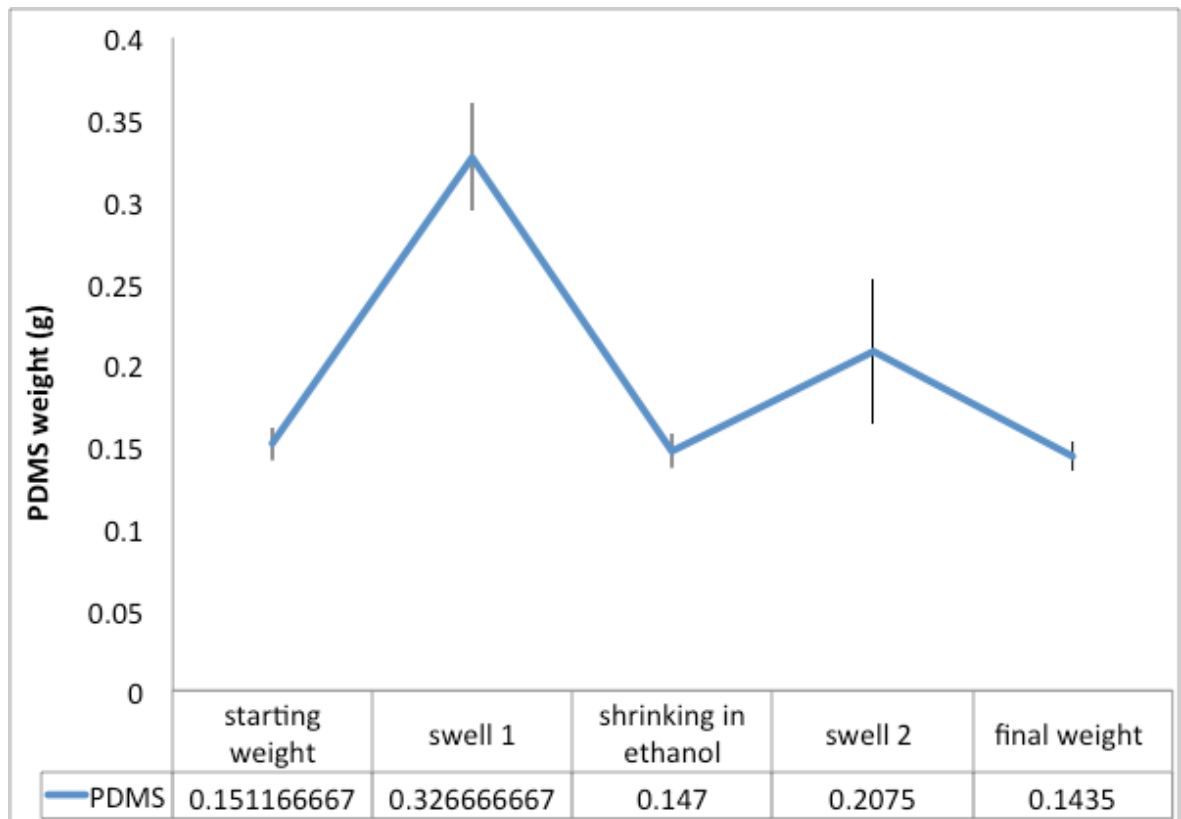


Figure 10: PDMS weight change with swelling. The above graph represents the average weight changes of 18 PDMS samples. A total decrease of 5% was established.

### 2.2.2.8 X-ray photoelectron spectroscopy (XPS)

XPS was carried out by Dr Rasmus Peterson on a SAGE 100 system (Specs GmbH, Germany). Base pressure in the analysis chamber was approximately  $2e^{-7}$  mbar. The X-ray source was AlK $\alpha$  or MgK $\alpha$  operated at an anode voltage of 9.5 kV and 140 W. Spectra were recorded at a take-off angle of 90°. The pass energy for the hemispherical analyzer was 50 eV. Spectra were analysed using commercial casaXPS software, and atomic composition was determined by integration of peak areas using a standard Shirley background.

Prior to analysis, samples were sterilised and protein coated as described previously. To monitor the presence of His-tagged protein on the surfaces by Cu<sup>2+</sup> binding, samples were soaked in a 0.5 mM solution of copper sulphate for 30 minutes before rinsing the samples with water to wash off any excess protein and air-dried for analysis

## Chapter 2

### 2.2.2.9 Topas® sample preparation

Patterned Topas samples were made by Dr. Neven Steinmetz as follows: Microposit™ S1818™ photoresist was spun onto 2.2 cm x 2.2 cm hydrophobic Topas® samples. A UV lithography mask with feature sizes ranging from 200 µm to 15 µm was utilised and samples were exposed in a custom-built (LED Engin 365 nm 11W UV LED) exposure chamber for 14 seconds. The samples were developed using Shipley Microposit® developer to generate a patterned, masked surface. These samples were given an O<sub>2</sub> plasma treatment (100W for 1 minute) to increase the hydrophilicity of the patterns. Water contact angle measurement (KSV CAM 100) was performed on the plasma treated surface ( $45.0^{\circ} \pm 2.8^{\circ}$ ) and the untreated Topas® surface ( $71.5^{\circ} \pm 2.5^{\circ}$ ), (n=5).

#### 2.2.2.10 Data analysis – cell number timeline

Images of the cell nuclei were obtained using an automated fluorescent microscope (Olympus - BX51) controlled by ImageProPlus (Media Cybernetics, UK) obtaining nine images in a grid pattern distributed over the surface with a randomized starting point. The pictures were analysed using Image J (Rasband, 1997-2012) by adjusting the threshold of the image and counting particles by defining the size of the nucleus of the timeline (day 1, 5 and 7) and dividing by the total area covered by the cells. Statistical analysis was performed on SPSS statistics using ANOVA analysis with a Dunnett post test for significance between parameters.

## Chapter 2

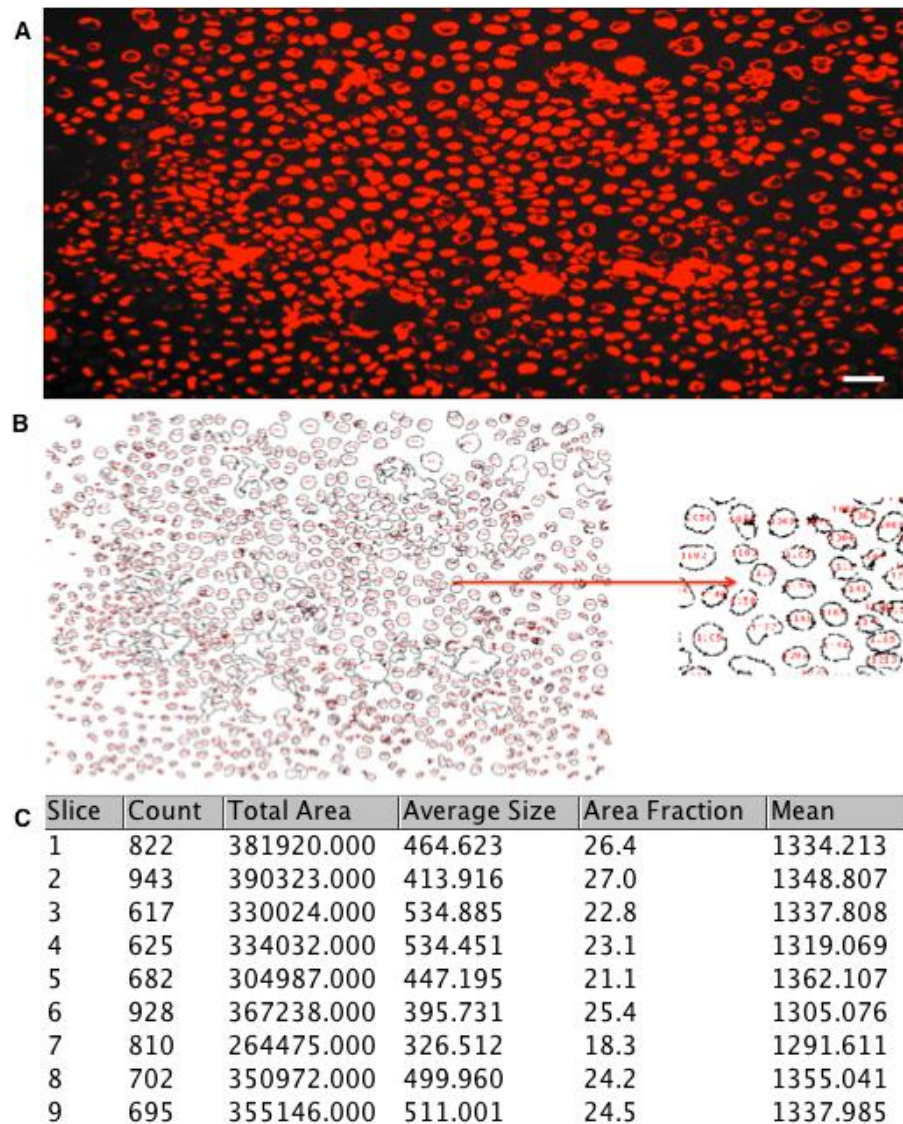


**Figure 11:** Image analysis using the Analyse particle tool of Image J software. (A) Represents the cell nuclei selected by adjusting the threshold. (B) Represents the particles counted and (C) is the completed computation of the number of particles selected. Scale bar = 50  $\mu\text{m}$ .

### 2.2.2.11 Quantification of linear ZO-1 staining

Images of the tight junction ZO-1 were obtained by taking Z-stacks of fluorescent images with a 20x objective (N.A, 0.5) using a motorized Zeiss Axiovert 200m microscope; from 10 random fields of view acquired for each surface treatment and time point. From the Z-stack, using the extended depth of focus plugin in ImagePro+ (Media Cybernetics), one maximum contrast image was obtained for each stack. Each of the resulting images was calibrated and processed on Image J (Rasband, 1997-2012) using the Neuron J plugin (Meijering *et al.*, 2004), which traces the lines selected giving the total length of the tight

**Chapter 2**

junctions in  $\mu\text{m}$ . Total ZO-1 length per field was calculated in Microsoft Excel, and statistical analysis was performed on SPSS statistics using ANOVA analysis with a Dunnett post test for significance between parameters.

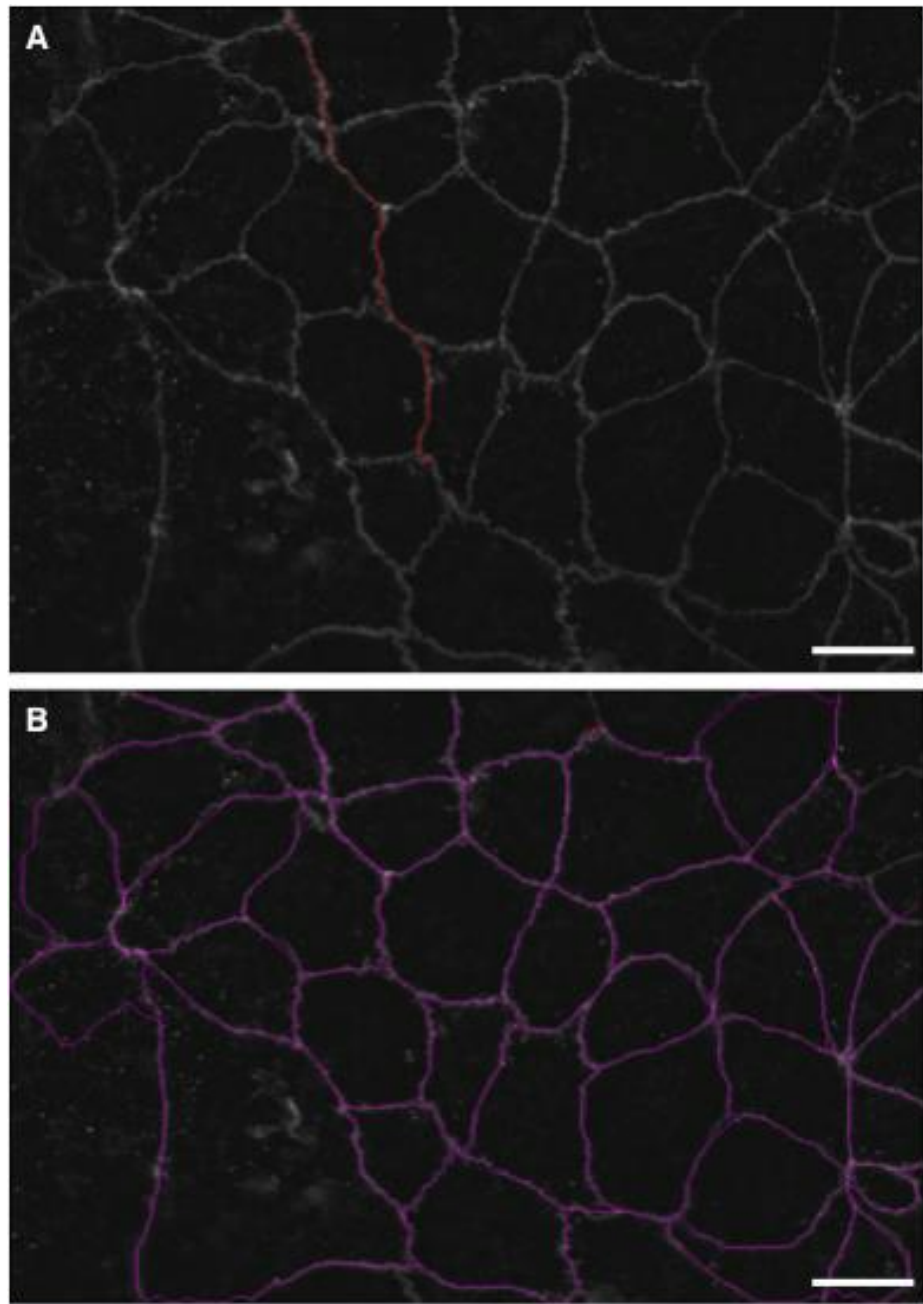


**Figure 12: Image analysis using Neuron J tool of Image J software. The fluorescence image of the ZO-1 immunostaining (A) in the process of tight junction selection – once a trace has been made the line changes colour to pink (B). Once all the tight junctions are selected the program is run to compute the length of the selection and the results are obtained in  $\mu\text{m}$ . scale bar = 50  $\mu\text{m}$ .**

## Chapter 2

### 2.3 Results

#### 2.3.1 Expression and purification of Rsn2 and iLOV-Rsn2

A test expression was carried out using pET28-Rsn2/BL21 (DE3) and pET28-iLOV-Rsn2/BL21 (DE3), constructs were analysed by SDS-PAGE, from which the best colony was selected to perform a large-scale expression (figure 13).

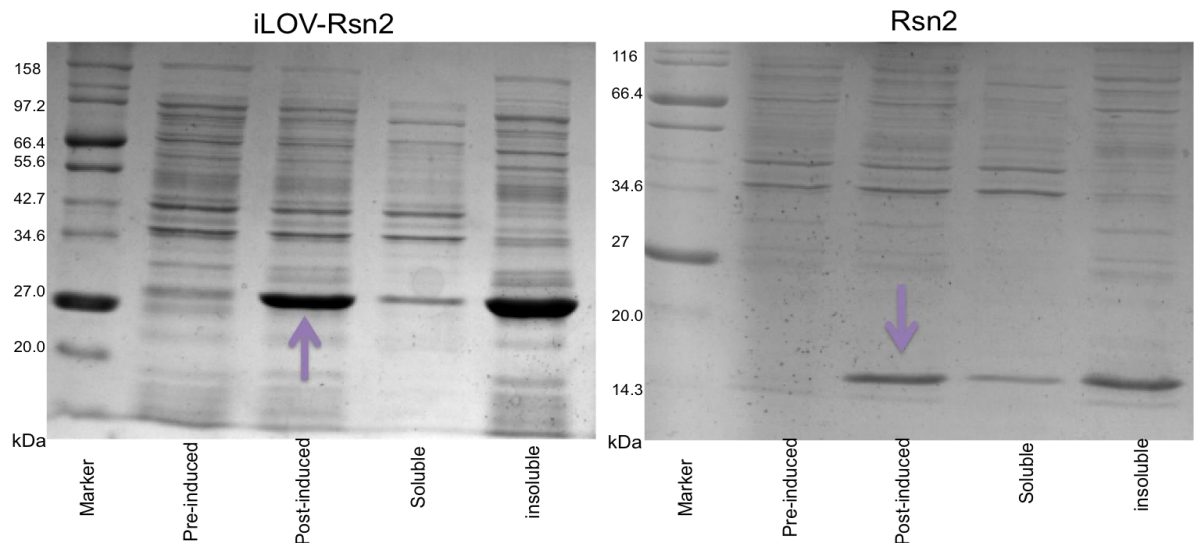


**Figure 13: SDS-PAGE analysis of iLOV-Rsn2 (left) and Rsn2 (right) expression samples. A distinct band is visible for iLOV-Rsn2 at ~ 27 KDa (arrow) and ~14 KDa for Rsn2 (arrow) indicating the presence of protein which could be confirmed by purification.**

The chosen colony was then used to set up a large scale expression of the respective protein (Rsn2 and iLOV-Rsn2) as described in the Methods, followed by nickel affinity purification. The respective samples were run on an SDS-PAGE gel to determine if the protein was eluted (figure 14).

## Chapter 2

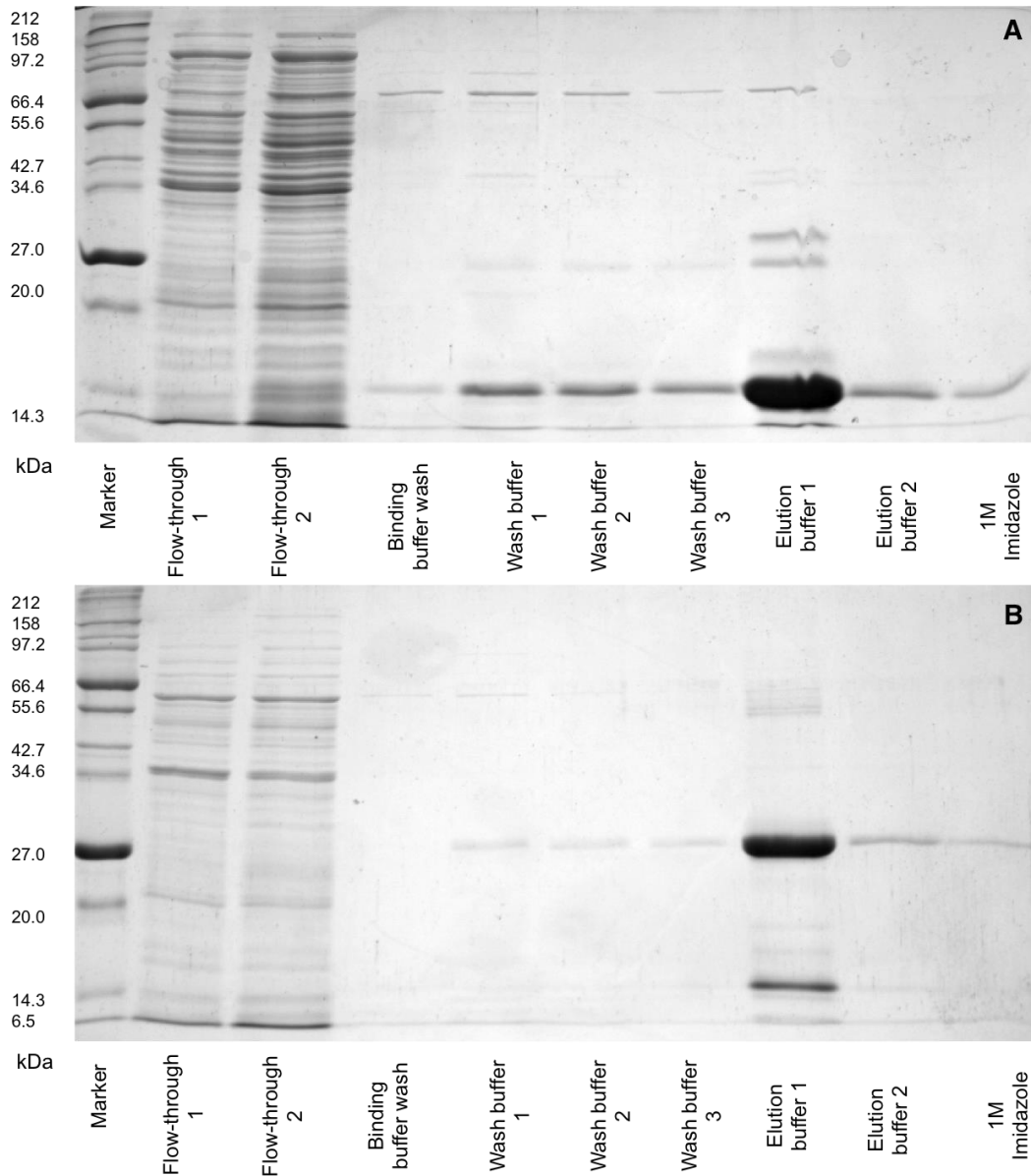


**Figure 14: SDS-PAGE analysis of Rsn2 (A) and iLOV-Rsn2 (B) nickel affinity column samples. To elute the bound His-tagged protein, a solution containing a high concentration of Imidazole is used which displaces the bound histidines. Contaminant proteins seen in columns (5-7) were removed by a series of washes using (5-30mM) imidazole concentrations before eluting for the target protein. The gels confirm that the protein was eluted successfully as a distinct band is visible in the first elution wash ~ 27 kDa for iLOV-Rsn2 and ~14 kDa for Rsn2.**

The SDS-PAGE gels shown above confirm that both Rsn2 and iLOV-Rsn2 were purified. These proteins were used to coat the biomaterial surfaces for all the experiments carried out in this chapter.

## Chapter 2

### 2.3.2 Adsorption of Rsn2 onto a hydrophobic surface

Surfaces constructed of cyclic olefin copolymer were micro-patterned using plasma oxidation, where the inside of the pattern is either more hydrophilic or more hydrophobic than the background. By applying a fluorescently tagged version of Rsn2, iLOV-Rsn2 to the patterned surfaces it was possible to image the differential adsorption using fluorescence microscopy. The iLOV-Rsn2 protein adsorbs differentially on both hydrophilic and hydrophobic regions in one application (Figure 15).

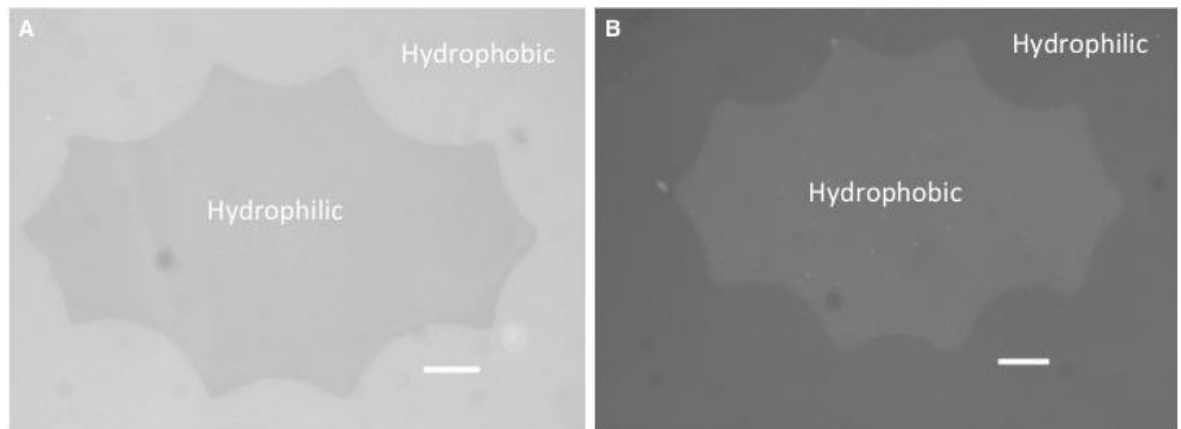


**Figure 15: Fluorescence images of iLOV-Rsn2 adsorbed surfaces with holly leaf shaped patterned hydrophilic (contact angle  $45.0^{\circ} \pm 2.8^{\circ}$ ) and hydrophobic ( $71.5^{\circ} \pm 2.5^{\circ}$ ) surfaces. (A) hydrophilic surface inside, hydrophobic outside, and (B) Hydrophilic surface outside, hydrophobic inside. These images show that the surface properties guide the differential adsorption of iLOV-Rsn2. Imaging of iLOV fluorescence showed consistently, that the relative amount of iLOV-Rsn2 was lower on the hydrophilic substrate and that this difference was independent of the pattern type (inside/outside hydrophobic). Scale bar =  $30\mu\text{m}$ .**

## Chapter 2

## 2.3.3 Verification of protein attachment – XPS

To initially verify protein attachment on a hydrophobic polymer (PDMS), XPS analysis was performed on a blank PDMS substrate to measure its chemical surface composition as well as substrates coated with Rsn2. As seen from figure 16, the nitrogen 1s signal is a clear marker for the presence of protein on the surface; no signal is seen on the protein-free PDMS.

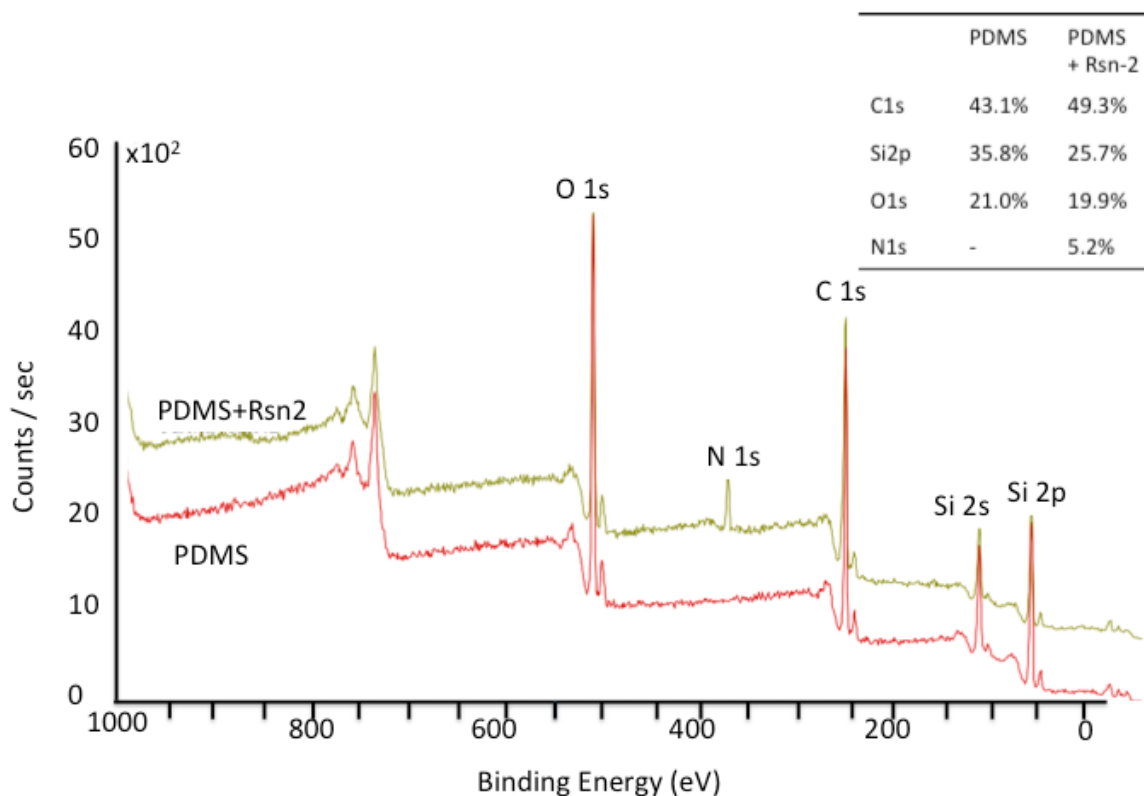


**Figure 16: XPS spectra (MgK $\alpha$  X-ray source) of blank PDMS substrate (lower, red trace) and PDMS coated with Rsn2 (upper, brown trace). The nitrogen 1s signal is a clear marker for the presence of protein on the surface, and can only be seen on the Rsn-2 coated surface. The respective peaks are indicated. The inset table gives the relative percentage surface coverage for C1, Si2p, O1s, and N1s.**

## Chapter 2

### 2.3.4 DRG cultures

To test the ability of Rsn2 and iLOV-Rsn2 to create cell compatible PDMS surfaces, DRG explants were cultured on samples of PDMS coated with either of the proteins. Both these surfaces showed initial compatibility with extension of growth cones and the formation of an axonal network extending from the DRGs. However, after ~6 days these networks started to retract (figure 17B & C). In comparison, DRGs cultured on PDMS surfaces initially oxidized, and then PLL coated could be maintained for more than 30 days (figure 17A).

This network retraction could be due to three main causes:

- A) The nature of the PDMS polymer,
- B) Protein displacement and
- C) Degradation of the explants.

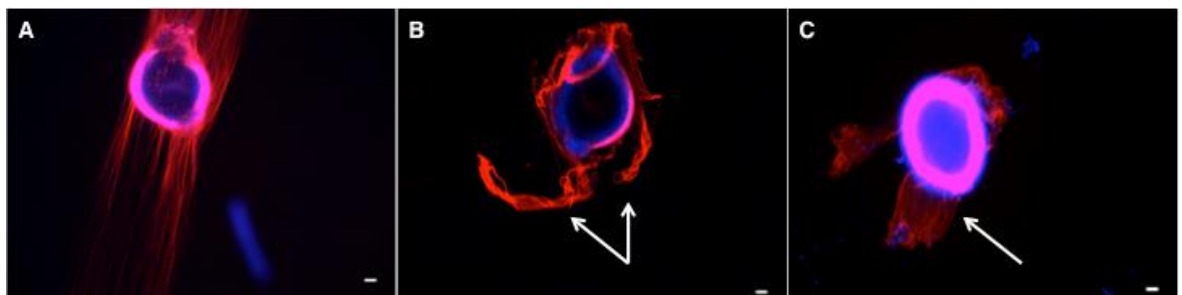


**Figure 17: Immunofluorescence images of DRG explants immuno-labelled for  $\beta$ 3-tubulin (red) and nuclei (blue) grown for 6 days on: (A) PLL coated PDMS (grooves). (B) On Rsn2 coated PDMS (grooves) (C) on iLOV-Rsn2 coated PDMS (grooves). Images B and C are showing the retraction of the nerve fibres when cultured on Rsn2/iLOV-Rsn2 surfaces (see arrows), whereas the positive control (A) is showing extended and growing nerve fibres. (Observation of n=9 DRG cells) Scale bar = 100 $\mu$ m.**

## Chapter 2

To establish whether the nature of the polymer was the reason for cell retraction, two other polymers, PCL and PC were used for comparison (Figure 18 and 19 respectively). DRGs cultured on Rsn2 or iLOV-Rsn2 coated PCL and PC were cultured for up to 10 days with no sign of axonal retraction, suggesting that the retraction observed on PDMS was due to the nature of the material.

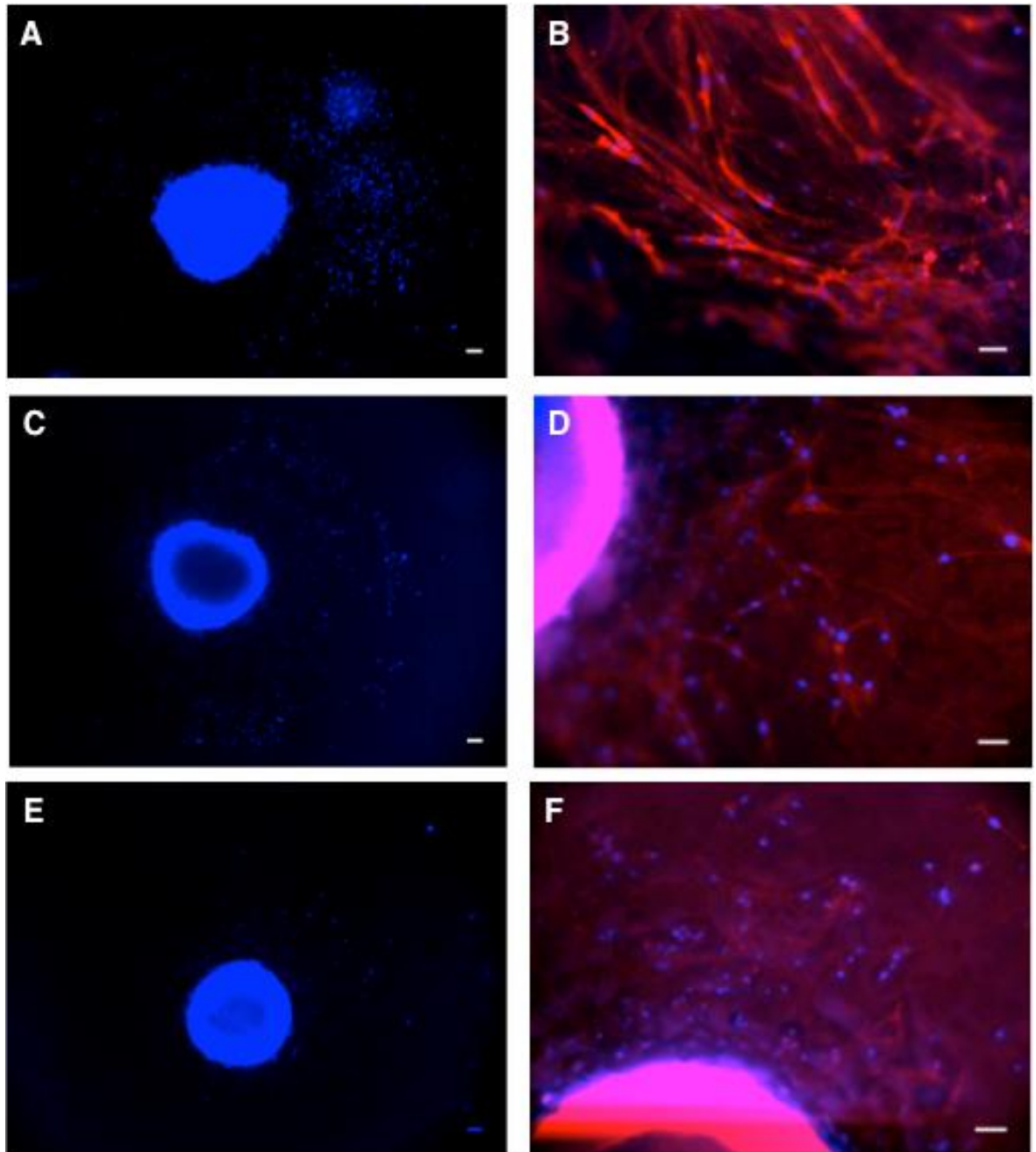


**Figure 18:** Immunofluorescence images of DRG explants immuno-labelled for F-Actin (red) and nuclei (blue) cultured on PCL for 10 days coated with (A&B) PLL, (C&D) Rsn2 and (E&F) iLOV-Rsn2. The images show that the DRG cells adhered onto the PCL surfaces without showing any neurite retraction. (Observation of n=9 DRG cells) Scale bar for images A, C&E = 100  $\mu\text{m}$  and B, D&F = 50  $\mu\text{m}$ .

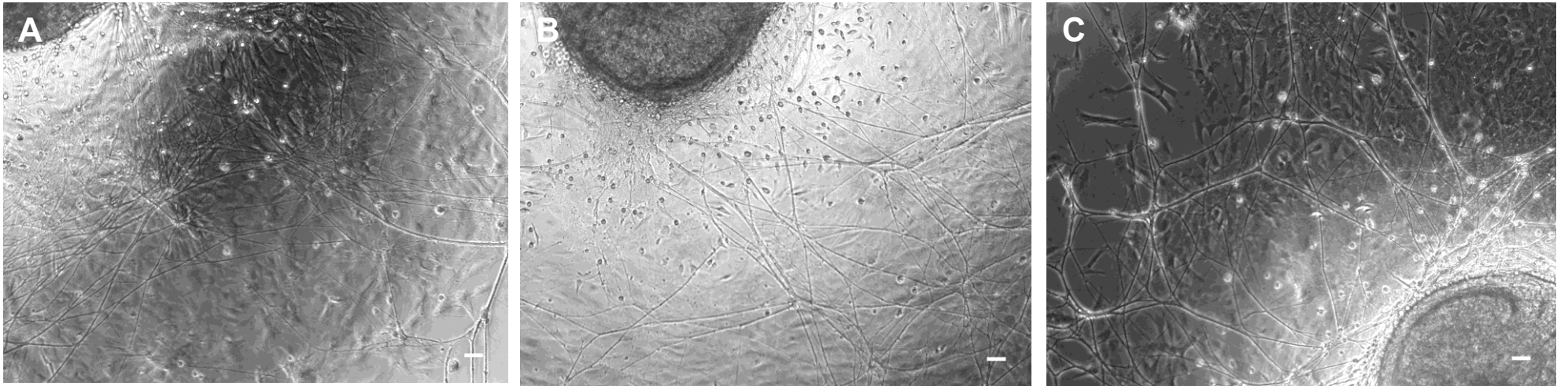


**Figure 19: Bright field images of DRG explants cultured on PC substrates for 10 days coated with (A) PLL (B) Rsn2 and (C) iLOV-Rsn2. The images show that the DRG cells adhered onto the PC substrates without showing any neurite retraction. (Observation of n=9 DRG cells) Scale bar = 50  $\mu$ m.**

## Chapter 2

To further validate that the issue was material specific, a set up was used where samples were pre-incubated in media 6 days prior to seeding in presence and absence of FBS. This was necessary to assess whether the proteins in FBS had a higher affinity to the biomaterial surface than Rsn2. Results using PC (figure 20) indicate that pre-incubation of the samples did not affect the outgrowth of the nerve fibres. The outgrowth observed in Figure 20 (images B & C) was similar, but there was improved outgrowth on the sample that had been pre-incubated in media in absence of 10% FBS (20D).

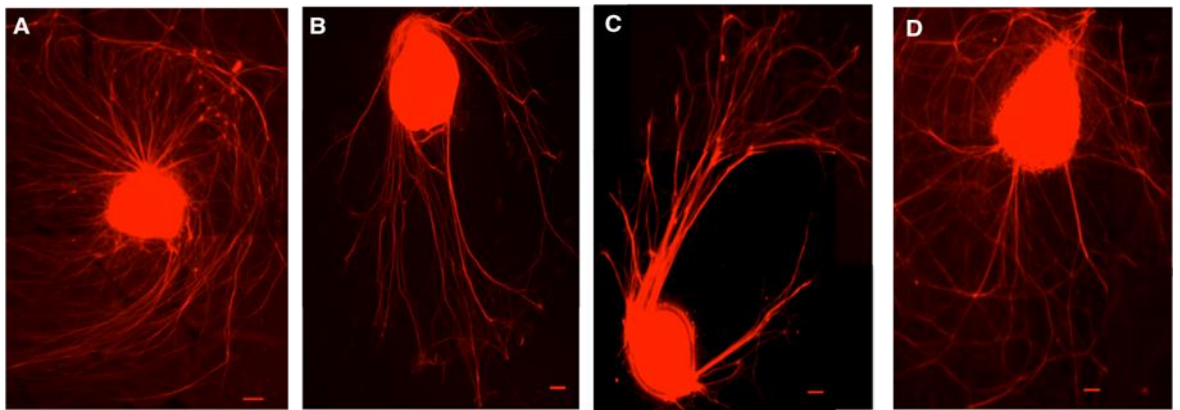


**Figure 20:** Immunofluorescence images of DRG explants immuno-labelled for  $\beta$ 3-tubulin (red) grown for 10 days on (A), PLL coated PC (B), iLOV-Rsn2 coated PC (C), iLOV-Rsn2 coated PC and pre incubated in L15 media 6 days prior to seeding (D), iLOV-Rsn2 coated PC and pre incubated in L15 media (in absence of FBS). (Observation of n=9 DRG cells) Scale bar = 50 $\mu$ m.

### 2.3.5 Caco -2 cell cultures

Based on the initial observation of the DRG explants' network retraction it was hypothesised that this loss of cell-substrate interaction could be exploited as a tool for cell sheet harvesting. A series of experiments were set up using PDMS as a substrate for the epithelial sheet forming Caco-2 cell line. Caco-2 cells resemble enterocytes lining the small intestine, but under the right condition can give rise to all cells of the gut epithelium (Huh *et al.*, 2011). These cells are contact inhibited, and post proliferation start to differentiate, developing functional tight junctions after 14-21 days in culture. To begin with, cell proliferation on the different surfaces was assessed. Rsn2/iLOV-Rsn2 coated PDMS was compared to plasma treated PLL coated substrates as a positive control, with the negative control being untreated PDMS. A cell count of Caco-2

## Chapter 2

cells cultured on the various surfaces at 1, 5 and 7 days showed that these cells proliferated well when cultured on Rsn2, iLOV-Rsn2, and on the positive control substrate (plasma and PLL) figure 21, but not on untreated PDMS.

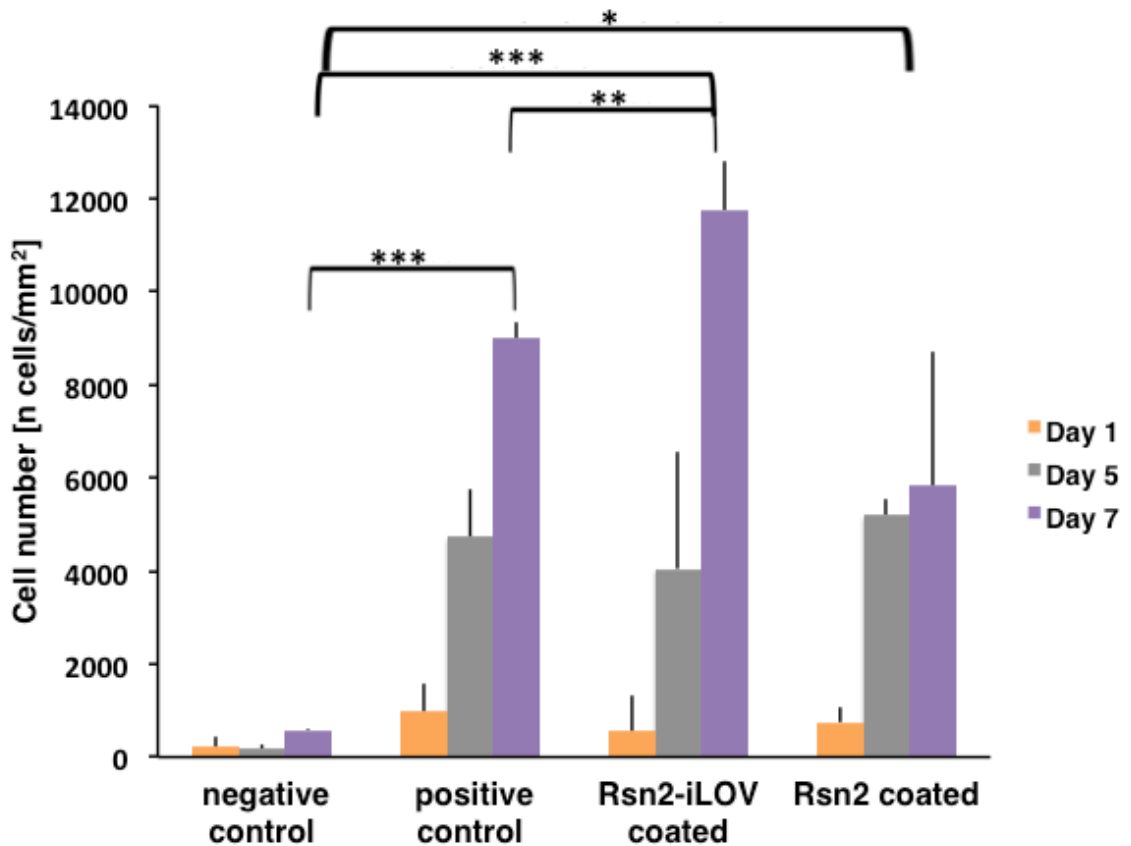
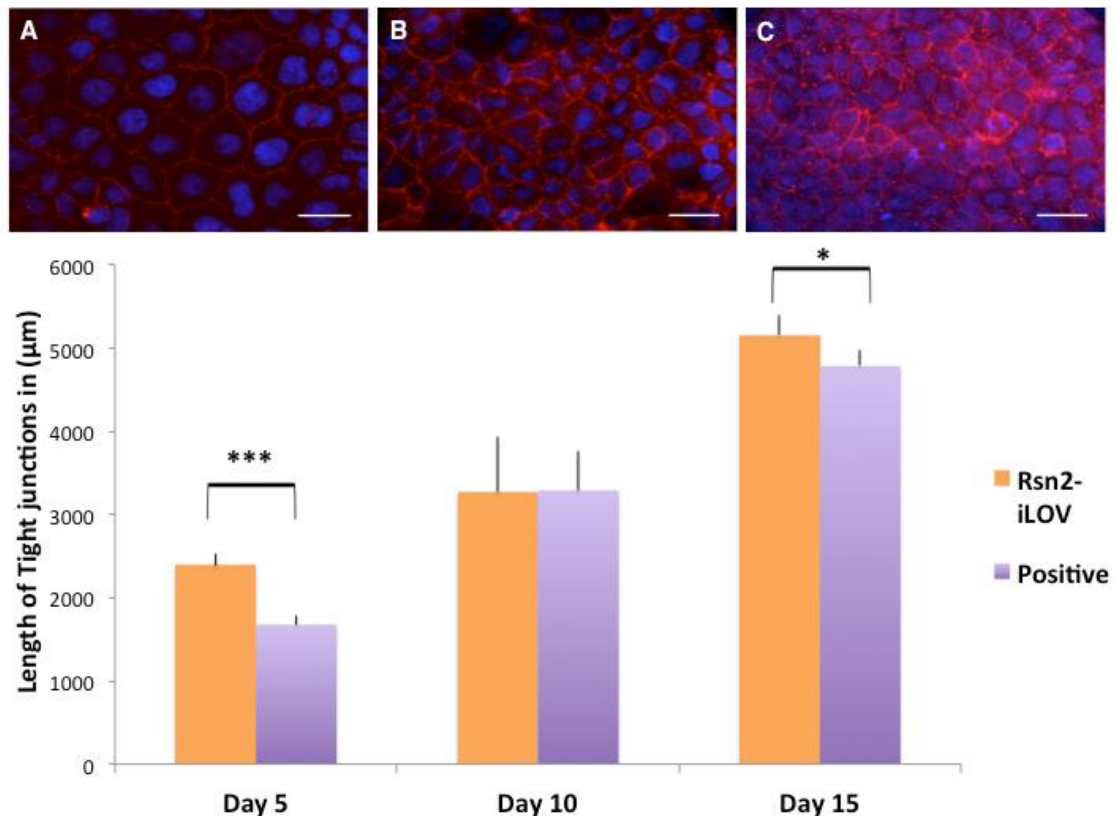


Figure 21: The graph represents the average number of Caco-2 cells/mm<sup>2</sup> after 1,5 and 7 days on plain PDMS – negative control, PLL coated PDMS –positive control, and Rsn2 and iLOV-Rsn2 coated PDMS. Stars indicate significant differences between groups as determined by ANOVA and a Dunnett post hoc test \*p<0.05 \*\*p<0.01 and \*\*\*P<0.001. (n=3 biological repeats, multiple fields of view (9 per sample) were examined for analysis). The bars indicate standard deviation.

As iLOV-Rsn2-coated PDMS surfaces gave the best results in the previous study, these surfaces were also used to test differentiation of the Caco-2 cells. Caco-2 cells express tight junction proteins, forming functional tight junctions, which interconnect the apicolateral membranes of neighbouring cells by tetraspan proteins. These proteins include claudins, which colocalize with proteins such as ZO-1 to form a tight junction and have been shown to determine paracellular barrier properties (Rosenthal *et al.*, 2012, Furuse *et al.*, 1998). ZO-1 antibody detection was used over a 15-day period to gain quantitative data of tight junction formation. Tight junction length was measured with NeuronJ (Meijering

## Chapter 2

*et al.*, 2004), an image analysis tool normally used to measure neuron length, but that can also be applied to measure tight junction length by tracing the stained cell-cell interfaces. Tight junction formation increased over the culture period as evident from figure 22- Images A-C. The graph D in figure 22 is a representation of the tight junction lengths measured at the different time points in Caco-2 cultures on either iLOV-Rsn2 or PLL coated PDMS. Both surfaces show an increase in overall cell-cell junction length over time confirming the use of Rsn2 as means to aid in fostering and maintaining a differentiated state.



**Figure 22:** ZO-1 tight junction staining 5, 10 and 15 days (A-C) on iLOV-Rsn2 coated PDMS and analysis of tight junction length ZO-1 (red), and DNA (blue). Scale bar = 30µm. The graph (D) shows the average length of tight junction formation (ZO-1) by Caco-2 cells after 5, 10 and 15 days on PLL coated –positive control and iLOV-Rsn2 coated PDMS. Stars indicate significant differences between groups as determined by ANOVA and a Dunnett post hoc test \* $p < 0.05$  and \*\*\* $P < 0.001$ . (n=3 biological repeats, multiple fields of view (10 per sample) were examined for analysis). The bars indicate standard deviation.

After reaching confluence and differentiating, the Caco-2 cells peeled off as a confluent sheet. Cell sheet peeling was only observed on Rsn2/iLOV-Rsn2 coated PDMS. The results presented so far demonstrate that Caco-2 cells are being supported by Rsn2 on PDMS, as indicated by the formation of a confluent cell layer with mature ZO-1 positive tight junctions, before the peeling takes effect.

## Chapter 2

The cell layer starts to peel off after ~20 days in culture releasing a sheet of Caco-2 cells. This was not observed on the plasma treated PLL-coated PDMS where cell sheets remained firmly attached for up to 28 days in culture (longest time followed up) as depicted in figure 23.

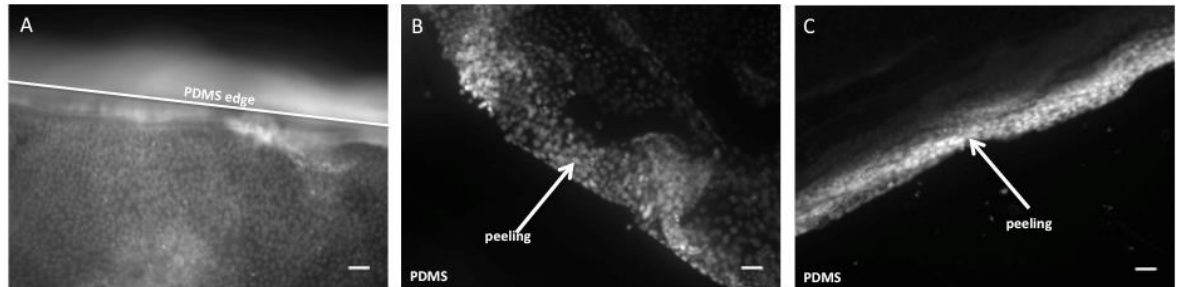


**Figure 23:** Immunofluorescence images of Caco-2 cells immuno-labelled for nuclei (grey-scale) cultured for 28 days on (A) PLL coated PDMS- no cell peeling on the edge (edge indicated by white line). (B) iLOV-Rsn2 coated PDMS – cell-peeling starting from the edge. (C) Rsn2 coated PDMS – cell peeling on the edges (indicated by the arrow). (Observation of n=9 samples) Scale bar = 50 $\mu$ m.

To determine if cell peeling caused by the effect of Rsn2 was destructive to the cell associated ECM, samples post cell peel off were stained for the ECM protein fibronectin. Image A figure 24 is of the PLL coated sample where there is no cell peeling and fibronectin can be seen localized over the whole surface of the substrate. Image B in figure 24 shows no protein remaining post peeling where the cells have peeled off, further indicating that the Caco-2 cells peel off with their ECM intact and suggesting that the cell peeling is non-destructive to the cells.

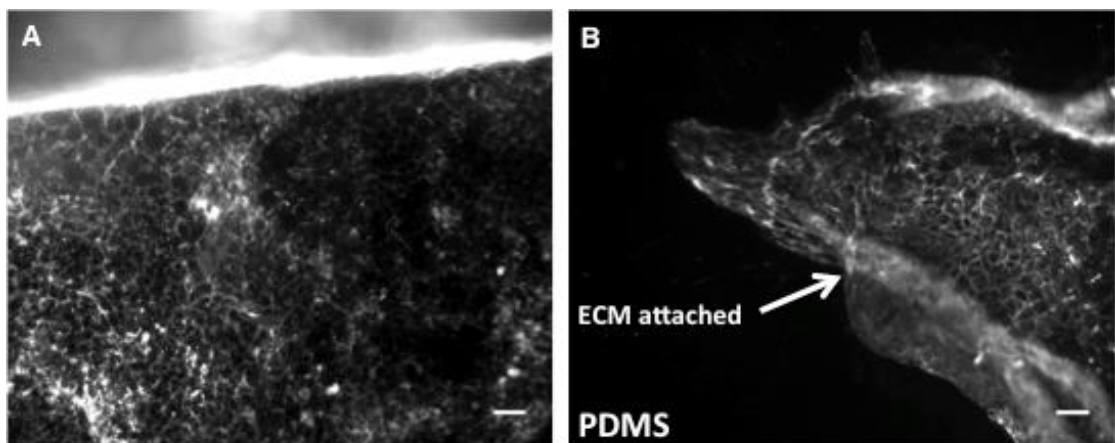


**Figure 24:** Immunofluorescence images of Caco-2 cells immuno-labelled for fibronectin (grey-scale) cultured on (A) PLL-coated PDMS: there is no cell peeling and ECM is associated with the whole surface. (B) Post cell peel-off from iLOV-Rsn2 PDMS (peeling indicated by arrow): no fibronectin is present on surface after peeling. (Observation of n=9 samples) Scale bar = 50 $\mu$ m.

## Chapter 2

To further understand the material specific mechanism of the polymer in aiding cell release, XPS analysis was carried out to study the PDMS surface post cell peeling. The suitability of copper (II) as a marker for the presence of the recombinant proteins Rsn2 & iLOV-Rsn2, based on the presence of the His-tag sequence, which binds metal ions, was verified (figure 25). For detection of  $\text{Cu}^{2+}$ , the X-ray source was switched to  $\text{MgK}\alpha$  rather than the standard  $\text{AlK}\alpha$ , since  $\text{Cu}^{2+}$  has a higher photoionization cross section at the lower X-ray energy of the  $\text{MgK}\alpha$  source, thus improving the detection capability which results in a slightly higher sensitivity to the  $\text{Cu}2\text{p}$  peak. Because of this switch the oxygen Auger peaks normally present around 750 eV are absent. As figure 25 shows  $\text{Cu}^{2+}$  can indeed be observed when bound to the protein on the surface. The two control samples show no  $\text{Cu}^{2+}$  signal.

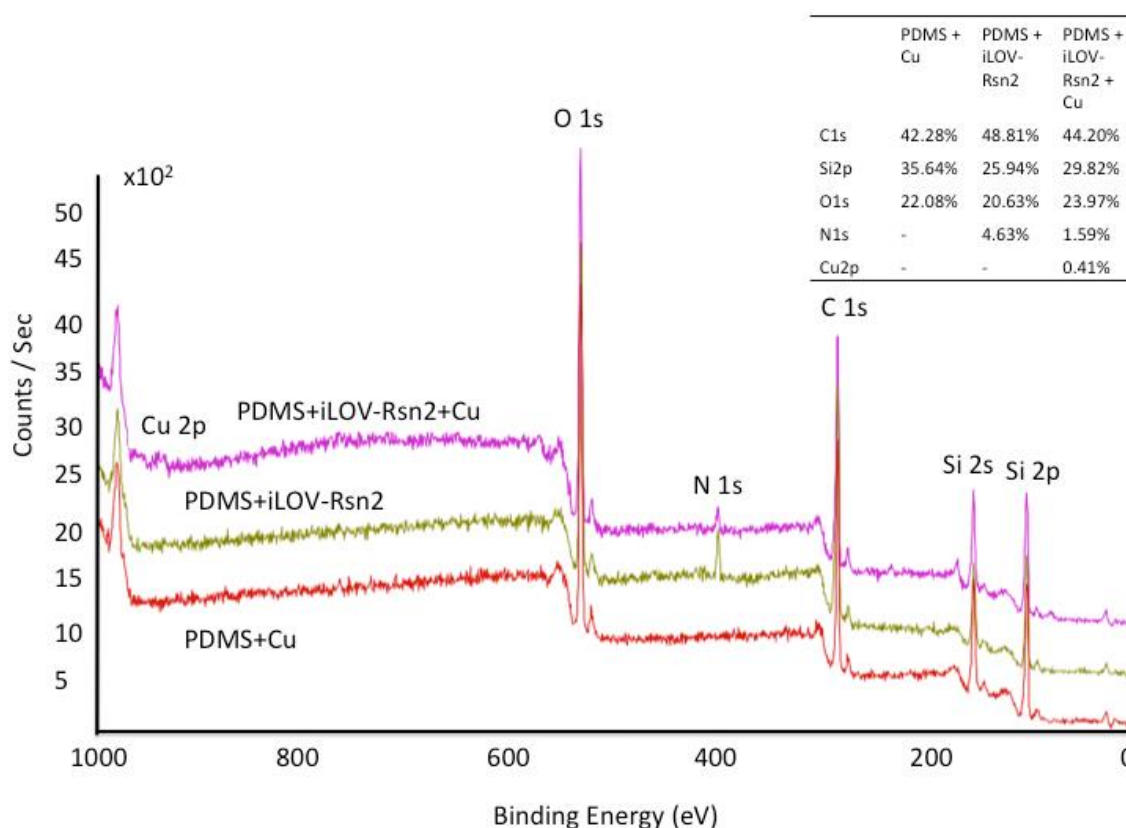


**Figure 25: XPS spectra ( $\text{AlK}\alpha$  X-ray source) to verify the use of  $\text{Cu}^{2+}$  as a tag to detect Rsn2.  $\text{Cu}^{2+}$  is observed when bound to Rsn2 on the surface (upper trace) – two control samples (middle and lower trace) were tested to ensure that  $\text{Cu}^{2+}$  does not bind the material and that the signal is only observed when  $\text{Cu}^{2+}$  is chelated by Rsn2. The respective peaks are indicated, and the inset table gives the relative percentage surface coverage for C1s, Si2p, O1s, and N1s.**

## Chapter 2

Finally, XPS analysis was carried out after cell peeling had taken place (figure 26); neither Cu2p nor N1s peaks were observed on the PDMS. This result indicates that firstly, the Rsn2 protein is no longer present on the surface and secondly, that it has not been replaced with a different protein either secreted by the cells, or adsorbed from serum.

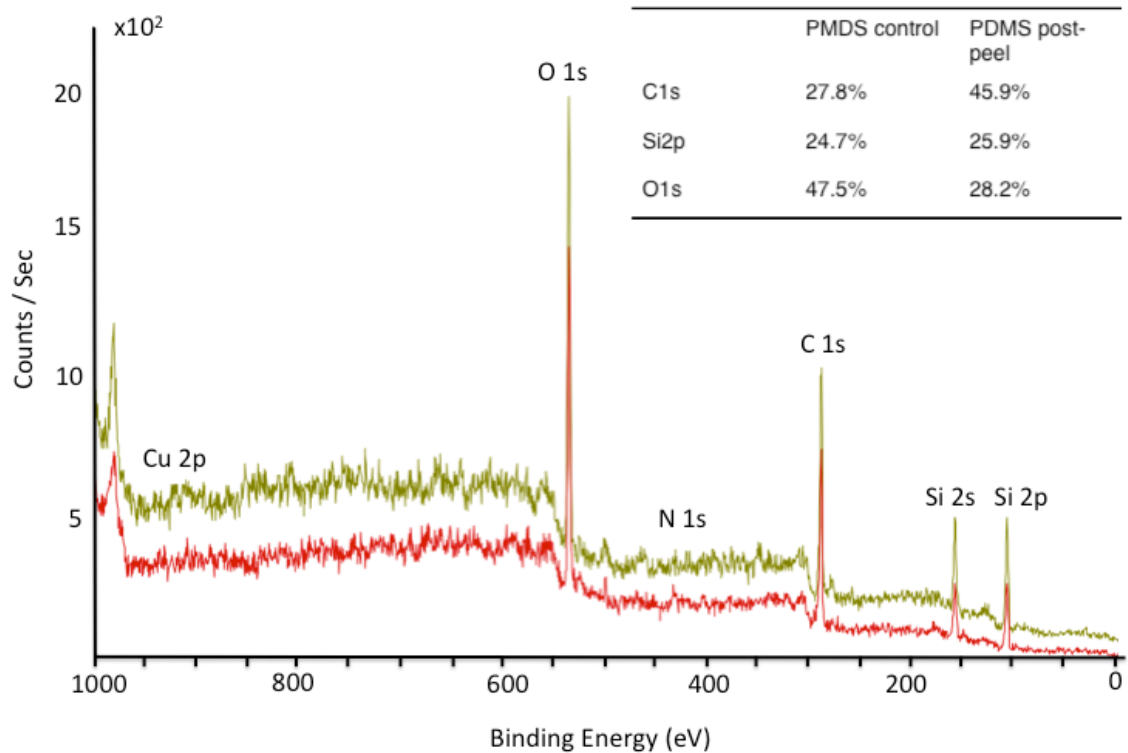


**Figure 26:** XPS spectra (AlK $\alpha$  X-ray source) analysing the PDMS surface post peel off. Neither Cu2p nor N1s peak are observed on the PDMS surface post cell peel off (upper trace) confirming that Rsn2 is no longer present on the surface and that the PDMS as the blank substrate (lower trace) is reverted back to its original chemistry before being coated with Rsn2. The respective peaks are indicated, and the inset table gives the relative percentage surface coverage for C1, Si2p, O1s, and N1s.

From the XPS data, it can be concluded that the post cell PDMS surface when coated with Rsn2/iLOV-Rsn2 had returned back to its original chemistry after 20 days in culture and in the process released a sheet of Caco-2 cells.

To be able to establish if the movement of the LMW species was the main cause for the return of the hydrophobic PDMS surface when coated with Rsn2 (discussed in detail in section 1.4), therefore causing cell peeling, serial extractions were used with sequential heptane and ethanol washes, until the sample weight was constant prior to Rsn2 coating and cell seeding. When the un-

**Chapter 2**

reacted base component was extracted from the PDMS by swelling/shrinking the polymer by repeated sequential immersion in n-heptane and ethanol prior to coating with Rsn2, no cell sheet peeling was observed after 20 days. The cell morphology was similar to that of cells cultured on Rsn2 coated PC, a comparison material that did not allow the Caco-2 cells to peel, instead the cells clustered together as shown in (figure 27). This further supports that the Caco-2 cell sheet peeling is due to the return of the hydrophobicity of PDMS.

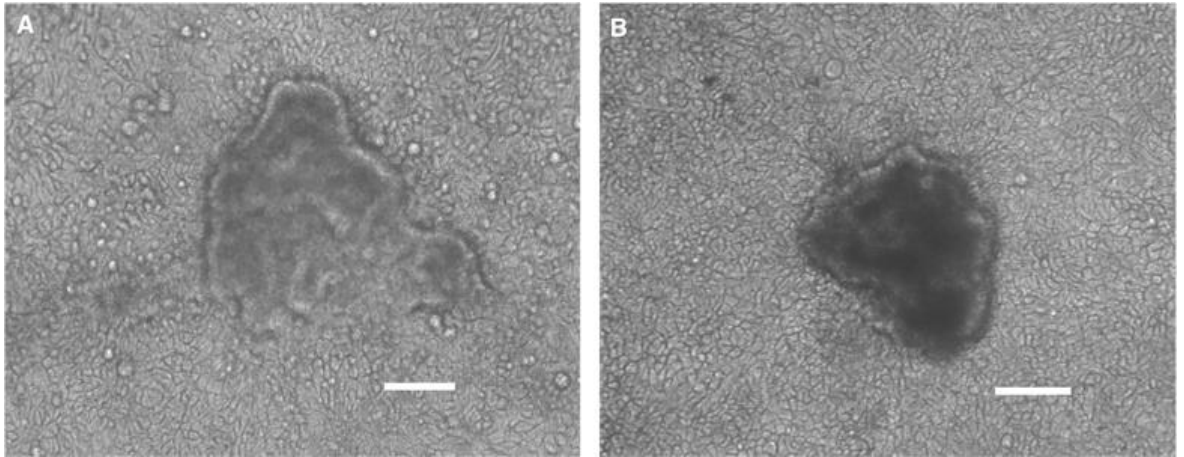


**Figure 27: Phase contrast images of Caco-2 cell sheets cultured on (A) PC and (B) leached PDMS cultured for 21 days. Both show no peeling and similar cell clustering morphology. Representative images. Scale bar = 50  $\mu$ m.**

## Chapter 2

### 2.4 Discussion/conclusion

It is well understood that the protein conformation on a surface of a biomaterial plays a major role in cell attachment (Grinnell and Feld, 1982). The current model for Rsn2's mechanism of surface activity suggests that the surface-active conformation has amphiphilic properties, and we have previously observed that Rsn2 will coat glass as well as hydrophobic surfaces. To show this visually, hydrophilically micro-patterned Topas surfaces were coated with iLOV-Rsn2 and, as expected, the protein coated either region (hydrophilic and hydrophobic). However, by image analysis of the relative fluorescence intensities it can be concluded that iLOV-Rsn2 binds 18% more efficiently to the hydrophobic than to the hydrophilic region. This amphiphilic coating makes Rsn2 a suitable tool for an alternative method of coating both hydrophilic as well as hydrophobic polymers.

In order to achieve a cell compatible surface, both the physical and the chemical properties of the biomaterial can be modified to improve the biocompatibility of the original surface. Various techniques such as plasma treatment, (Hegemann *et al.*, 2003), NaOH treatment (Yang *et al.*, 2002) and photochemical surface modification (Ma *et al.*, 2003) have been widely used to result in a pro-adhesive surface.

When a protein like Rsn2 adsorbs onto a biomaterial surface, this leads to conformational changes and exposure of otherwise buried features. Rsn2 was used in the aim of achieving cell compatibility without the need to plasma treat materials, such as PDMS. The protein supported the DRG cells for a limited period of time. After ruling out cell degradation and protein displacement caused by the so called Vroman effect, which describes the process of protein displacement by less motile proteins that have a higher affinity to the surface (Vroman and Adams, 1969), the cause of the limitation was narrowed down to the nature of the polymer. In summary, experiments using DRGs, indicate that the axonal retraction is polymer dependent and this was confirmed by using a different material as well as the pre-incubation of the samples prior to seeding to show that the Rsn2 protein was still delivering a hydrophilic surface on application.

## Chapter 2

This finding was further explored as a tool for cell sheet extraction of Caco-2 cells which are epithelial cells that are representative of the enterocytes lining of the small intestine and are the best cell culture model available of absorptive small enterocytes extensively used for toxicological and pharmacological studies (Ferruzza *et al.*, 2012). To begin with, a timeline of the cell number at 1,5 and 7 days on PDMS showed that the cells did not adhere or grow on the non-treated control PDMS, probably due to its low biocompatibility. Proliferation on iLOV-Rsn2 however was significantly higher than on the positive, plasma treated and PLL coated control, indicating that this fluorescent amphiphile provides a surface very supportive of cell adhesion, growth and proliferation, with cells having a much higher affinity compared to the simple Rsn2 construct alone. The preference of cells for iLOV-Rsn2 over Rsn2 is not clearly understood, although surface density and conformation of polypeptide sequences exposed on the surface are all parameters important for recognition by cells (Lee *et al.*, 2004, Thoumine *et al.*, 2000).

Expression of tight junction proteins is an indication of Caco-2 cell differentiation after reaching a confluent cell layer. This establishment of cell-cell junctions allows the cells to control paracellular permeability across the cell layer (Nasdala *et al.*, 2002). Once cell-cell adhesion is established, the tight junction seals the apical from the baso-lateral space through its protein components, including the transmembrane proteins claudin and occludin, and associated cytoplasmic adaptor proteins such as ZO-1 (Shen, 2012). Tight junction formation was measured; calculating the total lengths at 5,10 and 15 days on both iLOV-Rsn2 and PLL coated PDMS. Both surfaces show an increase in overall cell-cell junction length over time confirming the utility of either Rsn2 as a means to aid in fostering and maintaining a differentiated state.

It is already understood that when PDMS is treated with plasma, over time the polymer undergoes hydrophobic recovery (Fritz and Owen, 1995). Possible explanations for the recovery of surface oxidized PDMS are, according to Fritz & Owen (1995), cracking of the silica like region produced by plasma treatment producing a path for the migration of free PDMS chains from the bulk material to the surface, or due to the migration of free, unreacted polymer chains (particularly LMW species) through the bulk matrix to the surface. Another well-

## Chapter 2

known term “leaching” describes the movement of the LMW species when in contact with solution (Berthier *et al.*, 2012), where the LMW species leach out of the bulk and into the solution. We suspect that although the PDMS that we coated with Rsn2/iLOV-Rsn2 had not been plasma treated, its surface, over time, undergoes a similar process to that termed hydrophobic recovery and/or leaching. Castner and Ratner (2002) demonstrated that the composition of the adsorbed protein layer can differ from the fluid phase composition and changes with time adsorbed. This correlates to the observations of the ability of Rsn2 to support long-term cell culture, as the changes occurring in polymer chemistry are in turn altering the initial layer composition protein formed to change over time.

The ECM is known to be vital to the adhesion, proliferation and differentiation of cells (Gospodarowicz *et al.*, 1978). The removal of cells cultured on a substrate usually requires enzymatic or a mechanical method for removal, which has an effect on cell morphology and the underlying ECM of the cells is damaged. Methods like pNIPAAm and low temperature lift-off techniques in obtaining cell sheets are less-destructive to the ECM layer underlying the cells than other methods as shown by a set of studies carried out by Canavan *et al.*, (2005) comparing the effects on the ECM using pNIPAAm as a non-destructive means for cell harvest alternative compared to the traditional enzymatic methods

PDMS curing is a time and temperature dependent process that does not achieve 100% crosslinking (Regehr *et al.*, 2009). It has been shown that as much as 5% (w/w) of the PDMS remains unreacted, and that these LMW species are mainly responsible for the surface undergoing hydrophobic recovery over time after plasma treatment (Lee *et al.*, 2003). Techniques that have been used to suppress this are either to complete crosslinking, or to neutralize or remove uncured oligomers e.g. by Soxhlet extraction (Kim *et al.*, 2001), serial extractions in organic solvents (Lee *et al.*, 2003) and extended oven baking (Eddington *et al.*, 2006). Due to its hydrophobic nature, PDMS has a high solubility in nonpolar organic solvents resulting in swelling of the polymer (Lee *et al.*, 2003) and the swelling of the polymer network increases solvent availability to uncured oligomers within the bulk and facilitates the removal of these oligomers (Regehr *et al.*, 2009).

## Chapter 2

In order to establish whether the movement of LMW species was the prime reason for cell peeling, serial extractions of PDMS were carried out prior to seeding and the cell morphology was comparable to that of cells cultured on PC. To further confirm the PDMS surface had become hydrophobic after peeling, XPS was used to assess surface chemistry after peeling. To enable this, it was important to tag Rsn2, making it distinguishable from other proteins that may have replaced the PDMS surface. Typically iodine is used to label proteins, however in this instance the iodine would most likely disrupt the Rsn2 function. Alternatively, the His tag already placed in Rsn2 for purification purposes was used to directly label Rsn2 using copper. Copper ions bind to the His tag very efficiently, with a higher binding affinity than other metals like nickel or cobalt.

The complete detachment of cells from surfaces may indicate an unfavourable interaction between the cell and its local environment (Lee *et al.*, 2004). Lee *et al.*, (2004) discusses how excess curing agent in the polymer may inhibit certain cell types from reaching confluence. In keeping with this paper, the authors further discuss that the growth of a particular cell type can be suitably cultured by choosing the correct processing conditions of PDMS and assembling devices suitably to favour cell attachment and growth of the chosen cell type.

The work in this chapter has shown that Rsn2 can be successfully adsorbed to PDMS substrates and modifies this surface from one that is hydrophobic, and prevents cell attachment, to a more hydrophilic, cell adhesion compatible surface. The iLOV version was more effective as seen from greater proliferation rates and better tight junction formation and is suitable for producing cell sheets without the need for enzymatic or mechanical dissociation, enabling the use of these cell sheets for various tissue-engineering applications.

## **Chapter 3**

### **Physical substrates factors affect NGF response in individual neurons**

## Chapter 3

### 3.1 Introduction

Nerve repair is still a major challenge in surgery as the use of nerve conduits is limited to short distance repair. To replace the gold standard of autologous nerve transplantation, research has focused on functionalizing nerve guidance channels in order to enhance regeneration across larger nerve gaps. Many modifications to the common hollow tube have been designed to increase the gap length that can be successfully/reliably bridged and improve their characteristics; these include growth permissive substrates, surface modifications, trophic factors and glial cells or other support cells (Bellamkonda, 2006).

Growth factors play a major role in nerve regeneration as they enhance functional regeneration by supporting axonal growth, Schwann cell migration and proliferation. Research using growth factors to aid repair has focused on the use of NGF, as it is a known promoter of neuronal outgrowth and branching. The NGF concentration usually present in human and rat serum is in the range of pg/ml (Fawcett and Asher, 1999), the concentration however is increased at an injury site where NGF is secreted by Schwann cells in the bands of Bungner aiding the regeneration process (Fu and Gordon, 1997). The dose of NGF required to achieve optimal regeneration is still under investigation.

The effect of NGF on neuronal cells is varied as it influences: proliferation, differentiation, survival and death of neuronal cells. NGF signals through the *trkA* receptor that activates common intracellular signalling intermediates including Ras, MAPK, phosphoinositide 3-kinase (PI 3-K) and the serine-threonine kinase Akt (Kaplan and Miller, 2000). The signal transduction pathway responsible for regulating cytoskeletal organisation is the Rho-ROCK pathway (Guan and Rao, 2003), and the molecules responsible for the assembly of contractile actin and myosin filaments are Rho, Rac and cell division cycle-42 (Cdc42). Rho has three isomers: Rho-A, Rho-B and Rho-C, the isomer which is mainly found in a neuron is Rho-A (Erschbamer *et al.*, 2005). Rho exists in two forms, one is the non-activated form combined with Guanosine-5'-diphosphate (GDP) and the other is the activated form combined with Guanosine-5'-triphosphate (GTP) (Fauré and Dagher, 2001). The exchange of Rho-GDP to Rho-GTP is mediated by guanine exchange factors (GEFs). Activated Rho is linked

### Chapter 3

to an increase in acto-myosin contractility by regulating the phosphorylation of myosin light chain (MLC). (Amano *et al.*, 1996) (Summarised in figure 28).

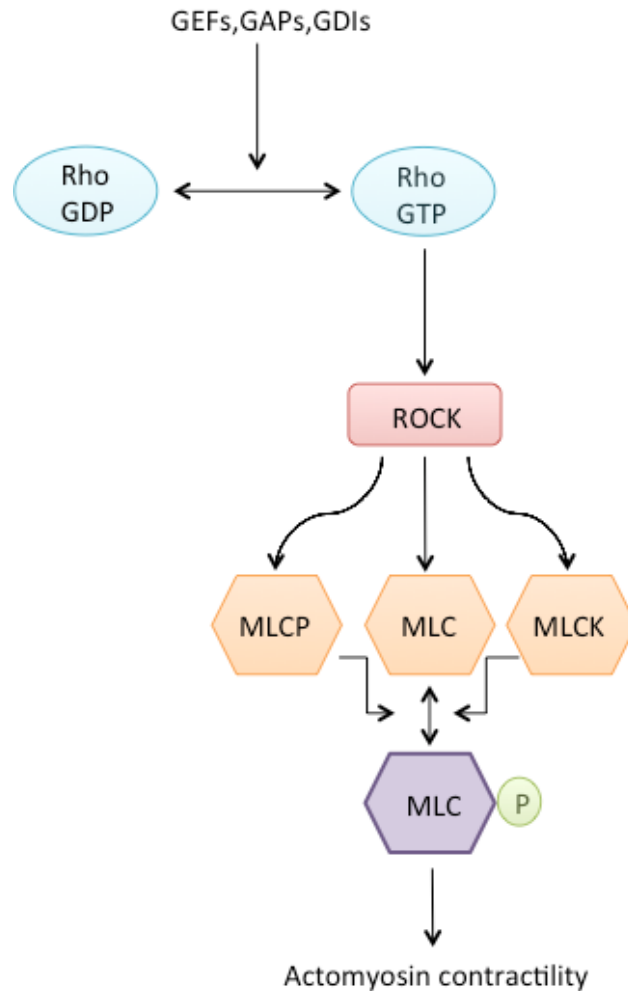


**Figure 28: Signal transduction pathway of the Rho GTPases in regulation of cytoskeleton organisation. Adapted from (Guan and Rao, 2003). The Rho GTPases are regulated by GEFs (guanine nucleotide exchange factors) and inactivated by GAPs (GTPase activating protein). Activated ROCK regulates MLC and its phosphorylation results in an increase in actomyosin contractility.**

### Chapter 3

Surface topography and mechanical properties of substrates are crucial factors to consider in nerve tube design as these structures can have profound effects on cell formation and function (Flanagan *et al.*, 2002). Grooved substrates have been used to guide astrocytes and neurites in *in vitro* models of the CNS and PNS with success (Deumens *et al.*, 2004, Johansson *et al.*, 2006, Sorensen *et al.*, 2007). In our lab, varying groove widths and depths have been previously studied and the best cell response was achieved using 12.5  $\mu\text{m}$  width and 5  $\mu\text{m}$  depth.

As discussed previously, numerous ECM proteins have been considered suitable candidates for surface functionalization of nerve guidance tubes including collagen, fibronectin and laminin (Koh *et al.*, 2010). As laminin appears to be among the most potent ECM proteins, affecting virtually all neurons of the PNS, it is widely used to coat biomaterials for its capacity to enhance neuronal survival. Many researchers that study various aspects of individual neurons *in vitro*, use laminin to treat the surface of chosen scaffolds (Huang *et al.*, 2008, Liu *et al.*, 2013). In this study two surface coatings were analysed, one of which was laminin and the other PLL.

The background work to this chapter was carried out by Théophile Déjardin (Déjardin, 2013) who has shown that a whole DRG was influenced by modulations of substrate stiffness, topography and NGF concentration, where substrate cues interact with growth factor activity to modulate axonal outgrowth. The findings show that the area covered by axonal networks on flat PDMS increased with higher NGF concentrations whereas on grooved PDMS, the length of the axons decreased with increasing NGF concentrations. This suggests that the modulation is the result of the combination of the topographical cue and NGF signalling.

When studying the response of explants, more than 5 different cell types could have been responsible for the modulation observed. The aim of this chapter was to establish which of these cell types is responsible; therefore individual sensory neurons dissociated from the DRGs were used, to determine if factors such as topography and differing NGF concentrations similarly affect axonal outgrowth at the single cell level. This was achieved by seeding dissociated DRG neurons onto PDMS substrates with or without micro-grooves, and cultured with varying NGF concentrations of 10, 50 and 100 ng/ml. As the changes in outgrowth are likely to do with cytoskeletal organisation, the cells were further characterised

**Chapter 3**

to find a relationship between how the changes affect cell morphology and axonal outgrowth. To understand if cytoskeletal contractility was responsible for the observed differences in axonal outgrowth, ROCK (Y-27632) and myosin II (Blebbistatin) inhibitors were used.

## Chapter 3

### 3.2 Materials and methods

#### 3.2.1 PDMS fabrication (flat and Grooves)

PDMS 184 polymer solution 90% (wt/wt) (Sylgard® 184 Silicone Elastomer, Dow Corning, UK) was added to 10% (wt/wt) curing agent. This was mixed very well in a disposable cup and the mixture was degassed under vacuum for 20 mins. For planar controls, the degassed PDMS was poured directly into a petri dish to make a flat surface while grooved PDMS substrates were created by syringing the PDMS mixture into a casting jig with the grooved silicon wafer master (12.5  $\mu\text{m}$  width, 5  $\mu\text{m}$  depth). The PDMS was cured in an 80°C oven for 2 hours then left to cool before removing and cutting the samples to individual 11 mm diameter devices with a cork borer.

#### 3.2.2 Sample sterilization and preparation

Samples were sterilized prior to seeding by immersing them in 70% ethanol for 30 mins followed by 2 washes in PBS and then dried with a flow of 0.22  $\mu\text{m}$  filtered compressed air in a laminar flow cabinet to avoid contamination. Samples of PDMS were treated at for 1 min with air plasma generated using a Harrick Plasma PDC-002 cleaner at 29.6 W. After plasma treatment, the surfaces were coated in PLL solution for 30 mins at 37°C. For laminin coating, the samples were first coated in PLL solution as described, followed by a 2-hour incubation at 37°C with laminin (12  $\mu\text{g}/\text{ml}$ , Sigma). Each sample was rinsed 2x in PBS before seeding cells.

#### 3.2.3 Dissociation of DRGs into single cells

DRGs were isolated from neonatal (1-5 days old) Sprague-Dawley rats. Rats were euthanized by a Euthatal® injection (500mg/Kg) according to Home Office regulations and then dissected. After extraction, the DRGs were placed in a 35mm culture dish containing 2 ml trypsin/EDTA (0.125%/0.05%, Sigma, UK) and incubated at 37°C for 30 mins. After digestion, ganglia were transferred to a centrifuge tube containing 5 ml L15 media containing FBS (10%, Life technologies, UK) and DNase (10  $\mu\text{g}/\text{ml}$ , Life technologies, UK). This was titrated with a Pasteur pipette until suspension was homogenous after which it was centrifuged at 250 g for 10 mins. The cells were cultured in Neurobasal® media

### Chapter 3

(Life technologies, UK) containing B27 supplement (2%, Life technologies, UK), Pen/strep (1%, Sigma, UK), L-Glutamine (0.5 mM, Life technologies, UK), Glucose (2.5g/L, Fisher Scientific), FBS (1%, Life Technologies, UK) and NGF (10, 50 or 100 ng/ml, 2.5 S Invitrogen, UK). Cells were seeded at low density onto PDMS samples and were incubated at 37°C 5% CO<sub>2</sub> for 1, 4 or 10 days. The media was exchanged every 2 days when required.

#### 3.2.4 Immunofluorescence

After growth, DRGs were washed with PBS and fixed for 15 mins in a formaldehyde (10%, Fisher Scientific)/PBS solution containing sucrose (2% w/v, Fisher Scientific). Following fixation, the cells were permeabilised using a solution of sucrose (10.3%), NaCl (0.292%, AnalaR Normapur), MgCl<sub>2</sub> (0.06%, AnalaR Normapur), HEPES (0.476%, Fisher Scientific) and Triton X-100 (0.5%, Sigma, UK) per 100ml PBS at 4°C for 5 mins, followed by an incubation at 37°C in PBS/BSA (1%, Sigma, UK) for 5 mins. The blocking solution was replaced by PBS/BSA solution containing anti-β3-tubulin antibody (1:100, mouse anti-TU-20 Santa Cruz, California) and anti-S100β antibody (1:100 rabbit S100 Abcam, UK). The samples were incubated at 37°C for 2 hours. Samples were then washed thrice with a PBS/Tween®20 (0.5%, Sigma, UK) and then further incubated for an hour in PBS/BSA solution containing biotinylated anti-mouse secondary antibody (1:50, Vector Laboratories) and Texas Red conjugated anti-rabbit antibody (1:50, Vector Laboratories). After incubation, samples were washed thrice with PBS/Tween®. Fluorescein streptavidin (1:50, Vector Laboratories) in PBS/BSA was then added to the samples and incubated at 4°C for 30 mins before washing thrice with PBS/Tween®. To prepare the slides, a small drop of mounting medium containing DAPI (vectorshield-DAPI) was placed on a labelled microscope slide. Samples were viewed on Zeiss Axiovert200 microscope and Zeiss Axiophot (epifluorescence). . DAPI Excitation/Emission (nm) = 358/461, Texas red (FITC) Excitation/Emission (nm) = 596/615 and Fluorescein (TRITC) Excitation/Emission (nm) = 490/525.

Anti-talin antibody (1:500, mouse monoclonal, Sigma, UK) was used for focal adhesion analysis and rhodamine phalloidin (1:200, life technologies) was used to assess F-actin organization, following the same protocol.

### Chapter 3

For sub-population analysis, the primary antibodies used were anti-NF200 (1:1000, rabbit or chicken polyclonal, abcam), somatostatin (1:100, rabbit polyclonal, Santa Cruz), Substance P (1:100, rat monoclonal, Santa Cruz) and anti-CGRP (1:100, mouse monoclonal, Abcam). For secondary antibodies goat anti-rat and anti-chicken (Alexa Fluor® 488, Abcam) as well as Texas Red anti-rabbit were used to identify the different proteins.

#### 3.2.5 Rho & ROCK inhibitors

For inhibitor studies, the dissociated DRG cells were allowed to attach onto the surfaces for 4 hours before the addition of either blebbistatin (50  $\mu\text{M}$  or 100  $\mu\text{M}$ , Abcam) or Y-27632 dihydrochloride (50  $\mu\text{M}$ , Abcam). The samples were incubated in the inhibitors for 24 hours before fixation.

#### 3.2.6 Cell sizing analysis

On a light microscope, brightfield images of dissociated DRG cells were taken 1 hour after seeding. The images were exported to Image J to calculate cell area by using the set measurement tool. In Microsoft Excel, bin widths were defined and the frequency of cell sizes analysed.

#### 3.2.7 Branching analysis

After images of the dissociated DRG cells were obtained and assembled in Photoshop (Adobe), the number of branches was counted manually and a histogram was created on Microsoft Excel.

#### 3.2.8 Neuron length analysis

After images of the individual axons were obtained and assembled in Photoshop (Adobe), each image was processed on Image J (Rasband, 1997-2012) using the Neuron J plugin (Meijering *et al.*, 2004) which allows tracing and quantification of the total neuron length in  $\mu\text{m}$ . Statistical analysis was performed using ANOVA with Dunnett or Tukey post-hoc test for significance between parameters.

## Chapter 3

### **3.3 Results**

#### **3.3.1 Cell characterisation**

The size of individual sensory neurons 1 hour after seeding was determined as shown in figure 30. The variation in size within the culture was due to the presence of different sub-populations within the DRG cells. The cells were stained for a number of neuroactive peptides present in the DRG neuron subpopulations. These included substance P (SP), somatostatin (SOM), Calcitonin gene-related peptide (CGRP) and 200-kilodalton subunits of neurofilaments (NF200) figure 29.

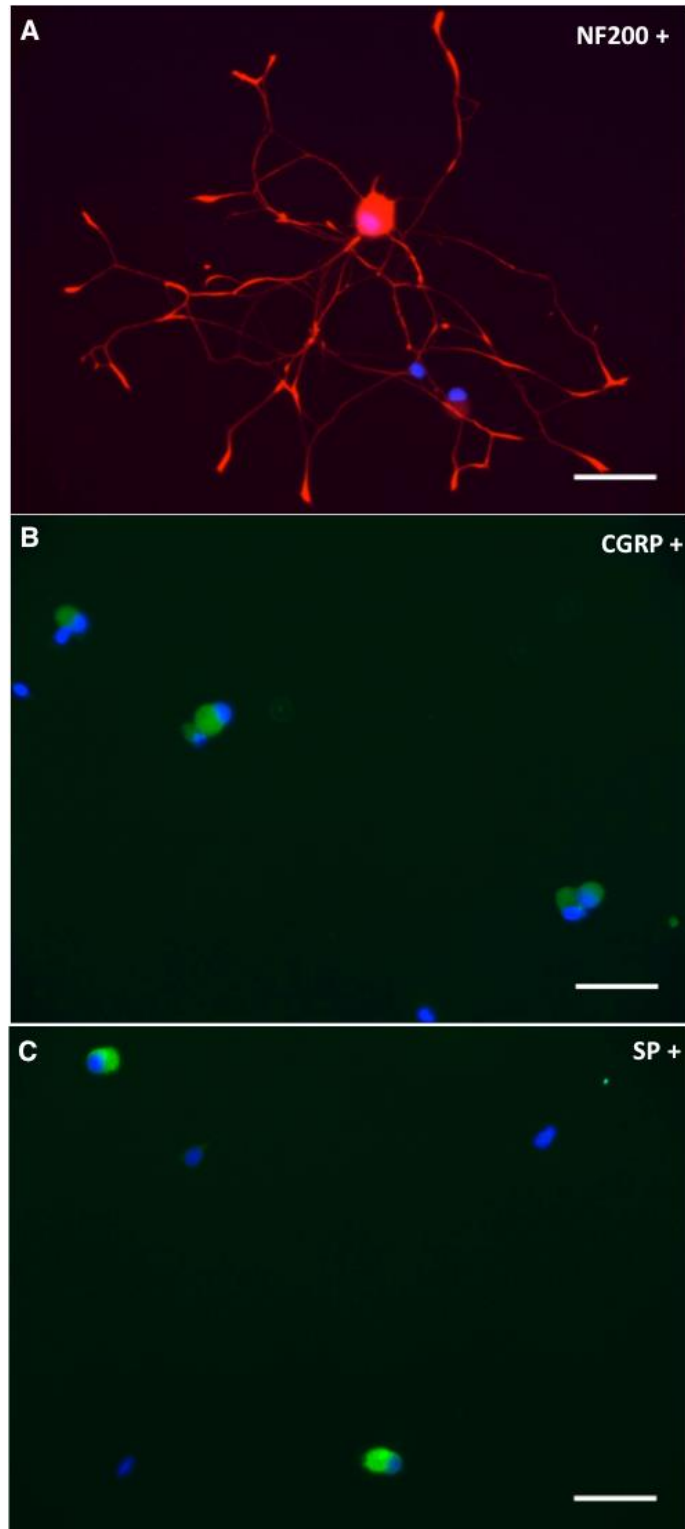
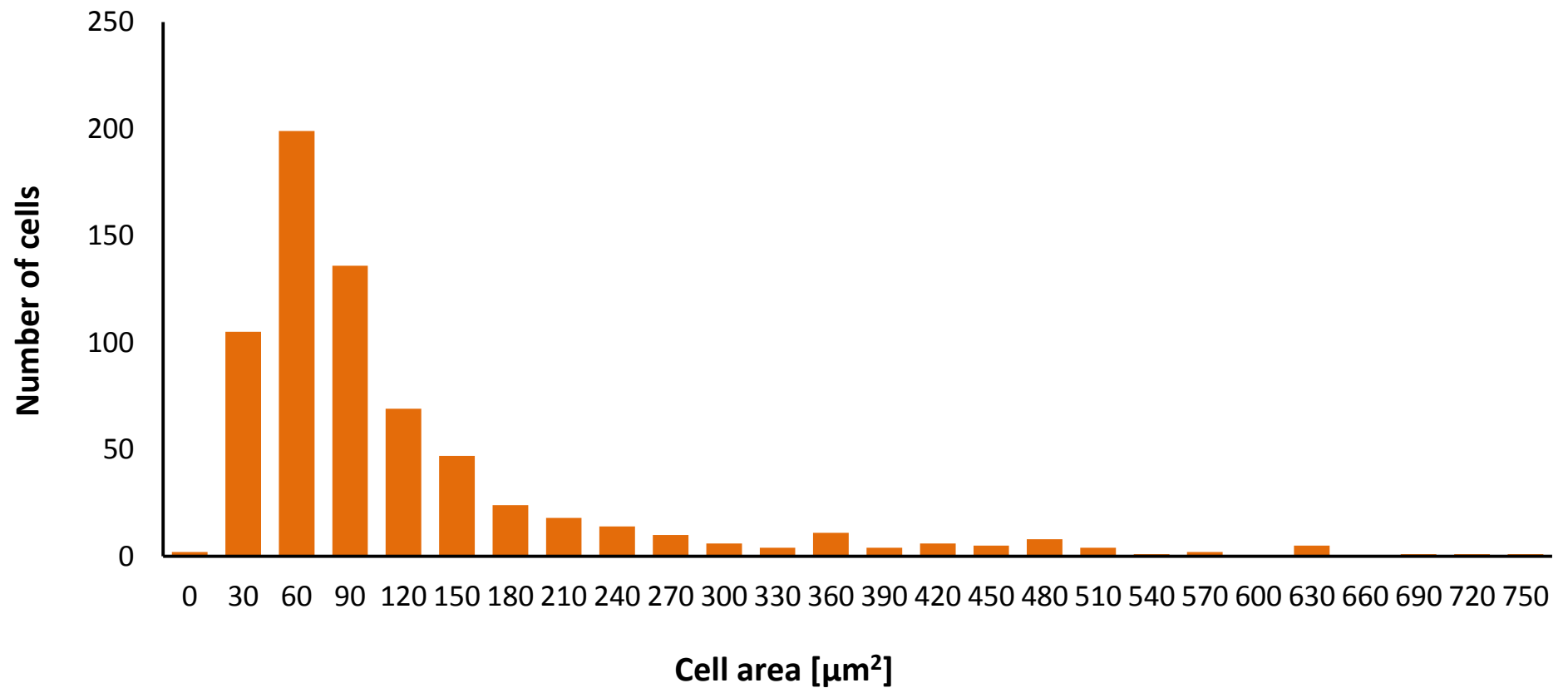


Figure 29: Immunofluorescence images of sensory neurons immuno-labelled for neuroactive peptides NF200 (red), SP or CGRP (green) and nuclei (blue) to determine cell population distribution. The cells were cultured on PLL coated PDMS (flat). The images represent NF200 positive cell (A), CGRP positive cells (B) and SP positive cells (C). No SOM positive cells were detected. Representative images. Scale bar =50  $\mu$ m.



**Figure 30:** The graph represents the cell area ( $\mu\text{m}^2$ ) of individual sensory neurons after seeding on PLL and laminin coated PDMS (flat). The variation of cell size is due to the presence of different cell subpopulations within the DRG neurons. (n= 3 biological repeats, multiple fields of view were examined for analysis, total of 686 cells).

## Chapter 3

### 3.3.2 Length of individual neurons (10 day culture)

The axonal length of individual neurons isolated from a DRG and cultured on flat PLL coated PDMS substrates increased with increasing NGF concentrations (figure 31,  $p < 0.05$ ), when cultured for a period of 10 days. In contrast, the overall axonal length decreased with increasing NGF concentration for DRG neurons cultured on the flat laminin coated PDMS (figure 32,  $p < 0.01$ ). The different coatings also affected the network shape. Axons associated with neurons cultured on PLL extended in a linear fashion at all concentrations of NGF (figure 31). In comparison neurons cultured on laminin demonstrated extensive branching at the lowest concentrations of NGF with the number of branches decreasing with increasing NGF concentrations (figure 32).

Axonal networks extending from cells cultured on microstructured PDMS were guided along the grooves. Axons on both PLL and laminin coated grooved PDMS, decreased with increasing NGF concentrations. Although the overall axonal length decreased on both protein coatings, the shape of the network is dissimilar. Axons extending on the PLL coating followed the grooves in a less structured manner (figure 33 & 36) particularly at the highest concentration of NGF. Extensions formed on the laminin-coated substrates follow the pattern of the grooves effectively on all the NGF concentrations tested (figure 34 & 36).

Overall axonal lengths recorded on the different surfaces after a 10 day culture are represented in figure 35. From this, we have shown that the individual neurons extracted from a DRG are also influenced by variation in NGF concentration. In order to gain a full understanding of the mechanisms underlying the outcome of this data, it was deemed necessary to reduce the complexity of the results by reducing the time of culture to 24 hours.

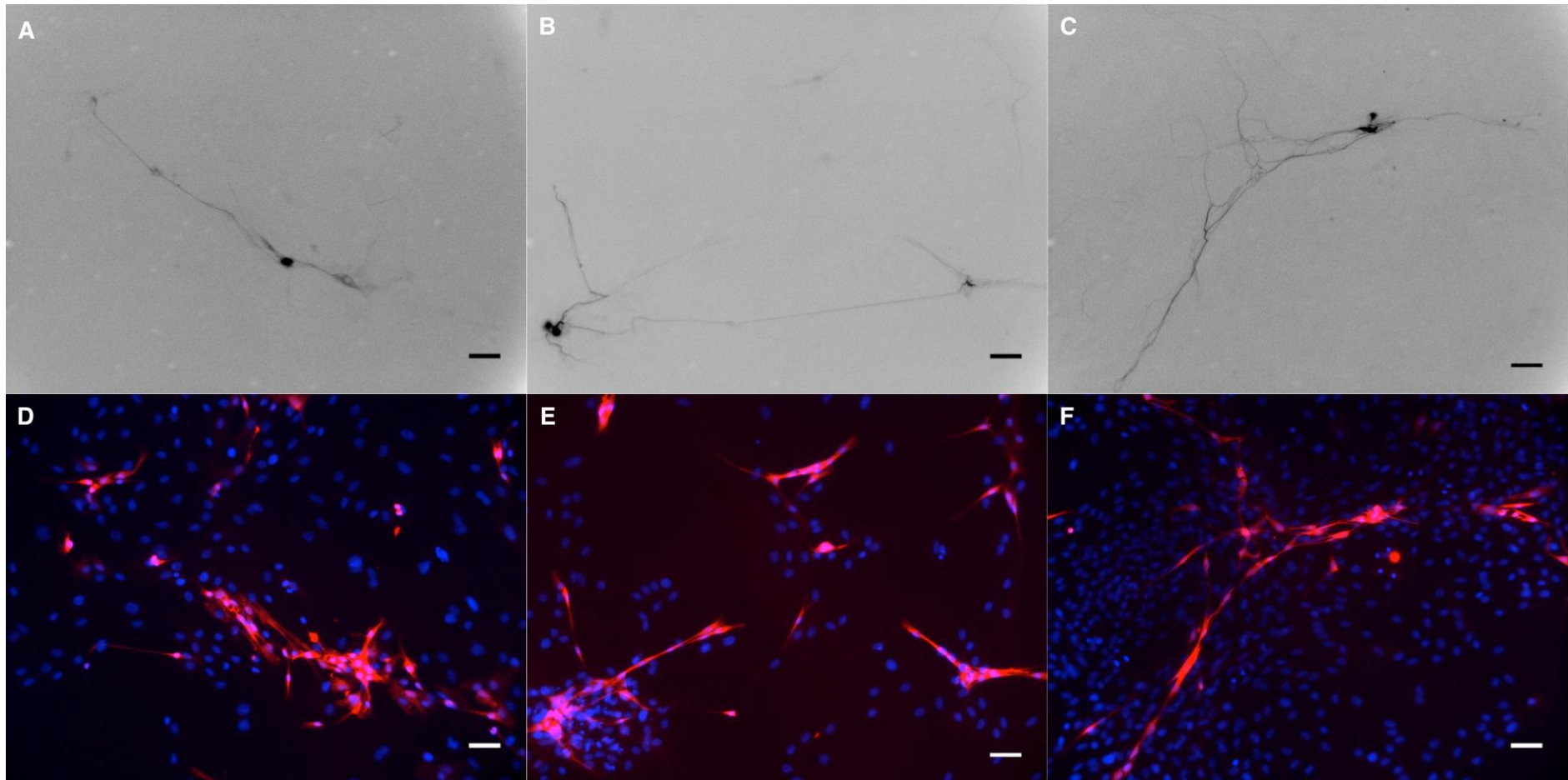


**Figure 31: Immunofluorescence images of sensory neurons immuno-labelled for  $\beta$ 3-tubulin (A-C inverted grey-scale images) on PLL coated PDMS (flat). Cells were cultured for 10 days at (A) 10 ng/ml (B) 50 ng/ml (C) 100 ng/ml of NGF. The axons extend from the neurons after plating, with the length of the axons increasing with NGF concentration. Images (D-F) show the S100 $\beta$  positive Schwann cells (red) that follow the outgrowth of the axons and the nuclei (blue, DNA) of all other structural cells. Scale bar = 50  $\mu$ m**

## Chapter 3

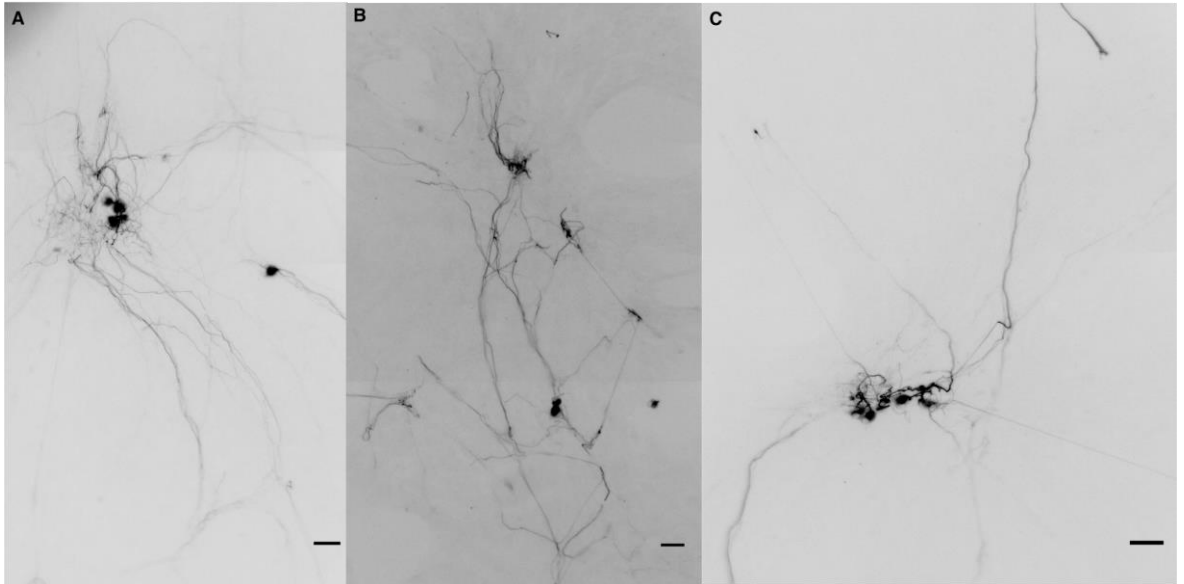


**Figure 32:** Immunofluorescence images of sensory neurons immuno-labelled for  $\beta$ 3-tubulin (inverted grey-scale images) on laminin coated PDMS (flat). Cells were cultured for 10 days at (A) 10 ng/ml, (B) 50 ng/ml, and (C) 100 ng/ml of NGF. The axons branch out in a random manner, the length of the total axonal outgrowth decreases with NGF concentration. Scale bar = 50  $\mu$ m

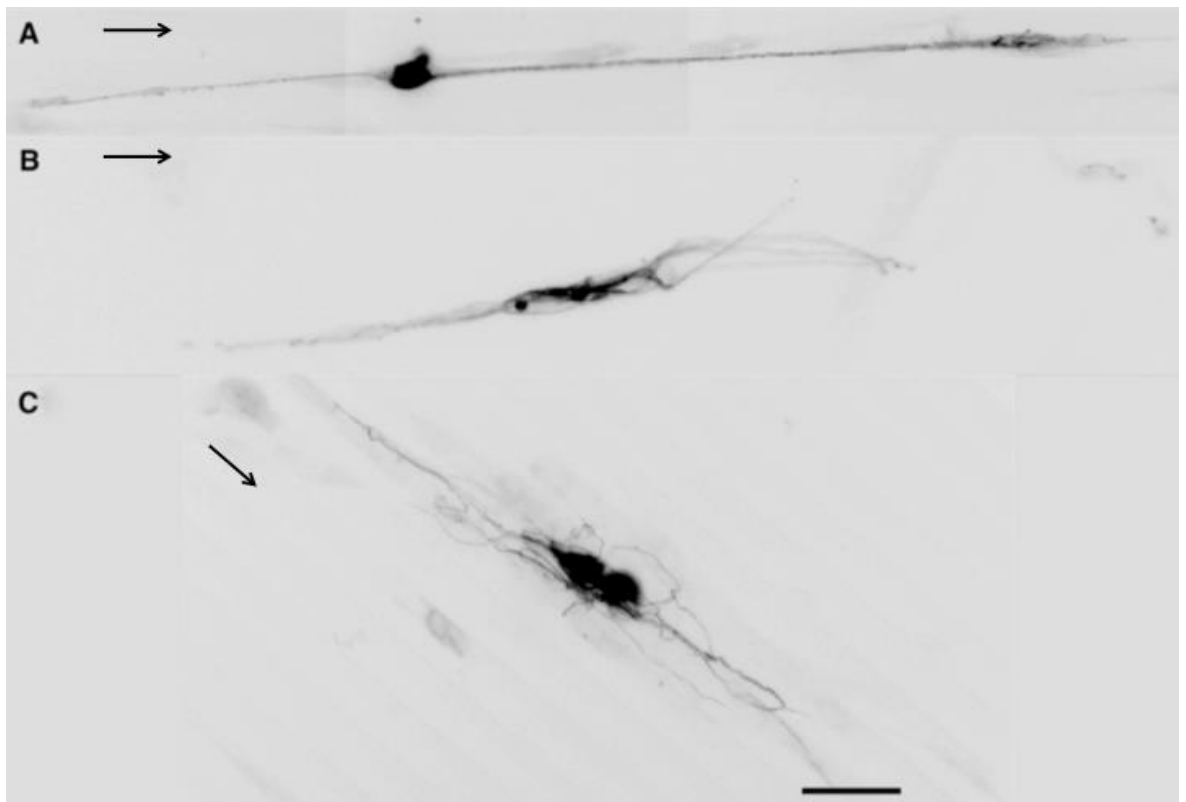


**Figure 33:** Immunofluorescence images of sensory neurons immuno-labelled for  $\beta$ 3-tubulin (inverted grey-scale images) on PLL coated PDMS (grooves). Cells were cultured for 10 days at (A) 10 ng/ml, (B) 50 ng/ml, and (C) 100 ng/ml of NGF. The axons extend by following the orientation of the grooves, but less so with increasing NGF concentration as seen in B (50 ng/ml) and C (100 ng/ml). The length of the total axonal outgrowth decreases with NGF concentration. Arrows show groove orientation. Scale bar = 50  $\mu$ m.

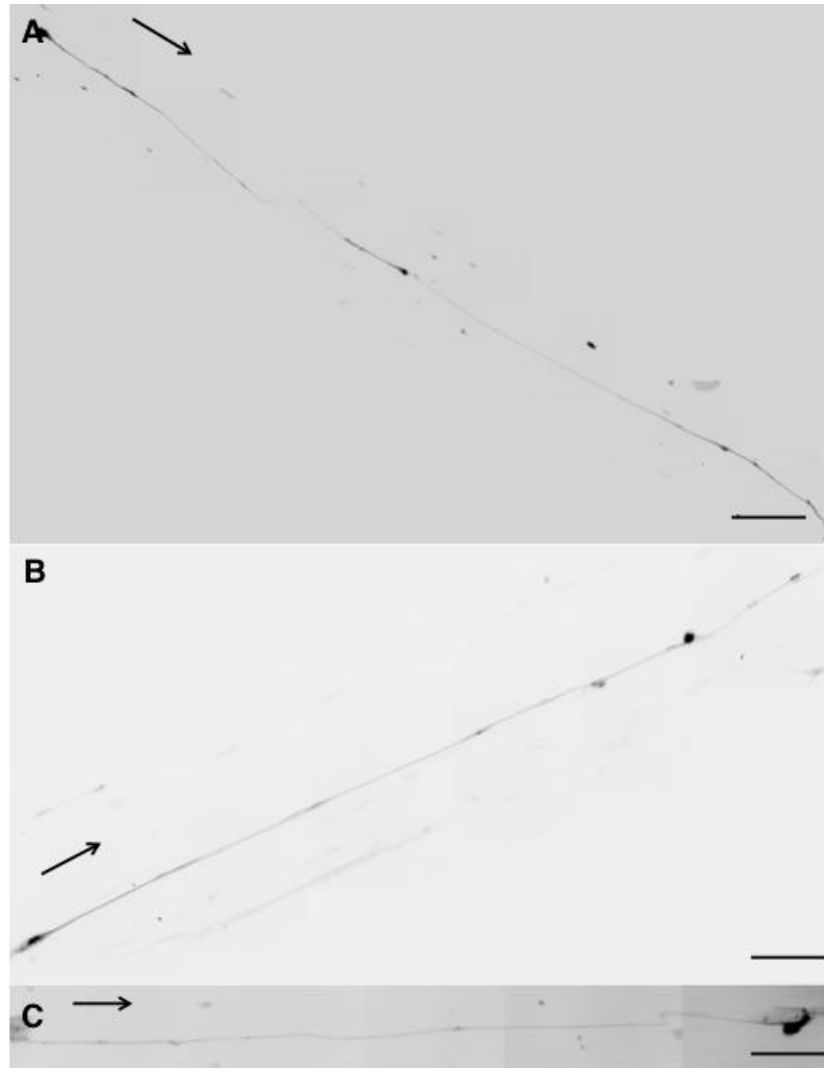


**Figure 34:** Immunofluorescence images of sensory neurons immuno-labelled for  $\beta$ 3-tubulin (inverted grey-scale images) on laminin coated PDMS (grooves). Cells were cultured for 10 days at (A) 10 ng/ml, (B) 50 ng/ml, and (C) 100 ng/ml of NGF. The axons extend along the grooves following their orientation, the length of the total axonal outgrowth decreases with increasing NGF concentrations. Arrows show groove orientation. Scale bar = 50  $\mu$ m

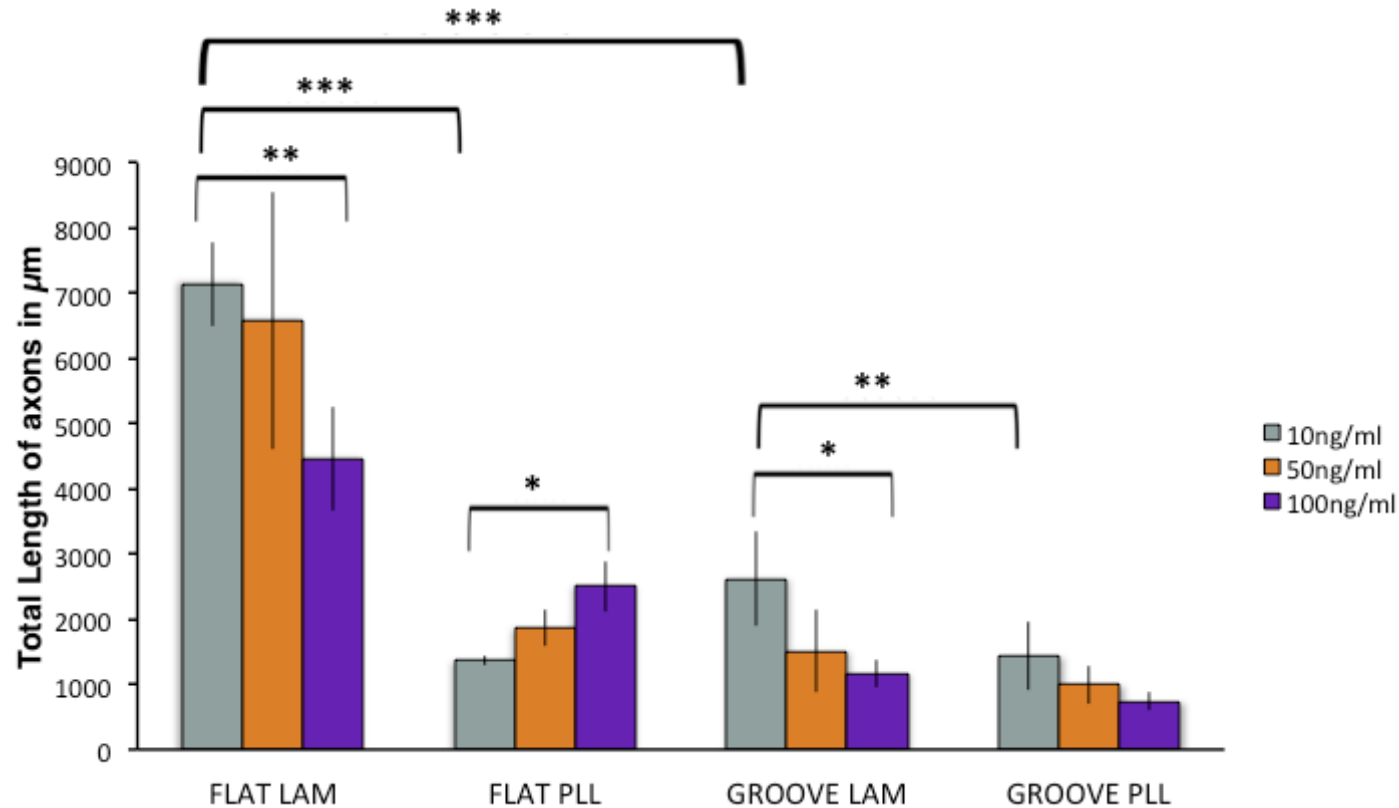


**Figure 35: Axon length of individual sensory neurons after a 10-day culture on PLL coated (flat or microgrooved) and laminin coated (flat or microgrooved) PDMS. On the PLL coated PDMS (flat), axonal length increased significantly with increasing NGF concentration. Compared to the flat, on microgrooves axon length was reduced with increasing NGF concentration. On the laminin coated PDMS (flat) axon length decreased significantly from 10ng/ml to 100ng/ml as did the length of the axons on the microgrooves. Stars indicate significant differences between groups as determined by ANOVA and Tukey's post hoc test \* $p < 0.05$  \*\* $p < 0.01$  and \*\*\* $P < 0.001$ . (n=3 biological repeats, multiple fields of view (10 per sample) were examined for analysis). The bars indicate standard deviation.**

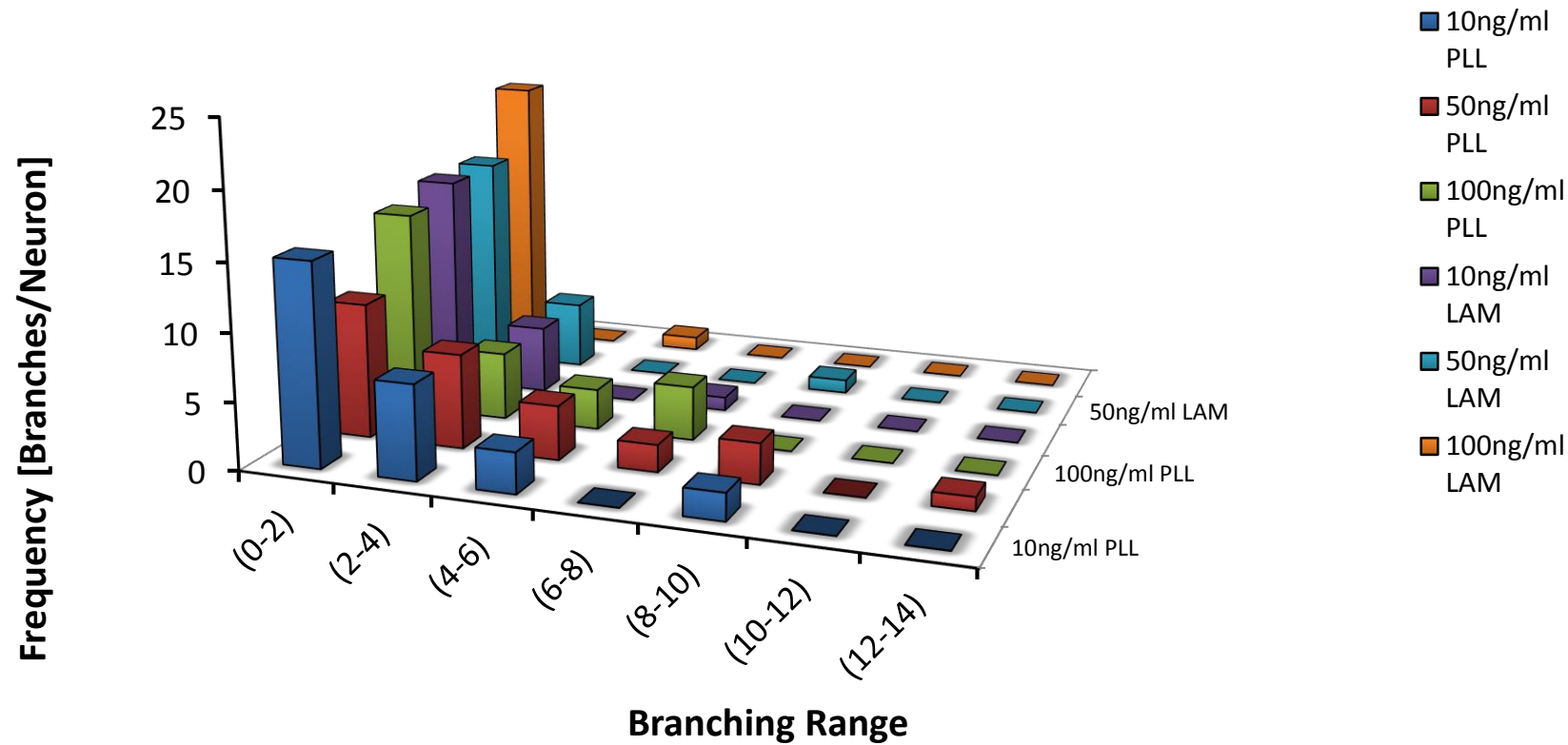


**Figure 36:** The graph represents the number of branches formed on PDMS (grooves) coated with either PLL or laminin (LAM) cultured for 10 days in varying NGF concentrations of 10 ng/ml, 50 ng/ml and 100 ng/ml ng/ml. No change in branching was observed with increasing NGF concentrations, however the laminin surface reduced the number of branches. (n=3 biological repeats, multiple fields of view (10 per sample) were examined for analysis).

## Chapter 3

### 3.3.3 24-hours outgrowth and contractility tests

By reducing the time of culture to 24 hours, the presence of Schwann cells was minimized, and the neurons followed the same behavioural trend, where increasing the NGF concentration resulted in increased axon outgrowth, similar to that observed at the 10-day time point on both the flat and grooved surfaces (figure 37).

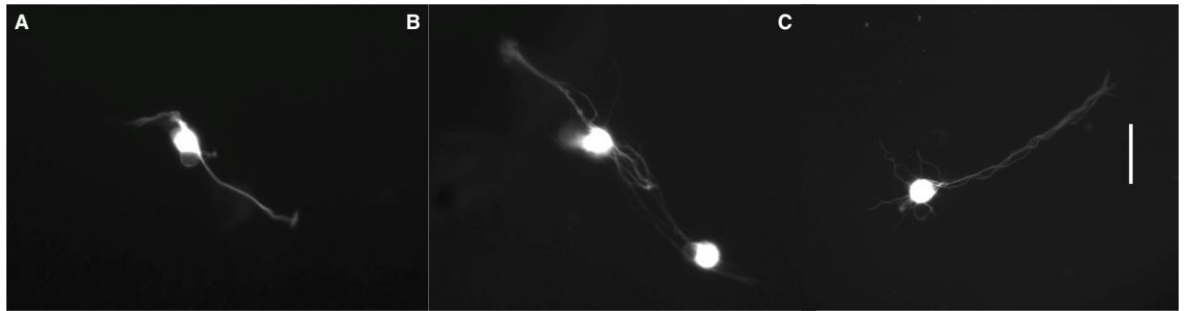


**Figure 37:** Immunofluorescence images of sensory neurons immuno-labelled for  $\beta$ 3-tubulin (grey-scale) cultured on PLL coated PDMS (flat). Cells were cultured for 24hs at (A) 10 ng/ml, (B) 50 ng/ml and (C) 100 ng/ml of NGF. The axons extended from the neurons after plating, with the length of the axons increasing with NGF concentration. Scale bar = 50  $\mu$ m.

The behaviour of the individual neurons after a 24-hour culture suggests that the modulation in axonal outgrowth observed after 10 days on flat vs. grooved topography is not a collaborative effect involving other cell types. To understand if cytoskeletal contractility was responsible for the differences observed in axonal outgrowth, a ROCK and a myosin II inhibitor, which affect cytoskeletal contractility, were used to influence growth cone dynamics. The inhibitors work by blocking the NGF signalling pathway that is involved in regulating actin dynamics at the growth cone, and by inhibiting actin/myosin contractility.

Analysis of the 24-hour axonal outgrowth on PLL coated flat PDMS shows that the neurons followed the same trend of increasing axonal length with increasing NGF concentrations, as observed on explant and the 10-day culture using dissociated individual cells. Upon the addition of Blebbistatin, the outgrowth was accelerated but still mirroring the trend of longer axonal extensions with increasing NGF concentrations. When the ROCK inhibitor Y-27632 was added, the extent of outgrowth observed was comparatively small, and neither influenced

### Chapter 3

by the amount of NGF present, nor by topography (summarised in figure 38 & 39).

The outgrowth on PLL coated grooved PDMS, again shows a similar trend to that observed on the explant and 10-day culture of individual cells when overall axonal length decreased with increasing NGF concentration. In contrast upon the addition of blebbistatin, outgrowth increased and it followed the same trend as blebbistatin treated flat PDMS, meaning that with increasing concentrations of NGF (figure 40) the length of outgrowth increased. These suggest that by inhibiting the acto-myosin contractility and Rho-ROCK pathway, the topographical cue given by the grooves is ignored by the cells. When the ROCK inhibitor Y-27632 was added, the outgrowth was grossly reduced and the trend of an increased outgrowth with increasing NGF concentrations, observed on the control is inhibited (results summarised in figure 40 & 41).

Staining for actin was carried out to assess how the addition of the inhibitors affected the actin cytoskeleton. The non-treated control demonstrated well-structured axonal extensions typical of a healthy neuron (figure 42A&B). However, the addition of Blebbistatin resulted in accelerated outgrowth, which in turn caused damage to the underlying actin where the actin was unstructured when forming extensions (figure 42C). The inhibition of ROCK by Y-27632 reduced outgrowth significantly ( $p < 0.001$ ,  $n=3$ ) with very little evidence for the presence of F-actin (figure 42D).

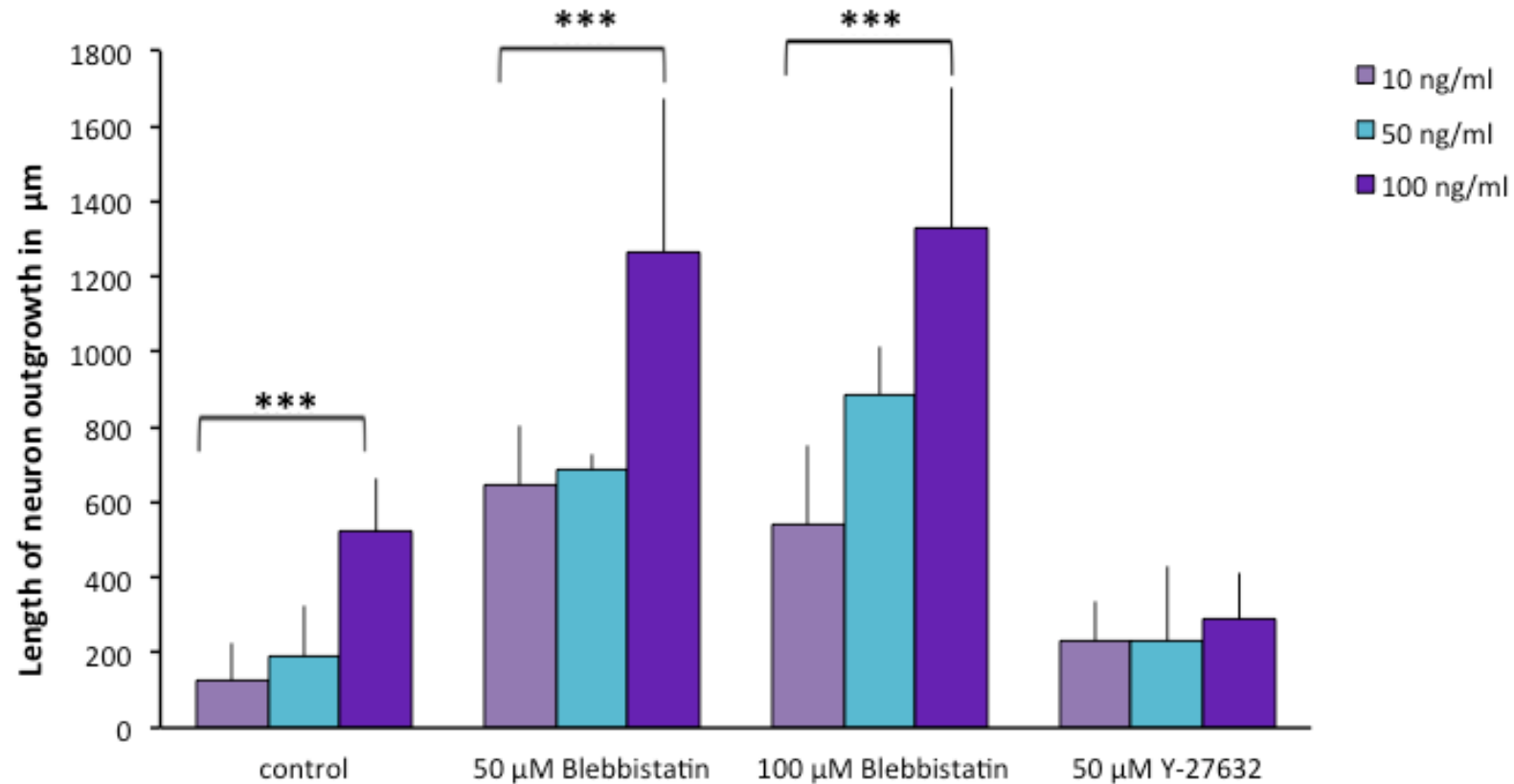


**Figure 38:** Axon length of individual sensory neurons after 24-hour culture on PLL coated PDMS (flat) samples with varying NGF concentrations of 10 ng/ml, 50 ng/ml and 100 ng/ml. Positive control – PLL coated PDMS (non-treated). Inhibition of myosin II was achieved by the addition of Blebbistatin (50 μM or 100 μM). The Rho-ROCK pathway was inhibited by the addition of Y-27632 (50μM). The pattern observed on the control was comparable to the 10-day time point where the axon length increased significantly with increasing NGF concentration. Upon the addition of blebbistatin, the pattern of outgrowth was similar to that of the control but with larger axonal extensions. Y-27632 inhibited the pattern of outgrowth observed with increasing NGF concentrations. Stars indicate significant differences between groups as determined by ANOVA and a Dunnett post hoc test \*\*\*P<0.001. (n=3 biological repeats, multiple fields of view (10 per sample) were examined for analysis). The bars indicate standard deviation.

## Chapter 3

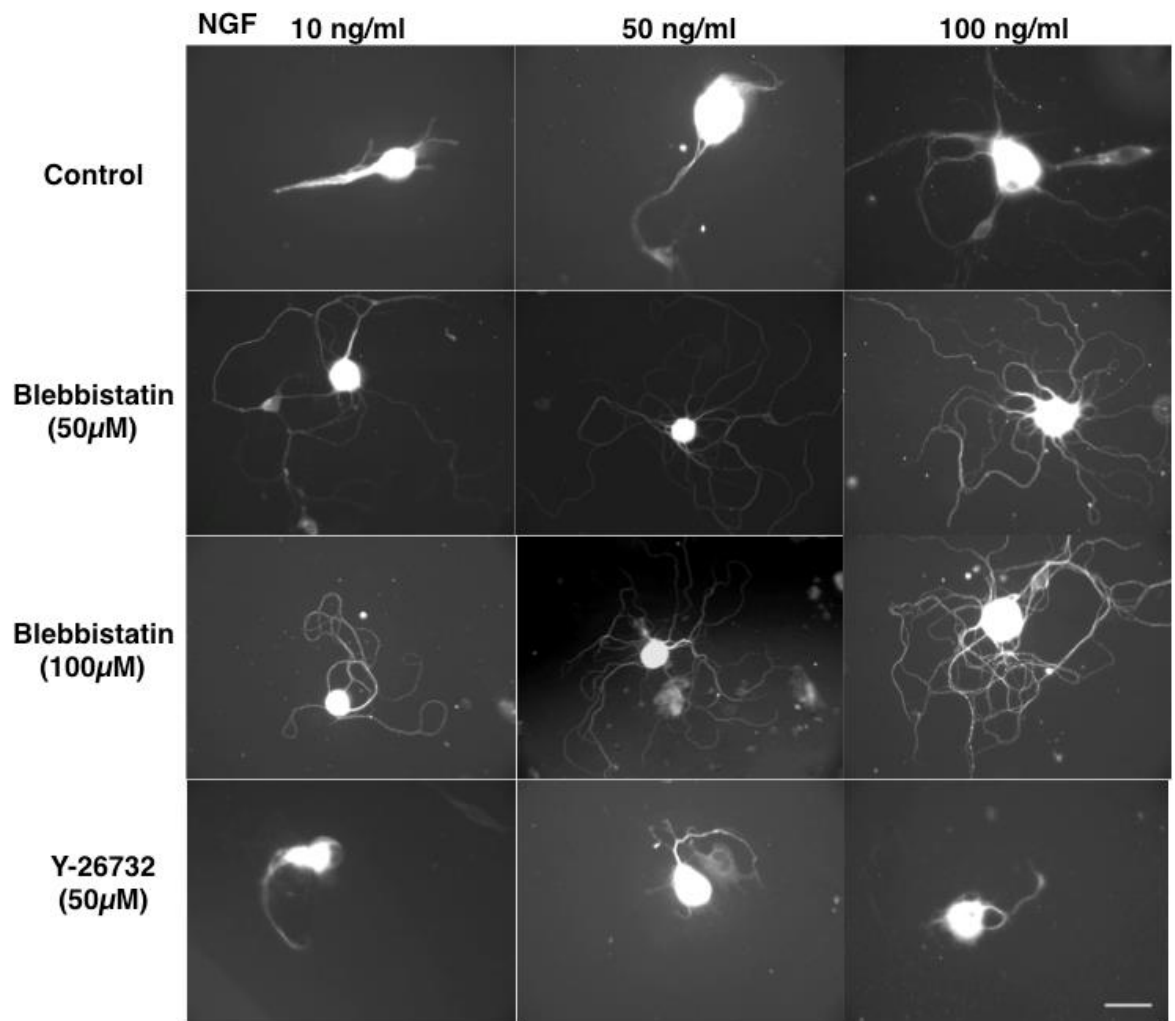


**Figure 39:** Immunofluorescence images of sensory neurons immuno-labelled for  $\beta$ 3-tubulin (grey-scale) cultured on PLL coated PDMS (flat) at 10 ng/ml, 50 ng/ml and 100 ng/ml of NGF. Inhibition of myosin II was achieved by the addition of Blebbistatin (50  $\mu$ M or 100  $\mu$ M). The Rho-ROCK pathway was inhibited by the addition of Y-27632 (50  $\mu$ M). Pattern observed on the control was comparable to the 10-day time point where the axonal length increased significantly with increasing NGF concentration. Upon the addition of Blebbistatin, the pattern of outgrowth was similar to that of the control but with longer axonal extensions. Y-27632 grossly inhibited overall outgrowth and no change in outgrowth could be seen with increasing NGF concentrations. Scale bar = 50  $\mu$ m.

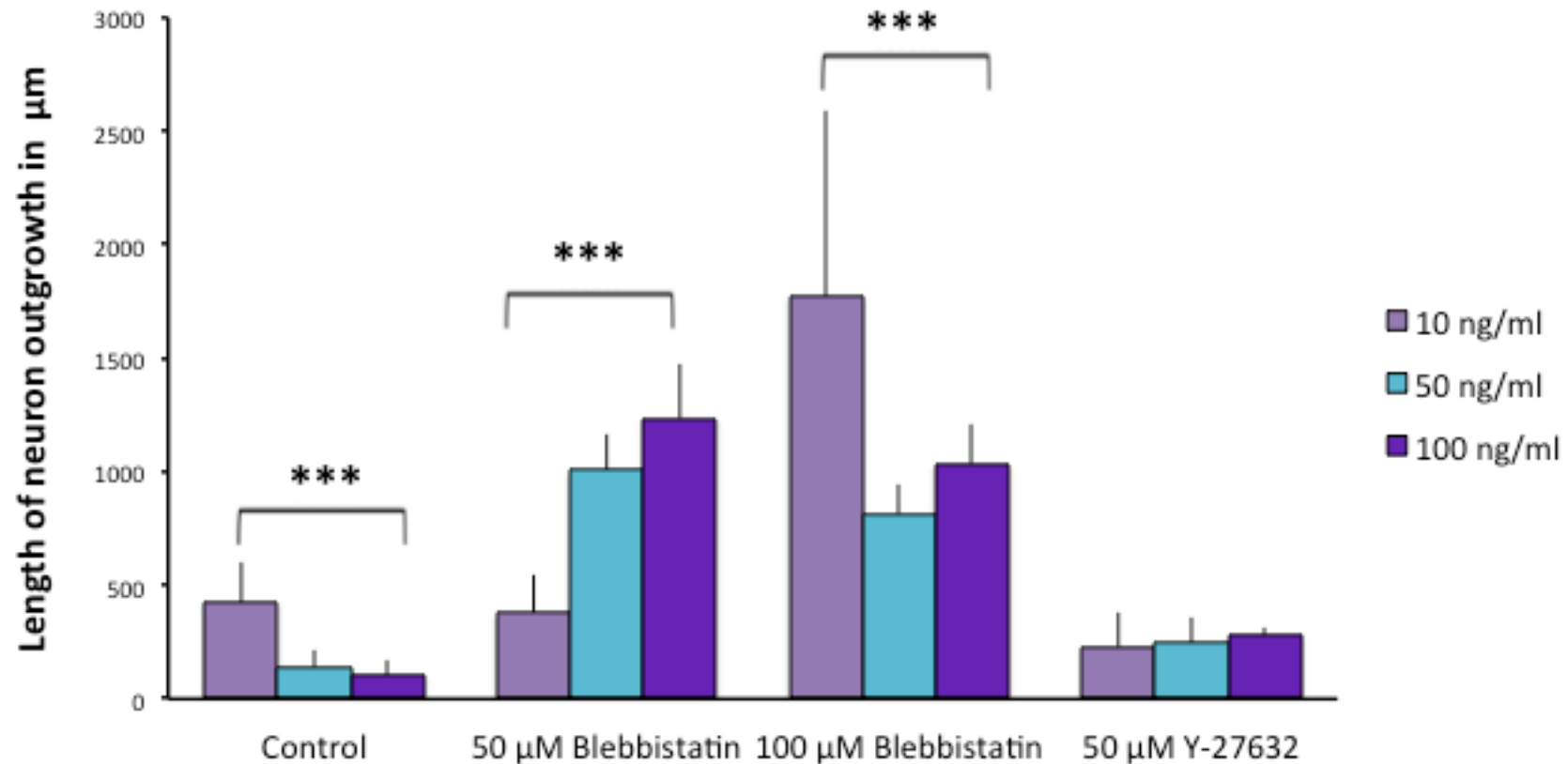
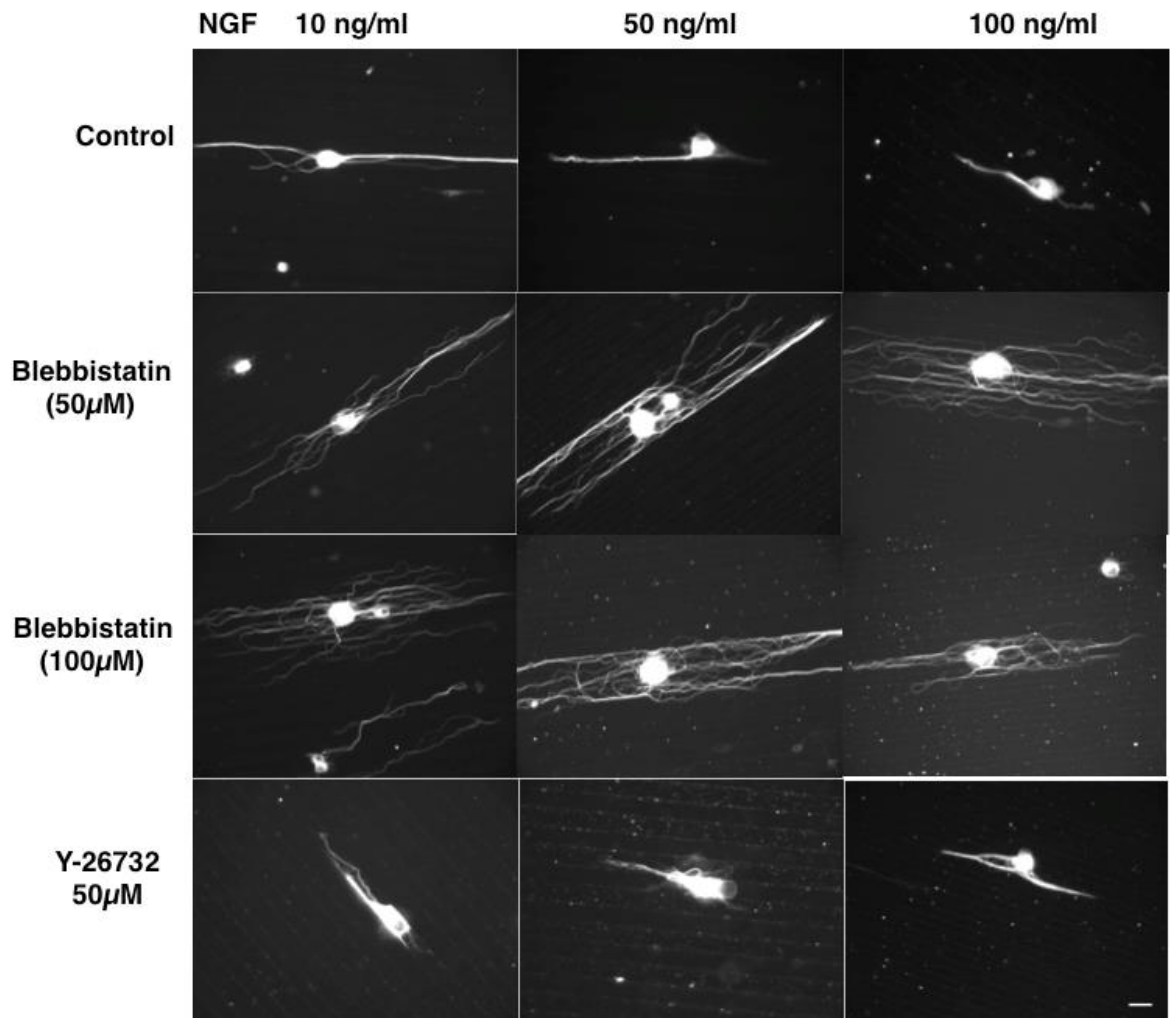


Figure 40: Axon length of individual sensory neurons after 24-hour culture on PLL coated PDMS (grooves) samples with varying NGF concentrations of 10, 50 and 100 ng/ml. Positive control – PLL coated PDMS (non-treated). Inhibition of myosin II was achieved by the addition of blebbistatin (50  $\mu$ M or 100  $\mu$ M). The Rho-ROCK pathway was inhibited by the addition of Y-27632 (50 $\mu$ M). The pattern observed on the control was comparable to the 10-day time point where the axonal length decreased significantly with increasing NGF concentration. The addition of blebbistatin resulted in larger axonal extensions. Y-27632 inhibited the pattern of outgrowth observed with increasing NGF concentrations. Stars indicate significant differences between groups as determined by ANOVA and a Dunnett post hoc test \*\*\* $P < 0.001$ . (n=3 biological repeats, multiple fields of view (10 per sample) were examined for analysis). The bars indicate standard deviation.

## Chapter 3



**Figure 41:** Immunofluorescence images of sensory neurons immuno-labelled for  $\beta$ 3-tubulin (grey-scale) cultured on PLL coated PDMS (grooves) at 10 ng/ml, 50 ng/ml and 100 ng/ml of NGF. Inhibition of myosin II was achieved by the addition of Blebbistatin (50  $\mu$ M or 100  $\mu$ M). The Rho-ROCK pathway was inhibited by the addition of Y-27632 (50  $\mu$ M). Pattern observed on the control was comparable to the 10-day time point where the axonal length decreased significantly with increasing NGF concentration. Upon the addition of Blebbistatin, the pattern of outgrowth was similar to that of the control but with larger axonal extensions (non-responsive to topographical cue). Y-27632 inhibited the pattern of outgrowth seen with the differing NGF concentrations. Scale bar = 50  $\mu$ m.

## Chapter 3

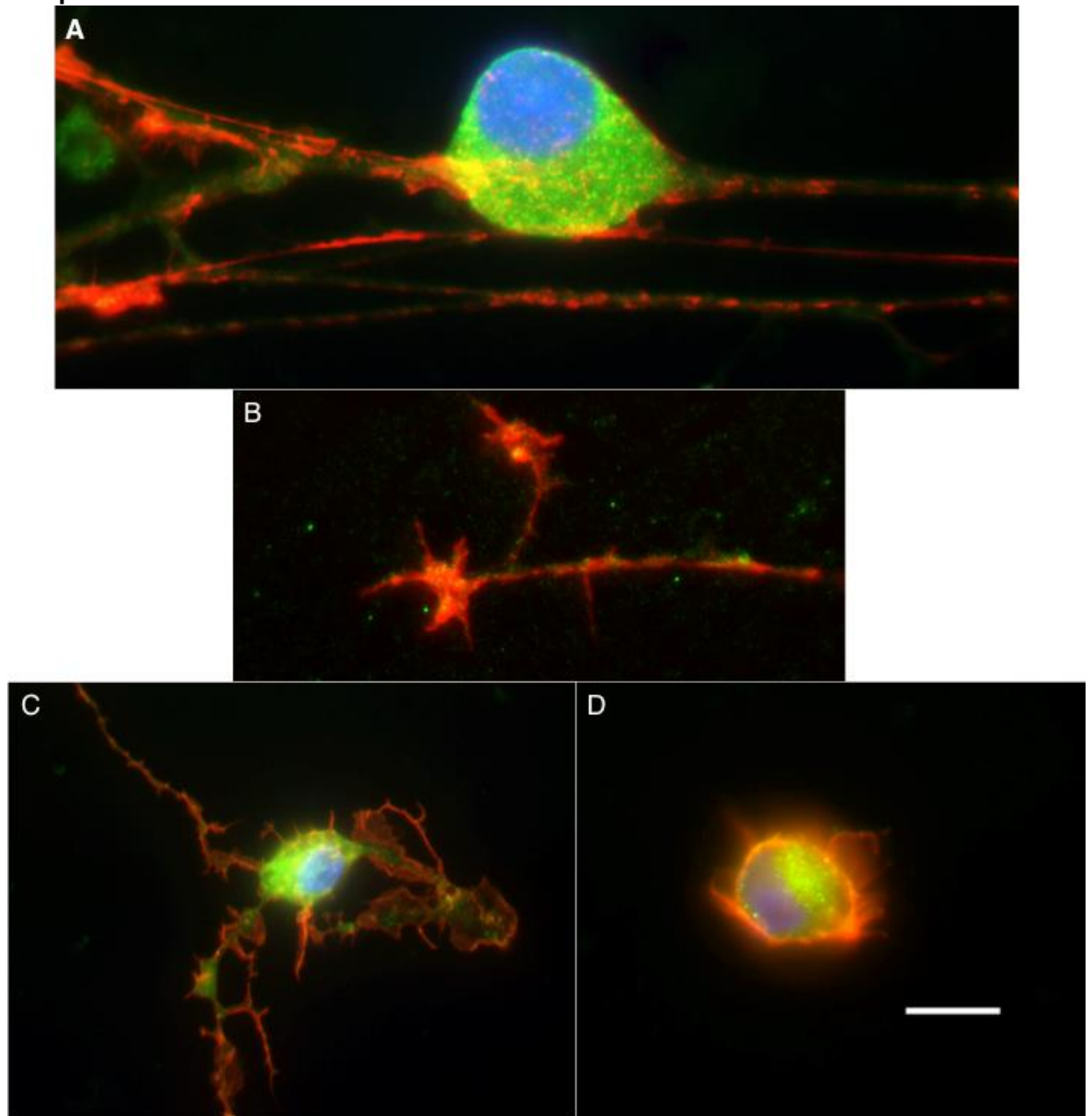


Figure 42: Immunofluorescence images of sensory neurons immuno-labelled for F-actin (red), the focal adhesion marker talin (green), and DNA in nuclei (blue). The cells were cultured for 24-hours on glass coverslips where (A&B) No inhibitor (C) 100  $\mu$ M Blebbistatin (D) 50  $\mu$ M Y-27632. Scale bar = 10  $\mu$ m.

## Chapter 3

### 3.4 Discussion/Conclusion

It is known that a DRG is composed of heterogeneous populations of neurons that convey a variety of sensory information from peripheral and visceral tissues to the central nervous system. DRG neurons have been classified according to the size of their cell bodies, duration and amplitude of their action potential, the extent of myelination, expression of neurofilaments and their axonal conduction velocities (Ho and O'Leary, 2011). Histologically, DRG neurons have also been described as 'large light' and 'small dark' (Lawson, 1979). In order to link the histological classifications to the functional ones, the use of neuroactive peptides found within the DRG neurons have been widely used. Two most common ones are SP (Hökfelt et al., 1975) and SOM (Hökfelt et al., 1976). Others include CGRP (Rosenfeld et al., 1983) and tyrosine hydroxylase (TH) (Price and Mudge, 1983).

It has been shown that NGF affects specific subpopulations of adult sensory neurons. It is still not clear which of these is NGF dependent, but it has been reported that NGF increases the content of SP and SOM (Otten et al., 1980). Others have demonstrated that CGRP and SP positive neurons possess NGF receptors and that NGF enhances the expression of these neuropeptide genes in adult sensory neurons (Lindsay and Harmar, 1989). Approximately half of adult sensory neurons have high affinity NGF receptors (Verge et al., 1989).

Much of the literature agrees that laminin is a known promoter of neural process outgrowth and survival *in vitro*. It is capable of enhancing the extensions and growth of neural processes. A study carried out on hippocampal neurons has shown that laminin resulted in enhanced neuritic outgrowth and accelerates the development of its polarity (Lein *et al.*, 1992). The same paper assessed the effect PLL substrates have on the neurons, this resulted in the outgrowth of relatively short neurites. Our observation in the 10-day study similarly demonstrates that laminin stimulates enhanced branching on the flat PDMS, with extensions emerging earlier, growing more rapidly and branching much more frequently, compared to the neurons that were cultured on PLL.

### Chapter 3

From the shape of the axonal outgrowth emanating from neurons cultured on grooves it is evident that these topographic features constrain the number of neurites that the cells extend. The grooved topography promotes a bipolar phenotype unlike the cells cultured on the flat substrates, which exhibit a branching phenotype. As evident from figure 35 the overall outgrowth of axons on grooves with either laminin or PLL decreases with increasing NGF concentrations. These results align with those reported by Foley *et al.*, (2005) who describe how topography acts to modulate neuritogenesis under conditions of sub-optimal NGF signaling. In their experiments reducing the NGF concentration resulted in a decrease of overall neurite formation by PC12 cells. The paper goes on to discuss potential explanations for how topography might cooperate with NGF signaling to promote neurite formation. Focal adhesion contacts are major sites for intracellular signaling and have been demonstrated to affect cytoskeletal organization and the adhesive properties of cells. Another potential mechanism related to focal contact assembly is that the scale of topography affects the ability of growth cones to extend. Growth cone migration is dependent on a highly regulated series of events that include adhesion and the generation of contractile forces (Foley *et al.*, 2005).

Myosin II, the mechanism responsible for muscle contraction is present in most non-muscle cells to regulate cytoplasmic contraction (Taylor *et al.*, 1973). There are two isoforms of Myosin, IIA and IIB, which are differentially distributed within cells (Vicente-Manzanares *et al.*, 2009). In neurons myosin IIB is considerably elevated over myosin IIA in the margins of the growth cone (Cheng *et al.*, 1992). A lot of changes in axon branching stimulated by laminin and other proteins are known to depend on myosin II activity (Liu *et al.*, 2013).

Taking recent work on mechanotransduction in differentiating mesenchymal cells by the groups around Dalby (Dalby *et al.*, 2007), Disher (Discher *et al.*, 2005) and Killian and Mrksich (2012) into account it was hypothesised that the topography induced changes in the neuronal response to varying concentrations of NGF may correlate to a difference in intracellular tension. These groups showed that topography and cell shape lead to a change in intracellular tension within mesenchymal stem cells that in turn can be correlated to the direction of differentiation (fat, muscle, bone), that these cells take. By taking the work by

### Chapter 3

Franze *et al.*, (2009) into account who show that mechanical impact may act as a guidance cue for neural growth, the mechanisms responsible for growth cone tension were inhibited to assess how cellular tension affects axonal outgrowth.

By inhibiting the ATPase activity of the A and B isoforms of non-muscle myosin II using Blebbistatin (Straight *et al.*, 2003), axonal outgrowth from the neurons was significantly increased and implicitly accelerated in comparison to the control on both the flat and grooved substrates. This correlates to the data presented by Hur *et al.*, (2011) where myosin II activity was inhibited by Blebbistatin and axon growth of embryonic DRG neurons was enhanced in a dose dependent manner on permissive substrates. The same paper showed that blocking myosin II activity enabled neurons to completely overcome axon inhibition induced by CSPGs. They propose that inhibiting myosin II leads to a reorganization of both F-actin and microtubules in the growth cone resulting in microtubule reorganization that allows rapid axon extension over non-permissive or even inhibitory substrates.

Upon the addition of Y-27632, a specific ROCK inhibitor, axonal outgrowth of the cells was grossly inhibited on all substrates tested. The literature on Y-27632 is varied and, especially in primary neuronal cells, the effect of ROCK inhibitor treatment seems to be dependent on the age of the animal from which the cultures originated. Embryonic cells demonstrate enhanced outgrowth, and in adult DRG neurons outgrowth is inhibited. This difference in response to the exposure to Y-27632 has been correlated to intracellular cAMP levels: in embryonic cells, which have high levels of endogenous cAMP the growth potential is conserved (Borisoff *et al.*, 2003, Monnier *et al.*, 2003); in adult cells neurite outgrowth is only possible when a cAMP drive is added (Ahmed *et al.*, 2009). It has been shown that the effect of Y-27632 is also dependent on close contact with Schwann cells: the neurite length of neurons treated with Y-27632 of cells in contact with Schwann cell increased significantly compared to neurons with no contact to Schwann cells (Fuentes *et al.*, 2008). Y-26732 treatment has divergent effects on regeneration of sensory and motor neurons in a non-growth permissive environment. It is less effective in sensory as compared to motor neurons (Joshi *et al.*, 2015).

It was observed that the inhibitors altered not only the F-actin cytoskeleton and the outgrowth of the axons, but also affected the morphology of the Schwann

### Chapter 3

cells. Changes in Schwann cell morphology upon the addition of ROCK inhibitors have been described in detail and ROCK has been shown to regulate Schwann cell branching and myelin morphology (Melendez-Vasquez *et al.*, 2004).

ECM molecules and growth factors are two classes of extracellular ligands that have crucial effects on axonal growth *in vivo* and *in vitro* (Paveliev *et al.*, 2007, Chen and Strickland, 2003). How axonal outgrowth is modulated by growth factor concentration is something rarely studied in the literature. Taken together, these results suggest that surface topography, protein layer and NGF concentration act through interacting pathways to influence axonal outgrowth behavior. A laminin layer promoted the most growth on all NGF concentrations tested in comparison to a PLL layer. Both PLL and laminin showed a modulation in outgrowth depending on NGF concentration available in the media and topography. ECM molecules regulate axonal growth by activating integrins (Tomaselli *et al.*, 1993), which trigger several intracellular signalling pathways. One particular pathway we manipulated is the Rho-ROCK pathway as myosin II plays a major role in force generation of DRG filopodia and lamellipodia (Sayyad *et al.*, 2015). Interestingly, the inhibition of the myosin II pathway lead to increased outgrowth with all NGF concentrations, whereas the inhibition of ROCK lead to a halt in outgrowth on all tested substrates independent of NGF. As the integral behaviour of the signalling network converting receptor activation into axonal growth remains largely unknown (Tucker *et al.*, 2005), the investigation of these parameters will help to refine parameters for nerve repair tube design in general.

The findings of this chapter highlight the importance of crosstalk between the parameters tested on cellular response and the balance between events required for neurite growth. Overall the results highlight that topography and growth factor availability work together and, cytoskeletal assembly in the axons affects extensions with respect to contractility, which is guided by the substrate coating. The best parameters for increased outgrowth can be selected for further investigation or for advancement in *in vivo* studies.

## **Chapter 4**

### **Rsn2 modifications and neural response**

## Chapter 4

### 4.1 Introduction

The surface properties of a biomaterial, especially hydrophobicity, influence cell adhesion (Chauvel-Lebret *et al.*, 1999). Surface properties of polymers used in tissue engineering often do not meet the demand to support good cell adhesion, thus surface modifications are usually required to enhance these properties. For nerve repair guides this is required for enhanced regeneration. Effective surface modifications include changes in chemical functionality, surface charge, hydrophilicity, hydrophobicity and wettability (Williams *et al.*, 1999, Yang *et al.*, 2002). Cell adhesion is mediated by specific interaction of the cell surface receptors with extracellular glycoproteins. CAMs involved in cell-surface adhesion are the integrins (Hynes, 2004). Once bound to a ligand, integrins initiate the formation of focal adhesion complexes, which in turn facilitate cell migration and signal transduction. Biomimetic surface modifications have been used to drive specific cell interactions mediated by bio-molecular recognition, which can be manipulated by altering the design parameters of the material (Shin *et al.*, 2003). One way this can be achieved is to use specific integrin ligand sequences (such as the tripeptide RGD) (Ruoslahti and Pierschbacher, 1986) to drive specific cell adhesion and interaction with the substrate (Sanchez-Cortes and Mrksich, 2011, Kilian and Mrksich, 2012).

Laminin, a large glycoprotein, mediates cell adhesion, migration, proliferation, differentiation and neurite outgrowth (Koh *et al.*, 2010, Itoh *et al.*, 2001). Laminin contains a variety of potential cell binding sequences with seventeen different ones having been identified on the  $\alpha 1$ ,  $\beta 1$ , and  $\gamma 1$  chains (Nomizu *et al.*, 1998, Graf *et al.*, 1987). RGD, the principal integrin-binding domain present within ECM proteins, is also found in laminins and collagens, however RGD may be inaccessible within these molecules (depending upon conformation), and other amino acid motifs are known to serve as alternative binding modules for laminin selective receptors (von der Mark *et al.*, 2010, Bellis, 2011). Many of the cell adhesive peptide sequences found within laminin have been used in the context of peripheral nerve repair. These include the five amino acid motif IKVAV that is found in the  $\alpha 1$  chain of laminin (Tashiro *et al.*, 1989) and YIGSR, a peptide motif found on the  $\beta 1$  chain, (Graf *et al.*, 1987) which has also been shown to promote neurite outgrowth (Itoh *et al.*, 1999).

## Chapter 4

The use of peptide sequences over native ECM proteins has been well debated in literature (Bellis, 2011, Williams *et al.*, 1999). Using short peptides that represent the bioactive sequences within native proteins (e.g. RGD, IKVAV, YIGSR etc.), minimises the risk of immune reactivity, and peptides can also be coupled to material surfaces in controlled densities and orientations (Bellis, 2011). Methods that have been used to incorporate functional-, specifically adhesive-peptides include surface grafting (Massia and Stark, 2001), self assembling nanofibers (Silva *et al.*, 2004), self assembly scaffolds containing IKVAV (Powell *et al.*, 2000) and matrix metalloproteinase sensitive IKVAV containing hydrogels (Park *et al.*, 2010).

The aim of this chapter is to combine the surface-active protein Rsn2 (function described in detail in chapter 1) with the functionality of specific peptides to present a hydrophilic and cell specific surface to drive neurite outgrowth. Five<sup>2</sup> different variations of Rsn2 were made, where the peptide sequences RGD, proline-histidine-serine-arginine-asparagine (PHSRN), IKVAV, leucine-aspartic acid-valine-proline (LDVP) or phenylalanine-histidine-arginine-isoleucine-lysine-lysine-alanine (FHRIKKA) were added to the N-terminus of the protein. The proteins were expressed, cleaned, and used to coat PDMS substrates to increase their wettability. The underlying hypothesis was that by using Rsn2 constructed to display specific adhesion peptides, the attachment of identified cell types would be promoted by allowing integrin subtype specific adhesion.

---

<sup>2</sup> The molecular work constructing and characterising the modified, peptide bearing Rsn2 vectors was done by Vibuthi Desai. Here I grew the stably transfected bacteria from glycerol stocks, expressed, isolated, cleaned, and characterised the proteins and did all the work otherwise described in this chapter.

## Chapter 4

# 4.2 Materials and methods

## 4.2.1 Protein expression

Rsn-2 was overexpressed as a thrombin-cleavable N-terminal His<sub>6</sub> fusion-tagged form in *Escherichia coli* (*E.coli*) BL21 (DE3) cells (Novagen) using the pET28-Rsn2 plasmid. A second construct containing an additional fluorescent tag (iLOV) (Chapman *et al.*, 2008) was prepared by sub cloning a synthetic, codon optimised iLOV insert into the NdeI site of pET28-Rsn2 to create pET28-iLOV-Rsn2. (vector made and characterised by Dr. S.Vance). Similarly, integrin sequences, IKVAV, RGD, LDVP, PHSRN and FHRIKKA were sub cloned into the NdeI site of pET28-Rsn2 to create 5 new Rsn2 protein constructs (vectors made and characterised by Ms. V. Desai). The proteins Rsn2, iLOV-Rsn2, RGD-Rsn2, FHRIKKA-Rsn2 and PHSRN-Rsn2 were expressed as described in section 2.2.1. IKVAV-Rsn2 and LDVP-Rsn2 were expressed overnight at 15 °C with all other conditions being the same as described as section 2.2.1.

## 4.2.2 Size Exclusion Chromatography

Size exclusion chromatography was carried out on a pre-packed Superdex 75 10/300 GL column (GE healthcare), connected to the AKTA chromatography system in a cold room (+4°C). After equilibration with running buffer (10 mM NaH<sub>2</sub>PO<sub>4</sub>, 10 mM Na<sub>2</sub>HPO<sub>4</sub> and 50 mM salt), a 500 µl protein sample was injected into the sample loop. Size exclusion chromatography was then carried out at 0.1 ml/min running buffer for 1.5 column volumes, and monitored by UV absorbance at 220 and 280 nm. Fractions of 0.5 ml elutant were collected and fractions that showed absorbance at 280 nm were analysed by SDS-PAGE.

## 4.2.3 PDMS fabrication

PDMS 184 polymer solution 90% (wt/wt) (Sylgard® 184 Silicone Elastomer, Dow Corning, UK) was added to 10% (wt/wt) curing agent. The polymer and curing agent were mixed very well in a disposable cup and then degassed under vacuum for 20 mins. The degassed PDMS was poured into a petri dish or a silicon wafer mould and cured in an 80 °C oven for 2 hours; it was left to cool before removing and cutting the samples to individual 11 mm diameter devices with a cork borer.

## Chapter 4

### 4.2.4 Sample preparation

Samples were sterilised prior to seeding by immersing them in 70% ethanol for 30 mins after which each sample was rinsed 2x in PBS followed by drying with a flow of 0.22µm filtered compressed air in a laminar flow cabinet to avoid contamination.

For Rsn2, iLOV-Rsn2, RGD-Rsn2, IKVAV-Rsn2, PHSRN-Rsn2, LDVP-Rsn2 and FHRIKKA-Rsn2 coating - no plasma treatment was required, protein solution (0.1 mg/ml) was added to each surface and left to incubate for up to an hour. After this, the surfaces were rinsed in water and air-dried ready for seeding with cells.

The positive control samples of PDMS surfaces were treated for 1 min with air plasma generated using a Harrick Plasma PDC-002 Plasma cleaner at 29.6 W. After plasma treatment, the surfaces were coated in PLL solution for 30 mins at 37°C before seeding with cells. For laminin coating, samples were first coated in PLL as described, followed by a 2-hour incubation at 37°C with laminin (12 µg/ml, Sigma). Each sample was rinsed 2x in 1x PBS before seeding cells.

For the 10-day time points, the unreacted component of the crosslinked PDMS was extracted by three cycles of swelling the polymer in n-hexane (Riedel-de Haën), followed by n-hexane/PDMS extraction and shrinking of the samples in ethanol.

### 4.2.5 Dissociation of DRGs into single cells

DRGs were isolated from neonatal (1-5 days old) Sprague-Dawley rats. Rats were euthanized by a Euthatal® injection (500mg/Kg) according to Home Office regulations and then dissected. After extraction, the DRGs were placed in a 35mm culture dish containing 2 ml trypsin/EDTA (0.125%/0.05%, Sigma, UK) and incubated at 37°C for 30 mins. After digestion, ganglia were transferred to a centrifuge tube containing 5 ml L15 media, FBS (10%, Life technologies, UK) and DNase (10 µg/ml, Life technologies, UK). The cell suspension was triturated with a Pasteur pipette until it was homogenous after which the cells were pelleted at 250 g for 10 mins. The cells were cultured in Neurobasal® media (Life technologies, UK) containing B27 supplement (2%, Life technologies), Pen/strep

## Chapter 4

(1%, Sigma), L-Glutamine (0.5 mM, Life technologies, UK), glucose (2.5g/L, Fisher Scientific), FBS (1%, Life Technologies) and NGF (10, 50 or 100 ng/ml, 2.5 S Invitrogen). Dissociated DRG cells were seeded at a low density onto PDMS samples and were incubated at 37°C 5% CO<sub>2</sub> for 1 or 10 days. The media was exchanged every 2 days as required.

### 4.2.6 Immunofluorescence staining

After growth, DRG neurons were washed with PBS and fixed for 15 mins in a formaldehyde (10%, Fisher Scientific)/PBS solution containing sucrose (2% w/v, Fisher Scientific). Following fixation, the cells were permeabilised using a solution of sucrose (10.3%), NaCl (0.292%, AnalaR Normapur), MgCl<sub>2</sub> (0.06%, AnalaR Normapur), HEPES (0.476%, Fisher Scientific) and Triton X-100 (0.5%, Sigma) per 100 ml PBS at 4°C for 5 mins, followed by an incubation at 37°C in PBS/BSA (1%, Sigma, UK) for 5 mins. The blocking solution was replaced by PBS/BSA solution containing anti- $\beta$ 3-tubulin antibody (1:100, mouse anti-TU-20 Santa Cruz) and anti-S100  $\beta$  antibody (1:100 rabbit S100 Abcam). The samples were incubated at 37°C for 2 hours then washed thrice with a PBS/Tween<sup>®</sup>20 (0.5%, Sigma) and further incubated for an hour in PBS/BSA solution containing biotinylated anti-mouse antibody (1:50, Vector Laboratories) and Texas red anti-rabbit antibody (1:50, Vector Laboratories). After incubation, samples were washed thrice with PBS/Tween<sup>®</sup>. Fluorescein streptavidin (1:50, Vector Laboratories) in PBS/BSA was then added to the samples and incubated at 4°C for 30 mins before washing thrice with PBS/Tween<sup>®</sup>. To prepare the slides, a small drop of mounting medium containing DAPI (vectorshield-DAPI) was placed on a labelled microscope slide. Samples were viewed on a Zeiss Axiovert200 and Zeiss Axiophot microscope with 10x 0.25 N.A. Ph1, 20x 0.5 N.A. Ph2, and 40x 0.75 N.A. Ph2 objectives, images were taken using a Qimaging Click or Retiga 2000 camera. DAPI Excitation/Emission (nm) = 358/461, Texas red (FITC) Excitation/Emission (nm) = 596/615 and Fluorescein (TRITC) Excitation/Emission (nm) = 490/525.

## Chapter 4

**4.2.7 Water Contact Angle (WCA)**

WCA measurement was carried out using the static drop technique with an Attension Theta (Biolin Scientific) instrument. High contrast images were recorded for 30 seconds after a droplet was placed on the surface. The OneAttension software was used to define the contact angle by fitting Young-Laplace equation around the droplet to determine the contact angles across the series of images taken. Three different sets of data were recorded for each protein coating used and averages were pooled.

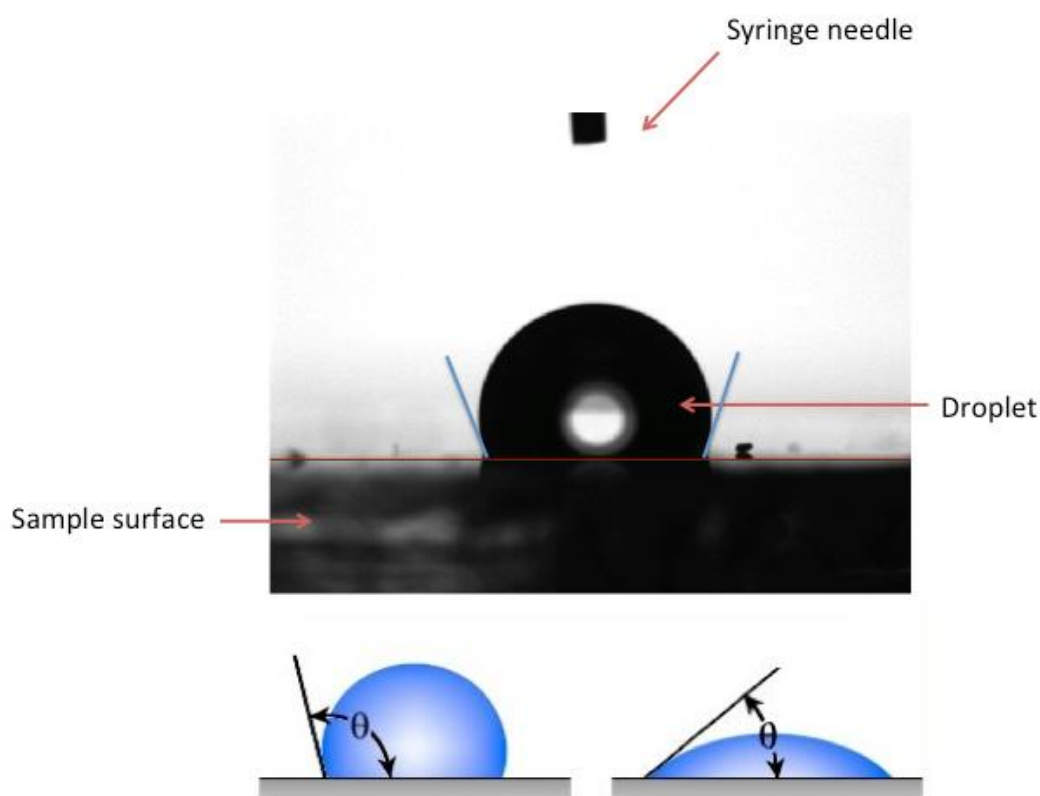


**Figure 43:** Contact angles were measured using the static drop technique on a PDMS surface and fitted with a circular line to determine angles. As depicted the contact angle varies depending on the hydrophobicity of the surface (WCA  $<90^\circ$  = high wettability, WCA  $>90^\circ$  = low wettability).

## Chapter 4

### 4.2.8 PDMS microcontact stamp

Grooved PDMS cast from a microstructured master as described above was plasma treated for 2 mins (air plasma at 29.6 W) and coated with iLOV-Rsn2, RGD-Rsn2 or IKVAV-Rsn2 at a concentration of 0.1 mg/ml for 30 mins at room temperature. After incubation excess protein was washed off with PBS and the  $\mu$ CP stamp was dried with a flow of 0.22 $\mu$ m-filtered compressed air. The stamp was used to print the various types of Rsn2 onto a flat untreated PDMS sample by putting the two surfaces into conformal contact and then keeping the stamp in contact with the substrate for a further 30 mins. The cells were seeded on both surfaces to address the question if hydrophilic materials are suitable materials for Rsn2 based modification.

### 4.2.9 Data analysis

After images of the dissociated DRG neurons were obtained and assembled in Photoshop (Adobe), each image was processed on Image J (Rasband, 1997-2012) using the Neuron J plugin (Meijering *et al.*, 2004) which allows tracing and quantification of the total neuron length in  $\mu$ m. The intersections of the neuron were estimated using the segment number tool using the same plugin. Statistical analysis was performed using ANOVA with a Dunnett post-hoc test for significance between parameters.

## Chapter 4

## 4.3 Results

## 4.3.1 Expression and purification of the proteins

Large-scale expressions of the proteins Rsn2, iLOV-Rsn2, RGD-Rsn2, IKVAV-Rsn2, PHSRN-Rsn2, LDVP-Rsn2 and FHRIKKA-Rsn2 were set up as described in the methods, followed by nickel affinity purification. The respective samples were run on an SDS-page gel to determine if the protein was eluted correctly (example of RGD-Rsn2 gel - figure 44). After collecting the eluted protein samples, they were buffer exchanged in a low salt solution and another SDS-page gel was run to confirm that all the proteins had been purified (figure 45).

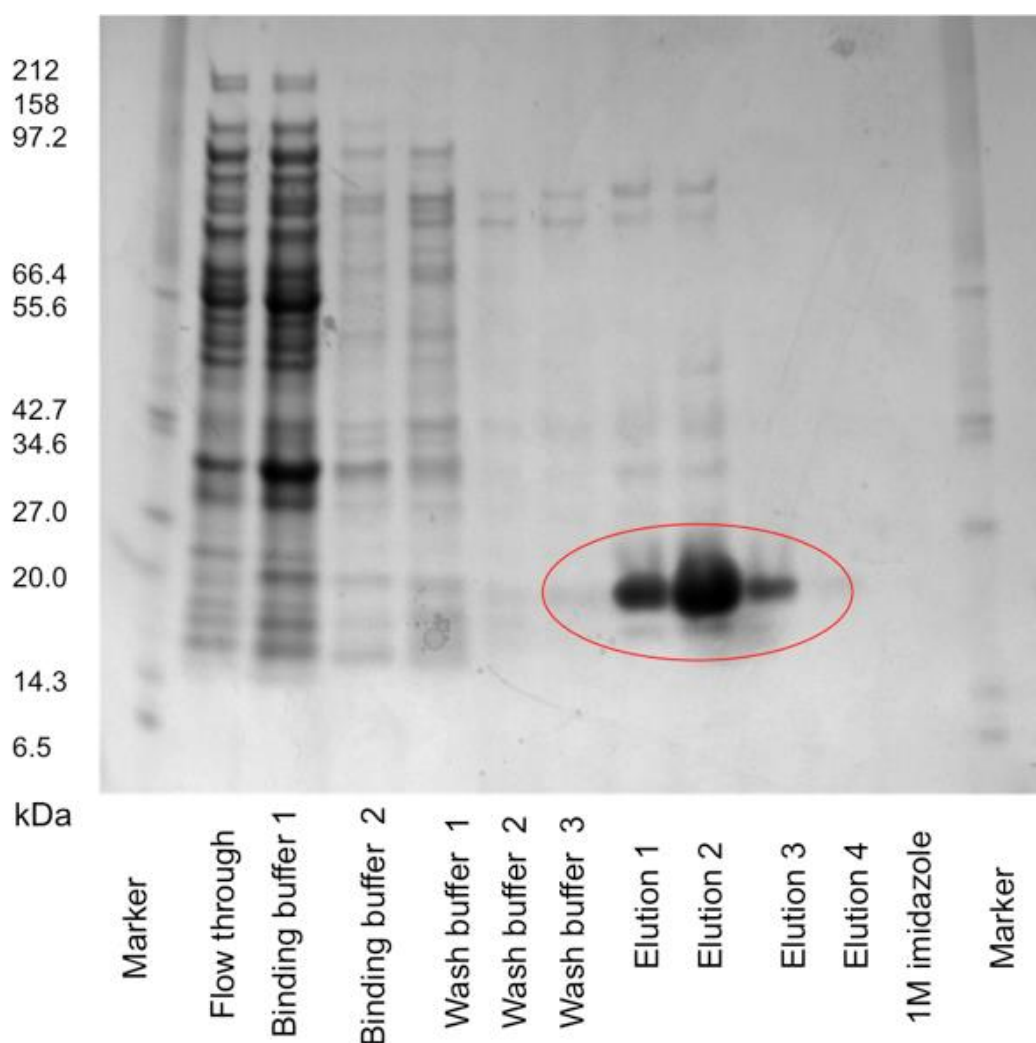


**Figure 44: SDS-PAGE analysis of RGD-Rsn2 nickel affinity column samples. To elute the bound His-tagged protein, a solution containing a high concentration of Imidazole is used which displaces the bound histidines. Contaminant proteins seen in columns (5-7) were removed by a series of washes using (5-30mM) imidazole before eluting the target protein. The gels confirm that the protein was eluted successfully, as a distinct band is visible in the first elution wash at the molecular weight (~14 kDa) expected for RGD-Rsn2.**

## Chapter 4

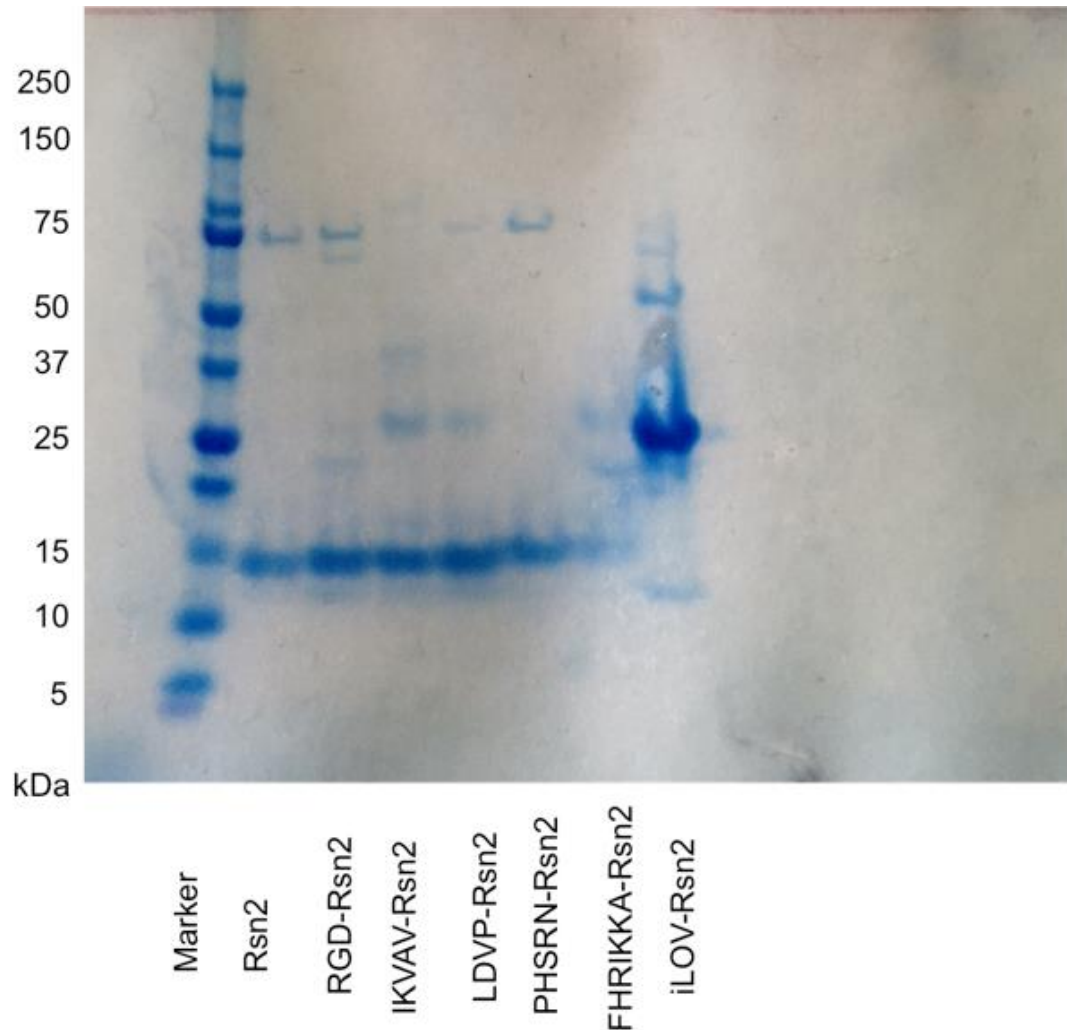


**Figure 45: SDS-PAGE analysis of purified and buffer exchanged protein samples. Distinct bands are present at ~ 14 kDa for (from left to right after the markers): Rsn2, RGD-Rsn2, IKVAV-Rsn2, LDVP-Rsn2, PHSRN-Rsn2, FHRIKKA-Rsn2. For iLOV-Rsn2 a distinct band is present at ~ 27 kDa. The other much weaker bands seen at 75 kDa (Rsn2, RGD-Rsn2, PHSRN-Rsn2) and 25 kDa could be E.coli proteins.**

### 4.3.2 WCA measurements

To establish how well the proteins coated a hydrophobic polymer such as PDMS, WCA measurements were taken and compared to untreated PDMS and plasma treated PDMS. Two other controls were also set up where PDMS was treated with plasma, and the surface was then coated with PLL or LAM (table 1). The WCA measurements were observed to change between the different conditions, where the untreated PDMS was very hydrophobic ( $111.9 \pm 0.7^\circ$ ). Upon plasma treatment, the contact angle significantly dropped to ( $7 \pm 4.1^\circ$ ). Treating the surface with LAM or PLL after plasma gave a reading of ( $100.8 \pm 0.3^\circ$ ) and ( $92.8 \pm 4.3^\circ$ ) respectively. Coating with the different Rsn2 proteins, resulted in similar readings to that of LAM and PLL coated samples (Table 1).

PDMS condition	Contact angle (deg)
Untreated	111.9±0.69
Plasma-treated	7±4.1
PLL-coated	92.8±4.3
LAM-coated	100.8±0.27
Rsn2-coated	98.1±1.45
iLOV-Rsn2-coated	83.8±8.1
RGD-Rsn2-coated	92.2±3.2
IKVAV-Rsn2 coated	88.9±1.6
PHSRN-Rsn2-coated	97.8±0.8
LDVP-Rsn2-coated	94.6±8.4
FHRIKKA-Rsn2 -coated	97.9±0.95

**Table 1: CA measurement values of the eleven different conditions tested. Measurements were taken immediately after coating with the proteins. Values and standard deviation were calculated using 30 readings per data set, which were taken across 3 substrates.**

### 4.3.3 Axonal outgrowth on all protein variations

The first experiment using the proteins was set up to establish which coating was best suitable for promoting axonal outgrowth on flat PDMS. Initial results obtained show that IKVAV-Rsn2 and RGD-Rsn2 both enhanced axonal extensions in comparison to the controls (PLL, and LAM) (figure 46 - controls highlighted in red). PHSRN-Rsn2, LDVP-Rsn2, FHRIKKA-Rsn2 and iLOV-Rsn2 were not investigated any further as they did not provide a surface that promoted axonal outgrowth.

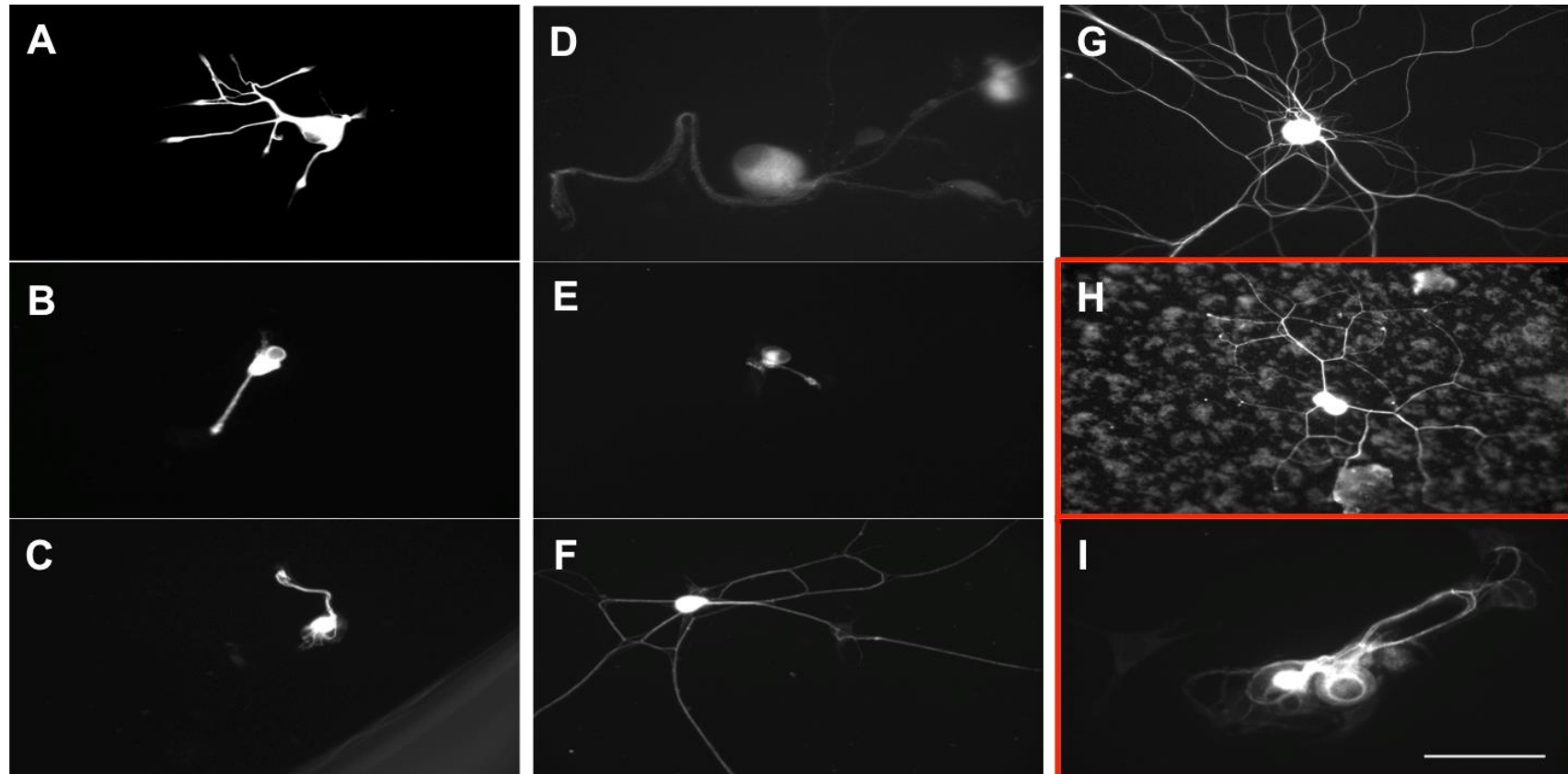


Figure 46: Immunofluorescence images of sensory neurons immuno-labelled for  $\beta$ 3-tubulin (grey-scale) cultured for 24 hours on PDMS (flat) coated with (A) Rsn2, (B) LDVP-Rsn2, (C) PHSRN-Rsn2, (D) iLOV-Rsn2, (E) FHRIKKA-Rsn2, (F) RGD-Rsn2, (G) IKVAV-Rsn2 and highlighted in red are the two controls for this experiment (H) laminin (LAM) and (I) PLL. IKVAV-Rsn2 and RGD-Rsn2 were taken forward as suitable coatings to promote axonal outgrowth, Rsn2 was also used as a control. (Observation of n=9 cells) Scale bar = 50  $\mu$ m.

## Chapter 4

### 4.3.4 Analysis of axonal outgrowth on IKVAV-Rsn2 and RGD-Rsn2

IKVAV-Rsn2 and RGD-Rsn2 were further investigated as potential coatings for promoting axonal outgrowth. The cells were cultured on flat PDMS for 24-hours in media containing 10 ng/ml of NGF. Three controls were set up where Rsn2 alone was used to be able to compare how the addition of the peptides influences the outgrowth, as well as a PLL coated control and a laminin coated control. The morphology of the neurons varied greatly with respect to the coating. A large network formed on the IKVAV-Rsn2 coating. Laminin also promoted branching. In contrast, smaller networks formed on the RGD-Rsn2 and the RGD-Rsn2/IKVAV-Rsn2 mix. Additionally, fewer and shorter neurites extended on the PLL and Rsn2 coated samples. The level of neurite outgrowth on IKVAV-Rsn2 was significantly higher ( $p < 0.001$ ) compared to all the other coatings, which confirmed that the IKVAV peptide would be a suitable candidate to promote neurite outgrowth (results presented in figure 47, 48 and 49).

When cultured on the grooved PDMS surfaces, selective adhesion of the cells along the patterned grooves was observed on all the samples (figure 52). Laminin provided the best outgrowth condition for cells on grooves, where the overall axonal length was significantly higher in comparison to IKVAV-Rsn2 ( $p < 0.01$ ). IKVAV-Rsn2 provided a better surface for the cells in comparison to PLL, Rsn2, RGD-Rsn2 and a 1/1 RGD-Rsn2/IKVAV-Rsn2 mix ( $p < 0.01$ ) (results presented in figure 50, 51 and 52).

Mixing RGD-Rsn2 and IKVAV-Rsn2 did not enhance the cellular outgrowth on the flat surface. The use of the peptides individually delivered a surface more suitable for neuron adhesion and outgrowth. The mix of IKVAV/RGD on the flat surface encouraged the initial adhesion of other cell types (Schwann and other structural cells) (figure 53). On the grooves, the RGD/IKVAV-Rsn2 mix provided a better adhesion surface for the neurons than RGD-Rsn2 alone.

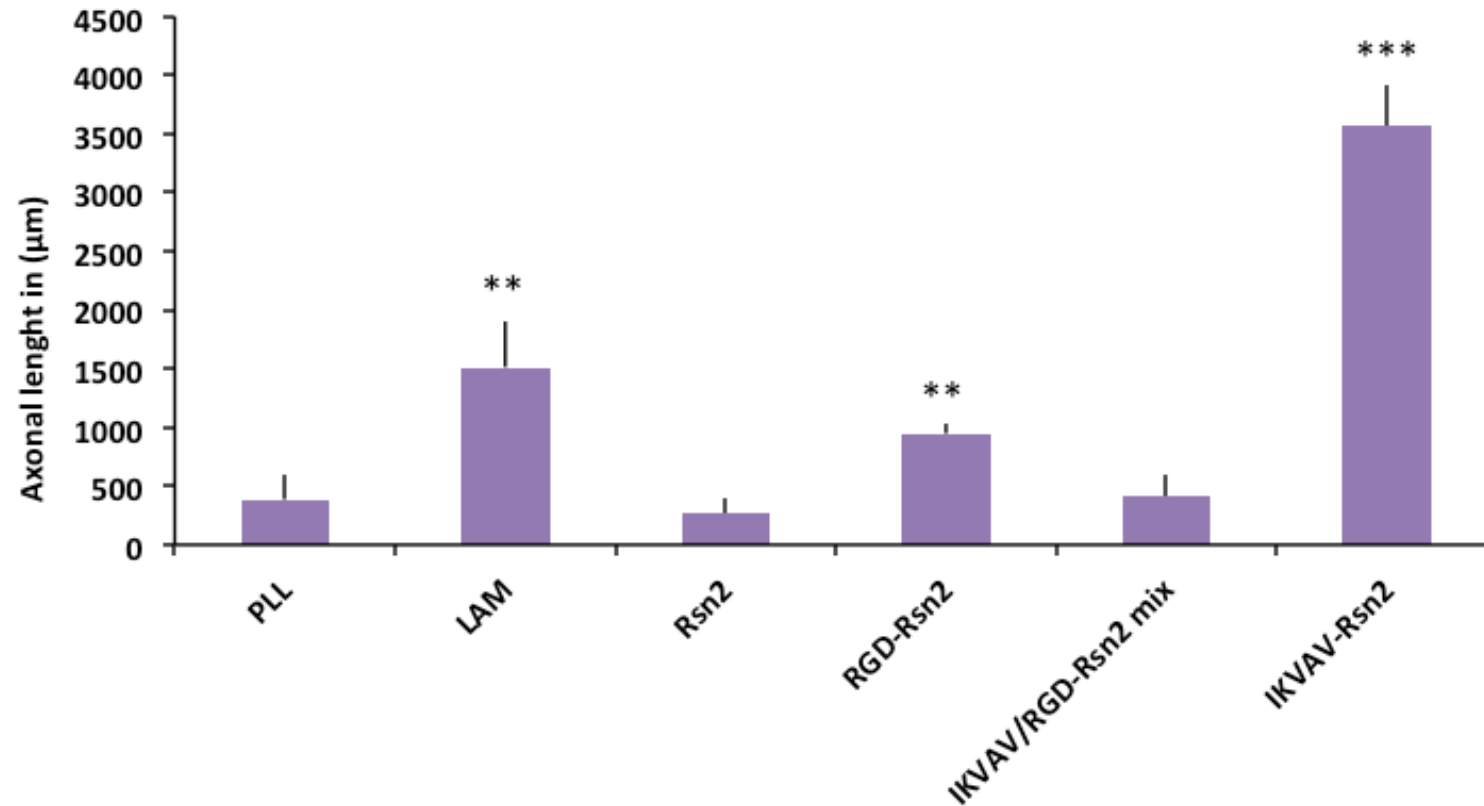


Figure 47: This graph represents the average length of axon outgrowth of individual neurons cultured for 24-hours PDMS (flat) coated with: PLL, LAM, Rsn2, RGD-Rsn2, IKVAV/RGD-Rsn2 mix and IKVAV-Rsn2 in 10 ng/ml NGF. The outgrowth on IKVAV-Rsn2 was significantly higher than on all the other substrates tested. Stars indicate significant differences between groups compared to control sample PLL as determined by ANOVA and a Dunnett post hoc test \*\* $p < 0.01$  and \*\*\* $P < 0.001$ . (n=3 biological repeats, multiple fields of view (10 per sample) were examined for analysis). The bars indicate standard deviation.

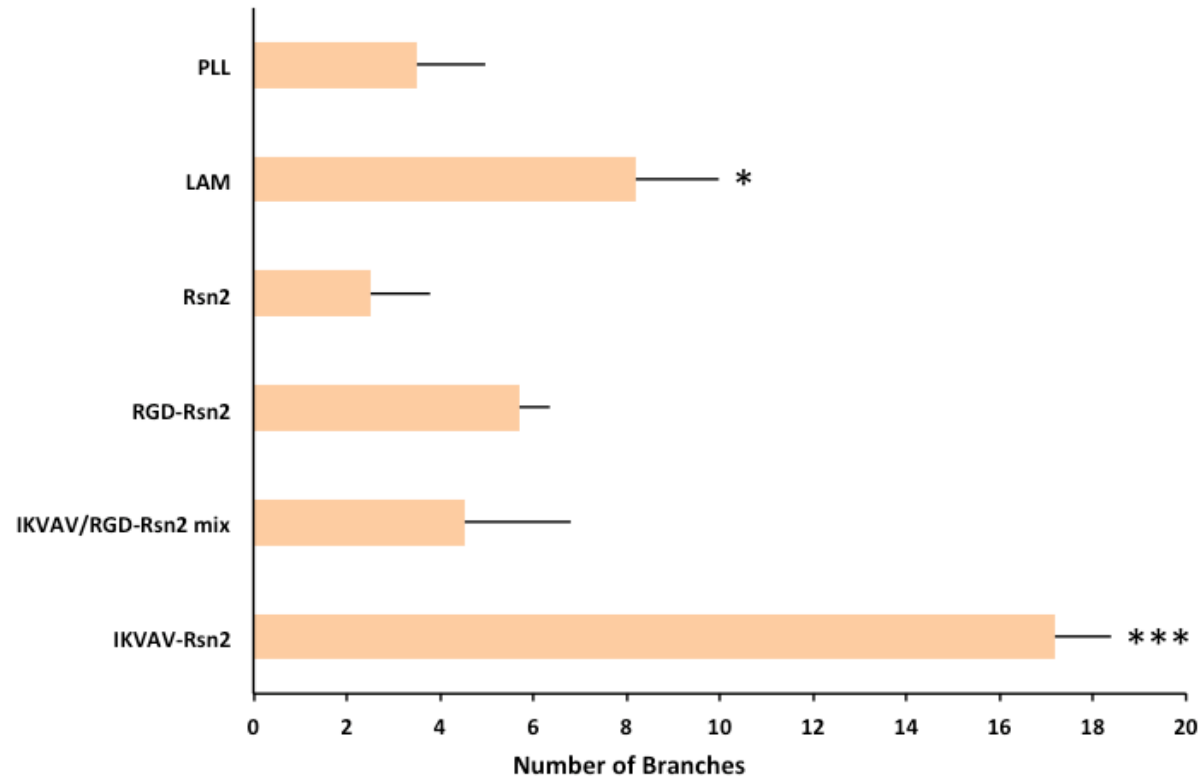
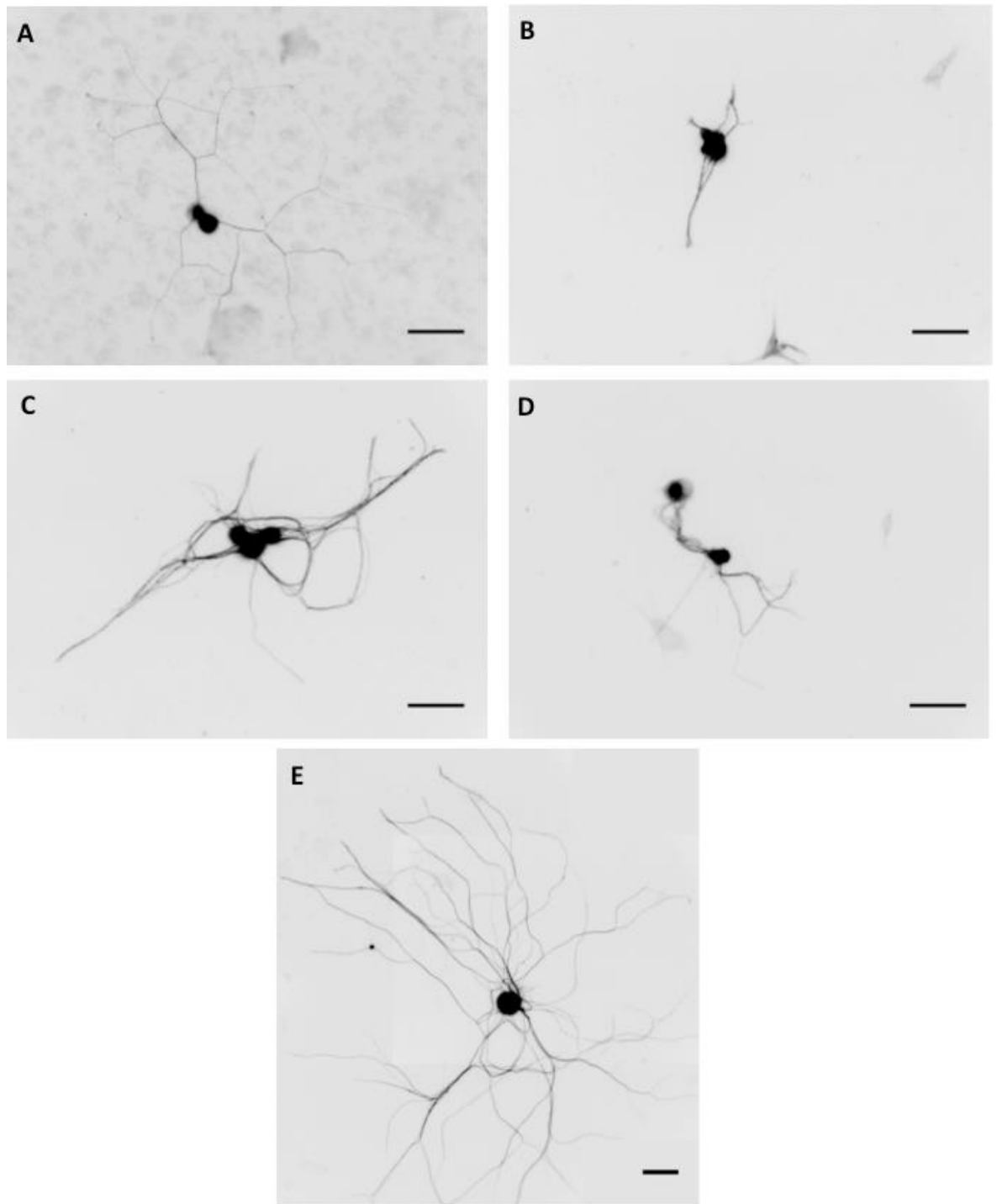


Figure 48: The graph represents the number of branches of individual neurons cultured for 24-hours on PDMS (flat) coated with: PLL, LAM, Rsn2, RGD-Rsn2, IKVAV/RGD-Rsn2 mix and IKVAV-Rsn2 in 10 ng/ml NGF. Neurons growing on IKVAV-Rsn2 branched significantly more than those seeded onto the other coatings tested. Stars indicate significant differences between groups compared to control sample PLL as determined by ANOVA and a Dunnett post hoc test \* $p < 0.05$  and \*\*\* $P < 0.001$ . (n=3 biological repeats, multiple fields of view (10 per sample) were examined for analysis). The bars indicate standard deviation.

## Chapter 4



**Figure 49:** Immunofluorescence images of sensory neurons immuno-labelled for  $\beta$ 3-tubulin (inverted grey-scale images) cultured for 24-hours on PDMS (flat) coated with (A) Laminin, (B) PLL, (C) RGD-Rsn2, (D) Rsn2, and (E) IKVAV-Rsn2. A large network of axons was formed on the IKVAV-Rsn2 coating, fewer and smaller networks were formed on all the other surfaces. Scale bar = 50  $\mu$ m applies to all parts of the figure.

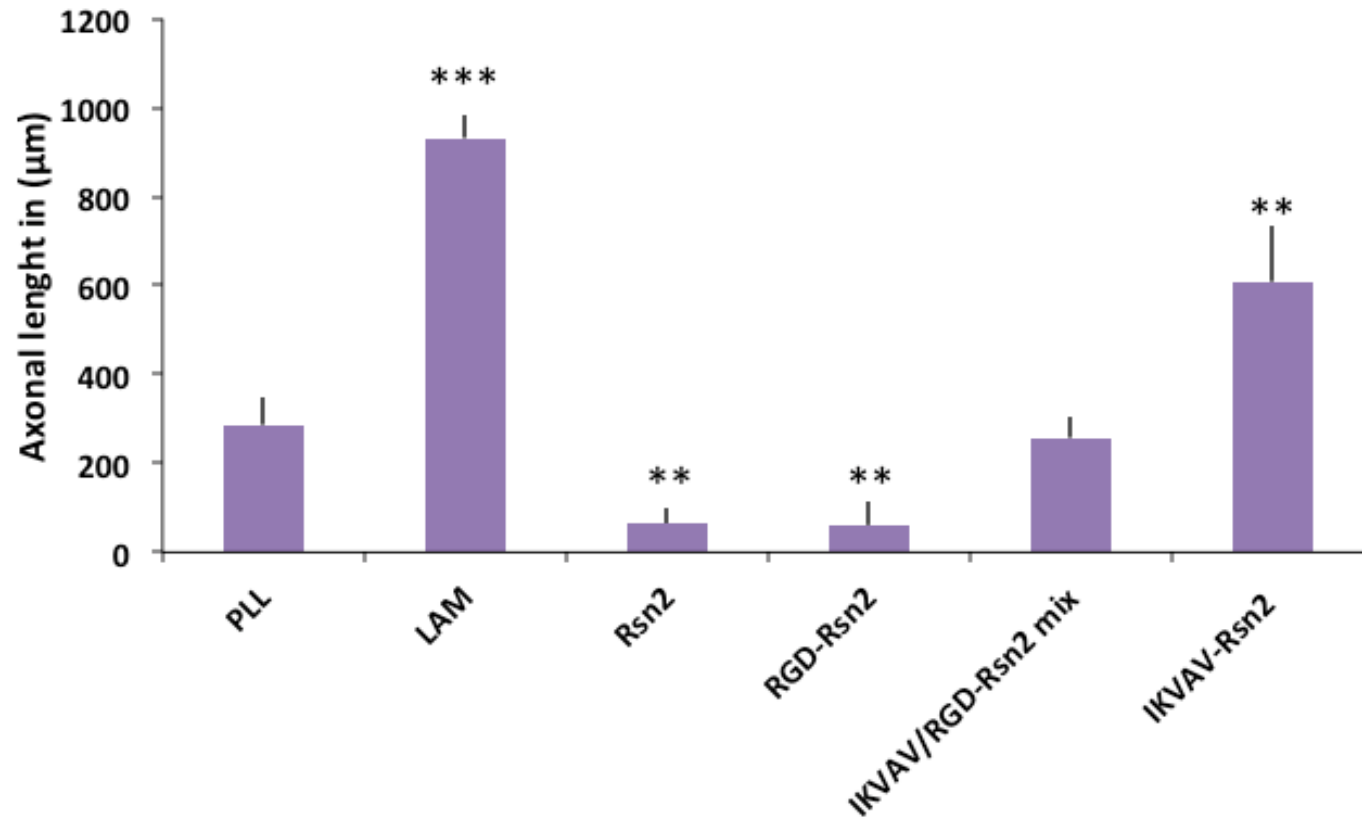


Figure 50: The graph represents the average axon length of individual neurons cultured for 24-hours on PDMS (grooves) coated with: PLL, LAM, Rsn2, RGD-Rsn2, IKVAV/RGD-Rsn2 mix and IKVAV-Rsn2 in 10 ng/ml NGF. The neurite length of cells cultured on IKVAV-Rsn2 and LAM were significantly longer in comparison to PLL. Stars indicate significant differences between groups compared to control sample PLL as determined by ANOVA and a Dunnett post hoc test \*\* $p < 0.01$  and \*\*\* $P < 0.001$ . (n=3 biological repeats, multiple fields of view (10 per sample) were examined for analysis). The bars indicate standard deviation.

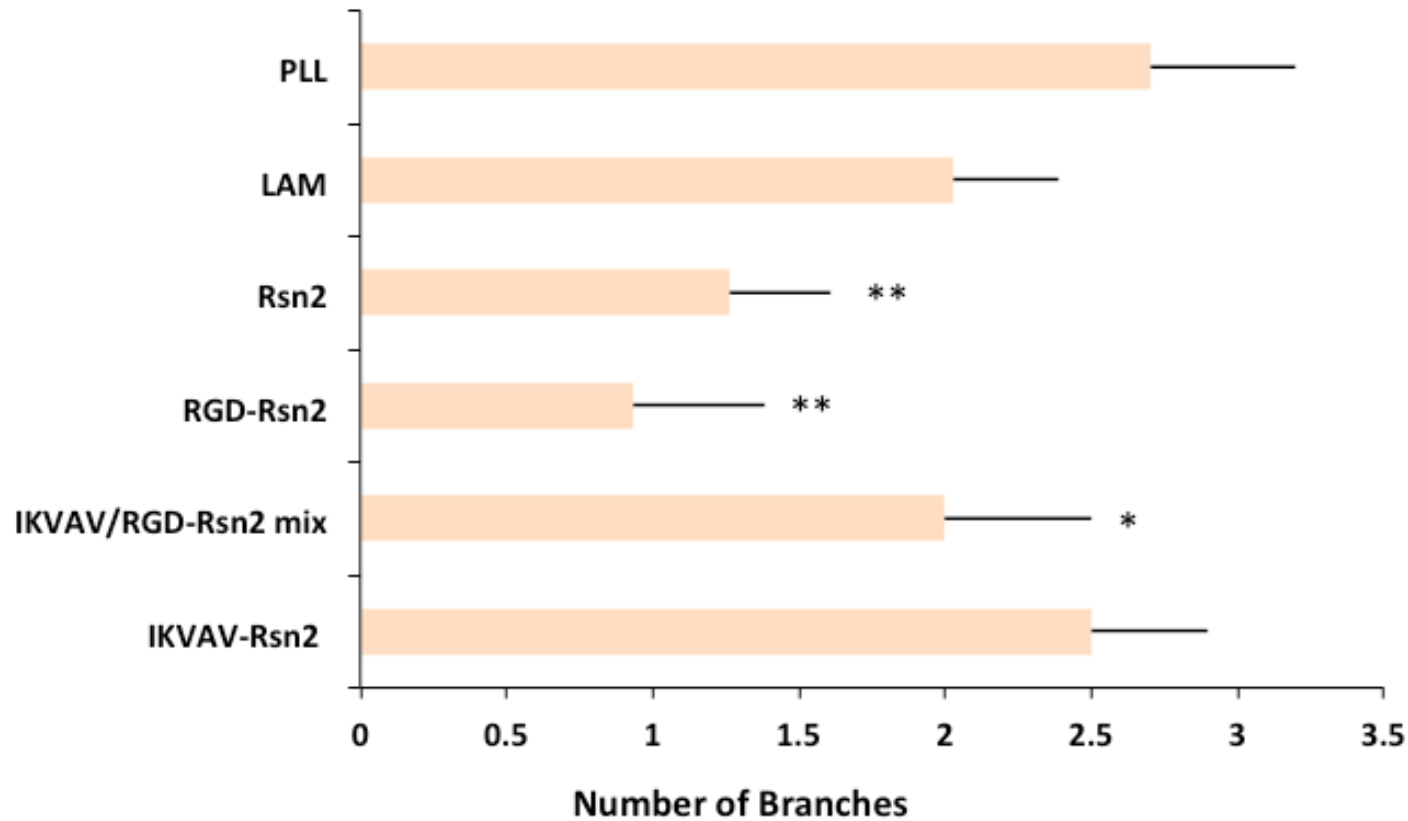
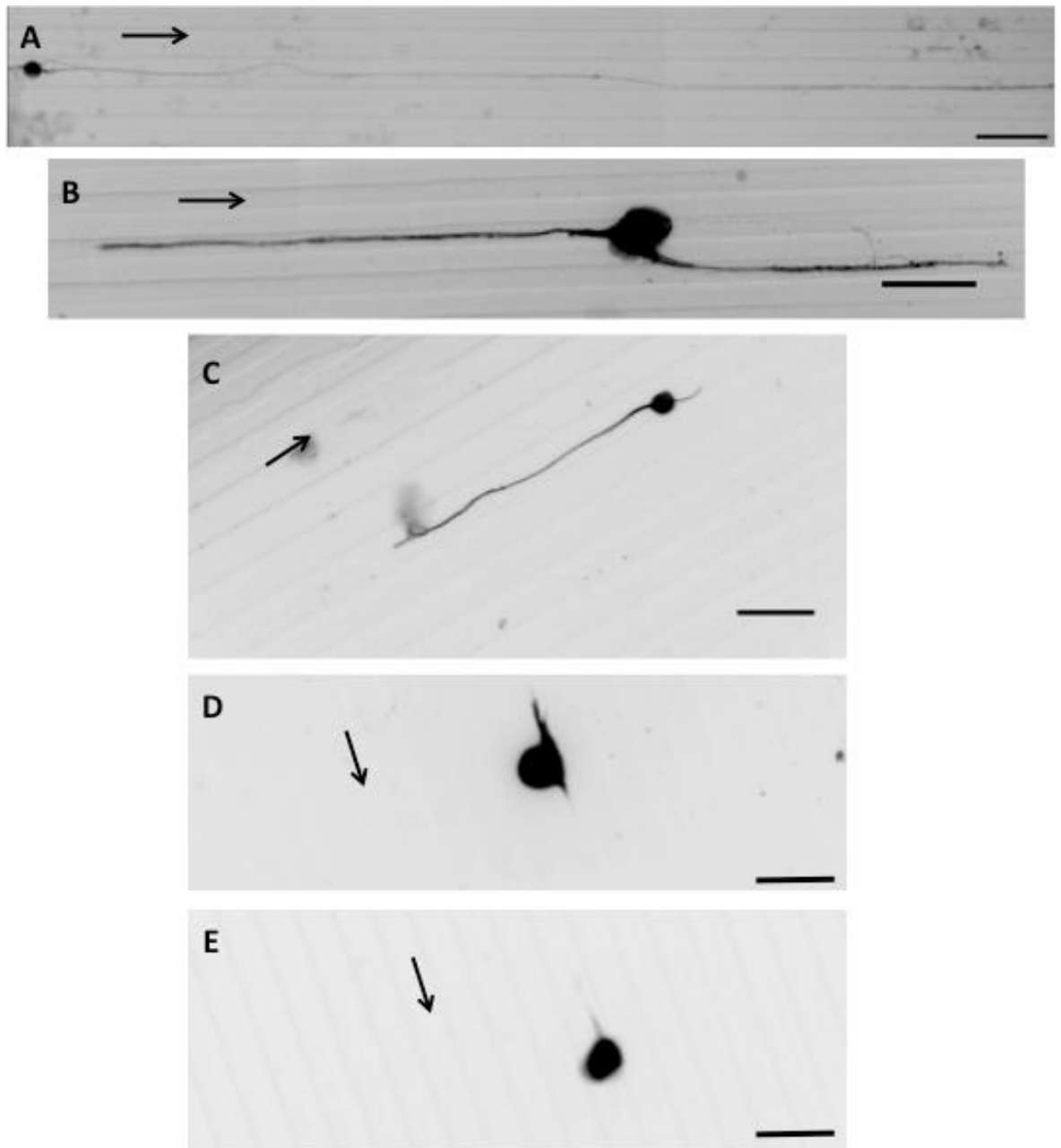


Figure 51: The graph represents the number of branches of individual neurons cultured for 24-hours on PDMS (grooves) coated with PLL, LAM, Rsn2, RGD-Rsn2, IKVAV/RGD-Rsn2 mix and IKVAV-Rsn2 in 10 ng/ml NGF. Axons on IKVAV-Rsn2 branch significantly, more often in comparison to RGD-Rsn2 and plain Rsn2. Stars indicate significant differences between groups compared to control sample PLL as determined by ANOVA and a Dunnett post hoc test \* $p < 0.05$  and \*\* $p < 0.01$  ( $n=3$  biological repeats, multiple fields of view (10 per sample) were examined for analysis). The bars indicate standard deviation.

## Chapter 4



**Figure 52:** Immunofluorescence images of sensory neurons immuno-labelled for  $\beta$ 3-tubulin (grey-scale inverted images) cultured for 24-hours on PDMS (grooves – arrows represent direction of grooves) coated with (A) laminin (B) IKVAV-Rsn2 (C) PLL (D) RGD-Rsn2 and (E) Rsn2. All the surfaces allowed for guided directional outgrowth where laminin provided the best outgrowth compared to the other surfaces. Scale bar = 50  $\mu$ m applies to all substrates.

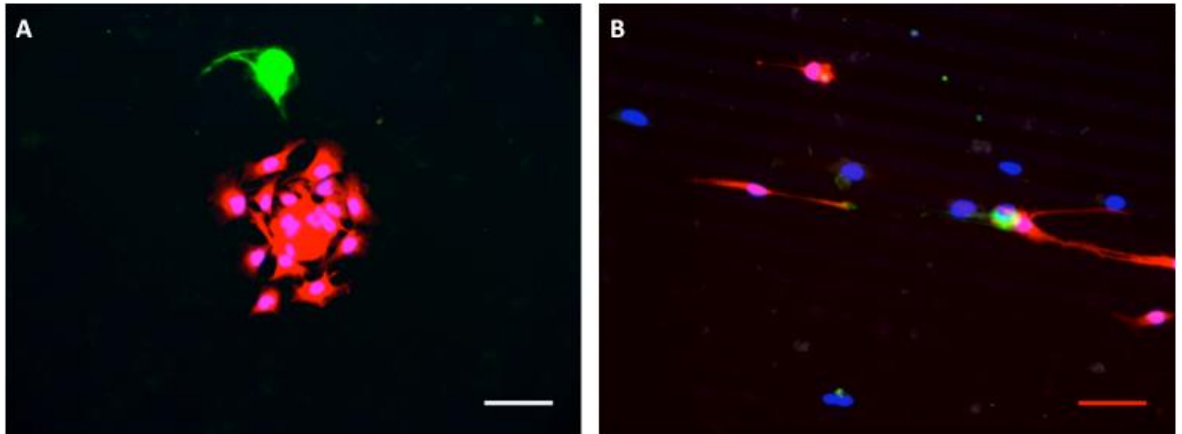
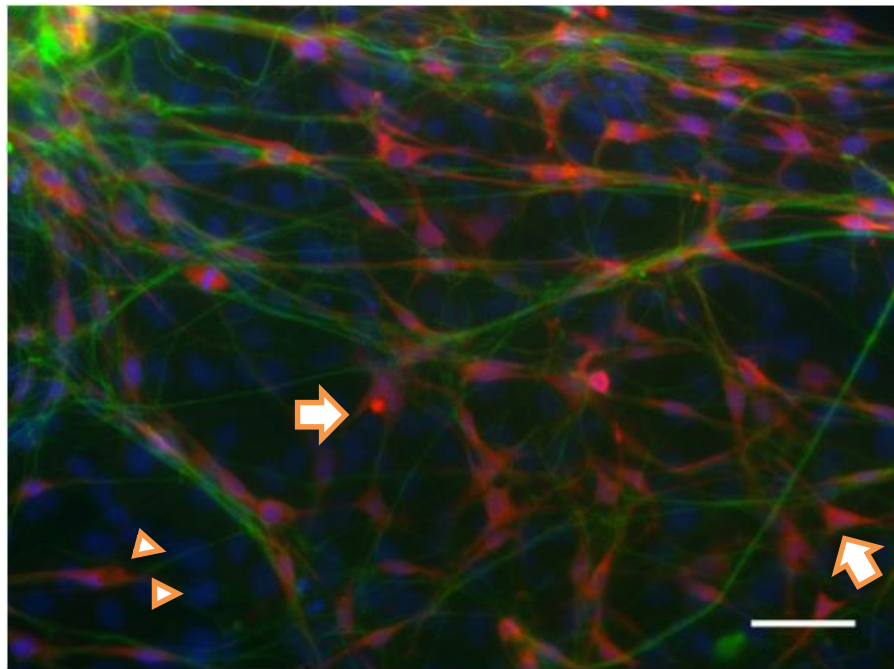


Figure 53: Immunofluorescence images of sensory neurons immuno-labelled for  $\beta$ 3-tubulin (green), Schwann cell marker S100 $\beta$  (red) and DNA (blue) cultured for 24-hours on (A) PDMS (flat) and (B) PDMS (grooves) coated with a 1/1 mix of RGD-Rsn2/IKVAV-Rsn2. The peptide mix seems to have increased the attachment of Schwann cells and other structural cells (only nuclei, not S100 $\beta$  positive). (Observation of n=10 cells) Scale bar = 50  $\mu$ m.

#### 4.3.5 Long term time points (10-day)

To assess if IKVAV peptide sequence is cell supportive long term, a 10-day culture was set up using PDMS samples that have been leached (described in detail in chapter 2) prior to seeding. The protein was supportive for up to the 10-day time point tested (figure 54 & 55). The networks formed on the flat surface were very complex, and by day 10, the attachment and proliferation of other cells was observed (Schwann cells and other structural cells). The surfaces with grooves also maintained the neurons during the 10-day culture where aligned extensions were formed.

## Chapter 4



**Figure 54:** Immunofluorescence images of sensory neurons immuno-labelled for  $\beta$ 3-tubulin (green), Schwann cell marker S100 $\beta$  (red) and DNA (blue) cultured for 10 day on PDMS (flat) coated with IKVAV-Rsn2. At the 10-day time point, the axons formed a very complex network. Also evident were a large number of Schwann (e.g. see arrows, S100 $\beta$  positive) and other supporting cells (e.g. arrowheads, only nuclei, not S100 $\beta$  positive). Scale bar = 50  $\mu$ m.

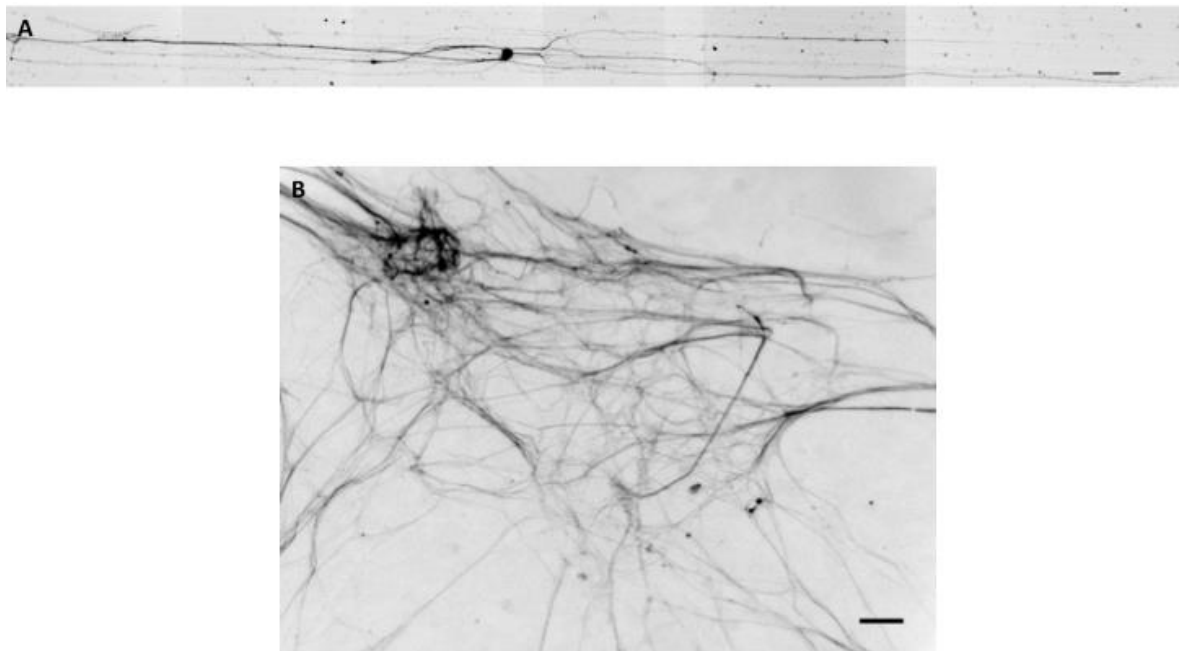


**Figure 55:** Immunofluorescence images of sensory neurons immuno-labelled for  $\beta$ 3-tubulin (inverted grey-scale images) cultured for 10 days on (A) PDMS (grooves) and (B) PDMS (flat) both coated with IKVAV-Rsn2. The grooves resulted in aligned outgrowth whereas the flat cultures have formed a very complex network of axons. Scale bar = 50  $\mu$ m.

## Chapter 4

## 4.3.6 PDMS microcontact stamp

As discussed in detail previously (chapter 2), Rsn2 is assumed to bind to a surface by undergoing a conformational change when in contact with a hydrophobic surface and exposing its hydrophilic side or vice versa. To confirm the basis of this hypothesis,  $\mu$ CP was used to transfer stripes using the hydrophobicity of the protein. To do this a grooved PDMS sample was plasma treated and coated with the fluorescent protein iLOV-Rsn2 to allow visualization of the protein. This was contact printed to a non-treated flat PDMS sample, where it was expected that the pattern would transfer due to both samples being hydrophobic. The transfer of the stripes by conformal contact between the top of the ridges and the flat substrate was successful as visualised by the iLOV fluorescence (figure 56). To assess if the stripe transfer was sufficient for cell growth, cells were cultured on both surfaces (A&B figure 56). Cells adhered to the plasma treated surface coated with iLOV-Rsn2, however no adherence was established on the surface with  $\mu$ CP stripe transfer.

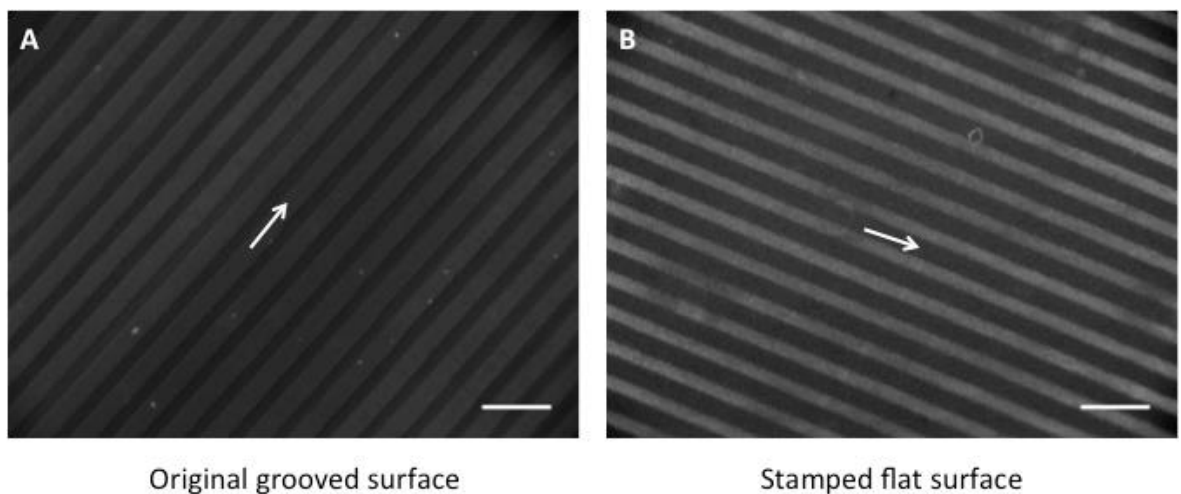


**Figure 56:** Fluorescence images of iLOV-Rsn2 adsorbed surfaces on (A) PDMS (grooves) – plasma treated and iLOV-Rsn2 coated after  $\mu$ CP (B) non-treated PDMS (flat) after  $\mu$ CP transferred iLOV-Rsn2 from (A). These images show that the lines formed by the ridges were successfully transferred from sample A to B (arrows show direction of grooves). Scale bar = 50 $\mu$ m.

**Chapter 4**

Taking the results of the  $\mu$ CP transfer into account, an experiment was set up to assess how plasma treating the PDMS prior to coating with Rsn2 would affect axonal outgrowth. The protein IKVAV-Rsn2 and RGD-Rsn2 were used to coat plasma treated and untreated PDMS, to assess if the peptides are exposed to the cells in both conformations. Results show that there was no significance difference in the axonal length between treating the PDMS prior to protein coating (figure 57).

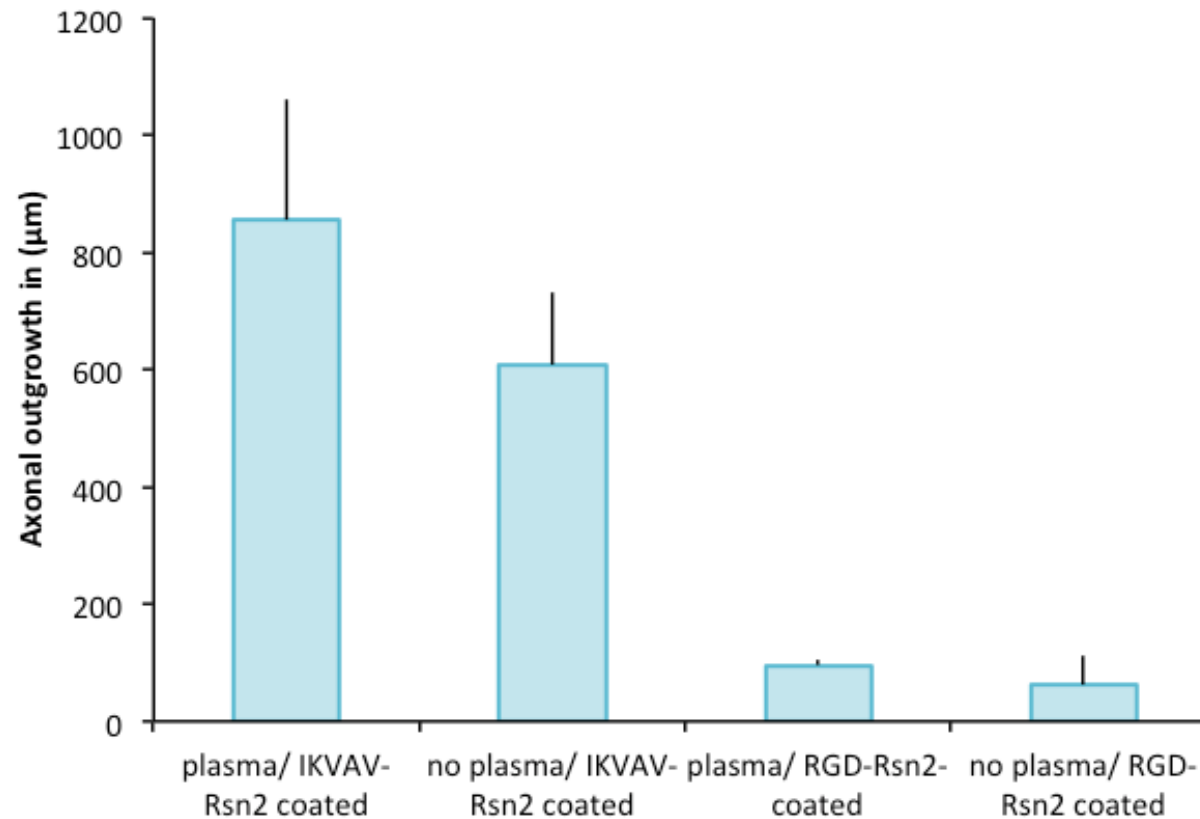


**Figure 57:** The graph represents the average axon outgrowth length of individual neurons cultured for 24-hours on PDMS (flat) (with and without plasma treatment) coated with either IKVAV-Rsn2 or RGD-Rsn2 in 10 ng/ml NGF. The differences between plasma and no plasma treatment were not considered significant at  $p < 0.05$  using ANOVA ( $n=3$  biological repeats, multiple fields of view (10 per sample) were examined for analysis). The bars indicate standard deviation.

## Chapter 4

### 4.4 Discussion & conclusion

The surface properties of a material, such as hydrophilicity/hydrophobicity as well as surface texture (Cortese *et al.*, 2013) are very important determinants of cell adhesion and the resulting cellular morphology (Lee *et al.*, 2004). Treating PDMS with plasma reduced the WCA to less than  $10^\circ$ , this finding also agrees with those of other groups as the formation of hydroxyl groups from the  $O^-$  in the air plasma treatment process significantly increases the hydrophilicity of the surfaces (Sia and Whitesides, 2003). To generate substrates that are favourable for cell adhesion, a routine procedure is to coat the substrate with a layer of adhesive protein. Plasma treated PDMS when coated with LAM and PLL resulted in fairly hydrophobic readings (see table 1). Two groups have discussed a similar observation, and explained it based on the knowledge that ECM molecules such as fibronectin have no electron donor components thus layers of these proteins, adsorbed to surfaces will have an inherently low surface energy. Materials coated with ECM molecules could thus not form hydrogen bonds with water molecules so they would therefore become hydrophobic (Toworfe *et al.*, 2004, Chang, 2009).

Biomaterials play an important role in nerve tissue engineering as they serve as the substrates that form the guidance tubes, they form the interface where cells can attach to and migrate on. To enhance the performance of biomaterials many methods have been used including growth factor delivery systems (Wood *et al.*, 2010), covalent surface modifications and the use of peptide mimetics, modified to contain biologically active motifs such as RGD, YIGSRR and IKVAV (Chung and Park, 2007, Itoh *et al.*, 1999). Various studies have shown that the incorporation of the IKVAV sequence enhances the regenerative potential of nerve cells. A study by Zou *et al.*, (2009) showed that self assembly nanofiber scaffolds containing the IKVAV sequence promoted good biocompatibility with adult sensory neurons. The same paper also incorporated IKVAV into nanofiber gels, which also improved sensory neuron adhesion and promoted neurite outgrowth. Silva *et al.*, (2004) developed IKVAV nanofibres that assembled into a gel-like matrix once exposed to a positive ions - for example, in living tissue. Mouse neural progenitor cells were added to the matrix and the cells differentiated rapidly into neurons as indicated by the expression of specific gene markers and neurite outgrowth.

## Chapter 4

The work presented in this chapter agrees with the above studies as the results successfully show that the neonatal neurons have a preference for the IKVAV sequence, where neurite outgrowth was significantly higher when compared to the RGD peptide and the RGD/IKVAV mix coated substrates as well as laminin. Massia *et al.*, (2004) highlighted this observation, where PC12s (neuron like cell line) were seeded onto dextran-coated materials grafted with an RGD sequence, in its presence the adhesion of fibroblasts and glia cells was significantly higher than that of the neuron like PC12 cells. In contrast when seeded onto IKVAV coated substrates neuronal cell adhesion (PC12) was increased whilst a smaller number of fibroblast and glial cells could adhere. The IKVAV sequence has been identified as one of the principal sites in laminin which differentially regulates cellular behaviour (Tashiro *et al.*, 1989).

The chemical and physical characteristics of a surface influences the quantity, density and conformation of the protein layer adsorbed (Lenk *et al.*, 1991, Sigal *et al.*, 1998, Ta and McDermott, 2000). Rsn2 has been described as a surface-active protein, where it was thought that it undergoes a conformational change where the alpha helix unfolds away from the beta-sheet, exposing the protein's hydrophobic core to the air and aligning the hydrophilic exterior in one plane, directed to the water (detailed in section 1.5). This was described as a “clam-shell” like opening of the protein and would give rise to the amphiphilicity required for the surfactant activity (Mackenzie *et al.*, 2009, Fleming *et al.*, 2009).

The hydrophobicity of Rsn2 enabled the transfer of grooves from one substrate to another using  $\mu$ CP (see figures 56 a & b), and the protein was successfully able to coat both hydrophilic and hydrophobic PDMS and as figure 57 shows both these configurations enabled the functional display of the attached adhesion peptides. This finding suggests that the adsorption of the Rsn2 protein onto a surface is a complex process that involves van der Waals, hydrophobic and electrostatic interactions and hydrogen bonding and further development into using  $\mu$ CP will be necessary.

The work of this chapter has described a method to coat PDMS to improve its biocompatibility and bioactivity by using the protein Rsn2 in combination with IKVAV, a penta-peptide domain found in laminin that advanced adhesion and the outgrowth potential of individual sensory neurons. This induced a much stronger

**Chapter 4**

neuronal cell adhesion and outgrowth after a 24-hour culture on flat PDMS, than any of the other coatings tested (RGD, IKVAV/RGD-Rsn2 mix PLL, and laminin). The outcome on the grooved PDMS coated with the same Rsn2 constructs, PLL and laminin was different, as axonal outgrowth on IKVAV-Rsn2 was significantly less pronounced than on laminin.

The work of this chapter has shown that Rsn2 protein based surface coating has led to the development of well-defined modifications that allow the precise control of cellular interactions at the biomaterial interface and tested for up to 10 days in culture using PDMS scaffolds. Application of IKVAV peptide can be used where stimulation sites to promote neurite outgrowth near the sites for optimal signal transfer between neurons and implants.

**Chapter 5**  
**Discussion-Conclusion**

## Chapter 5

### 5.1 General discussion

Research into PNS injuries has advanced as small defects can be treated with autografts or with nerve guidance tubes (Arslantunali *et al.*, 2014). However, large injuries remain a challenge in surgery. A variety of research techniques using biodegradable scaffolds to stimulate outgrowth through the delivery of permissive cues such as growth factors (Dodla and Bellamkonda, 2008), supportive cells (di Summa *et al.*, 2010, You *et al.*, 2011) and the use of aligned nanotopography (Sorensen *et al.*, 2007) have been developed. On going research to enhance the internal modifications of nerve conduits is necessary for improved clinical outcome.

Biomaterials play a vital role in the field of tissue engineering as their characteristics, such as stiffness (Engler *et al.*, 2006) and degradability (Yang and El Haj, 2006) are considered to play an important role to influence the differentiated cell phenotype and stem cell fate (Leipzig and Shoichet, 2009, Trappmann *et al.*, 2012). The surface topography of a biomaterial, plays an important role e.g. Dalby *et al.*, (2007) have shown, that stem cells can be differentiated into bone cells as a function of the order within the surface features and Spivey *et al.*, (2012) discuss the fundamentals of incorporating surface topography for the restoration of nerve function. One of the great challenges that remain in this field is the translation of the relationship between topography, neural response and the mechanisms by which neurons translate physical cue to biological responses.

## Chapter 5

### 5.1.1 Rsn2 for temporary surface modification of PDMS

PDMS has been extensively used as a material to study cell behaviour because of its biocompatibility and the tunable mechanical properties that cover a wide range of biological tissue stiffness (Trappmann *et al.*, 2012, Murrell *et al.*, 2011, Balaban *et al.*, 2001). As the surface of PDMS is naturally hydrophobic (not conducive to cell attachment), and not conducive to cell adhesion, various techniques, such as physical and chemical treatments, have been utilized to alter this. For example, oxygen plasma has been used to modify the surfaces of PDMS as this treatment reduces hydrophobicity and improves cell attachment (Ferguson *et al.*, 1993). One aspect that is seen as a disadvantage when using surface modified PDMS, is that the hydrophilic surface gradually changes and recovers its hydrophobicity over time (Eddington *et al.*, 2006). This is believed to be a result of LMW chains diffusing to the surface (Kim *et al.*, 2001). The LMW species are either uncrosslinked linear PDMS chains or residual crosslinking agent. Many researchers agree that removing the LMW species improves the biocompatibility of PDMS. Other reasons for removing the uncured PDMS is that these can complicate the interpretation of data, and may interfere with normal cell behaviour upon incorporation into the plasma membrane (Regehr *et al.*, 2009). It is widely accepted that a PDMS network where the LMW species have been removed e.g. by swelling/shrinking in differential solvent systems will retain its hydrophilicity for a much greater time (Eddington *et al.*, 2006, Bodas and Khan-Malek, 2006).

Chapter two of this thesis focused on using the surfactant protein Rsn2 as a means to coat hydrophobic polymers to improve axonal outgrowth, this led to the discovery of a cell sheet harvest method exploiting the interaction of the surface mobility of PDMS containing LMW. Rsn2 acts as a temporary coat that enables cell adhesion to PDMS without the need for prior surface oxidation. By selecting the pre-processing condition for PDMS before coated with Rsn2 (by removing LMW or not), we were able to define a method of Caco-2 cell attachment and growth of a confluent cell sheet which detached after ~21 days with no enzymatic digestion or mechanical dissociation. Cell sheet engineering has been progressing rapidly during the past few years and has emerged as a novel approach for cell based therapy. This allows the fabrication of viable, transplantable cell sheets for various tissue-engineering applications. This Rsn2

## Chapter 5

coating is temporary and allows the retrieval of differentiated cell sheets. The loss of Rsn2 from the surface of PDMS was suppressed if LMW species had been leached out of the bulk of the polymer prior to Rsn2 coating. This can lead to a rational interface design which can be precisely tuned to cell type specific adhesion or different cell sheet retention times on PMDS applied to any cell type.

### 5.1.2 Physical substrates factors affect NGF response in individual neurons

It is now well understood that for peripheral nerve regeneration to improve beyond the state of the art, a combinatorial approach of multiple strategies is required to achieve optimal recovery. Therefore, the third chapter of this thesis tested how surface topography influences the growth of regenerating dissociated DRG neurons with varying NGF concentrations. The use of growth factors and the effect of their concentrations in neuro tissue engineering have been widely studied (Cao and Shoichet, 2001, Madduri *et al.*, 2009, Kaselis *et al.*, 2014). The interaction of substrate stiffness, microtopography and NGF concentration was previously shown to be effective in PC12 neuronal cells (Foley *et al.*, 2005). Dissociated DRG neurons demonstrated a modulation in outgrowth in response to the protein coating of the PDMS substrate. On flat PLL coated PDMS, increasing the range of NGF from 10 ng/ml to 100 ng/ml was associated with increased axonal outgrowth. The inverse effect was found when outgrowth followed micro-grooved topography. On laminin coated PDMS, increasing the range of NGF from 10 ng/ml to 100 ng/ml was associated with decreased axonal outgrowth on both the flat and grooved surfaces. This demonstrated that the interaction between growth factor concentration, protein coating and micro-topography is an important relationship determining the response of the growing axon to their regenerative potential.

Cytoskeletal dynamics are believed to be a central factor in topography-induced responses. Koch and Claesson Welsh (2012) showed that the traction force interactions between the cytoskeleton network and the substrate, which determines growth cone movements, migration and guidance mechanisms occur by integrin mediated mechanisms that sense substrate rigidity. Axon branching requires interactions between dynamic microtubules and actin filaments and

## Chapter 5

integrin activation is linked to myosin II dependent changes in growth cone motility (Dent and Kalil, 2001). It is believed that growth on grooved surfaces induces changes in cellular stiffness (McPhee *et al.*, 2010) as well as differential gene regulation (Dalby *et al.*, 2003). We thus tested how the integrity of the cytoskeleton affects branching by using topography and variation of the NGF concentrations in combination with Blebbistatin, a specific inhibitor of non-muscle myosin II ATPase activity (Limouze *et al.*, 2004). The inhibition of myosin II accelerated the axonal outgrowth at all NGF concentrations and topographies tested. Inhibiting Rho-kinase by using Y-27632 had the opposite effect where outgrowth reduced significantly in comparison to the controls. This demonstrates that cellular tension plays an important role in developing the type and length of axonal outgrowth and is likely to be responsible for the differences observed in outgrowth on flat and grooved surfaces of the dissociated DRG neurons. Signals derived from integrins and other guidance cue receptors converge and act to change growth cone motility, coordinating the direction and rate of outgrowth. This chapter has shown that extracellular cues, through NGF signal transduction mechanisms are transformed into a reorganization of the cytoskeleton resulting in differences in axonal outgrowth. This chapter has also established the most effective combinations of topographies, surface coating and growth factor concentrations to be used in further studies and it adds to the knowledge that cooperative effects between topography, surface coating and NGF signalling play an important role in creating an environment suitable for regeneration by influencing growth cone dynamics.

### 5.1.3 Rsn2 modifications and neural response

In cell and tissue engineering, controlling cell function is vital. One way this can be achieved is by modifying the surface chemistry of a substrate by covalently linking specific proteins to the surface (Niepel *et al.*, 2013). Studies on the adhesive properties of various amphiphilic proteins subjected to conformational changes at an interface include; mussel proteins (Lee *et al.*, 2007), Latherin (Vance *et al.*, 2013), hydrophobins (Janssen *et al.*, 2002) and various palate, lung and nasal epithelium clone proteins (PLUNC) (Gakhar *et al.*, 2010). These have generated interest for their use as agents for surface modification and fabrication of various substrates for biomimetic studies. The work in chapter 2 has shown that the amphiphilic protein Rsn2 can be used to coat biomaterials

## Chapter 5

(leached PDMS, PC and PCL) and sustained neurite outgrowth in culture.

Modifying the protein with specific adhesion peptides for specialised functional surface chemistry can expand its potential use.

Laminin, a major component of the basal lamina, including that produced by Schwann cells, has positive effects on neurite extension, proliferation and migration, and overall has exhibited the ability to improve nerve regeneration (Koh *et al.*, 2010, Itoh *et al.*, 2001). However there are limitations in using laminin *in vivo* as it cannot be produced in a pure form and has a large molecular weight making it difficult to synthesise (Itoh *et al.*, 2003, Santiago *et al.*, 2009). To overcome this, Rsn2 with incorporated N-terminal RGD which is short peptide sequence found in several native ECM proteins including laminin and fibronectin, was created to increase cellular adhesion. To deliver a neuron specific adhesion Rsn2 was combined with IKVAV, a short peptide found only on the alpha chain of laminin.

The effect of the surface chemistry displayed on outgrowth differed depending on the topography and if Rsn2 displayed peptide or whole protein was used. When tested on flat PDMS, IKVAV-Rsn2 surfaces promoted substantial neuron cell adhesion and outgrowth was significantly increased compared to the control using whole laminin and the RGD-Rsn2 coated substrates. These results are in agreement with other reports in the literature that have shown IKVAV to be more effective than the other substrates tested (Xie *et al.*, 2013, Heiduschka *et al.*, 2001, Zou *et al.*, 2009). IKVAV can recognize and bind to a 110-kDa protein (LBP110) located on the surface of neurons, this protein has been found to promote the differentiation and neurite outgrowth of neurons (Kibbey *et al.*, 1993, Kibbey *et al.*, 1995). Another reason that IKVAV can enhance outgrowth is the available epitope density around the cells could be remarkably higher than that of laminin alone. Silva *et al.*, reported that on a IKVAV presenting nanofibre network the epitope density was increased relative to a laminin monolayer by factor of  $10^3$  (Silva *et al.*, 2004). However, on the grooved topography, laminin as a whole protein molecule showed better efficacy compared to all the peptides used, even when combinations of different peptides were used. The difference in outgrowth between neurons on flat and grooved substrates could be related to growth cone morphology as described by Micholt *et al.*, (2013) where the change

## Chapter 5

of the growth cone shape ensures robust neurite outgrowth compared to outgrowth on a flat surface. This determines the speed of outgrowth and is a possible reason for the difference in results between flat and grooved topographies.

Rsn2 is not only an effective protein for improving surface hydrophobicity but is also an ideal carrier for anchoring functional molecules for precision in cell adhesion and response. This chapter has shown that IKVAV-Rsn2 but not RGD-Rsn2 can enhance neuron outgrowth and maintain outgrowth long term. These together with the findings in chapter 3 hold great promise for the advancement of research in this field.

## 5.2 Future work

### 5.2.1 Further investigation in using Rsn2 in culture

This thesis initially started testing the prospect of using Rsn2 as a surface coating to functionalise hydrophobic materials, this led to the discovery of a technique for harvesting cell sheets without the use of mechanical or enzymatic forces. This method allows for the harvest of confluent sheets with their excreted ECM that therefore preserves their biological function.

Further research is required to optimise the method of transferring the cell sheets to another substrate after they detach e.g. a coverslip. This technique can then be tuned for any particular cell type required. These can be patterned and assembled together to mimic the microarchitecture of native tissue, which is crucial for functional tissue regeneration. For the purpose of nerve repair, it would be interesting to investigate this technique for Schwann cell cultures and adipose derived stem cells as sheets that can be used to promote for axonal outgrowth. This will require investigation of the time required to establish a confluent sheet and how long the peeling effect would take.

The work of chapter 4 provided promising results for using IKVAV-Rsn2 in nerve repair strategies. Currently in our lab, Dr Jemma Roberts is investigating the potential use of IKVAV-Rsn2 and RGD-Rsn2 in dissociated DRG adult rat cells and adult pig cells. Provisional data has shown that the adult rat and pig cells

## Chapter 5

prefer a mixture of RGD-Rsn2 and IKAVA-Rsn2 for their outgrowth, on going studies will define the best parameters for the adult cell cultures.

As the majority of experiments in this thesis have focused on the use of PDMS, testing on other materials will be required as PDMS is unsuitable for *in vivo* use. PCL has been widely used for nerve tissue engineering (Oliveira *et al.*, 2010, Donoghue *et al.*, 2012) making it a good candidate biomaterial for further *in vitro* and *in vivo* studies. The suitability of Rsn2 to coat other materials has briefly been investigated in chapter 2, using PC and PCL; however further research will be required for the fusion protein. For the purpose of translational development, this will require confirmation that human neurons respond to the same protein peptides or mixture of peptides. This will require access to human neurons of the PNS, which is current the focus of our group also.

### 5.2.2 Quantifying myosin II

Chapter 3 demonstrated that axonal outgrowth modulation by growth factor concentration, substrate microtopography and protein coating in dissociated DRG neurons was due to the changes in cytoskeletal tension that feeds in to the NGF pathway. Staining of Phospho-Myosin light chain 2 (Ser19) antibody was attempted on the dissociated cells. It was very difficult to define the myosin presence because of the small scale it occurs and because it did vary so much between cell types. To overcome this it will be necessary to use a quantitative technique such as a Western blot to quantify the difference of active myosin (phosphorylated) in the presence and absence of the inhibitors.

For this, non-neuronal cells need to be eliminated from the culture, as a pure population of neurons is required for such analysis. Ara-C an antimetabolic agent has been previously used to kill fibroblasts and glial cells (Aguayo *et al.*, 1975, Eccleston *et al.*, 1989). This was briefly tested, however, due to time limitations this was not fully optimized. Future work will involve optimising the best Ara-C concentration to use to eliminate glial cells by imaging and using cell type-specific antibodies. As the NGF pathway is responsible for the modulation of many genes, further investigation of responsible mechanical, trophic and tropic pathways by qPCR analysis can be used to analyse the genes involved in the process of nerve regeneration.

## Chapter 5

### 5.3 General conclusion

Although there are currently several nerve conduits available for clinical use, none meet the criteria of autologous nerve grafting. An integrated research approach into combinations of the factors (material stiffness, NGF concentration, topography and surface coating) may result in improved performance of nerve conduits by supporting regeneration over long nerve gaps and in large diameter nerves. It has been clearly demonstrated that axonal outgrowth from dissociated DRG neurons can be enhanced on PDMS and directed by microtopography. We have shown that guidance cues of the growth cone and NGF signal transduction mechanisms influence the axonal outgrowth, which is a fundamental relationship to understand for therapeutic purposes.

We have also demonstrated that Rsn2 with its unique structural properties and surfactant activity is beneficial for the studies of surface modification of biomaterials. The data in this thesis suggests IKVAV-Rsn2 is an ideal specific coating agent to functionalise hydrophobic materials in the application of neural tissue engineering. The future prospects of Rsn2 may contribute to the advances in the technology of cell and tissue engineering.

This work will contribute to the on-going effort to develop improved treatment for peripheral nerve repair. This area of research, although popular, is not as successful in clinical translation as desired. The results will help establish the most effective combinations of topographies, biomaterial coating (IKVAV-Rsn2) and growth factors improving our understanding in this field and contributing to improved peripheral nerve repair treatments.

## List of References

- AGUAYO, A. J., ROMINE, J. S. & BRAY, G. M. 1975. Experimental necrosis and arrest of proliferation of Schwann cells by cytosine arabinoside. *J Neurocytol*, 4, 663-74.
- AHMED, Z., BERRY, M. & LOGAN, A. 2009. ROCK inhibition promotes adult retinal ganglion cell neurite outgrowth only in the presence of growth promoting factors. *Molecular and Cellular Neuroscience*, 42, 128-133.
- AKINS, M. R. & BIEDERER, T. 2006. Cell-cell interactions in synaptogenesis. *Curr Opin Neurobiol*, 16, 83-9.
- ALLODI, I., UDINA, E. & NAVARRO, X. 2012. Specificity of peripheral nerve regeneration: Interactions at the axon level. *Progress in Neurobiology*, 98, 16-37.
- AMANO, M., ITO, M., KIMURA, K., FUKATA, Y., CHIHARA, K., NAKANO, T., MATSUURA, Y. & KAIBUCHI, K. 1996. Phosphorylation and activation of myosin by Rho-associated kinase (Rho-kinase). *J Biol Chem*, 271, 20246-9.
- ANTON, E. S., KREIDBERG, J. A. & RAKIC, P. 1999. Distinct Functions of  $\alpha 3$  and  $\alpha V$  Integrin Receptors in Neuronal Migration and Laminar Organization of the Cerebral Cortex. *Neuron*, 22, 277-289.
- ARSLANTUNALI, D., DURSUN, T., YUCEL, D., HASIRCI, N. & HASIRCI, V. 2014. Peripheral nerve conduits: technology update. *Medical Devices (Auckland, N.Z.)*, 7, 405-424.
- AUMAILLEY, M., BRUCKNER-TUDERMAN, L., CARTER, W. G., DEUTZMANN, R., EDGAR, D., EKBLUM, P., ENGEL, J., ENGVALL, E., HOHENESTER, E., JONES, J. C., KLEINMAN, H. K., MARINKOVICH, M. P., MARTIN, G. R., MAYER, U., MENEGUZZI, G., MINER, J. H., MIYAZAKI, K., PATARROYO, M., PAULSSON, M., QUARANTA, V., SANES, J. R., SASAKI, T., SEKIGUCHI, K., SOROKIN, L. M., TALTS, J. F., TRYGGVASON, K., UITTO, J., VIRTANEN, I., VON DER MARK, K., WEWER, U. M., YAMADA, Y. & YURCHENCO, P. D. 2005. A simplified laminin nomenclature. *Matrix Biol*, 24, 326-32.
- AUMAILLEY, M., GERL, M., SONNENBERG, A., DEUTZMANN, R. & TIMPL, R. 1990. Identification of the Arg-Gly-Asp sequence in laminin A chain as a latent cell-binding site being exposed in fragment P1. *FEBS Letters*, 262, 82-86.
- BALABAN, N. Q., SCHWARZ, U. S., RIVELINE, D., GOICHBURG, P., TZUR, G., SABANAY, I., MAHALU, D., SAFRAN, S., BERSHADSKY, A., ADDADI, L. & GEIGER, B. 2001. Force and focal adhesion assembly: a close relationship studied using elastic micropatterned substrates. *Nat Cell Biol*, 3, 466-472.
- BEELEY, J. G., EASON, R. & SNOW, D. H. 1986. Isolation and characterization of latherin, a surface-active protein from horse sweat. *Biochemical Journal*, 235, 645-650.
- BELLAMKONDA, R. V. 2006. Peripheral nerve regeneration: An opinion on channels, scaffolds and anisotropy. *Biomaterials*, 27, 3515-3518.
- BELLIS, S. L. 2011. Advantages of RGD peptides for directing cell association with biomaterials. *Biomaterials*, 32, 4205-10.
- BENDER, M. D., BENNETT, J. M., WADDELL, R. L., DOCTOR, J. S. & MARRA, K. G. 2004. Multi-channeled biodegradable polymer/CultiSpher composite nerve guides. *Biomaterials*, 25, 1269-78.

- BERTHIER, E., YOUNG, E. W. & BEEBE, D. 2012. Engineers are from PDMS-land, Biologists are from Polystyrenia. *Lab Chip*, 12, 1224-37.
- BODAS, D. & KHAN-MALEK, C. 2006. Formation of more stable hydrophilic surfaces of PDMS by plasma and chemical treatments. *Microelectron. Eng.*, 83, 1277-1279.
- BORISOFF, J. F., CHAN, C. C. M., HIEBERT, G. W., OSCHIPOK, L., ROBERTSON, G. S., ZAMBONI, R., STEEVES, J. D. & TETZLAFF, W. 2003. Suppression of Rho-kinase activity promotes axonal growth on inhibitory CNS substrates. *Molecular and Cellular Neuroscience*, 22, 405-416.
- BRADSHAW, A. D., MCNAGNY, K. M., GERVIN, D. B., CANN, G. M., GRAF, T. & CLEGG, D. O. 1995. Integrin  $\alpha 2\beta 1$  mediates interactions between developing embryonic retinal cells and collagen. *Development*, 121, 3593-3602.
- BRUCK, W. 1997. The role of macrophages in Wallerian degeneration. *Brain Pathol*, 7, 741-52.
- BURNETT, M. G. & ZAGER, E. L. 2004. Pathophysiology of peripheral nerve injury: a brief review. *Neurosurg Focus*, 16, E1.
- CAMPBELL, W. W. 2008. Evaluation and management of peripheral nerve injury. *Clinical Neurophysiology*, 119, 1951-1965.
- CANAVAN, H. E., CHENG, X., GRAHAM, D. J., RATNER, B. D. & CASTNER, D. G. 2005. Surface characterization of the extracellular matrix remaining after cell detachment from a thermoresponsive polymer. *Langmuir*, 21, 1949-55.
- CAO, X. & SHOICHET, M. S. 2001. Defining the concentration gradient of nerve growth factor for guided neurite outgrowth. *Neuroscience*, 103, 831-40.
- CASTNER, D. & RATNER, B. 2002. Biomedical surface science: Foundations to frontiers. *Surface Science*, 500, 28-60.
- CHANG, C. J. 2009. Effects of nerve growth factor from genipin-crosslinked gelatin in polycaprolactone conduit on peripheral nerve regeneration--in vitro and in vivo. *J Biomed Mater Res A*, 91, 586-96.
- CHAPMAN, S., FAULKNER, C., KAISERLI, E., GARCIA-MATA, C., SAVENKOV, E. I., ROBERTS, A. G., OPARKA, K. J. & CHRISTIE, J. M. 2008. The photoreversible fluorescent protein iLOV outperforms GFP as a reporter of plant virus infection. *Proceedings of the National Academy of Sciences*, 105, 20038-20043.
- CHAUVEL-LEBRET, D. J., PELLEN-MUSSI, P., AUROY, P. & BONNAURE-MALLET, M. 1999. Evaluation of the in vitro biocompatibility of various elastomers. *Biomaterials*, 20, 291-299.
- CHEN, Y.-S., HSIEH, C.-L., TSAI, C.-C., CHEN, T.-H., CHENG, W.-C., HU, C.-L. & YAO, C.-H. 2000. Peripheral nerve regeneration using silicone rubber chambers filled with collagen, laminin and fibronectin. *Biomaterials*, 21, 1541-1547.
- CHEN, Z.-L. & STRICKLAND, S. 2003. Laminin  $\gamma 1$  is critical for Schwann cell differentiation, axon myelination, and regeneration in the peripheral nerve. *The Journal of Cell Biology*, 163, 889-899.
- CHENG, T. P. O., MURAKAMI, N. & ELZINGA, M. 1992. Localization of myosin IIB at the leading edge of growth cones from rat dorsal root ganglionic cells. *FEBS Letters*, 311, 91-94.
- CHIONO, V., CIARDELLI, G., VOZZI, G., CORTEZ, J., BARBANI, N., GENTILE, P. & GIUSTI, P. 2008. Enzymatically- Modified Melt- Extruded Guides for Peripheral Nerve Repair. *Engineering in Life Sciences*, 8, 226-237.
- CHUNG, H. J. & PARK, T. G. 2007. Surface engineered and drug releasing pre-fabricated scaffolds for tissue engineering. *Adv Drug Deliv Rev*, 59, 249-62.

- CIARDELLI, G. & CHIONO, V. 2006. Materials for peripheral nerve regeneration. *Macromolecular Bioscience*, 6, 13-26.
- CLARK, P., CONNOLLY, P., CURTIS, A. S., DOW, J. A. & WILKINSON, C. D. 1990. Topographical control of cell behaviour: II. Multiple grooved substrata. *Development*, 108, 635-44.
- CORDEIRO, P. G., SECKEL, B. R., LIPTON, S. A., D'AMORE, P. A., WAGNER, J. & MADISON, R. 1989. Acidic fibroblast growth factor enhances peripheral nerve regeneration in vivo. *Plast Reconstr Surg*, 83, 1013-9; discussion 1020-1.
- CORTESE, B., RIEHLE, M. O., D'AMONE, S. & GIGLI, G. 2013. Influence of variable substrate geometry on wettability and cellular responses. *Journal of Colloid and Interface Science*, 394, 582-589.
- DALBY, M. J., GADEGAARD, N., TARE, R., ANDAR, A., RIEHLE, M. O., HERZYK, P., WILKINSON, C. D. W. & OREFFO, R. O. C. 2007. The control of human mesenchymal cell differentiation using nanoscale symmetry and disorder. *Nat Mater*, 6, 997-1003.
- DALBY, M. J., RIEHLE, M. O., YARWOOD, S. J., WILKINSON, C. D. W. & CURTIS, A. S. G. 2003. Nucleus alignment and cell signaling in fibroblasts: response to a micro-grooved topography. *Experimental Cell Research*, 284, 272-280.
- DALY, W., YAO, L., ZEUGOLIS, D., WINDEBANK, A. & PANDIT, A. 2012. A biomaterials approach to peripheral nerve regeneration: bridging the peripheral nerve gap and enhancing functional recovery. *Journal of the Royal Society Interface*, 9, 202-221.
- DEISTER, C. & SCHMIDT, C. E. 2006. Optimizing neurotrophic factor combinations for neurite outgrowth. *J Neural Eng*, 3, 172-9.
- DÉJARDIN, T. P. E. 2013. *New strategies for nerve regeneration* University of Glasgow
- DENT, E. W. & KALIL, K. 2001. Axon Branching Requires Interactions between Dynamic Microtubules and Actin Filaments. *The Journal of Neuroscience*, 21, 9757-9769.
- DEUMENS, R., KOOPMANS, G. C., DEN BAKKER, C. G., MAQUET, V., BLACHER, S., HONIG, W. M., JEROME, R., PIRARD, J. P., STEINBUSCH, H. W. & JOOSTEN, E. A. 2004. Alignment of glial cells stimulates directional neurite growth of CNS neurons in vitro. *Neuroscience*, 125, 591-604.
- DI SUMMA, P. G., KINGHAM, P. J., RAFFOUL, W., WIBERG, M., TERENCEHI, G. & KALBERMATTEN, D. F. 2010. Adipose-derived stem cells enhance peripheral nerve regeneration. *J Plast Reconstr Aesthet Surg*, 63, 1544-52.
- DISCHER, D. E., JANMEY, P. & WANG, Y. 2005. Tissue Cells Feel and Respond to the Stiffness of Their Substrate. *Science*, 310, 1139.
- DODLA, M. C. & BELLAMKONDA, R. V. 2008. Differences between the effect of anisotropic and isotropic laminin and nerve growth factor presenting scaffolds on nerve regeneration across long peripheral nerve gaps. *Biomaterials*, 29, 33-46.
- DONOGHUE, P. S., LAMOND, R., BOOMKAMP, S. D., SUN, T., GADEGAARD, N., RIEHLE, M. O. & BARNETT, S. C. 2012. The Development of a  $\epsilon$ -Polycaprolactone Scaffold for Central Nervous System Repair. *Tissue Engineering Part A*, 19, 497-507.
- DREPPER, T., EGGERT, T., CIRCOLONE, F., HECK, A., KRAUSZ, U., GUTERL, J.-K., WENDORFF, M., LOSI, A., GARTNER, W. & JAEGER, K.-E. 2007. Reporter proteins for in vivo fluorescence without oxygen. *Nat Biotech*, 25, 443-445.

- ECCLESTON, P. A., BANNERMAN, P. G., PLEASURE, D. E., WINTER, J., MIRSKY, R. & JESSEN, K. R. 1989. Control of peripheral glial cell proliferation: enteric neurons exert an inhibitory influence on Schwann cell and enteric glial cell DNA synthesis in culture. *Development*, 107, 107-112.
- EDDINGTON, D. T., PUCCINELLI, J. P. & BEEBE, D. J. 2006. Thermal aging and reduced hydrophobic recovery of polydimethylsiloxane. *Sensors and Actuators B: Chemical*, 114, 170-172.
- EL-ALI, J., SORGER, P. K. & JENSEN, K. F. 2006. Cells on chips. *Nature*, 442, 403-11.
- ENGLER, A. J., SEN, S., SWEENEY, H. L. & DISCHER, D. E. 2006. Matrix Elasticity Directs Stem Cell Lineage Specification. *Cell*, 126, 677-689.
- ERSCHBAMER, M. K., HOFSTETTER, C. P. & OLSON, L. 2005. RhoA, RhoB, RhoC, Rac1, Cdc42, and Tc10 mRNA levels in spinal cord, sensory ganglia, and corticospinal tract neurons and long-lasting specific changes following spinal cord injury. *The Journal of Comparative Neurology*, 484, 224-233.
- EVANS, G. R. 2001. Peripheral nerve injury: a review and approach to tissue engineered constructs. *Anat Rec*, 263, 396-404.
- EZRATTY, E. J., BERTAUX, C., MARCANTONIO, E. E. & GUNDERSEN, G. G. 2009. Clathrin mediates integrin endocytosis for focal adhesion disassembly in migrating cells. *The Journal of Cell Biology*, 187, 733-747.
- FAURÉ, J. & DAGHER, M.-C. 2001. Interactions between Rho GTPases and Rho GDP dissociation inhibitor (Rho-GDI). *Biochimie*, 83, 409-414.
- FAWCETT, J. W. & ASHER, R. A. 1999. The glial scar and central nervous system repair. *Brain Res Bull*, 49, 377-91.
- FENRICH, K. & GORDON, T. 2004. Canadian Association of Neuroscience review: axonal regeneration in the peripheral and central nervous systems--current issues and advances. *Can J Neurol Sci*, 31, 142-56.
- FERGUSON, G. S., CHAUDHURY, M. K., BIEBUYCK, H. A. & WHITESIDES, G. M. 1993. Monolayers on disordered substrates: self-assembly of alkyltrichlorosilanes on surface-modified polyethylene and poly(dimethylsiloxane). *Macromolecules*, 26, 5870-5875.
- FERRUZZA, S., ROSSI, C., SCARINO, M. L. & SAMBUY, Y. 2012. A protocol for differentiation of human intestinal Caco-2 cells in asymmetric serum-containing medium. *Toxicol In Vitro*, 26, 1252-5.
- FLANAGAN, L. A., JU, Y. E., MARG, B., OSTERFIELD, M. & JANMEY, P. A. 2002. Neurite branching on deformable substrates. *Neuroreport*, 13, 2411-5.
- FLEMING, R. I., MACKENZIE, C. D., COOPER, A. & A KENNEDY, M. W. 2009. Foam nest components of the tu' ngara frog: a cocktail of proteins conferring physical and biological resilience. *Proceedings of the Royal Society of London Series B: Biological Sciences*, 276, 1787-1795.
- FLETCHER, D. A. & MULLINS, R. D. 2010. Cell mechanics and the cytoskeleton. *Nature*, 463, 485-92.
- FOLEY, J. D., GRUNWALD, E. W., NEALEY, P. F. & MURPHY, C. J. 2005. Cooperative modulation of neuritogenesis by PC12 cells by topography and nerve growth factor. *Biomaterials*, 26, 3639-44.
- FOX, M. A. 2008. Novel roles for collagens in wiring the vertebrate nervous system. *Curr Opin Cell Biol*, 20, 508-13.
- FRANZE, K., GERDELMANN, J., WEICK, M., BETZ, T., PAWLIZAK, S., LAKADAMYALI, M., BAYER, J., RILLICH, K., GÖGLER, M., LU, Y.-B., REICHENBACH, A., JANMEY, P. & KÄS, J. 2009. Neurite Branch Retraction Is Caused by a Threshold-Dependent Mechanical Impact. *Biophysical Journal*, 97, 1883-1890.

- FRITZ, J. L. & OWEN, M. J. 1995. Hydrophobic recovery of Plasma-Treated Polydimethylsiloxane. *J. Adhesion*, 54, 33-45.
- FU, S. Y. & GORDON, T. 1997. The cellular and molecular basis of peripheral nerve regeneration. *Mol Neurobiol*, 14, 67-116.
- FUENTES, E. O., LEEMHUIS, J., STARK, G. B. & LANG, E. M. 2008. Rho kinase inhibitors Y27632 and H1152 augment neurite extension in the presence of cultured Schwann cells. *Journal of Brachial Plexus and Peripheral Nerve Injury*, 3, 19-19.
- FURUSE, M., FUJITA, K., HIIRAGI, T., FUJIMOTO, K. & TSUKITA, S. 1998. Claudin-1 and -2: Novel Integral Membrane Proteins Localizing at Tight Junctions with No Sequence Similarity to Occludin. *The Journal of Cell Biology*, 141, 1539-1550.
- GAKHAR, L., BARTLETT, J. A., PENTERMAN, J., MIZRACHI, D., SINGH, P. K., MALLAMPALLI, R. K., RAMASWAMY, S. & MCCRAY, P. B., JR. 2010. PLUNC Is a Novel Airway Surfactant Protein with Anti-Biofilm Activity. *PLoS ONE*, 5, e9098.
- GAMBLE, H. J. & EAMES, R. A. 1964. An Electron Microscope Study of the Connective Tissues of Human Peripheral Nerve. *J Anat*, 98, 655-63.
- GEORGE, E. B., GLASS, J. D. & GRIFFIN, J. W. 1995. Axotomy-induced axonal degeneration is mediated by calcium influx through ion-specific channels. *J Neurosci*, 15, 6445-52.
- GEORGE, P. M., SAIGAL, R., LAWLOR, M. W., MOORE, M. J., LAVAN, D. A., MARINI, R. P., SELIG, M., MAKHNI, M., BURDICK, J. A., LANGER, R. & KOHANE, D. S. 2009. Three-dimensional conductive constructs for nerve regeneration. *J Biomed Mater Res A*, 91, 519-27.
- GESELLCHEN, F., BERNASSAU, A. L., DEJARDIN, T., CUMMING, D. R. S. & RIEHLE, M. O. 2014. Cell patterning with a heptagon acoustic tweezer - application in neurite guidance. *Lab on a Chip*, 14, 2266-2275.
- GIANCOTTI, F. G. & RUOSLAHTI, E. 2006. Integrin Signaling. *Science* 285, 1028.
- GOODMAN, C. S. 1996. Mechanisms and molecules that control growth cone guidance. *Annu Rev Neurosci*, 19, 341-77.
- GOSPODAROWICZ, D., GREENBURG, G. & BIRDWELL, C. R. 1978. Determination of cellular shape by the extracellular matrix and its correlation with the control of cellular growth. *Cancer Res*, 38, 4155-71.
- GRAF, J., IWAMOTO, Y., SASAKI, M., MARTIN, G. R., KLEINMAN, H. K., ROBEY, F. A. & YAMADA, Y. 1987. Identification of an amino acid sequence in laminin mediating cell attachment, chemotaxis, and receptor binding. *Cell*, 48, 989-996.
- GRAVVANIS, A. I., TSOUTSOS, D. A., TAGARIS, G. A., PAPALOIS, A. E., PATRALEXIS, C. G., ICONOMOU, T. G., PANAYOTOU, P. N. & IOANNOVICH, J. D. 2004. Beneficial effect of nerve growth factor-7S on peripheral nerve regeneration through inside-out vein grafts: an experimental study. *Microsurgery*, 24, 408-15.
- GRINNELL, F. & FELD, M. K. 1982. Fibronectin adsorption on hydrophilic and hydrophobic surfaces detected by antibody binding and analyzed during cell adhesion in serum-containing medium. *J Biol Chem*, 257, 4888-93.
- GUAN, K. L. & RAO, Y. 2003. Signalling mechanisms mediating neuronal responses to guidance cues. *Nat Rev Neurosci*, 4, 941-56.
- GUILLAUME-GENTIL, O., SEMENOV, O. V., ZISCH, A. H., ZIMMERMANN, R., VOROS, J. & EHRBAR, M. 2011. pH-controlled recovery of placenta-derived mesenchymal stem cell sheets. *Biomaterials*, 32, 4376-84.

- GUPTON, S. L. & GERTLER, F. B. 2010. Integrin signaling switches the cytoskeletal and exocytic machinery that drives neuritogenesis. *Dev Cell*, 18, 725-36.
- HAKIM, A. M. 1999. The neuron: Cell and molecular biology, 2nd edition. *Journal of Psychiatry & Neuroscience* 24, 355-356.
- HALL, S. 2005. The response to injury in the peripheral nervous system. *J Bone Joint Surg Br*, 87, 1309-19.
- HANANI, M. 2005. Satellite glial cells in sensory ganglia: from form to function. *Brain Res Brain Res Rev*, 48, 457-76.
- HANNACHI, I. E., YAMATO, M. & OKANO, T. 2009. Cell sheet engineering: a unique nanotechnology for scaffold-free tissue reconstruction with clinical applications in regenerative medicine. *Journal of internal medicine* 267, 54-70.
- HANZ, S., PERLSON, E., WILLIS, D., ZHENG, J. Q., MASSARWA, R., HUERTA, J. J., KOLTZENBURG, M., KOHLER, M., VAN-MINNEN, J., TWISS, J. L. & FAINZILBER, M. 2003. Axoplasmic importins enable retrograde injury signaling in lesioned nerve. *Neuron*, 40, 1095-104.
- HARAGUCHI, Y., SHIMIZU, T., YAMATO, M., KIKUCHI, A. & OKANO, T. 2006. Electrical coupling of cardiomyocyte sheets occurs rapidly via functional gap junction formation. *Biomaterials*, 27, 4765-74.
- HARAGUCHI, Y., SHIMIZU, T., YAMATO, M. & OKANO, T. 2012. Concise review: cell therapy and tissue engineering for cardiovascular disease. *Stem Cells Transl Med*, 1, 136-41.
- HARRISON, R. G. 1912. The cultivation of tissues in extraneous medium as a method of morphogenetic study. *Anat.Rec.*, 6, 181-93.
- HEGEMANN, D., BRUNNER, H. & OEHR, C. 2003. Plasma treatment of polymers for surface and adhesion improvement. *Nuclear Instruments and Methods in Physics Research Section B: Beam Interactions with Materials and Atoms*, 208, 281-286.
- HEIDUSCHKA, P., ROMANN, I., ECKEN, H., SCHÖNING, M., SCHUHMANN, W. & THANOS, S. 2001. Defined adhesion and growth of neurones on artificial structured substrates. *Electrochimica Acta*, 47, 299-307.
- HEKTOR, H. J. & SCHOLTMEIJER, K. 2005. Hydrophobins: proteins with potential. *Curr Opin Biotechnol*, 16, 434-9.
- HERDEGEN, T., KUMMER, W., FIALLOS, C. E., LEAH, J. & BRAVO, R. 1991. Expression of c-JUN, JUN B and JUN D proteins in rat nervous system following transection of vagus nerve and cervical sympathetic trunk. *Neuroscience*, 45, 413-22.
- HIGUCHI, A., HAMAMURA, A., SHINDO, Y., KITAMURA, H., YOON, B. O., MORI, T., UYAMA, T. & UMEZAWA, A. 2004. Photon-modulated changes of cell attachments on poly(spiropyran-co-methyl methacrylate) membranes. *Biomacromolecules*, 5, 1770-4.
- HIKITA, S. T., CANN, G. M., WINGERD, K. L., MULLICK, L. H., WAYNE, W. C., WEBB, S. W. & CLEGG, D. O. 2003. Integrin alpha4beta1 (VLA-4) expression and activity in retinal and peripheral neurons. *Mol Cell Neurosci*, 23, 427-39.
- HO, C. & O'LEARY, M. E. 2011. Single-cell analysis of sodium channel expression in dorsal root ganglion neurons. *Molecular and cellular neurosciences*, 46, 159-166.
- HOFFMAN-KIM, D., MITCHEL, J. A. & BELLAMKONDA, R. V. 2010. Topography, cell response, and nerve regeneration. *Annu Rev Biomed Eng*, 12, 203-31.

- HÖKFELT, T., ELDE, R., JOHANSSON, O., LUFT, R., NILSSON, G. & ARIMURA, A. 1976. Immunohistochemical evidence for separate populations of somatostatin-containing and substance P-containing primary afferent neurons in the rat. *Neuroscience*, 1, 131-124.
- HÖKFELT, T., KELLERTH, J. O., NILSSON, G. & PERNOW, B. 1975. Substance p: localization in the central nervous system and in some primary sensory neurons. *Science*, 28, 889-90.
- HUANG, J. H., ZAGER, E. L., ZHANG, J., GROFF, R. F., PFISTER, B. J., COHEN, A. S., GRADY, M. S., MALONEY-WILENSKY, E. & SMITH, D. H. 2008. Harvested human neurons engineered as live nervous tissue constructs: implications for transplantation. *Laboratory investigation. J Neurosurg*, 108, 343-7.
- HUBERT, T., GRIMAL, S., CARROLL, P. & FICHARD-CARROLL, A. 2009. Collagens in the developing and diseased nervous system. *Cell Mol Life Sci*, 66, 1223-38.
- HUH, D., HAMILTON, G. A. & INGBER, D. E. 2011. From Three-Dimensional Cell Culture to Organs-on-Chips. *Trends in cell biology*, 21, 745-754.
- HUMPHRIES, M. J., AKIYAMA, S. K., KOMORIYA, A., OLDEN, K. & YAMADA, K. M. 1988. Neurite extension of chicken peripheral nervous system neurons on fibronectin: relative importance of specific adhesion sites in the central cell-binding domain and the alternatively spliced type III connecting segment. *J Cell Biol*, 106, 1289-97.
- HUR, E.-M., YANG, I. H., KIM, D.-H., BYUN, J., SAIJILAFU, XU, W.-L., NICOVICH, P. R., CHEONG, R., LEVCHENKO, A., THAKOR, N. & ZHOU, F.-Q. 2011. Engineering neuronal growth cones to promote axon regeneration over inhibitory molecules. *Proceedings of the National Academy of Sciences of the United States of America*, 108, 5057-5062.
- HYNES, R. O. 1996. Targeted mutations in cell adhesion genes: what have we learned from them? *Dev Biol*, 180, 402-12.
- HYNES, R. O. 2004. The emergence of integrins: a personal and historical perspective. *Matrix Biol*, 23, 333-40.
- ISHIZAKI, T., MAEKAWA, M., FUJISAWA, K., OKAWA, K., IWAMATSU, A., FUJITA, A., WATANABE, N., SAITO, Y., KAKIZUKA, A., MORII, N. & NARUMIYA, S. 1996. The small GTP-binding protein Rho binds to and activates a 160 kDa Ser/Thr protein kinase homologous to myotonic dystrophy kinase. *The EMBO Journal*, 15, 1885-1893.
- ITO, A., HAYASHIDA, M., HONDA, H., HATA, K., KAGAMI, H., UEDA, M. & KOBAYASHI, T. 2004. Construction and harvest of multilayered keratinocyte sheets using magnetite nanoparticles and magnetic force. *Tissue Eng*, 10, 873-880.
- ITOH, S., TAKAKUDA, K., ICHINOSE, S., KIKUCHI, M. & SCHINOMIYA, K. 2001. A study of induction of nerve regeneration using bioabsorbable tubes. *J Reconstr Microsurg*, 17, 115-23.
- ITOH, S., TAKAKUDA, K., SAMEJIMA, H., OHTA, T., SHINOMIYA, K. & ICHINOSE, S. 1999. Synthetic collagen fibers coated with a synthetic peptide containing the YIGSR sequence of laminin to promote peripheral nerve regeneration in vivo. *J Mater Sci Mater Med*, 10, 129-34.
- ITOH, S., YAMAGUCHI, I., SUZUKI, M., ICHINOSE, S., TAKAKUDA, K., KOBAYASHI, H., SHINOMIYA, K. & TANAKA, J. 2003. Hydroxyapatite-coated tendon chitosan tubes with adsorbed laminin peptides facilitate nerve regeneration in vivo. *Brain Res*, 993, 111-23.
- JANSSEN, M. I., VAN LEEUWEN, M. B., SCHOLTMEIJER, K., VAN KOOTEN, T. G., DIJKHUIZEN, L. & WOSTEN, H. A. 2002. Coating with genetic

- engineered hydrophobin promotes growth of fibroblasts on a hydrophobic solid. *Biomaterials*, 23, 4847-54.
- JO, B. H., VAN LERBERGHE, L. M., MOTSEGOOD, K. M. & BEEBE, D. J. 2000. Three-dimensional micro-channel fabrication in poly- dimethylsiloxane (PDMS) elastomer. *J. Microelectromech. Syst.* , 9, 76-81.
- JOHANSSON, F., CARLBERG, P., DANIELSEN, N., MONTELIUS, L. & KANJE, M. 2006. Axonal outgrowth on nano-imprinted patterns. *Biomaterials*, 27, 1251-8.
- JOSHI, A. R., BOBYLEV, I., ZHANG, G., SHEIKH, K. A. & LEHMANN, H. C. 2015. Inhibition of Rho-kinase differentially affects axon regeneration of peripheral motor and sensory nerves. *Experimental Neurology*, 263, 28-38.
- KALBERMATTEN, D. F., ERBA, P., MAHAY, D., WIBERG, M., PIERER, G. & TERENCEHI, G. 2008. Schwann cell strip for peripheral nerve repair. *J Hand Surg Eur Vol*, 33, 587-94.
- KALLURI, R. 2003. Basement membranes: structure, assembly and role in tumour angiogenesis. *Nat Rev Cancer*, 3, 422-33.
- KANG, H., TIAN, L. & THOMPSON, W. 2003. Terminal Schwann cells guide the reinnervation of muscle after nerve injury. *J Neurocytol*, 32, 975-85.
- KAPLAN, D. R. & MILLER, F. D. 2000. Neurotrophin signal transduction in the nervous system. *Current Opinion in Neurobiology*, 10, 381-391.
- KASELIS, A., TREINYS, R., VOSYLIUTE, R. & SATKAUSKAS, S. 2014. DRG axon elongation and growth cone collapse rate induced by *Sema3A* are differently dependent on NGF concentration. *Cell Mol Neurobiol*, 34, 289-96.
- KATER, S. B. & REHDER, V. 1995. The sensory-motor role of growth cone filopodia. *Curr Opin Neurobiol*, 5, 68-74.
- KEELEY, R. D., NGUYEN, K. D., STEPHANIDES, M. J., PADILLA, J. & ROSEN, J. M. 1991. The artificial nerve graft: a comparison of blended elastomer-hydrogel with polyglycolic acid conduits. *J Reconstr Microsurg*, 7, 93-100.
- KEHOE, S., ZHANG, X. F. & BOYD, D. 2012. FDA approved guidance conduits and wraps for peripheral nerve injury: A review of materials and efficacy. *Injury-International Journal of the Care of the Injured*, 43, 553-572.
- KEMP, S. W., WALSH, S. K. & MIDHA, R. 2008. Growth factor and stem cell enhanced conduits in peripheral nerve regeneration and repair. *Neurol Res*, 30, 1030-8.
- KENEA, N. L. & MEHMET, H. 2002. Neural stem cells. *J Pathol*, 197, 536-50.
- KIBBEY, M. C., JOHNSON, B., PETRYSHYN, R., JUCKER, M. & KLEINMAN, H. K. 1995. A 110-kD nuclear shuttling protein, nucleolin, binds to the neurite-promoting IKVAV site of laminin-1. *J Neurosci Res*, 42, 314-22.
- KIBBEY, M. C., JUCKER, M., WEEKS, B. S., NEVE, R. L., VAN NOSTRAND, W. E. & KLEINMAN, H. K. 1993. beta-Amyloid precursor protein binds to the neurite-promoting IKVAV site of laminin. *Proceedings of the National Academy of Sciences of the United States of America*, 90, 10150-10153.
- KILIAN, K. A. & MRKSICH, M. 2012. Directing stem cell fate by controlling the affinity and density of ligand-receptor interactions at the biomaterials interface. *Angew Chem Int Ed Engl*, 51, 4891-5.
- KIM, J., CHAUDHURY, M. K., OWEN, M. J. & ORBECK, T. 2001. The Mechanisms of Hydrophobic Recovery of Polydimethylsiloxane Elastomers Exposed to Partial Electrical Discharges. *Journal of Colloid and Interface Science*, 244, 200-207.
- KINGHAM, P. J., KALBERMATTEN, D. F., MAHAY, D., ARMSTRONG, S. J., WIBERG, M. & TERENCEHI, G. 2007. Adipose-derived stem cells differentiate into a

- Schwann cell phenotype and promote neurite outgrowth in vitro. *Experimental Neurology*, 207, 267-274.
- KIRSCH, M., TERHEGGEN, U. & HOFMANN, H. D. 2003. Ciliary neurotrophic factor is an early lesion-induced retrograde signal for axotomized facial motoneurons. *Molecular and Cellular Neuroscience*, 24, 130-138.
- KLEINMAN, H. K., SEPHEL, G. C., TASHIRO, K., WEEKS, B. S., BURROUS, B. A., ADLER, S. H., YAMADA, Y. & MARTIN, G. R. 1990. Laminin in neuronal development. *Ann N Y Acad Sci*, 580, 302-10.
- KLOSS, C. U., WERNER, A., KLEIN, M. A., SHEN, J., MENUZ, K., PROBST, J. C., KREUTZBERG, G. W. & RAIVICH, G. 1999. Integrin family of cell adhesion molecules in the injured brain: regulation and cellular localization in the normal and regenerating mouse facial motor nucleus. *J Comp Neurol*, 411, 162-78.
- KOCH, S. & CLAESSION-WELSH, L. 2012. Signal Transduction by Vascular Endothelial Growth Factor Receptors. *Cold Spring Harbor Perspectives in Medicine*, 2, a006502.
- KOH, H. S., YONG, T., TEO, W. E., CHAN, C. K., PUHAINDRAN, M. E., TAN, T. C., LIM, A., LIM, B. H. & RAMAKRISHNA, S. 2010. In vivo study of novel nanofibrous intra-luminal guidance channels to promote nerve regeneration. *J Neural Eng*, 7, 046003.
- KOKAI, L. E., GHAZNAVI, A. M. & MARRA, K. G. 2010. Incorporation of double-walled microspheres into polymer nerve guides for the sustained delivery of glial cell line-derived neurotrophic factor. *Biomaterials*, 31, 2313-2322.
- KOKAI, L. E., LIN, Y. C., OYSTER, N. M. & MARRA, K. G. 2009. Diffusion of soluble factors through degradable polymer nerve guides: Controlling manufacturing parameters. *Acta Biomater*, 5, 2540-50.
- KUMASHIRO, Y., YAMATO, M. & OKANO, T. 2010. Cell attachment-detachment control on temperature-responsive thin surfaces for novel tissue engineering. *Ann Biomed Eng*, 38, 1977-88.
- LABRADOR, L. O., BUTI, M. & NAVARRO, X. 1998. Influence of collagen and laminin gels concentration on nerve regeneration after resection and tube repair. *Exp Neurol*, 149, 243-252.
- LALLIER, T. & BRONNER-FRASER, M. 1993. Inhibition of neural crest cell attachment by integrin antisense oligonucleotides. *Science*, 259, 692-5.
- LAWSON, S. N. 1979. The postnatal development of large light and small dark neurons in mouse dorsal root ganglia: a statistical analysis of cell numbers and size. *J Neurocytol*, 8, 275-94.
- LEE, H., DELLATORE, S. M., MILLER, W. M. & MESSERSMITH, P. B. 2007. Mussel-inspired surface chemistry for multifunctional coatings. *Science*, 318, 426-30.
- LEE, J. N., JIANG, X., RYAN, D. & WHITESIDES, G. M. 2004. Compatibility of mammalian cells on surfaces of poly(dimethylsiloxane). *Langmuir*, 20, 11684-91.
- LEE, J. N., PARK, C. & WHITESIDES, G. M. 2003. Solvent Compatibility of Poly(dimethylsiloxane)-Based Microfluidic Devices. *Analytical Chemistry*, 75, 6544-6554.
- LEE, S. K. & WOLFE, S. W. 2000. Peripheral nerve injury and repair. *J Am Acad Orthop Surg*, 8, 243-52.
- LEIN, P. J., BANKER, G. A. & HIGGINS, D. 1992. Laminin selectively enhances axonal growth and accelerates the development of polarity by hippocampal neurons in culture. *Brain Res Dev Brain Res*, 69, 191-7.
- LEIPZIG, N. D. & SHOICHET, M. S. 2009. The effect of substrate stiffness on adult neural stem cell behavior. *Biomaterials*, 30, 6867-78.

- LEISS, M., BECKMANN, K., GIROS, A., COSTELL, M. & FASSLER, R. 2008. The role of integrin binding sites in fibronectin matrix assembly in vivo. *Curr Opin Cell Biol*, 20, 502-7.
- LENK, T. J., HORBETT, T. A., RATNER, B. D. & CHITTUR, K. K. 1991. Infrared spectroscopic studies of time-dependent changes in fibrinogen adsorbed to polyurethanes. *Langmuir*, 7, 1755-1764.
- LI, J., MCNALLY, H. & SHI, R. 2008. Enhanced neurite alignment on micro-patterned poly-L-lactic acid films. *J Biomed Mater Res A*, 87, 392-404.
- LIMOUZE, J., STRAIGHT, A. F., MITCHISON, T. & SELLERS, J. R. 2004. Specificity of blebbistatin, an inhibitor of myosin II. *J Muscle Res Cell Motil*, 25, 337-41.
- LINDER, M. B., SZILVAY, G. R., NAKARI-SETALA, T. & PENTTILA, M. E. 2005. Hydrophobins: the protein-amphiphiles of filamentous fungi. *FEMS Microbiol Rev*, 29, 877-96.
- LINDSAY, R. M. 1988. Nerve Growth Factors (NGF, BDNF) Enhance Axonal Regeneration but Are not Required for Survival of Adult Sensory Neurons. *The journal of Neuroscience* 8, 2394-2405.
- LINDSAY, R. M. & HARMAR, A. J. 1989. Nerve growth factor regulates expression of neuropeptide genes in adult sensory neurons. *Nature*, 337, 362-364.
- LINDWALL, C. & KANJE, M. 2005. Retrograde axonal transport of JNK signaling molecules influence injury induced nuclear changes in p-c-Jun and ATF3 in adult rat sensory neurons. *Mol Cell Neurosci*, 29, 269-82.
- LIU, B.-S., YAO, C.-H., HSU, S.-H., YEH, T.-S., CHEN, Y.-S. & KAO, S.-T. 2004. A Novel Use of Genipin-Fixed Gelatin as Extracellular Matrix for Peripheral Nerve Regeneration. *Journal of Biomaterials Applications*, 19, 21-34.
- LIU, H. M., YANG, L. H. & YANG, Y. J. 1995. Schwann cell properties: 3 C-fos expression, bFGF production, phagocytosis and proliferation during Wallerian degeneration. *J Neuropathol Exp Neurol*, 54, 487-496.
- LIU, W., XING, S., YUAN, B., ZHENG, W. & JIANG, X. 2013. Change of laminin density stimulates axon branching via growth cone myosin II-mediated adhesion. *Integr Biol (Camb)*, 5, 1244-52.
- LU, M. C., HUANG, Y. T., LIN, J. H., YAO, C. H., LOU, C. W., TSAI, C. C. & CHEN, Y. S. 2009. Evaluation of a multi-layer microbraided polylactic acid fiber-reinforced conduit for peripheral nerve regeneration. *J Mater Sci Mater Med*, 20, 1175-80.
- LUCKENBILL-EDDS, L. 1997. Laminin and the mechanism of neuronal outgrowth. *Brain Res Brain Res Rev*, 23, 1-27.
- MA, Z., GAO, C., GONG, Y. & SHEN, J. 2003. Chondrocyte behaviors on poly-l-lactic acid (PLLA) membranes containing hydroxyl, amide or carboxyl groups. *Biomaterials*, 24, 3725-3730.
- MACKENZIE, C. D., SMITH, B. O., MEISTER, A., BLUME, A., ZHAO, X., LU, J. R., KENNEDY, M. W. & COOPER, A. 2009. Ranaspumin-2: structure and function of a surfactant protein from the foam nests of a tropical frog. *Biophys J*, 96, 4984-92.
- MADDURI, S., DI SUMMA, P., PAPALOIZOS, M., KALBERMATTEN, D. & GANDER, B. 2010. Effect of controlled co-delivery of synergistic neurotrophic factors on early nerve regeneration in rats. *Biomaterials*, 31, 8402-9.
- MADDURI, S., PAPALOIZOS, M. & GANDER, B. 2009. Synergistic effect of GDNF and NGF on axonal branching and elongation in vitro. *Neurosci Res*, 65, 88-97.

- MANDOLESI, G., MADEDDU, F., BOZZI, Y., MAFFEI, L. & RATTO, G. M. 2004. Acute physiological response of mammalian central neurons to axotomy: ionic regulation and electrical activity. *FASEB J*, 18, 1934-6.
- MASSIA, S. P., HOLECKO, M. M. & EHTESHAMI, G. R. 2004. In vitro assessment of bioactive coatings for neural implant applications. *J Biomed Mater Res A*, 68, 177-86.
- MASSIA, S. P. & STARK, J. 2001. Immobilized RGD peptides on surface-grafted dextran promote biospecific cell attachment. *Journal of Biomedical Materials Research*, 56, 390-399.
- MCDONALD, J. C. & WHITESIDES, G. M. 2002. Poly(dimethylsiloxane) as a Material for Fabricating Microfluidic Devices. *Accounts of Chemical Research*, 35, 491-499.
- MCKERRACHER, L., CHAMOUX, M. & ARREGUI, C. O. 1996. Role of laminin and integrin interactions in growth cone guidance. *Mol Neurobiol*, 12, 95-116.
- MCPHEE, G., DALBY, M., RIEHLE, M. & YIN, H. 2010. Can common adhesion molecules and microtopography affect cellular elasticity? A combined atomic force microscopy and optical study. *Medical & Biological Engineering & Computing*, 48, 1043-1053.
- MEIJERING, E., JACOB, M., SARRIA, J. C. F., STEINER, P., HIRLING, H. & UNSER, M. 2004. Design and validation of a tool for neurite tracing and analysis in fluorescence microscopy images. *Cytometry Part A*, 58A, 167-176.
- MELLENDEZ-VASQUEZ, C. V., EINHEBER, S. & SALZER, J. L. 2004. Rho Kinase Regulates Schwann Cell Myelination and Formation of Associated Axonal Domains. *The Journal of Neuroscience*, 24, 3953-3963.
- MICHAJELEWSKI, I., MEDZIHRADESKY, K. F., LYNN, A., BURLINGAME, A. L. & FAINZILBER, M. 2010. Axonal Transport Proteomics Reveals Mobilization of Translation Machinery to the Lesion Site in Injured Sciatic Nerve. *Molecular & Cellular Proteomics : MCP*, 9, 976-987.
- MICHOLT, L., GARTNER, A., PRODANOV, D., BRAEKEN, D., DOTTI, C. G. & BARTIC, C. 2013. Substrate topography determines neuronal polarization and growth in vitro. *PLoS One*, 8, e66170.
- MILLER, C., JEFTINIJA, S. & MALLAPRAGADA, S. 2002. Synergistic effects of physical and chemical guidance cues on neurite alignment and outgrowth on biodegradable polymer substrates. *Tissue Eng*, 8, 367-78.
- MONNIER, P. P., SIERRA, A., SCHWAB, J. M., HENKE-FAHLE, S. & MUELLER, B. K. 2003. The Rho/ROCK pathway mediates neurite growth-inhibitory activity associated with the chondroitin sulfate proteoglycans of the CNS glial scar. *Molecular and Cellular Neuroscience*, 22, 319-330.
- MULLER, U., BOSSY, B., VENSTROM, K. & REICHARDT, L. F. 1995. Integrin  $\alpha 8 \beta 1$  Promotes Attachment, Cell Spreading, and Neurite Outgrowth on Fibronectin. *Molecular Biology of the Cell*, 6, 433-448.
- MURRELL, M., KAMM, R. & MATSUDAIRA, P. 2011. Substrate viscosity enhances correlation in epithelial sheet movement. *Biophys J*, 101, 297-306.
- MYERS, J. P., SANTIAGO-MEDINA, M. & GOMEZ, T. M. 2011. Regulation of axonal outgrowth and pathfinding by integrin-ECM interactions. *Dev Neurobiol*, 71, 901-23.
- NADARAJAH, B., ALIFRAGIS, P., WONG, R. O. & PARNAVELAS, J. G. 2002. Ventricle-directed migration in the developing cerebral cortex. *Nat. Neurosci.*, 5, 18-24.
- NAKAMURA, T., INADA, Y., FUKUDA, S., YOSHITANI, M., NAKADA, A., ITOI, S.-I., KANEMARU, S.-I., ENDO, K. & SHIMIZU, Y. 2004. Experimental study on the

- regeneration of peripheral nerve gaps through a polyglycolic acid-collagen (PGA-collagen) tube. *Brain Research*, 1027, 18-29.
- NASDALA, I., WOLBURG-BUCHHOLZ, K., WOLBURG, H., KUHN, A., EBNET, K., BRACHTENDORF, G., SAMULOWITZ, U., KUSTER, B., ENGELHARDT, B., VESTWEBER, D. & BUTZ, S. 2002. A transmembrane tight junction protein selectively expressed on endothelial cells and platelets. *J Biol Chem*, 277, 16294-303.
- NAVARRO, X., VIVO, M. & VALERO-CABRE, A. 2007. Neural plasticity after peripheral nerve injury and regeneration. *Prog Neurobiol*, 82, 163-201.
- NIEPEL, M., KÖWITSCH, A., YANG, Y., MA, N., AGGARWAL, N., GUDURU, D. & GROTH, T. 2013. Generic Methods of Surface Modification to Control Adhesion of Cells and Beyond. *Biomaterials Surface Science*. Wiley-VCH Verlag GmbH & Co. KGaA.
- NOMIZU, M., KURATOMI, Y., MALINDA, K. M., SONG, S.-Y., MIYOSHI, K., OTAKA, A., POWELL, S. K., HOFFMAN, M. P., KLEINMAN, H. K. & YAMADA, Y. 1998. Cell Binding Sequences in Mouse Laminin  $\alpha$ 1 Chain. *Journal of Biological Chemistry*, 273, 32491-32499.
- NOVIKOVA, L. N., PETTERSSON, J., BROHLIN, M., WIBERG, M. & NOVIKOV, L. N. 2008. Biodegradable poly-b-hydroxybutyrate scaffold seeded with Schwann cells to promote spinal cord repair. *Biomaterials*, 29, 1198-1206.
- OLIVEIRA, J. T., ALMEIDA, F. M., BIANCALANA, A., BAPTISTA, A. F., TOMAZ, M. A., MELO, P. A. & MARTINEZ, A. M. 2010. Mesenchymal stem cells in a polycaprolactone conduit enhance median-nerve regeneration, prevent decrease of creatine phosphokinase levels in muscle, and improve functional recovery in mice. *Neuroscience*, 170, 1295-303.
- OTTEN, U., GOEDERT, M., MAYER, N. & LEMBECK, F. 1980. Requirement of nerve growth factor for development of substance P-containing sensory neurones. *Nature*, 287, 158-159.
- OULAD HAMMOUCH, S., BEINERT, G. J. & HERZ, J. E. 1996. Contribution to a better knowledge of the crosslinking reaction of polydimethylsiloxane (PDMS) by end-linking: the formation of star-branched PDMS by the hydrosilylation reaction. *Polymer*, 37, 3353-3360.
- OWEN, M. J. & SMITH, P. J. 1994. Plasma treatment of polydimethylsiloxane. *J. Adhesion Sci*, 8, 1063-1075.
- PALCHESKO, R. N., ZHANG, L., SUN, Y. & FEINBERG, A. W. 2012. Development of polydimethylsiloxane substrates with tunable elastic modulus to study cell mechanobiology in muscle and nerve. *PLoS One*, 7, e51499.
- PARK, J., LIM, E., BACK, S., NA, H., PARK, Y. & SUN, K. 2010. Nerve regeneration following spinal cord injury using matrix metalloproteinase-sensitive, hyaluronic acid-based biomimetic hydrogel scaffold containing brain-derived neurotrophic factor. *Journal of Biomedical Materials Research Part A*, 93A, 1091-1099.
- PATEL, B. N. & VAN VACTOR, D. L. 2002. Axon guidance: the cytoplasmic tail. *Curr Opin Cell Biol*, 14, 221-9.
- PATEL, N. G. & ZHANG, G. 2013. Responsive systems for cell sheet detachment. *Organogenesis*, 9, 93-100.
- PAVELIEV, M., LUME, M., VELTHUT, A., PHILIPS, M., ARUMAE, U. & SAARMA, M. 2007. Neurotrophic factors switch between two signaling pathways that trigger axonal growth. *Journal of Cell Science*, 120, 2507-2516.

- POWELL, S. K., RAO, J., ROQUE, E., NOMIZU, M., KURATOMI, Y., YAMADA, Y. & KLEINMAN, H. K. 2000. Neural cell response to multiple novel sites on laminin-1. *Journal of Neuroscience Research*, 61, 302-312.
- PRICE, J. & MUDGE, A. W. 1983. A subpopulation of rat dorsal root ganglion neurones is catecholaminergic. *Nature*, 20;301, 241-3.
- QUARLES, R. H., MACKLIN, W. B. & MORELL, P. 2006. Myelin Formation, Structure and Biochemistry *Basic Neurochemistry: Molecular, Cellular and Medical Aspects*. Elsevier, Inc.
- RANSCHT, B. 2000. Cadherins: molecular codes for axon guidance and synapse formation. *Int J Dev Neurosci*, 18, 643-51.
- RASBAND, W. S. 1997-2012. ImageJ <http://imagej.nih.gov/ij/>,. U. S. National Institutes of Health , Bethesda, Maryland, USA.
- RATNER, B. D. & BRYANT, S. J. 2004. Biomaterials: where we have been and where we are going. *Annu Rev Biomed Eng*, 6, 41-75.
- REGEHR, K. J., DOMENECH, M., KOEPEL, J. T., CARVER, K. C., ELLISON-ZELSKI, S. J., MURPHY, W. L., SCHULER, L. A., ALARID, E. T. & BEEBE, D. J. 2009. Biological implications of polydimethylsiloxane-based microfluidic cell culture. *Lab on a Chip*, 9, 2132-2139.
- RIVAS, R. J., BURMEISTER, D. W. & GOLDBERG, D. J. 1992. Rapid effects of laminin on the growth cone. *Neuron*, 8, 107-15.
- ROSEN, B. & LUNDBORG, G. 2004. Sensory re-education after nerve repair: aspects of timing. *Handchir Mikrochir Plast Chir*, 36, 8-12.
- ROSENFELD, M. G., MERMOD, J. J., AMARA, S. G., SWANSON, L. W., SAWCHENKO, P. E., RIVIER, J., VALE, W. W. & EVANS, R. M. 1983. Production of a novel neuropeptide encoded by the calcitonin gene via tissue-specific RNA processing. *Nature*, 304, 129-35.
- ROSENTHAL, R., HEYDT, M. S., AMASHEH, M., STEIN, C., FROMM, M. & AMASHEH, S. 2012. Analysis of absorption enhancers in epithelial cell models. *Ann N Y Acad Sci*, 1258, 86-92.
- RUOSLAHTI, E. & PIERSCHBACHER, M. D. 1986. Arg-Gly-Asp: a versatile cell recognition signal. *Cell*, 44, 517-8.
- SANCHEZ-CORTES, J. & MRKSICH, M. 2011. Using self-assembled monolayers to understand alpha8beta1-mediated cell adhesion to RGD and FEI motifs in nephronectin. *ACS Chem Biol*, 6, 1078-86.
- SANCHEZ-RAMOS, J., SONG, S., CARDOZO-PELAEZ, F., HAZZI, C., STEDEFORD, T., WILLING, A., FREEMAN, T. B., SAPORTA, S., JANSSEN, W., PATEL, N., COOPER, D. R. & SANBERG, P. R. 2000. Adult bone marrow stromal cells differentiate into neural cells in vitro. *Exp Neurol*, 164, 247-56.
- SANTIAGO, L. Y., CLAVIJO-ALVAREZ, J., BRAYFIELD, C., RUBIN, J. P. & MARRA, K. G. 2009. Delivery of Adipose-Derived Precursor Cells for Peripheral Nerve Repair. *Cell Transplantation*, 18, 145-158.
- SAYYAD, W. A., AMIN, L., FABRIS, P., ERCOLINI, E. & TORRE, V. 2015. The role of myosin-II in force generation of DRG filopodia and lamellipodia. *Sci Rep*, 5, 7842.
- SCARAVILLI, F. 1984. Regeneration of the perineurium across a surgically induced gap in a nerve encased in a plastic tube. *J Anat*, 139 ( Pt 3), 411-24.
- SEDDON, H. J. 1942. A Classification of Nerve Injuries. *Br Med J*, 2, 237-9.
- SHAPIRO, L., FANNON, A. M., KWONG, P. D., THOMPSON, A., LEHMANN, M. S., GRUBEL, G., LEGRAND, J. F., ALS-NIELSEN, J., COLMAN, D. R. & HENDRICKSON, W. A. 1995. Structural basis of cell-cell adhesion by cadherins. *Nature*, 374, 327-37.

- SHEN, L. 2012. Tight junctions on the move: molecular mechanisms for epithelial barrier regulation. *Ann N Y Acad Sci*, 1258, 9-18.
- SHERMAN, M. A. & KENNEDY, J. P. 1998. Novel polyisobutylene/poly(dimethylsiloxane) bicomponent networks. I. Synthesis and characterization. *Journal of Polymer Science Part A: Polymer Chemistry*, 36, 1891-1899.
- SHIMIZU, T., SEKINE, H., ISOI, Y., YAMATO, M., KIKUCHI, A. & OKANO, T. 2006a. Long-term survival and growth of pulsatile myocardial tissue grafts engineered by the layering of cardiomyocyte sheets. *Tissue Eng*, 12, 499-507.
- SHIMIZU, T., SEKINE, H., YANG, J., ISOI, Y., YAMATO, M., KIKUCHI, A., KOBAYASHI, E. & OKANO, T. 2006b. Polysurgery of cell sheet grafts overcomes diffusion limits to produce thick, vascularized myocardial tissues. *FASEB J*, 20, 708-10.
- SHIN, H., JO, S. & MIKOS, A. G. 2003. Biomimetic materials for tissue engineering. *Biomaterials*, 24, 4353-64.
- SIA, S. K. & WHITESIDES, G. M. 2003. Microfluidic devices fabricated in poly(dimethylsiloxane) for biological studies. *Electrophoresis*, 24, 3563-76.
- SIGAL, G. B., MRKSICH, M. & WHITESIDES, G. M. 1998. Effect of Surface Wettability on the Adsorption of Proteins and Detergents. *Journal of the American Chemical Society*, 120, 3464-3473.
- SILVA, G. A., CZEISLER, C., NIECE, K. L., BENIASH, E., HARRINGTON, D. A., KESSLER, J. A. & STUPP, S. I. 2004. Selective Differentiation of Neural Progenitor Cells by High-Epitope Density Nanofibers. *Science*, 303, 1352-1355.
- SNIDER, W. D., ZHOU, F. Q., ZHONG, J. & MARKUS, A. 2002. Signaling the pathway to regeneration. *Neuron*, 35, 13-6.
- SORENSEN, A., ALEKSEEVA, T., KATECHIA, K., ROBERTSON, M., RIEHLE, M. O. & BARNETT, S. C. 2007. Long-term neurite orientation on astrocyte monolayers aligned by microtopography. *Biomaterials*, 28, 5498-508.
- SPIVEY, E. C., KHAING, Z. Z., SHEAR, J. B. & SCHMIDT, C. E. 2012. The fundamental role of subcellular topography in peripheral nerve repair therapies. *Biomaterials*, 33, 4264-76.
- STAATZ, W. D., FOK, K. F., ZUTTER, M. M., ADAMS, S. P., RODRIGUEZ, B. A. & SANTORO, S. A. 1991. Identification of a tetrapeptide recognition sequence for the alpha 2 beta 1 integrin in collagen. *Journal of Biological Chemistry*, 266, 7363-7367.
- STERNE, G. D., BROWN, R. A., GREEN, C. J. & TERENCE, G. 1997. Neurotrophin-3 delivered locally via fibronectin mats enhances peripheral nerve regeneration. *Eur J Neurosci*, 9, 1388-96.
- STETTLER, E. M. & GALILEO, D. S. 2004. Radial glia produce and align the ligand fibronectin during neuronal migration in the developing chick brain. *The Journal of Comparative Neurology*, 468, 441-451.
- STRAIGHT, A. F., CHEUNG, A., LIMOUZE, J., CHEN, I., WESTWOOD, N. J., SELLERS, J. R. & MITCHISON, T. J. 2003. Dissecting Temporal and Spatial Control of Cytokinesis with a Myosin II Inhibitor. *Science*, 299, 1743-1747.
- STRALEY, K. & HEILSHORN, S. C. 2009. Designer protein-based scaffolds for neural tissue engineering. *Conf Proc IEEE Eng Med Biol Soc*, 2009, 2101-2.
- STRITTMATTER, S. M., IGARASHI, M. & FISHMAN, M. C. 1994. GAP-43 amino terminal peptides modulate growth cone morphology and neurite outgrowth. *J Neurosci*, 14, 5503-13.

- SU, W. T., LIAO, Y. F., WU, T. W., WANG, B. J. & SHIH, Y. Y. 2013. Microgrooved patterns enhanced PC12 cell growth, orientation, neurite elongation, and neuritogenesis. *J Biomed Mater Res A*, 101, 185-94.
- SUNDERLAND, S. 1969. Nerves and nerve injuries. By Sydney Sunderland, C.M.G., M.D., B.S., D.Sc., F.R.A.C.S.(Hon.), F.R.A.C.P., F.A.A. (Melbourne). 10 x 7 in. Pp. 116 + xvi, with 197 illustrations. 1968. Edinburgh: E. & S. Livingstone Ltd. £ 12 10s. *British Journal of Surgery*, 56, 401-401.
- SUNDERLAND, S. & BRADLEY, K. C. 1961. Stress-strain phenomena in denervated peripheral nerve trunks. *Brain*, 84, 125-127.
- TA, T. C. & MCDERMOTT, M. T. 2000. Mapping interfacial chemistry induced variations in protein adsorption with scanning force microscopy. *Anal Chem*, 72, 2627-34.
- TAKEICHI, M. 2007. The cadherin superfamily in neuronal connections and interactions. *Nat Rev Neurosci*, 8, 11-20.
- TASHIRO, K., SEPHEL, G. C., WEEKS, B., SASAKI, M., MARTIN, G. R., KLEINMAN, H. K. & YAMADA, Y. 1989. A synthetic peptide containing the IKVAV sequence from the A chain of laminin mediates cell attachment, migration, and neurite outgrowth. *Journal of Biological Chemistry*, 264, 16174-16182.
- TATE, M. C., GARCIA, A. J., KESELOWSKY, B. G., SCHUMM, M. A., ARCHER, D. R. & LAPLACA, M. C. 2004. Specific beta1 integrins mediate adhesion, migration, and differentiation of neural progenitors derived from the embryonic striatum. *Mol Cell Neurosci*, 27, 22-31.
- TAYLOR, D. L., CONDEELIS, J. S., MOORE, P. L. & ALLEN, R. D. 1973. The contractile basis of amoeboid movement. I. The chemical control of motility in isolated cytoplasm. *J Cell Biol*, 59, 378-94.
- TERENGI, G. 1999. Peripheral nerve regeneration and neurotrophic factors. *Journal of Anatomy*, 194, 1-14.
- TERENGI, G., WIBERG, M. & KINGHAM, P. J. 2009. Chapter 21 Use of Stem Cells for Improving Nerve Regeneration. *International Review of Neurobiology*. Academic Press.
- THOLPADY, S. S., KATZ, A. J. & OGLE, R. C. 2003. Mesenchymal stem cells from rat visceral fat exhibit multipotential differentiation in vitro. *The Anatomical Record Part A: Discoveries in Molecular, Cellular, and Evolutionary Biology*, 272A, 398-402.
- THOMAS, P. K. 1989. Invited review: focal nerve injury: guidance factors during axonal regeneration. *Muscle Nerve*, 12, 796-802.
- THOMPSON, M. D. & BUETTNER, M. H. 2006. Neurite Outgrowth is Directed by Schwann Cell Alignment in the Absence of Other Guidance Cues. *Annals of Biomedical Engineering*, 34, 669-676.
- THOUMINE, O., KOCIAN, P., KOTTELAT, A. & MEISTER, J. J. 2000. Short-term binding of fibroblasts to fibronectin: optical tweezers experiments and probabilistic analysis. *Eur Biophys J*, 29, 398-408.
- TILLET, R. L., AFOKE, A., HALL, S. M., BROWN, R. A. & PHILLIPS, J. B. 2004. Investigating mechanical behaviour at a core-sheath interface in peripheral nerve. *J Peripher Nerv Syst*, 9, 255-62.
- TOMASELLI, K. J., DOHERTY, P., EMMETT, C. J., DAMSKY, C. H., WALSH, F. S. & REICHARDT, L. F. 1993. Expression of  $\beta 1$  Integrins in Sensory Neurons of the Dorsal Root Ganglion and Their Functions in Neurite Outgrowth on Two Laminin Isoforms. *The Journal of neuroscience : the official journal of the Society for Neuroscience*, 13, 4880-4888.

- TONGE, D. A., GOLDING, J. P., EDBLADH, M., KROON, M., EKSTROM, P. E. & EDSTROM, A. 1997. Effects of extracellular matrix components on axonal outgrowth from peripheral nerves of adult animals in vitro. *Exp Neurol*, 146, 81-90.
- TÖNGES, L., KOCH, J. C., BAHR, M. & LINGOR, P. 2011. ROCKing regeneration: Rho kinase inhibition as molecular target for neurorestoration. *Frontiers in Molecular Neuroscience*, 4.
- TOWORFE, G. K., COMPOSTO, R. J., ADAMS, C. S., SHAPIRO, I. M. & DUCHEYNE, P. 2004. Fibronectin adsorption on surface-activated poly(dimethylsiloxane) and its effect on cellular function. *Journal of Biomedical Materials Research Part A*, 71A, 449-461.
- TRAPPMANN, B., GAUTROT, J. E., CONNELLY, J. T., STRANGE, D. G., LI, Y., OYEN, M. L., COHEN STUART, M. A., BOEHM, H., LI, B., VOGEL, V., SPATZ, J. P., WATT, F. M. & HUCK, W. T. 2012. Extracellular-matrix tethering regulates stem-cell fate. *Nat Mater*, 11, 642-9.
- TUCKER, B. A., RAHIMTULA, M. & MEAROW, K. M. 2005. Integrin activation and neurotrophin signaling cooperate to enhance neurite outgrowth in sensory neurons. *J Comp Neurol*, 486, 267-80.
- VANCE, S. J., MCDONALD, R. E., COOPER, A., SMITH, B. O. & KENNEDY, M. W. 2013. The structure of latherin, a surfactant allergen protein from horse sweat and saliva. *J R Soc Interface*, 10, 20130453.
- VERGE, V. M., RIOPELLE, R. J. & RICHARDSON, P. M. 1989. Nerve growth factor receptors on normal and injured sensory neurons. *J Neurosci*, 9, 914-22.
- VICENTE-MANZANARES, M., MA, X., ADELSTEIN, R. S. & HORWITZ, A. R. 2009. Non-muscle myosin II takes centre stage in cell adhesion and migration. *Nat Rev Mol Cell Biol*, 10, 778-790.
- VON DER MARK, K., PARK, J., BAUER, S. & SCHMUKI, P. 2010. Nanoscale engineering of biomimetic surfaces: cues from the extracellular matrix. *Cell Tissue Res*, 339, 131-53.
- VROMAN, L. & ADAMS, A. L. 1969. Findings with the recording ellipsometer suggesting rapid exchange of specific plasma proteins at liquid/solid interfaces. *Surf. Sci.*, 16, 438-446.
- WALLER, A. 1850. Experiments on the section of the glossopharyngeal and hypoglossal nerves of the frog, observations of the alterations produced thereby in the structure of their primitive fibres. *Phil Transact Royal Soc London*, 140, 423-429.
- WALLQUIST, W., ZELANO, J., PLANTMAN, S., KAUFMAN, S. J., CULLHEIM, S. & HAMMARBERG, H. 2004. Dorsal root ganglion neurons up-regulate the expression of laminin-associated integrins after peripheral but not central axotomy. *J Comp Neurol*, 480, 162-9.
- WALSH, S. & MIDHA, R. 2009. Practical considerations concerning the use of stem cells for peripheral nerve repair. *Neurosurg Focus*, 26, E2.
- WERNER, A., WILLEM, M., JONES, L. L., KREUTZBERG, G. W., MAYER, U. & RAIVICH, G. 2000. Impaired axonal regeneration in alpha7 integrin-deficient mice. *J Neurosci*, 20, 1822-30.
- WILLIAMS, S. F., MARTIN, D. P., HOROWITZ, D. M. & PEOPLES, O. P. 1999. PHA applications: addressing the price performance issue: I. Tissue engineering. *International Journal of Biological Macromolecules*, 25, 111-121.
- WOOD, M. D., MACEWAN, M. R., FRENCH, A. R., MOORE, A. M., HUNTER, D. A., MACKINNON, S. E., MORAN, D. W., BORSCHER, G. H. & SAKIYAMA-ELBERT, S. E. 2010. Fibrin matrices with affinity-based

- delivery systems and neurotrophic factors promote functional nerve regeneration. *Biotechnol Bioeng*, 106, 970-9.
- XIAO, H. S., HUANG, Q. H., ZHANG, F. X., BAO, L., LU, Y. J., GUO, C., YANG, L., HUANG, W. J., FU, G., XU, S. H., CHENG, X. P., YAN, Q., ZHU, Z. D., ZHANG, X., CHEN, Z., HAN, Z. G. & ZHANG, X. 2002. Identification of gene expression profile of dorsal root ganglion in the rat peripheral axotomy model of neuropathic pain. *Proc Natl Acad Sci U S A*, 99, 8360-5.
- XIE, H., LI, J., LI, L., DONG, Y., CHEN, G.-Q. & CHEN, K. C. 2013. Enhanced proliferation and differentiation of neural stem cells grown on PHA films coated with recombinant fusion proteins. *Acta Biomaterialia*, 9, 7845-7854.
- XU, X., YEE, W.-C., HWANG, P. Y. K., YU, H., WAN, A. C. A., GAO, S., BOON, K.-L., MAO, H.-Q., LEONG, K. W. & WANG, S. 2003. Peripheral nerve regeneration with sustained release of poly(phosphoester) microencapsulated nerve growth factor within nerve guide conduits. *Biomaterials*, 24, 2405-2412.
- YANG, F., MURUGAN, R., RAMAKRISHNA, S., WANG, X., MA, Y. X. & WANG, S. 2004. Fabrication of nano-structured porous PLLA scaffold intended for nerve tissue engineering. *Biomaterials*, 25, 1891-1900.
- YANG, X., ZHAO, K. Z. & CHEN, G. 2002. Effect of surface treatment on the biocompatibility of microbial polyhydroxyalkanoates. *Biomaterials*, 23, 1391-1397.
- YANG, Y. & EL HAJ, A. J. 2006. Biodegradable scaffolds--delivery systems for cell therapies. *Expert Opin Biol Ther*, 6, 485-98.
- YEO, W. S., HODNELAND, C. D. & MRKSICH, M. 2001. Electroactive monolayer substrates that selectively release adherent cells. *Chembiochem*, 2, 590-593.
- YGGE, J. 1989. Neuronal loss in lumbar dorsal root ganglia after proximal compared to distal sciatic nerve resection: a quantitative study in the rat. *Brain Res*, 478, 193-5.
- YOU, H., WEI, L., LIU, Y., OUDEGA, M., JIAO, S.-S., FENG, S.-N., CHEN, Y., CHEN, J.-M. & LI, B.-C. 2011. Olfactory ensheathing cells enhance Schwann cell-mediated anatomical and functional repair after sciatic nerve injury in adult rats. *Experimental Neurology*, 229, 158-167.
- ZHANG, H., WEI, Y. T., TSANG, K. S., SUN, C. R., LI, J., HUANG, H., CUI, F. Z. & AN, Y. H. 2008. Implantation of neural stem cells embedded in hyaluronic acid and collagen composite conduit promotes regeneration in a rabbit facial nerve injury model. *J Transl Med*, 6, 67.
- ZOU, Z., ZHENG, Q., WU, Y., SONG, Y. & WU, B. 2009. Growth of rat dorsal root ganglion neurons on a novel self-assembling scaffold containing IKVAV sequence. *Materials Science and Engineering: C*, 29, 2099-2103.
- ZUO, J., HERNANDEZ, Y. & MUIR, D. 1998. Chondroitin sulfate proteoglycan with neurite-inhibiting activity is up-regulated following peripheral nerve injury. *Journal of Neurobiology* 34, 41-54.